Thermal optimisation of ground improvement for energy pile performance

M.E. Beh*[1], A. Al-Tabbaa[1], D.M.G Taborda[2], and R.Y.W. Liu[2]

*Correspondence: meb94@cam.ac.uk

[1] *Affiliation (The University of Cambridge, Cambridge CB2 1PZ)*
[2] *Affiliation (Imperial College, London SW7 2AZ)*

Abstract

Embedding ground source heat pump systems within concrete structures such as piled foundations saves time, space and money for new builds, while providing low-carbon heating and cooling. Despite many documented success cases, adoption of these energy piles is low, due to doubts surrounding their long-term efficiency and thermomechanical behaviour. Optimising the thermal characteristics of the surrounding soil body using ground improvement offers a solution to offsetting these effects, however little is known about the effects on long-term behaviour when subjected to realistic thermal loading. This research demonstrates how increasing both the radius and thermal conductivity of the improved zone has beneficial impacts on the thermal performance of the GSHP. Increased thermal conductivity also benefits the long-term thermomechanical behaviour, however only at smaller radii.

Introduction

Previous studies have demonstrated that energy pile performance and thermomechanical response is greatly improved for soil bodies with higher thermal conductivity. Ground improvement methods such as jet grouting and deep soil mixing provide a means of increasing the thermal conductivity of the soil through cementation of soil particles, while offering an opportunity to further optimise thermal properties through tailored grout mixes. Taborda et al. (2023) investigated the impact of introducing a zone of improved thermal conductivity surrounding an energy pile on the generation of thermally induced axial stress, with promising results. However, questions remain around the long-term effectiveness of this zone, as well as the impacts on the thermal efficiency of the GSHP system. This study aims to examine the thermomechanical impacts of improving the thermal conductivity of a zone surrounding an energy pile subject to realistic long term cyclic thermal loading. Recommendations on the optimisation of the thermal conductivity and diameter of the zone of improvement will be made.

Methodology

The response of a single 900mm diameter energy installed within London Clay to a depth of 25m and subjected to five cycles of heating and cooling over a period of 1800 days is investigated. Applied thermal boundary conditions for the heat exchanger pipes are modelled after Taborda et al. (2023) and assume an extraction/injection of 99W/m. Mechanical boundary conditions include static loading of the pile to 2600kN (4560kPa), equating to a FoS of approximately 2.6. Key considerations of these analyses are the impact on the magnitude of the thermally induced axial stresses and the rate of heat dissipation surrounding the pile. The modelling of this problem would normally require a three-dimensional numerical model to accurately simulate the discrete locations of the heat exchanger pipes. Such models are computationally expensive, and therefore a simplified method proposed by Liu et al. (2020) is adopted, which uses the combination of a plane-strain cross section model with an axisymmetric model for a more accurate 2D analysis. The London Clay is modelled using the Imperial College Small Strain Stiffness Model (IC.3GS), developed by Taborda (2023). Ten cases are analysed and compared against a control scenario ($\lambda_{gi} = \lambda_{soil}$).

Results

To improve thermal efficiency of the GSHP system, it is imperative to increase the rate at which thermal energy moves to and from the pile. As seen below in Figure 1 an increase in

λ_{GI} has a significant impact on the amount of thermal energy transferred into the surrounding soil.

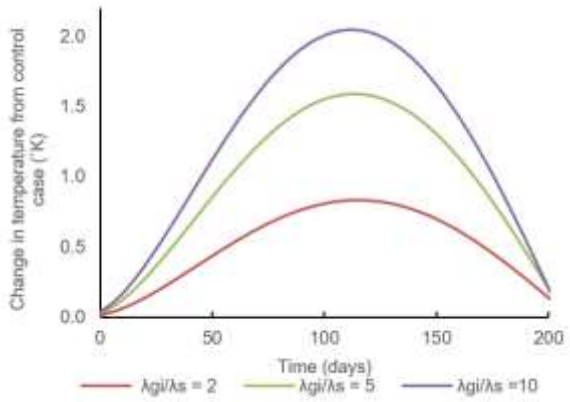

Figure 1: Effect of λ_{GI} on temperature 2m offset from centre of pile for r_{GI}/r_{pile} = 3 (first 200 days of operation)

These promising results are continued when considering thermomechanical behaviour. Figure 2 depicts how increasing both λ_{GI} and r_{GI} can reduce the thermally induced axial stress during the first heating cycle by up to 86%. This increase from the results of Taborda et al. (2023) is due to the difference gradient of the applied temperature function.

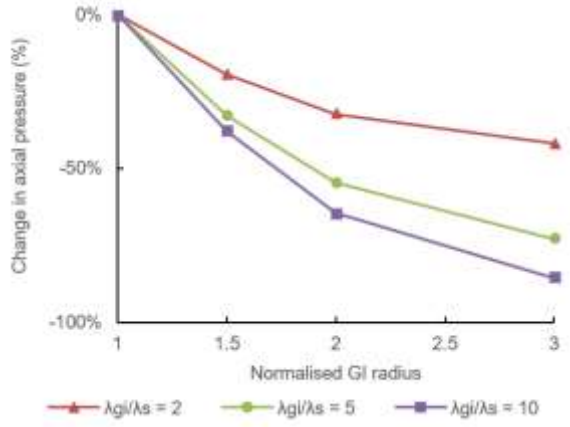

Figure 2: Effect of λ_{GI} and r_{GI} on thermally induced axial stress within pile during first heating cycle

However, when considering 5 years of continuous operation, this effect is reversed for some values of λ_{GI} and r_{GI}, as seen below in *Figure* 3. This is thought to be a possible effect of a build up of thermal energy or due to an increase of negative excess pore pressures at the pile toe, a numerical side-effect of the assumption of a homogenous soil profile. Therefore, a smaller GI radius is recommended for long-term operation.

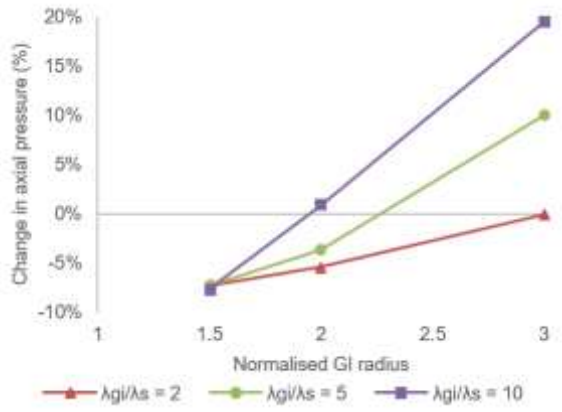

Figure 3: Effect of λ_{GI} and r_{GI} on maximum thermally induced axial stress within pile over all 5 cycles

Further Work

Further work will widen the range of optimised thermal properties to include heat capacity and the coefficient of thermal expansion of the improved zone. This will then be expanded to analyse pile group behaviour. From these promising results, it is likely that an optimised ground improvement mix can suggested for pile groups to offset the differential raft displacement and pile-raft-pile load transfer that has been observed in multiple energy pile group tests.

References

This work, as well as any further work, is completed as part of the SaFEGround (Sustainable, Flexible and Efficient Ground-source heating and cooling systems) Project, funded by the Engineering and Physical Sciences Research Council (EPSRC).

Liu, R. Y. W., Sailer, E., Taborda, D. M. G., Potts, D. M., & Zdravković, L. (2020). A practical method for calculating thermally-induced stresses in pile foundations used as heat exchangers. Computers and geotechnics, 126. https://doi.org/10.1016/j.compgeo.2020.103743

Taborda, D. K., S; Tsiampousi, A. (2023). IC MAGE Model 01 – strainhardening/softening Mohr-Coulomb failure criterion with isotropic small strain stiffness

Taborda, D. M. G., Bortolotto, M. S., & Liu, R. Y. W. (2023). Influence of pipe arrangement and improved thermal conductivity on the response of thermo-active piles NUMGE, Imperial College, London.

17th BGA YGES
University of Cambridge
1-3 July, 2024

A novel foundation design for the hybrid marine renewable energy harvest system

Yukun Ma*[1], Liang Cui[1], and Suby Bhattacharya[1]

*km01614@surrey.ac.uk

[1] *University of Surrey (School of Sustainability, Civil and Environment Engineering, Guildford, UK)*

Abstract

Establishing a hybrid marine renewable energy harvest system (HMREHS) on a shared platform can reduce the energy costs, increase production, and promote the United Nation Sustainable Development Goals. The aims of this paper are to propose a novel design of a HMREHS supported by foundation consisting of a monopile and a plate to integrate various marine renewable energy harvest devices and to establish a foundation design methodology based on FE simulations using Plaxis 3D. Taking the Sheringham shoal wind farm as a case study, the monopile dimensions are determined using monopile design guidance. Based on this monopile designed, considering multiple environmental loads, a series of numerical simulations of foundation with different steel plate sizes were performed to determine the most reasonable combination.

Introduction

The marine renewable energy includes many types, the wind energy harvested by offshore wind turbine (OWT), the wave energy harvested by wave energy converter (WEC), and the current energy collected by current turbine (CT), etc. They are characterised as clean, effective and sustainable (Cui et al., 2024).

Although these energy sources are green and renewable, they face substantial obstacles in their development. For example, high foundation installation costs and energy transmission losses. All of them directly result in a higher levelised cost of energy (LCOE), making these energy sources less accessible to users. Therefore, if a shared infrastructure can be designed to integrate different energy harvest device, it would significantly reduce construction costs and increase energy production. This would greatly promote the utilisation of marine renewable energy and make it a widely acceptable energy for users.

This paper proposes a HMREHS supported by a fixed-base foundation consisting of a monopile and a steel plate. Taking the Sheringham shoal wind farm as the case study, the loads on the HMREHS are calculated and the fixed foundation parameters are determined.

HMREHS overview

The HMREHS consists of an OWT, four WECs, two CTs and a set of hydrogen production devices. The OWT is located at the centre of the system; the WECs are connected by tubular steel arms with a diameter of 0.5m, a wall thickness of 0.05m, and a length of 10m; the CTs are connected by tubular steel arms with a diameter of 1 m, a wall thickness of 0.01 m, and a length of 15 m. The hydrogen production devices are installed on a circular platform with a diameter of 6 m. Based on the marine meteorological data and geotechnical data, the 50-year extreme operating gust wind load and 1-year extreme wave height are considered. The wind load exerting on the OWT is 1.62 MN, the wave load exerting on the foundation is 2.36 MN, the current load exerting on the foundation, current turbine and CT connection arm are 20.2 kN /m, 461 kN and 3.37 kN/m. The vertical load and horizontal load exerting on the WEC are 135.6 kN and 129.8 kN, respectively.

Foundation design

Based on the monopile design method proposed by Arany et al. (2017), the initial design specifies a monopile with 6 m diameter, 35 m embedded depth and 0.07 m wall thick-ness. FEM verified that the rotation and displacement at the mudline level are 0.22° and 9 cm, respectively, which meet the design requirements. Integrating a steel plate with monopile is an innovative hybrid foundation design. It

can provide additional capacity to resist the lateral load with reduced embedded length (Lp) (Wang et al., 2018). In order to obtain the optimum combination of steel plate diameter (D) and embedded depth, a comparative study is performed using FE modelling using Plaxis 3D. The numerical schemes are listed in Table 1(M – monopile, MP – hybrid foundation).

Table 1. Simulation schemes

Scheme	L_p	D	System	Foundation
A-1	35	0	HMREHS	M
B-1~B-10	30	8~17	HMREHS	MP
C-1~C-5	27	8,10, 12,14, 16	HMREHS	MP
C-6~C-10	30		HMREHS	MP
C-11~C-15	33		HMREHS	MP

A set of indices, η_{HL}, η_{SL}, η_{ML}, and δ_i, are proposed to quantify the different responses between different schemes, as shown in Eq. 1.

$$\delta_i = \left|\frac{D_{i-HL} - D_{M-HL}}{D_{M-HL}}\right| + \left|\frac{D_{i-SL} - D_{M-SL}}{D_{M-SL}}\right| + \left|\frac{D_{i-ML} - D_{M-ML}}{D_{M-ML}}\right| \quad (1)$$

$$\delta_i = |\eta_{HL}| + |\eta_{SL}| + |\eta_{ML}| \quad (2)$$

where D_{i-x} is the lateral deformation of scheme i at x level, where x can be ML, SL, and HL, corresponding to mudline level, sea surface level, and hub level, respectively.

Results

The effect of steel plate diameter on the lateral displacement at different levels from Scheme B are shown in Figure 1. With the increase in steel plate diameter, the lateral deformation reduced more significantly at the mudline level compared to the sea level and hub level.

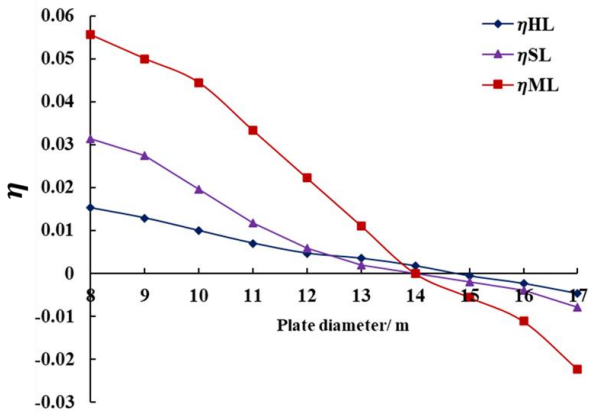

Figure 1. Effect of plate diameter on lateral displacement

In order to obtain an optimum combination of D and Lp, Scheme C are simulated. The sum of relative differences in lateral deformation at three levels are analysed, as listed in Table 2. The evaluation index, δ_i, for the M-14-30 scheme is the smallest This indicates that the deformation profile obtained from the hybrid monopile with an embedded depth of 30 m and a steel plate with a diameter of 14 m is most similar to that of the monopile with 35m embedded depth.

Table 2. Lateral deformation (m) (*MP-8-27: 8 – plate diameter; 27 – embedded length)

	D_{i-HL}	D_{i-SL}	D_{i-ML}	δ_i
M	1.703	0.255	0.09	-
MP-8-27*	1.854	0.299	0.11	0.483
MP-8-30	1.729	0.263	0.095	0.102
MP-8-33	1.681	0.248	0.087	0.073
MP-10-27	1.841	0.296	0.11	0.46
MP-10-30	1.72	0.26	0.094	0.074
MP-10-33	1.672	0.246	0.084	0.120
MP-12-27	1.826	0.292	0.108	0.417
MP-12-30	1.711	0.256	0.092	0.030
MP-12-33	1.664	0.243	0.08	0.181
MP-14-27	1.814	0.288	0.106	0.372
MP-14-30	1.706	0.255	0.09	0.001
MP-14-33	1.657	0.241	0.077	0.226
MP-16-27	1.713	0.262	0.098	0.122
MP-16-30	1.699	0.254	0.089	0.017
MP-16-33	1.651	0.24	0.082	0.178

Conclusions

The monopile with a steel plate exhibits higher stiffness and higher resistance to lateral deformation. Adding a steel plate with suitable diameter can reduce the monopile embedment depth by approximately 15%, resulting in higher cost saving.

References

Arany L, Bhattacharya S, Macdonald J, et al. 2017. Design of monopiles for offshore wind turbines in 10 steps. Soil Dynamics and Earthquake Engineering, 92: 126-152.

Cui L, Amani S, Gabr M, et al. 2024. Synergistic Hybrid Marine Renewable Energy Harvest System. Energies, 17(5): 1240.

Wang X, Zeng X, Li J, et al. 2018. Lateral bearing capacity of hybrid monopile-friction wheel foundation for offshore wind turbines by centrifuge modelling. Ocean Engineering, 148: 182-192.

Development of an Iterative Static Soil-Structure Interaction Methodology for a Nuclear Facility

R. Hamilton Carmichael*[1], T. Anderson[1], J. Meehan[1] and H. Jethmalani[1]

* Correspondence: ross.hamiltoncarmichael@mottmac.com

[1] *Mott MacDonald, 8-10 Sydenham Road, London*

Abstract

Soil-structure interaction is crucial in understanding the behaviour of massive structures, such as nuclear power plants, during static and dynamic loading. UK sites are generally soft and produce a non-linear response, which makes typical methods unsuitable. This paper looks at a semi-coupled approach which used ANSYS and PDisp to assess structural forces and predict settlement, respectively. An innovative method was used to match the loading mesh from ANSYS to the PDisp mesh, allowing a smooth interface between both models which improved the efficiency of the iteration process. Tools were developed in Python to automate the production of graphical outputs of multiple variables across different iterations. Validation of this work was carried out using hand calculations, settlement assessments, and comparisons between a fully coupled structure and soil model in LS-DYNA.

Introduction

Most nuclear codes consider the Impedance Function Method and the Direct Method for the evaluation of Static Soil Structure Interaction (Ghosh, Kumar, Talby, Tan, & Tao, 2022). However, due to typically softer ground conditions in the UK, this method is unsuitable. This paper looks at matching the structural and geotechnical model meshes to improve the efficiency of the iteration process.

A geotechnical analysis of a large raft foundation was undertaken to provide soil springs for use in a structural analysis model. The analysis, which uses a semi-coupled approach, utilised ANSYS to model and analyse the behaviour of structural members. This model comprises the beams, columns, and load-bearing walls in the building, as well as the loads imposed on them and includes the reinforced concrete foundation raft. PDisp was used to predict the settlement of the raft foundation on a non-linear 3D soil continuum.

The response of the ground to applied pressure combined with the flexibility of the large raft foundation allows for structural forces and bending moments to redistribute. Several iterations of analysis allow this redistribution to be captured, and the iterations continue until the change in spring stiffnesses, settlements and structural forces becomes sufficiently low.

The raft is modelled in ANSYS as being supported by linear elastic springs. This is not a realistic assumption for the soil underlying the building, which is anticipated to exhibit non-linear behaviour. Given the sensitivity of nuclear structures, it is crucial to accurately model the expected behaviour of the ground. Therefore, the response of the loaded soil below the foundation must be obtained from Soil-Structure Interaction (SSI) analysis.

Methodology

The innovative Elastic Foundation Stiffness (EFS) method was used to match the loading mesh from the raft foundation in ANSYS exactly to the PDisp soil mesh. The ANSYS element centres align with the PDisp element centres, and the geometries of the mesh elements are the same.

Typically, the applied pressures from the structural model are manually grouped into similar zones and averaged before being input into the geotechnical model. However, using the EFS method allows a 1:1 element location and geometry match between ANSYS and PDisp. This improves the efficiency of the iteration process, ensures a smooth interface between the Structural and Geotechnical teams, and provides a consistent and repeatable automated process.

In the EFS method, each raft element is assigned an area spring stiffness based on the vertical settlement resulting from the applied pressure. The applied pressure from each ANSYS element is input into PDisp which then calculates the settlement of the element at its centre. An example iteration process is shown in Figure 1.

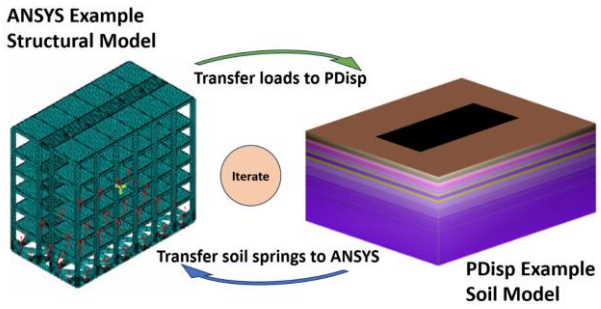

Figure 1. ANSYS – PDisp example iteration process. ANSYS Structural model for illustration purposes, from (Hong, Yang, & Jin, 2010).

Challenges and Improvements

Typically, the number of iterations required is increased due to the change of internal forces at the raft edges. This is because ANSYS doesn't model the soil and therefore can't redistribute stress beyond the building footprint. PDisp does model the soil, which provides a more realistic distribution of stress into the soil continuum.

To accelerate the convergence process, the area spring stiffness of the concrete raft edge elements is artificially increased by 25% (a factor of 1.25) (O'Brien, Burland, & Chapman, 2024). This "attracts" more load to the raft edges and thus accelerates convergence. When convergence is deemed to be complete, this "edge factor" is removed and a final iteration is performed to ensure that there are no significant differences concluding that these spring values are final.

Due to the large number of variables being checked (forces, moments, bearing pressure, spring stiffness and settlement) across multiple iterations, tools were created in Python to automate the production of graphical outputs.

Results and Validation

Figure 2 shows a relative rotation contour plot which was automated using Python scripts.

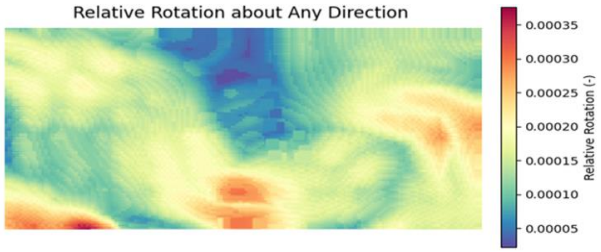

Figure 2. Rotation assessment plot for an area of the site.

Figure 3 shows, by spring stiffness and internal force, the number of elements changing by greater than 5% from the previous iteration.

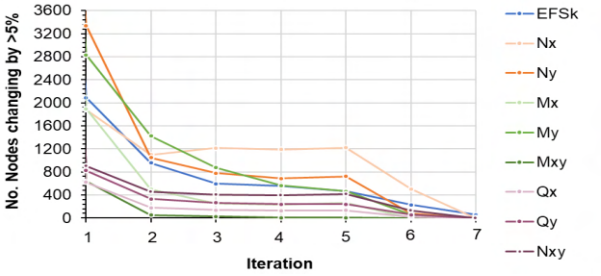

Figure 3. Number of nodes with a change of greater than 5% between iterations.

Validation of the results was carried out using the following methods: hand calculations, using a constant strain derived stiffness for all strata; settlement comparison at a fixed location in Settle3, using an equivalent linear stiffness; and comparisons between the fully coupled structure and soil model in LS-DYNA.

Conclusions

The EFS method improved the efficiency of the iteration process and allowed faster turnaround times between the structural and geotechnical teams, while retaining the high resolution of results in a critical nuclear facility. Automation of graphical outputs allowed easy visualisation of results between iterations across all model variables, making it easier to spot global trends.

References

Ghosh, B., Kumar, V., Talby, R., Tan, M., & Tao, Z. (2022). Iteractive Static Soil Structure Interaction Analysis for UK HPR1000. *26th International Conference on Structural Mechanics in Ractor Technology.* Blin: SMiRT-26.

Hong, Y., Yang, R., & Jin, H. (2010). Hong, Y., Yang, R., & Jin, H. (2010). The force analysis of frame structure building relocation based on ANSYS. 2010 International Conference on Future Information Technology and Management Engineering, 1, 353-356. *International Conference on Future Information Technology and Management Engineering* (pp. 353-356). Changzhou: IEEE.

O'Brien, T., Burland, J. B., & Chapman, T. (2024). Rafts and piled rafts. In M. Brown, J. Burland, T. Chapman, K. Higgins, H. Skinner, & D. Toll, *ICE manual of geotechnical engineering: Volume II* (pp. 897-935). Leeds: Emerald Publishing Limited.

Analytical method for thermal analysis of Energy Walls

A. Gupta*[1], F. Loveridge[1], I. Shafagh[2] and S.J. Rees[1]

*Correspondence: cnagu@leeds.ac.uk

[1] *School of Civil Engineering (University of Leeds, Woodhouse, Leeds, UK)*
[2] *School of Mechanical Engineering (University of Leeds, Woodhouse, Leeds, UK)*

Abstract

Decarbonising the energy system is one of the most essential steps for moving towards a carbon-neutral future. This can be assisted by thermally activating embedded components (most commonly piles and walls) of a structure which are in contact with the ground for space heating and cooling applications. While piles have been explored significantly, there is still a lack of an easy-to-apply analytical method for thermal analysis of walls to enable prediction of energy capacity. This work provides an analytical method which can be utilised for thermal analysis of thermally active embedded walls, also called energy walls. It uses the classical method of dividing the heat transfer components into time-dependent and -independent domains to simplify the overall analysis. Field data is used to test the analytical method that was developed.

Introduction

The heat energy in the ground, i.e., geothermal energy, can be exploited for space heating and cooling of structures through the substructural components, which are thermally activated through heat exchangers pipes that are embedded at the time of construction. These components are termed Energy Geostructures (EG); the case where the pipes are embedded within a retaining wall is called an Energy Wall (EW). There are no easy-to-apply analytical methods for thermal analysis of the energy walls which can be used in the design of energy capacity.

Heat transfer is generally divided into two components, time-dependent and -independent, which are used as an analytical method for thermal analysis for EG. The larger domain, soil, is considered to be in a transient or time-dependent state. On the other hand, the much smaller EG is considered to be in a steady or time-independent state (Laloui and Loria, 2019). A similar approach is adopted for the EW in this work. The method's accuracy is tested against field data collected from a site in Glorias, Spain. The details of the method are discussed in the next section.

Methodology

The field data studied here corresponds to an energy wall, which is fully buried, i.e., there is ground on both sides of the wall, as it is not excavated yet. Hence, the methodology here only discusses this case for brevity, but other cases are discussed in Gupta (2024). In the current case, the method predicts temperature changes in the outlet fluid. This can be done by considering only the heat transfer process on one side of the wall. The section closer to the ground is used (Fig. 1). Energy walls are considered as a planar heat source, and hence, the infinite place source (IPS) is applied to assess the transient heat transfer in the soil (e.g. Shafagh and Loveridge, 2020). This assumes heat transfer to occur in a semi-infinite soil solid. The temperature changes, ΔT due to a planar thermal load, q_p(W/m^2), at the ground wall interface at any time t, can be calculated through Eq. (1) given below:

$$\Delta T(t) = \frac{q_p}{2\lambda} g(x,t) = \frac{q_p}{2\lambda}\left(\sqrt{\frac{4\alpha t}{\pi}}\, e^{-x^2/4\alpha t} - x\, erfc\,\frac{x}{\sqrt{4\alpha t}}\right) \quad (1)$$

Where g(x,t) represents the g-function, x is the distance at which temperature changes are measured (here, x is the cover from the centre of the pipe), λ and α are, respectively, thermal conductivity and diffusivity of the ground, and erfc is the complementary error function. The steady-state heat transfer within the EW can be calculated through thermal resistances of three sections: (1). between the ground wall interface and the pipes; (2) the pipe materials; and (3) the fluid within the pipes.

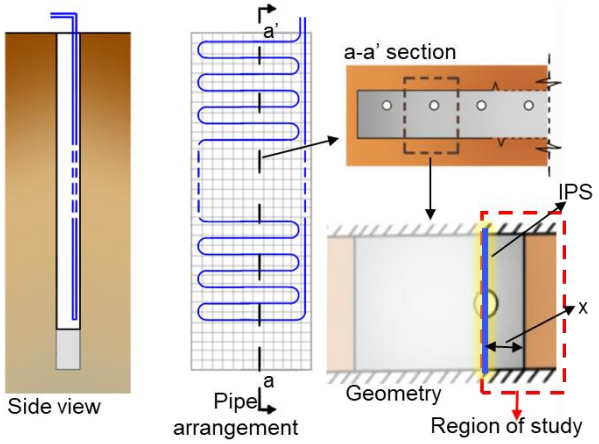

Figure 1: Schemetic represnetaion of energy wall in Barcelona and the region of the geometry (red box) used for the calculation of changes in fluid temperature.

Thermal resistances for pipe and fluid does not induce significant changes in the temperature, and they can be calculated from existing approaches (Laloui and Loria, 2019). Hence, only resistance, (R) between the wall and the pipe is discussed here. R can be calculated through the shape factor (S_F). S_F are simplified equations that can assess the heat transfer between two surfaces in a steady state. For the required section, the Eq. (2) can be used which is derived from rotational geometry and electrical analogy (Rohsenow et al., 1975).

$$S_F = \frac{1}{\lambda_W R} = \frac{\pi}{\ln\left(\frac{sinh\left(\frac{\pi(W-c')}{s}\right)}{sinh\left(\frac{\pi D}{2s}\right)}\right)} - \left(\frac{s}{W-2c'}\right) \quad \text{.....(2)}$$

Where W is the wall thickness, s is pipe spacing, D is pipe diameter, and c' is the cover from the centre of the pipe to the closest ground wall interface, as seen in Fig. 1. The transient response and steady-state response are combined to form Eq (3), which can be used for the calculation of fluid temperature.

$$T_{out}(t_n) = T_0 + \frac{q_p}{2\lambda} g(x,t) + \frac{q_p s}{2\lambda_W S_F} \quad \text{.....(3)}$$

Where T_0 is the initial fluid temperature. This equation was used for the calculation of the outlet temperature of the fluid. The principles of temporal superposition is used with Eq. (3) to assess temperature changes under time-varying thermal loads. The results are presented against the field data in the next section.

Results

A fully embedded energy wall of 15m deep, 3.5m wide and 0.6m thick was tested for 167.5 hours. The details regarding the thermal properties of the materials and thermal loading are extracted from Shafagh and Loveridge (2020). The results comparing the output temperature from field data and calculated data are presented in Fig. 2. As can be observed from the figure, the output temperature predicted by Eq. (3) almost traces the temperatures extracted from field data. The maximum difference between the two is 0.37ºC, which is 1.1%. This shows the high accuracy of the analysis method and proves its potential to be used for more complex cases.

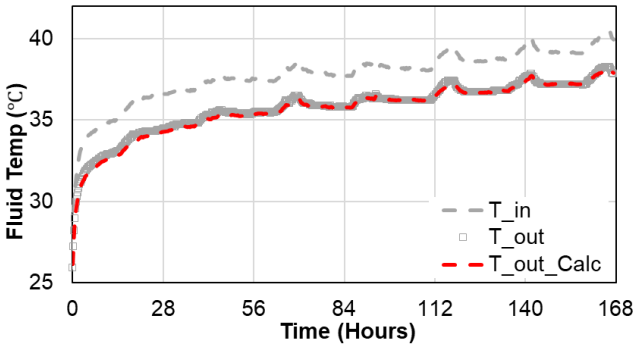

Figure 2. Temperature of the fluid collected from site (T_out) against calculated (T_out_calc)

Conclusions

The first easy-to-apply analytical method for the thermal analysis of energy walls is presented and validated against field data. The new method, based on superposition of a steady state solution for the wall and a transient solution for the ground, shows very good accuracy, and potential for rolling out to a wider range of geometry scenarios.

References

Gupta, A. 2024. An analytical method to de-ter-mine the amount of heat exchanged through thermally activated embedded retain-ing walls. *Doctoral Thesis. University of Leeds, UK*

Laloui, L. and Loria, A.F.R. 2019. Analysis and Design of Energy Geostructures: Theoretical Essentials and Practical Application.

Rohsenow, W.M., Hartnett, J.P. and Cho, Y.I. (eds.). 1975. Handbook of Heat Transfer *Third*. *New York: The McGraw-Hill Companies, Inc*.

Shafagh, I. and Loveridge, F. 2020. Developing analysis approaches for energy walls In: *E3S Web of Conferences, 2nd International Conference on Energy Geotechnics (ICEGT 2020)*, **205**, pp.8–12.

Settlement-Comparative Cost and CO_2 Emission Analysis of a Stone Column Enhanced Pile Foundation Using Finite Element Modelling

K.M. Sahin[1] and A. Ekinci*[2]

*Correspondence: ekincia@metu.edu.tr

[1] MSc Candidate (Civil Engineering Program, Middle East Technical University, Northern Cyprus Campus, Kalkanli, Guzelyurt, North Cyprus, via Mersin 10, Turkey)
[2] Associate Professor (Civil Engineering Program, Middle East Technical University, Northern Cyprus Campus, Kalkanli, Guzelyurt, North Cyprus, via Mersin 10, Turkey)

Abstract

Geotechnical applications frequently demand substantial quantities of concrete and steel, leading to elevated CO_2 emissions and costs. This study conducts a comparative settlement analysis of traditional piles versus piles combined with stone columns arranged in various geometrical configurations. The results demonstrate that integrating stone columns significantly reduces both costs and CO_2 emissions while maintaining comparable settlement values. This innovative approach offers a sustainable and cost-effective alternative for geotechnical engineering projects, contributing to environmental conservation without compromising structural integrity.

Introduction

Raft foundations are commonly selected for a wide range of construction applications due to their safety, ease of manufacture, and controllability. Settlement is typically the primary concern for foundations, especially in areas with poor soil conditions. To address this issue, piles can be installed alongside foundations to transfer structural loads from weaker topsoil to stronger subsoil strata (Ahmed et al., 2021). However, these piles are often constructed from materials like concrete and steel, which are chosen for their high strength but contribute significantly to CO2 emissions during construction (Al-Subari et al., 2022). To mitigate the cost and environmental impact of such materials, soil improvement techniques, such as stone column applications, can be employed. Stone columns are an effective ground improvement method, particularly in regions with soft clay and silt layers (Javed et al., 2019).

General Specifications

The region of Iskele in North Cyprus is known for weak topsoil which consists of silty clay with low strength properties. Analysis for a planned structure in this area which is to be 12 stories high with a raft foundation of 30 x 20 meters, showed large settlement values and required piles and/or soil improvement. Finite element analysis (FEM) was utilized using PLAXİS 3D software to find maximum settlement values. The interface used can be seen in Figure 1.

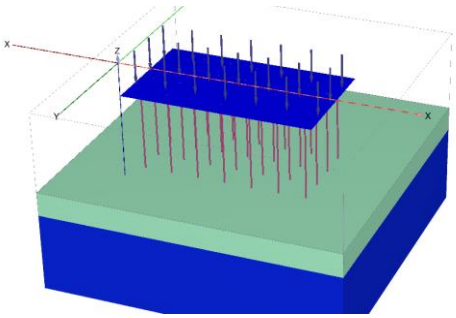

Figure 1. Model tested on PLAXİS 3D

Table 1 shows number of used elements (pile or Stone Column (SC)) along with their diameters and spacing.

Table 1. Properties of elements utilised for the project.

test ID	#of pile	Diameter(m) Pile	#of SC	Diameter(m) SC	Spacing
Pile only	28	1.5	0	-	4m
Pile+SC (a)	20	1.2	16	0.7	3m
Pile+SC (b)	18	1.2	18	0.7	3m

The piles were designed in accordance with the Turkish code TS-500, utilizing C30/35 grade concrete and S420 grade 24mm diameter steel. The same TS-500 code was applied

to the design of the stone columns. According to Durgunoğlu (1992) and Mungan (2023), natural crushed stone material with a grain size between 10 and 100 mm, a fine grain content of less than 5%, and no chemical reactivity with the environment is sufficient for stone column applications. The two geometrical configurations employed in this study are illustrated in Figure 2.

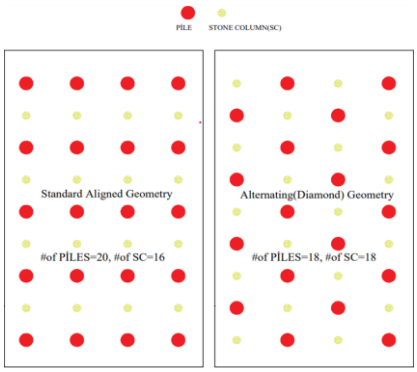

Figure 2. Standard geometry model(a) and Diamond geometry model(b).

Cost and CO_2 production for each stage was then calculated. Material volume required was calculated in accordance with TS-500, then their cost per volume which was provided by the supplier. CO_2 produced was found using coefficients for each materials production transportation and installation, taken from Al-Subari et.al, 2022.

Results and Discussion

Settlement results and distributions along the foundation for all geometries and combinations can be seen in Figure 3.

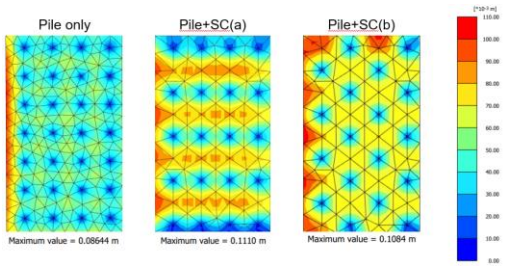

Figure 3. Settlement patterns for Pile only, Pile with regular and diamond configuration.

Installing only piles under foundations effectively reduces settlement but is also the most expensive option and produces the highest CO_2 emissions, as shown in Table 2.

Table 2. Cost, CO_2 emissions and Settlement values.

	Cost (€)	CO_2 (kg)	Settlement (mm)
Pile only	204,144	784280	86
Pile+SC(a)	131,078	362833	111
Pile+SC(b)	124,036	327476	108

It is seen that combining piles with stone columns lowers costs and environmental impact while maintaining decent settlement values. The geometry of application can enhance these results further, as model(b) performs better in terms of settlement than model(a), even though it costs less overall.

Conclusion

Installing only piles under foundations reduces settlement in weak soils but is costly and environmentally harmful due to high CO_2 emissions. Combining piles with soil improvement techniques, like stone columns arranged in a diamond geometry pattern, lowers costs and environmental impact while maintaining decent settlement properties.

References

Ahmed, D., Taib, S. N. L. B., Adat, T., & Hasan, A. (2021). A Review on the Behaviour of Combined Stone Columns and Pile Foundations in Soft Soils when Placed under Rigid Raft Foundation. ASM Science Journal, 16, 1–8.

Al-Subari, L., Yaqubi, N. A., Selcukhan, O., & Ekinci, A. (2022). Environmental and economical assessment of earth-retaining walls for design optimisation. Environmental Geotechnics, 1–18.

Durgunoğlu, H.T., Kulaç, F., İkiz, S. ve Karadayılar, T., (1992) An Application on Ground Improvement with Stone Columns'', 4th National Congress on Soil Mechanics and Foundation Engineering, Istanbul Technical University.

Javed, S. A., Salsabiyl, A., Jubaida, F. N., Islam, M. Z., & Islam, S. (2019). Comparative Cost Analysis of Pile Foundation with Soil Improvemnet of a Reclaimed Area. *Journal of Earthquake Science and Soil Dynamics Engineering*, *2*(3), 1-14.

Mungan, H. (2023). Stone Column Construction Methods and Applications, Nobel, 1–80.

Particle Size Distribution Effects in the Thaw Weakening in Soils

J. Leak*

*Correspondence: J.leak@napier.ac.uk

Edinburgh Napier University, School of Engineering and the Built Environment, Edinburgh

Abstract

Thaw weakening is detrimental to highway infrastructure. This work examines the relationship between PSD and thaw weakening susceptibility. Data used to establish the testing procedure for thaw weakening are examined in this work using grading entropy coordinates. It is seen that PSD is influential in the susceptibility to thaw weakening and changes in stability between freeze-thaw.

Introduction

Frost action describes two behaviours: frost heave and thaw weakening. Both are associated with damage to infrastructure. Whilst both behaviours associated with frost action are detrimental to infrastructure, susceptibility criteria are generally only specific to frost heave. Chamberlin (1981) drew attention to this:

"*Both seem to be major indicators of frost-susceptible soils. However, for decades there has been an almost universal tendency to define frost susceptibility in terms of frost heaving alone, i.e. a frost-susceptible soil was one which heaved when frozen*." *- Chamberlin (1981)*

A great deal of attention has been given to determining susceptibility to frost action. The simplest method of assessing frost action susceptibility (FAS) is the analysis of the particle size distribution (PSD). However, PSD is often considered unreliable as a means of determining frost susceptibility. This may be due to a reliance on common grading descriptors, that do not account for the full PSD (i.e. fines and gravel content).

There is a bias towards frost heave when considering FAS, particularly those orientated around the PSD. This investigation re-evaluates data from Jessberger & Carbee (1970), who proposed a commonly used testing procedure for thaw weakening susceptibility. Grading entropy coordinates are used to investigate the entire PSD curve. The relationship between thaw weakening is therefore investigated with the grading entropy stability criteria to establish a relationship between PSD, internal stability and thaw weakening.

Grading Entropy

Proposed by (Lorincz, 1986) grading entropy condenses the PSD to a single point on Cartesian plane by accumulating the grading entropy within each fraction. The total entropy is split into two components which form a coordinate pair:

$$A = \frac{S_0 - S_{0min}}{S_{0max} - S_{0min}} \quad B = \frac{\Delta S}{\ln(N)} \tag{1}$$

A is the normalised base entropy and *B* is the normalised entropy increment. S_0 and ΔS are the non-normalised base entropy and entropy increment coordinates, and *N* is the number of fractions in a PSD. These coordinates have simple physical meanings, *A* is a logarithmic mean of the average grain diameter, whereas *B* is a measure of how much a PSD is influenced by all its sieve fractions.

Grading Entropy Stability Criteria

Soils are suggested to be internally unstable if their A-coordinate is less than A=0.667 (known as the stability line), whereas soils are seen to be internally stable provided their A-coordinate is greater than A=0.667. Right of A=0.667, A-coordinates are large enough so that coarse grain skeletons may form. Moreover, larger B-coordinate ensures that there is ample material within the sieve fractions to provide support to coarse grain networks. Left of A=0.667, a

greater abundance of finer material is suggested to destabilise the internal stability of grains (Lorincz, 1986)

Results

Jessberger and Carbee (1970) undertook a series of freeze-thaw tests to determine a means of quantifying thaw weakening. Soils were subjected to a California Bearing Raito (CBR) test. Values were taken before and after freeze-thaw to investigate changes in bearing capacity. The testing procedure established in this work is commonly used to measure susceptibility to thaw weakening. Figure 1 shows the entropy coordinates for all soils from Jessberger & Carbee (1970):

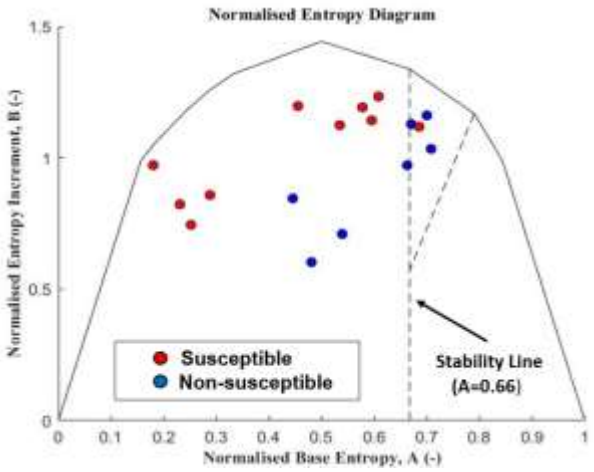

Figure 1. Entropy coordinates for soils form Jessberger & Carbee (1970). Susceptible soils are found left of A=0.667.

In Figure 1, soils that are susceptible after thaw are located in the unstable region (< A=0.667). Indicating that PSD may be an indicator of thaw weakening susceptibility. Figure 1 suggests that grading entropy coordinates may be used as an effective susceptibility criteria. In Figure 2, note that changes in CBR in excess of 20% are located primarily in the unstable region also, indicating significant changes in internal stability during thaw, which appear to be highly influenced by PSD.

These findings indicate that the PSD of highway infrastructure, such as road subgrades/subbases in cold and seasonally cold regions should give reference to the entire PSD in order to minimise road pavement defects induced via thaw weakening (such as potholes).

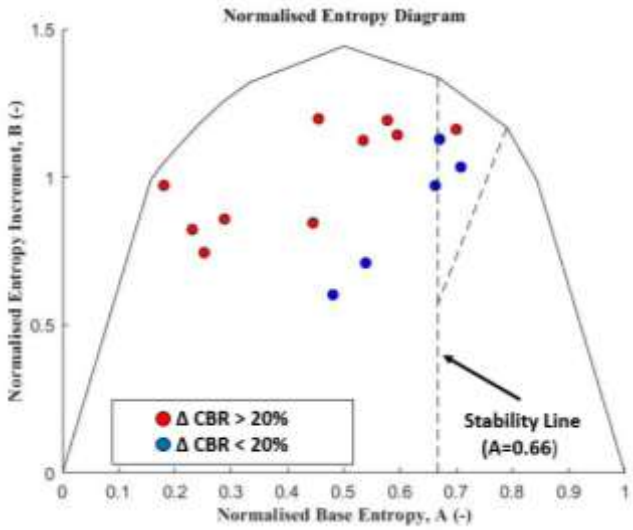

Figure 2. Soils are identified by their change in CBR % after freeze thaw. Greater changes in CBR are seen in Susceptible soils.

Discussion & Conclusion

This work has investigated data from Jessberger & Carbee (1970) using the grading entropy stability criteria. Results from this work show the following:

- Susceptibility to thaw weakening may be characterised by grading entropy coordinates, providing a criteria which assesses the entire PSD.
- Large changes in CBR, in excess of 20%, after thaw are primarily seen in soils within the unstable region of the grading entropy stability criteria.

References

1. Jessberger, H.L. and D.L. Carbee (1970) Influence of frost action on the bearing capacity of soils. Highway Research Record, no. 304, p. 14-26
2. Lőrincz J (1986) Grading entropy of soils. Dissertation, Technical University of Budapest (in Hung)
3. Chamberlain, E.J. (1981). Frost susceptibility of soil: Review of index tests. U.S. Army Corps of Engineers, Cold Regions Research & Engineering Laboratory

17th BGA YGES
University of Cambridge
1-3 July, 2024

Small Strain Stiffness and Stiffness Degradation of a Low to Medium Density Chalk

L.P. Rieman*[1], R.M. Buckley [1], and N.S. Shinde[1]

*Correspondence: l.rieman.1@research.gla.ac.uk

[1] *James Watt School of Engineering, University of Glasgow (Glasgow, UK)*

Abstract

Driven by ambitious climate targets and a uniquely exploitable wind resource, growth of the UK's offshore wind sector continues to accelerate. Most offshore wind turbines rely on driven monopile foundations, the design of which requires knowledge of the ground deformation parameters, including the small-strain shear modulus G_0. A range of in situ and laboratory methods exist to determine G_0, yet inter-method variability can be substantial and there is little agreement on which of these methods should be favoured. The EPSRC and industry funded SOURCE project aims to improve test interpretation and quantify uncertainties through comprehensive site investigation programmes conducted at three test sites representative of common offshore ground conditions. Preliminary results from the first of these, a chalk site in Kent, are presented.

Background

Chalk is a soft biomicrite rock found throughout Western Europe. It is highly porous, frequently contains hard flint nodules, and is often highly fractured with fracture spacing tending to increase with depth. Under high compressive stresses chalk readily de-structures to a soft, silt-like putty.

The test site is a disused chalk quarry near the village of St. Nicholas at Wade, Kent, for which previous characterisation has been conducted as part of the ALPACA JIP (Vinck *et al*., 2022) and others. New in-situ testing for SOURCE included cone penetration tests (CPT), seismic cone penetration tests (SCPT), pressuremeter tests, plus crosshole, downhole and PS suspension logging tests for four boreholes (three to 25m, one to 40m). Borehole logging was performed, and a large number of high-quality samples were preserved for testing. The laboratory programme comprises resonant column (RC) tests, cyclic triaxial (CT) and monotonic triaxial (MT) tests combined with bender element (BE) tests as well as associated unconfined compressive strength and index tests.

Sample Preparation

Preserved chalk cores require careful preparation prior to advanced laboratory testing. A water-fed diamond core drill and precision grinding machine were used to prepare specimens of nominal diameters 50 mm and 70 mm for testing. To facilitate testing in the RC apparatus where rigid torsional coupling with the specimen is critical, a preparation method was developed whereby a hatched groove pattern was scored into the specimen ends and infilled with fine gypsum plaster. This plaster bonded firmly to textured stainless steel discs at the apparatus top cap and pedestal. For tests incorporating bender elements, small slots were cut into the chalk and infilled with chalk putty prior to bender insertion.

Resonant Column Testing

Measurements of small-strain shear modulus of soils and rocks using the RC apparatus rely on accurate physical characterisation of the apparatus's drive components. This is typically achieved via a calibration exercise, yet existing methods yield inconsistent results, particularly for stiff specimens such as chalk, introducing uncertainty in subsequent interpretation of test data. An extensive calibration exercise using thirteen calibration bars was performed to fully characterise the device behaviour. Finite element analysis (shown in Figure 1) indicates that much of the observed behaviour at greater stiffnesses can be explained by compliance of the drive system components. A new linear elastic model of the resonant column apparatus introducing a drive stiffness parameter

was developed. This improved model was shown to be a robust means of characterising the apparatus behaviour, particularly for stiff specimens, whilst simplifying test data interpretation, and is discussed in detail by (Rieman *et al*., 2024).

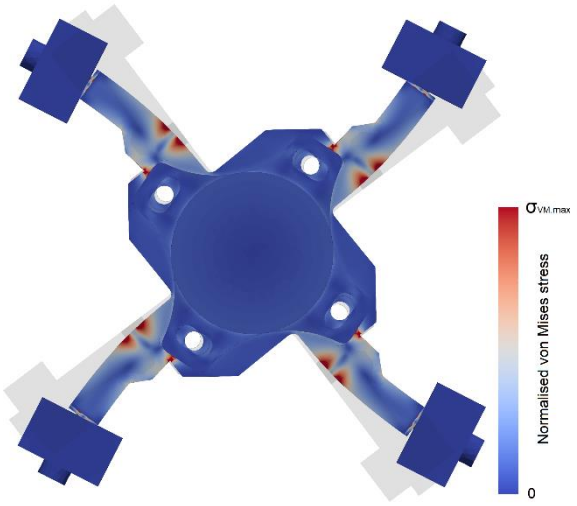

Figure 1. Finite element analysis of the resonant column drive system indicating concentrations of von Mises stress and deformation pattern under applied torque.

RC testing has been conducted on samples recovered from depths up to 43 m, with a diameter, D, of 50 mm and a range of heights of 1.7 to 2.5D. Each specimen was consolidated to between 2-5 different effective stress states with small-strain resonance testing performed at the end of each consolidation stage, with high-strain resonance testing being performed for the final stage of each test. Stiffness degradation behaviour for a subset of the stages performed at stresses representative of in situ ground conditions are shown in Figure 2.

Triaxial Testing

A number of CT tests are planned, the first of which have been completed and whose results are shown in Figure 3. Specimens of nominal D = 50mm and 70 mm were prepared and instrumented with local linear variable displacement transducers (LVDTs). Following an initial drained isotropic consolidation phase and an undrained monotonic 'pre-shear' phase to half of the predicted failure stress, compressive cyclic loading tests were conducted in stages of increasing load up until specimen failure. The planned testing programme includes additional targeted MT/BE as well as investigation of strain rate/frequency effects.

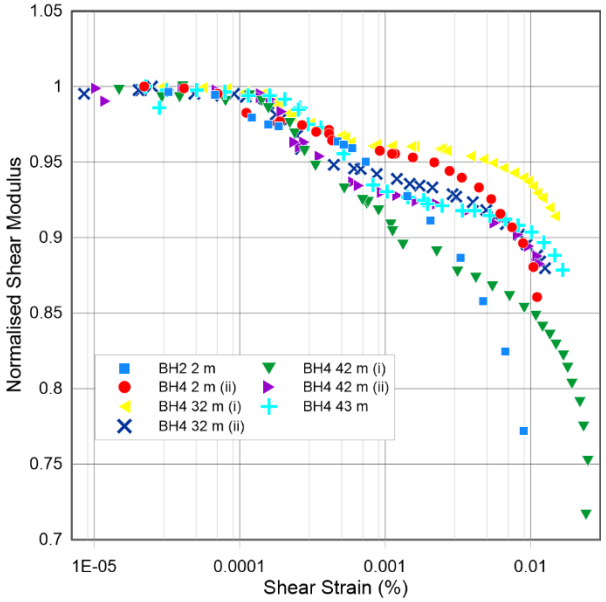

Figure 2. Normalised stiffness degradation behaviour from resonant column tests performed at stresses representative of in situ ground conditions. Samples obtained from three boreholes (BH) spaced linearly 4 m apart.

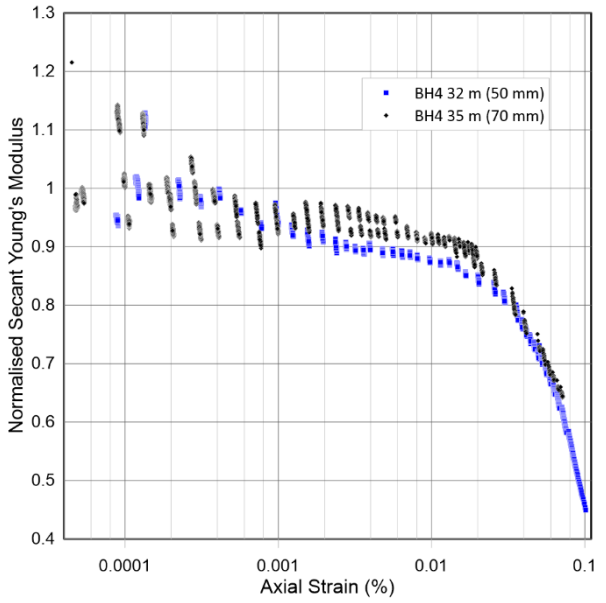

Figure 3. Normalised stiffness degradation behaviour from cyclic triaxial tests performed on specimens of two different sizes from similar depths.

References

Vinck, K. *et al.* 2022. Advanced in situ and laboratory characterisation of the ALPACA chalk research site. *Géotechnique*: (Online ahead of print) 1-15.

Rieman, L.P., Buckley R.M., Shinde, N.S., Wheeler, S.J. 2024. A modified linear-elastic model for calibration of resonant column devices accommodating drive system compliance. *Géotechnique*: (Online ahead of print) 1-14.

An Improved Nonlinear Dilatancy Equation Based on Dilatancy Properties of Gravelly Soil

Y.C. Li*[1,2], and X. Bin[1]

*Correspondence: liyichuan43@mail.dlut.edu.cn

[1] *School of Hydraulic Engineering, Faculty of Infrastructure Engineering, Dalian University of Technology, Dalian, China*
[2] *Department of Civil, Environmental and Geomatic Engineering, University College London, London, United Kingdom*

Abstract

Although the dilatancy equation is one of the core components for state prediction of gravelly soil, research on its liquefaction properties is still lacking. Therefore, this study uses static-dynamic triaxial tests to explore the dilatancy properties of gravelly soil. Then, a novel nonlinear dilatancy equation was improved to effectively describe the liquefaction properties of gravelly soil and fit the property track for solving current simulation problems.

Introduction

Due to its numerous advantageous engineering properties, gravelly soil is commonly used in foundational infrastructure projects. However, increasing evidence from seismic damage investigations shows that gravelly soil can liquefy under varying levels of seismic excitation, contrary to the traditional belief that it is non-liquefiable. So, even the dilatancy equation is a crucial component of elastoplastic constitutive models, indicating the direction of plastic flow, which also reflects the interconnection between the microscopic and macroscopic behaviour of soil (Marschi, Chan & Seed, 1972). Its effectiveness in describing the dilatancy properties of soil highly leads to the predictive accuracy of the constitutive model regarding soil deformation and pore pressure (Xiao, Liu, Zhu & Shi, 2011) and will affect the state evaluation directly. There is still an obvious gap between the real properties and current research. Therefore, this paper conducts systematic experimental studies on the static and liquefaction properties of gravelly soil using a static-dynamic triaxial apparatus. By investigating the dilatancy properties from triaxial tests, a dilatancy equation that reflects the liquefaction properties of gravelly soil was improved to help establish novel constitutive model for simulation (Wang, Xu, Tang, Zhou & Pang, 2022).

Nonlinear Dilatancy Equation Development of Gravelly Soil

To obtain the dilatancy properties of gravelly soil under different conditions, static-dynamic triaxial tests were conducted using a medium-sized triaxial apparatus, independently as shown in Fig. 1. A series of triaxial tests were conducted on gravelly soil samples with confining pressures of 100, 200, 300 kPa, and relative densities of Dr = 30%, 50%, 70%, respectively.

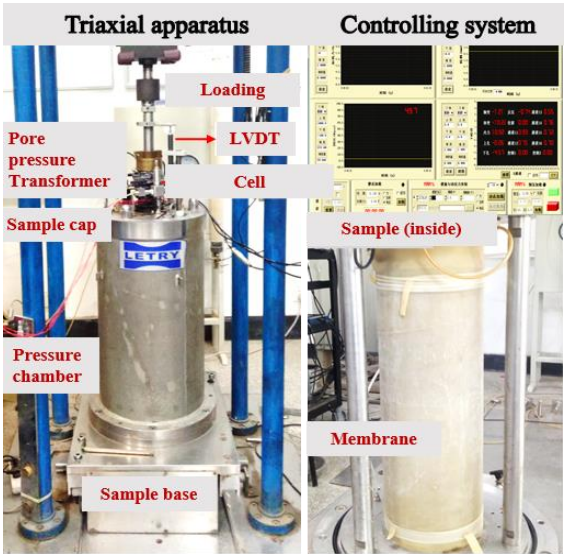

Figure 1. Static- dynamic triaxial platform

Based on the dilatancy properties of gravelly soil gained from previous triaxial tests and research, the development track of two typical stress-dilatancy relations of gravelly soil can be seen in Fig. 2. d_g is the magnitude of dilatancy, which is defined as the ratio of the increment of plastic volumetric strain $d\varepsilon_v^p$ to the increment of plastic shear strain $d\varepsilon_s^p$. And η is the stress ratio. Meanwhile, it can be observed from Fig. 2 that after reaching the phase transformation point *D*, the sample begins to exhibit dilative deformation, the pore pressure gradually decreases, and the average effective principal stress gradually increases, eventually reaching the critical state *C*. During the process from point *D* to *C*, the peak stress point *P* is encountered.

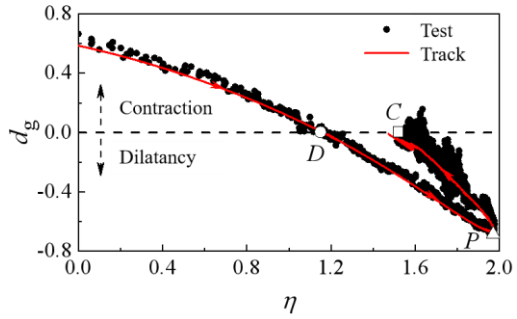

(a) Dr=30%, σ3=300kPa

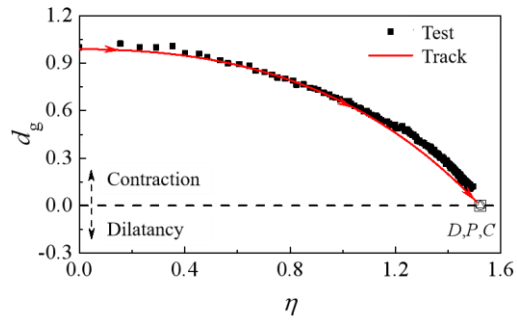

(b) Dr=70%, σ3=100kPa

Figure 2. Development track of typical stress-dilatancy relations of gravelly soils

However, the currently used dilatancy equations cannot accurately describe the variation of dilatancy properties throughout the entire shearing process of gravelly soil in Fig. 2. Therefore, this paper considers the relationship between the stress ratio at the phase transformation point and the shear strain. By introducing the cumulative plastic shear strain ξ which is defined as $\xi = \int \left| d\varepsilon_s^p \right|$ and the critical state stress ratio M_c, the phase transformation stress ratio M_d is expressed as:

$$M_d = M_c \exp\left(-\beta_g / (1+\xi)\right) \quad (1)$$

where β_g can be calculated from the cumulative plastic shear strain ξ_d at the phase transformation point and the phase transformation stress ratio M_d as Eq.(2):

$$\beta_g = -ln\left(M_d / M_c\right)(1+\xi_d) \quad (2)$$

Therefore, the expression of the nonlinear dilatancy equation considering the entire shearing process of gravelly in this paper is:

$$d_g = \alpha_g \left(M_c \exp\left(-\beta_g / (1+\xi)\right) - \eta\right) \exp\left(\eta / M_c\right) \quad (3)$$

where, α_g represents constitutive model parameter, which can be obtained by fitting the relationship between the cumulative plastic shear strain ξ. It can be observed that for the phase transformation point *D*, η equals M_d and ξ equals ξ_d, satisfying d_g equals 0; for the critical state point *C*, η equals M_c, and ξ tends to infinity, also satisfying d_g equals 0. Therefore, Eq.(3) meets the requirement that the shear dilation ratio is 0 at both the phase transformation and critical state points. The exponential term $exp(\eta/Mc)$ reflects the nonlinear characteristics of the shear-dilatancy relationship in gravelly soil.

In conclusion, the improved nonlinear dilatancy equation can describe the entire shearing process of gravelly soil well, which is also helpful for further state prediction.

References

Marschi, N.D., Chan, C.K., Seed, H.B. 1972. Evaluation of properties of rockfill materials. Journal of the Soil Mechanics and Foundations Division **98** (1):95-114.

Xiao, Y., Liu, H., Zhu, J., Shi, W.C. 2011. Dilatancy equation of rockfill material under the true triaxial stress condition. Science China Technological Sciences **54** (1):175-184.

Wang, X.l., Xu, B., Tang, C., Zhou, C.G., Pang, R. 2022. Elastoplastic Constitutive Model of Sand–Gravel Composites Considering the Whole Shearing Process. Journal of Engineering Mechanics **148** (9): 04022056.

The mechanics of a mineral sand tailings with a transitional behaviour

Y. Wang *[1] and Prof. M.R. Coop [1]

*Correspondence: ucesyw4@ucl.ac.uk

[1] *University College London, WC1E 6BT, UK.*

Abstract

From the gradings and mixed mineralogies the mode of transitional behaviour could be expected in some tailings, but a complete characterisation of this mode of behaviour is lacking in such materials. In this study, a series of oedometer and triaxial tests were conducted on samples of mineral sand tailings to investigate the characteristic of transitional behaviour. Soil fabric was investigated using mercury intrusion porosimetry (MIP) tests and scanning electron microscope (SEM) tests to determine the cause of the transitional behaviour. Overall, a clear transitional mode was defined but no striking differences of fabric were observed.

Introduction

Tailings are mining waste after extracting the economic minerals, metals or coal from the ore. The most common storage method is tailings dams. But there have been 257 tailings dam failures recorded since 1915, with catastrophic environmental and human impact (Piciullo, 2022). The stability analysis of current engineering practice for tailings dams relies on the critical state line (CSL) that is determined for reconstituted tailings samples (Mmbando, 2021). Therefore, accurate CSLs for in-situ tailings are required and any ambiguities in its location are a concern.

The mechanical behaviour of most soils can generally be described within a critical state framework so that the volumes in compression and shearing of the same soil under different stress states will converge into a unique Normal Compression Line (NCL) and CSL in the volumetric plane. However, it has been found that a transitional behaviour contradicts this framework, providing a different NCL and CSL for every initial density (Shipton & Coop, 2012). Although the exact causes of the transitional behaviour have not been identified, it is believed to be related to the robust soil fabric that will not be completely broken down even under high stress or strain levels (Todisco et. al, 2018). Tailings are typically the types of materials that have transitional behaviour due to the mixed mineralogies and mixed gradings (Coop, 2015). However, a complete characterisation of this mode of behaviour is lacking in such materials.

This work focuses the transitional behaviour of a mineral sand tailings from Australia. The transitional mode is evaluated by a series of oedometer tests and monotonic triaxial tests. To examine the cause of the transitional behaviour, the soil structure was examined by MIP tests and SEM tests.

Material and Methodology

The tailings used in this study were retrieved from a mine from Perth, Australia, the by-product of rutile and zircon ore processing. It is mineral sand tailings, with D_{min}=1μm, D_{50}=87μm and D_{max}=300μm. The mineralogy consists mainly of quartz (60%), kaolin (22%) and feldspar (18%). The specific gravity of the material is 2.53, and the plastic and liquid limits are 30.1% and 59.6% respectively.

A series of state-of-the-art oedometer and triaxial tests were conducted for samples with a wide range of initial specific volumes (v_i). The various v_i were achieved by adjusting the initial water content of the slurries. If the error of the calculated v_i is much smaller than the difference of the final v (v_f) at a given stress, it could be confidently concluded that compression lines are non-convergent. Therefore, the value and accuracy of the v_i are carefully determined

using six different equations proposed by Shipton and Coop (2012, 2015), resulting in a mean accuracy typically of about ±0.013.

Results and Discussion

The results of oedometer compression and triaxial compression and shearing are shown in Figure 1. It is clear that there is no clear unique NCL or CSL. The differences in the overall locations of compression lines and critical states are much larger than any possible inaccuracy of v_i. Therefore, the non-uniqueness of the NCLs and CSLs does not result from errors in the calculation of v_i.

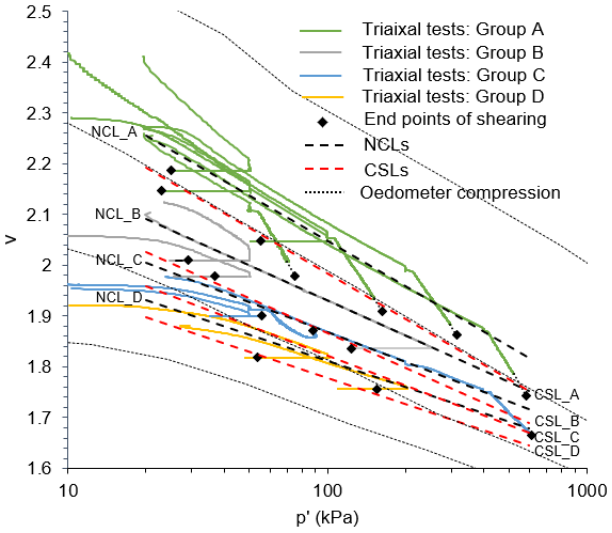

Figure 1. Volumetric behaviour of oedometer compression and triaxial compression and shearing (Wang et. al, under review).

The compression curves for the oedometer tests reach their individual NCLs, which do not converge even up to 8 MPa. This indicates a clear transitional behaviour. The isotropic compression behaviour shows a similar non-convergent trend to the one-dimensional compression curves. During shearing, samples with any initial density are predominantly contractive.

To investigate the transitional mode, the specimens of triaxial tests were divided into four groups A-D based on v_i. The NCLs and CSLs for each group were identified and were reasonably good fit with individual tests. The slopes of NCLs and CSLs for each group are quite similar with each other and decrease as the initial density increases. The spacing of the NCL and CSL for the denser group is smaller than that for the looser one.

For the microstructure, there is no striking difference between the loose and dense samples in the pore size distributions from the MIP tests or in the SEM images.

Conclusions

The transitional mode for tailings is identified by non-unique NCLs and CSLs. Notably, despite being transitional there is still some effect of initial density on the volumetric behaviour. As the v_i for the samples decreases, the slopes of NCLs and CSLs decrease and the spacings between the NCLs and CSLs decrease. However, the effect of initial density is slight, since samples with any initial density predominantly have compressive behaviour. Even the densest samples do not show the strong dilative that would be expected from a conventional soil with a unique NCL. Unfortunately, no striking differences of fabric are observed.

References

Coop, M. R. (2015, January). Limitations of a Critical State framework applied to the behaviour of natural and 'transitional' soils. In *Proceedings of 6th International Symposium on Deformation Characteristics of Geomaterials, IS-Buenos Aires* (pp.115-155).

Mmbando, E., Fourie, A., & Reid, D. (2023). Mechanics of an Iron Ore Tailings Exhibiting Transitional Behaviour. *Geotechnical and Geological Engineering*, 1-10.

Piciullo, L., Storrøsten, E. B., Liu, Z., Nadim, F., & Lacasse, S. (2022). A new look at the statistics of tailings dam failures. *Engineering Geology*, *303*, 106657.

Shipton, B., & Coop, M. R. (2012). On the compression behaviour of reconstituted soils. *Soils & Foundations, 52*(4), 668-681.

Shipton, B., & Coop, M. R. (2015). Transitional behaviour in sands with plastic and non-plastic fines. *Soils and Foundations,55*(1), 1-16.

Todisco, M., Coop, M. R., & Pereira, J.-M. (2018). Fabric characterisation in transitional soils. *Granular Matter*, *20*(2), 1-12.

Wang, Y., Cartwright, A., & Coop, M. R. (under review for *Engineering Geology*). The Mechanics of a Mineral Sand Tailings with a Transitional Behaviour. http://dx.doi.org/10.2139/ssrn.4808940.

A Thermal Analogy Method for Coupled Hydro-Mechanical Large-Deformation Analysis

Ahmad Foroutan Kalourazi*[1], Tingfa Liu[1], and Andrea Diambra[1]

*Correspondence: ahmad.foroutankalourazi@bristol.ac.uk

[1] *School of Civil, Aerospace and Design Engineering, University of Bristol, Bristol, UK*

Abstract

This paper outlines a novel numerical technique that utilises the analogy between water pressure and heat transfer for coupled hydro-mechanical analysis in geotechnical boundary value problems. This technique enables effective stress and consolidation analysis for saturated geomaterials and has important potential for resolving one of the long-standing limitations of the Coupled Eulerian-Lagrangian (CEL) method, that is currently applicable only for total stress analyses. The principle of the analogy is set out below, followed by validation cases of one-dimensional (1-D) consolidation problem against Terzaghi's analytical solutions.

1. Introduction

Numerical analysis of large deformation problems remains one of the most challenging areas in geotechnical engineering. Conventional finite element methods encounter severe mesh distortion issues when large strain develops that lead to numerical issues or inaccurate results. Various methods have been developed for analysing large deformation problems, including for example the CEL (Coupled Eulerian-Lagrangian) method as part of the Arbitrary Lagrangian-Eulerian (ALE) framework. In contrast to other ALE methods, CEL method maintains the original mesh and eliminates the need for re-meshing, offering enhanced numerical stability and efficiency. However, CEL method is primarily limited to total stress analysis and is not applicable for effective stress and consolidation analysis (Wang et al., 2015; Negula and Grabe, 2020).

To address this limitation, this paper explains the fundamentals of a novel procedures that utilises the analogy between water pressure and heat transfer for coupled hydro-mechanical analysis (Hamann et al., 2015; Staubach et al., 2021). The developed method offers a step change to the CEL method for large-deformation analysis in saturated geomaterials.

2. CEL method

CEL method incorporates Lagrangian and Eulerian descriptions of field movement within a single model. In model areas where large deformations occur, a Eulerian description is applied, while areas with only minor intrinsic deformations are modelled using the Lagrangian framework. The Eulerian region does not experience node movement but merely transports movement, thus avoiding mesh distortion caused by large deformations. The solution process involves advancing in time with a Lagrangian step where node displacements are determined, and then reverting to the original Eulerian mesh configuration in the remap step where nodes are repositioned if they have shifted significantly. The node displacements are temporary within each time increment. Interaction between the Eulerian and Lagrangian regions is facilitated through specialised contact algorithms (Hamman et al., 2015; Staubach et al., 2021).

3. Thermal Analogy

The intrinsic analogy between fluid flow and heat transfer in porous media is represented by thermo-hydromechanical coupling. This forms the basis for the numerical technique that utilises heat conduction analogous to Darcy's flow law. This relationship is further illustrated in Figure 1, which depicts one-dimensional transition systems for water and heat over the distance of Δx, with changes in hydraulic head from H_1 to H_2 and temperature from θ_1 to θ_2, respectively. Noting the similarities between

the generalised Darcy's law and heat conduction (Equations 1-2), the temperature can be analogous to excess pore pressure (p_w), and thermal conductivity (λ) to intrinsic permeability (k_i) divided by dynamic viscosity (μ). The mass balance of water and thermal energy balance are equated. The change in pore pressure due to the volumetric straining of the solid skeleton is simulated with volumetric heat production, and the diffusion of pore water is simulated with heat dissipation.

$$q = \lambda(-\nabla\theta) \quad (1)$$

$$q = \frac{k_i}{\mu}(-\nabla\Delta p_w) \quad (2)$$

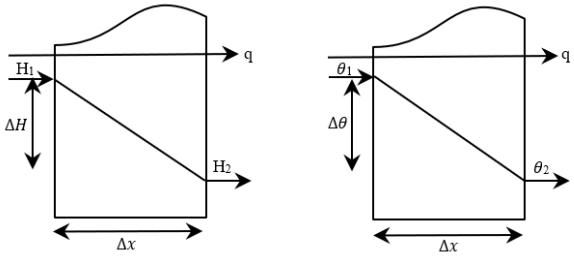

Figure 1. One-dimensional analogy between fluid flow and heat transfer system

4. Validations

Preliminary validation of the analogy method was undertaken by considering 1-D consolidation problems. The thermal analogy was implemented using a user-defined subroutine (VUMAT) in Abaqus/Explicit. A one-meter soil column, depicted in Figure 2(a), was modelled with impermeable boundaries at sides and bottom. Zero initial temperature was applied at the top boundary and throughout the body. A uniform stress of 10 kPa was applied at the top. A linear elastic model was employed while the effect of gravity was neglected. The soil characteristics are Young's modulus E = 10 MPa, Poisson's ratio v = 0.3, soil density ρ = 2650 kg/m³, intrinsic permeability $k_i = 1\times10^{-10}$ m², and dynamic viscosity $\mu = 1\times10^{-3}$ Pa·s. The numerical results are compared with Terzaghi's analytical solutions at different time factors (T_v), as illustrated in Figure 2(b). The results indicate that high accuracy is achieved by simulating the consolidation problem using temperature as a substitute for excess pore pressure.

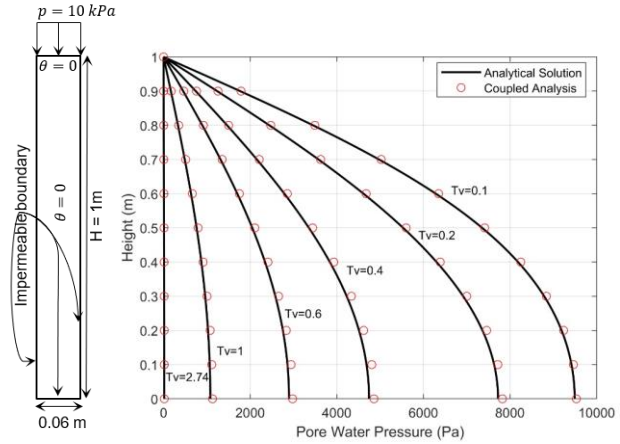

(a) (b)

Figure 2. Validation analyses: (a) Schematic diagram of the numerical model; (b) Comparison of pore pressure evolution with Terzaghi's analytical solutions

5. Conclusions

Geotechnical modelling using conventional Coupled Eulerian-Lagrangian (CEL) method is limited to total stress analysis. This paper outlines a novel numerical technique that utilises the analogy between water pressure and heat transfer for coupled hydro-mechanical analysis. This technique enables effective stress and consolidation analyses in saturated geomaterials undergoing small-to-large deformations. The accuracy and efficacy of the proposed method was validated in preliminary 1-D consolidation analysis. Further study and development is underway to apply the technique for modelling cone penetration test (CPT), offshore structure installation and other problems.

References

Hamann, T., Qiu, G., Grabe, J., 2015. Application of a Coupled Eulerian-Lagrangian approach on pile installation problems under partially drained conditions. *Computers and geotechnics,* 63: 279–290.

Nagula, S.S. and Grabe, J., 2020. Coupled Eulerian Lagrangian based numerical modelling of vibrocompaction with model vibrator. *Computers and geotechnics,* 123, 103545.

Staubach, P., Machaček, J., Skowronek, J. and Wichtmann, T., 2021. Vibratory pile driving in water-saturated sand: Back-analysis of model tests using a hydro-mechanically coupled CEL method. *Soils and Foundations*, 61(1): 144-159.

Wang, D., Bienen, B., Nazem, M., Tian, Y., Zheng, J., Pucker, T. and Randolph, M.F., 2015. Large deformation finite element analyses in geotechnical engineering. *Computers and geotechnics,* 65: 104-114.

Experimental testing of frozen ground with a newly developed frost heave apparatus with PIV capabilities

F. Lattuada*[1], G. Viggiani[1], and S. Stanier[1]

*Correspondence: fnl20@cam.ac.uk

[1] *University of Cambridge, Department of Engineering (Civil Engineering Building, JJ Thomson Avenue 7a Cambridge CB3 0FA, United Kingdom)*

Abstract

This study examines volumetric changes in frozen soil due to ice lens formation, using a newly developed Frost Heave Apparatus (FHA) with Particle Image Velocimetry (PIV). Focusing on frost-susceptible soils, primarily silts, the research tests materials range from non-frost susceptible soils with large pore sizes to frost susceptible soils made of fine-grained kaolin and sand in various proportions. The experiments, conducted under controlled thermal (-5°C to -15°C) and mechanical conditions (50 kPa to 400 kPa), utilize a novel FHA which features precise temperature control, a PID-controlled hydraulic system, and vacuum-sealed thermal insulation. Results show that lower mechanical loads promote more significant ice lens formation, especially with higher kaolin content. PIV analysis provides insights into the water redistribution in the soil, indicating increased water content above and decreased below the ice lens, influenced by temperature gradients and soil composition.

Introduction

Frost heave is a geotechnical issue occurring in cold climates where soil undergoes cycles of freezing and thawing. As the soil freezes, the water contained in the soil turns to ice and, due to cryogenic suction, more water is attracted to the freezing area, expanding and lifting the overlying soil. When it thaws, the soil settles back down. Repeated cycles can cause soil movement and significant damage to infrastructure (Peppin & Style, 2012). In frost susceptible soils, that mostly comprise silts (U.S. Army Corps of Engineers, 1984), the majority of heave is due to the formation of ice lenses upon freezing, which are layers of pure ice in the soil matrix. This paper investigates the volume change associate with frozen soil and the formation of ice lenses using a newly developed cutting-edge frost heave apparatus with PIV capabilities.

Tested Materials

The materials tested in the new frost heave apparatus are classified into two categories: non-frost susceptible and frost susceptible. Non-frost susceptible soils, characterized by a pore size distribution ranging from gravel to fine sand, are unlikely to exhibit frost heave due to inadequate pore sizes for generating cryogenic suction upon freezing. Because of the small size of their particles, silts or silty clay soils are amongst the most frost susceptible. When exposed to freezing temperatures, the water in their pores transitions to solid, but a thin film of unfrozen water is maintained around soil particles. This free energy of this film of water decreases with decreasing temperature, creating a potential gradient that moves water to colder areas, promoting ice accumulation and lens formation perpendicular to heat and water flow directions (Williams *et al*., 1989). In the experimental programme, frost susceptible soils were obtained mixing Speswhite Kaolin with a grain size of 2 μm and Leighton Buzzard Grade E sand (both described in Lam *et al*., 2012), in various proportions (75:25, 50:50, 25:75).

Frost Heave Apparatus (FHA)

The FHA (Fig. 1) is designed to accommodate a cylindrical soil sample with dimensions of 100mmx100mm, constrained horizontally. The freezing process is initiated vertically from top to bottom using two refrigerated circulators. At the upper end, a cold bath circulates a fluid at subfreezing temperature, while at the lower end, a warm bath maintained at +2°C prevents

freezing in the drainage line (Fig.2). Water intake and expulsion during testing are monitored using a volumometer. The FHA is housed within a loading frame. A feedback-based algorithm (PID), managed by the in-house CamLab software, controls the press and hydraulic system, enabling automated experiments. Thermal insulation is achieved by creating vacuum between the two perspex cylinders, which also prevents water vapor condensation during freezing. This ensures clear vision for the high-resolution imaging necessary for Particle Image Velocimetry (PIV). A new mathematical model corrects distortion from the curved perspex, enhancing camera calibration accuracy by up to 66% compared to existing models, converting measurements from 2D pixel space to 3D real-world space more precisely.

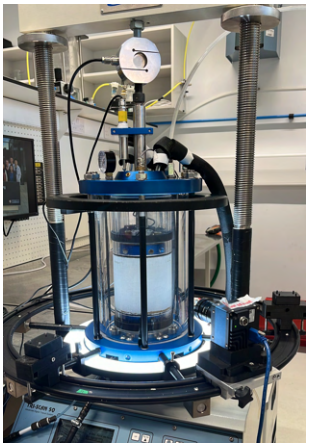

Figure 1. Frost heave apparatus during testing

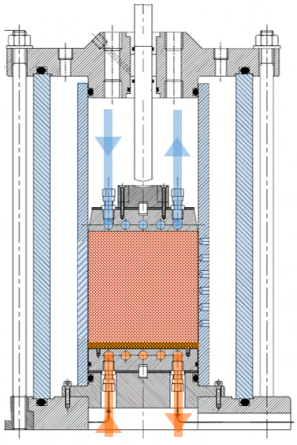

Figure 2. Diagram frost heave apparatus

Results

Mixtures of kaolin and sand in varying proportions were subjected to different thermal and mechanical conditions. The "cool" end temperatures ranged from -5°C to -15°C, while a constant +2°C was maintained at the "warm" end to prevent freezing in the drainage line. Stresses of 50 kPa, 100 kPa, 200 kPa, and 400 kPa were applied across various tests. It was found that under drained conditions, samples with lower loads showed greater heave, attributed to pronounced ice lens formation at the same freezing temperatures. The position of the ice lens within the soil sample depended on the thermal gradient, with no lens at -5°C, and progressively deeper lenses at -8°C, -10°C, and -15°C as the "cold bath" temperature decreased. For the same thermal gradient and imposed load the greater the proportion of kaolin the greater the have. Using PIV, water content redistribution within the soil was analysed, indicating increased water content above the ice lens where water freezes, and decreased below it due to cryogenic suction (Fig. 3).

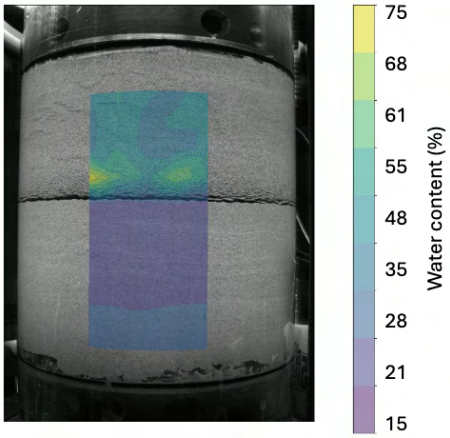

Figure 3. PIV inferred water content upon freezing, 100kPa, -10C top +2C bottom, drained, 50:50 kaolin sand

References

Lam, S. S. Y., Haigh, S., Elshafie, M. and Bolton, M. (2012), *A new apparatus for modelling excavations*, International Journal of Physical Modelling in Geotechnics **12:** 24–38.

Williams PJ, Smith MW, 1989. The Frozen Earth. Cambridge University Press.

Peppin, S. S. L. and Style, R. W. (2012), The physics of frost heave and ice-lens growth, Technical report.

U.S. Army Corps of Engineers (1984), Pavement Criteria for Seasonal Frost Conditions, Washington, D.C.

Modelling a Monopile Supported Offshore Wind Turbine in Liquefiable Soil

C. Espanol-Espinel*[1], S.P.G. Madabhushi*[1], S.K. Haigh*[1]

*Correspondence: ce411@cam.ac.uk

[1] *University of Cambridge, Department of Engineering (Schofield Centre, High Cross, Madingley Rd, Cambridge, CB3 0EF, United Kingdom.)*

Abstract

The sustained growth of the offshore wind sector is leading to the construction of offshore wind farms in highly seismic regions of the world. Hence, a large proportion of the potential sites may be exposed to liquefaction risk. Monopiles are directly affected by this phenomenon given their preference as a support system for offshore wind turbines over other foundation types. This paper includes a comprehensive study of the lateral response of monopiles against the combined action of earthquake induced liquefaction and environmental loading using centrifuge modelling.

Introduction

Offshore Wind Turbines (OWT) installed in seismic regions may encounter devastating earthquake effects during operation. Liquefaction is the most probable and detrimental to OWTs in such areas, as it effectively reduces the shear resistance and stiffness of the sand surrounding the monopile (Fig. 1). This may result in excessive rotation of the monopile and tower, exceeding the Serviceability Limit State (SLS) design requirements of a maximum turbine tilt of 0.5º (DNV, 2021).

This paper investigates the combined effects of static lateral loading and dynamic loading on monopile supported OWTs founded on liquefiable soils.

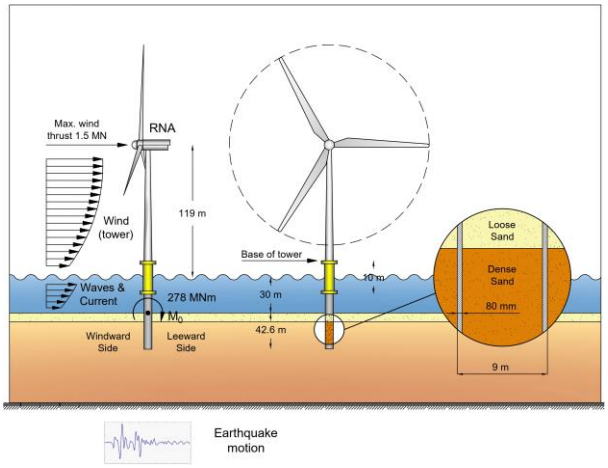

Figure 1. Dimensions and loads carried by the DTU 10 MW reference offshore wind turbine after Shaofeng et al. (2021).

Experimental Setup

The experimental setup was designed to test two different scenarios (Fig. 2). Firstly, the structure was subjected to dynamic and static lateral loading simultaneously. Secondly, the OWT and monopile were tested in calm air conditions. Both tests were conducted at 70 g, which allowed for modelling of a 17.5 m long and 4 m diameter monopile at prototype scale with an L/D ratio of 4.38. The soil profile includes a loose sand layer overlying a dense sand layer, both of which are fully saturated.

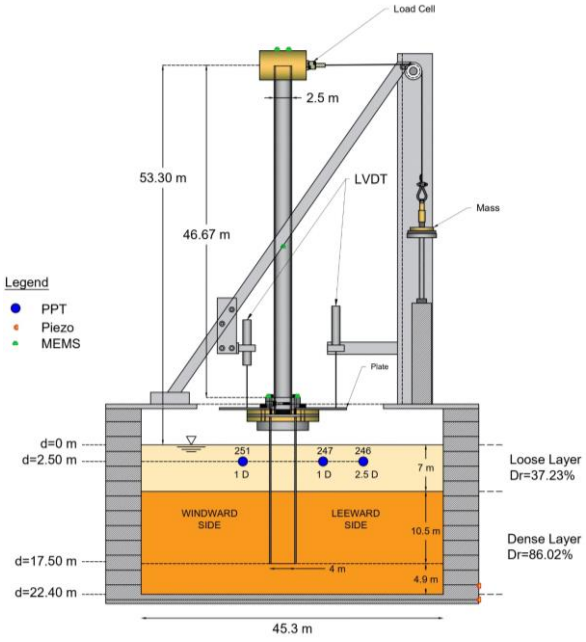

Figure 2. Monopile supported OWT at prototype scale.

The earthquake input motions were transferred to the model utilising a hydraulic earthquake actuator. (Madabhushi et al., 2015), (Madabhushi 2017).

The experimental data was collected using multiple instruments distributed across the models. Linear Variable Differential Transformers (LVDTs) were located on the windward and leeward sides of the tower to track rotation of the structure.

Results and Discussion

The excess pore pressure generated by the earthquakes in both, the laterally loaded, and non-laterally loaded scenarios reveals a substantial loss of effective stress in the soil surrounding the foundation. As a result, a rotation of approximately 3° is observed in the laterally loaded scenario. Even in calm air conditions, the rotation remains significant, at about 1.5° in the clockwise direction, as the tilting direction of the OWT is influenced by the response of the structure during the initial earthquake. In both cases, the tilt of the tower exceeds the allowable limit of 0.5° set by DNV (2021).

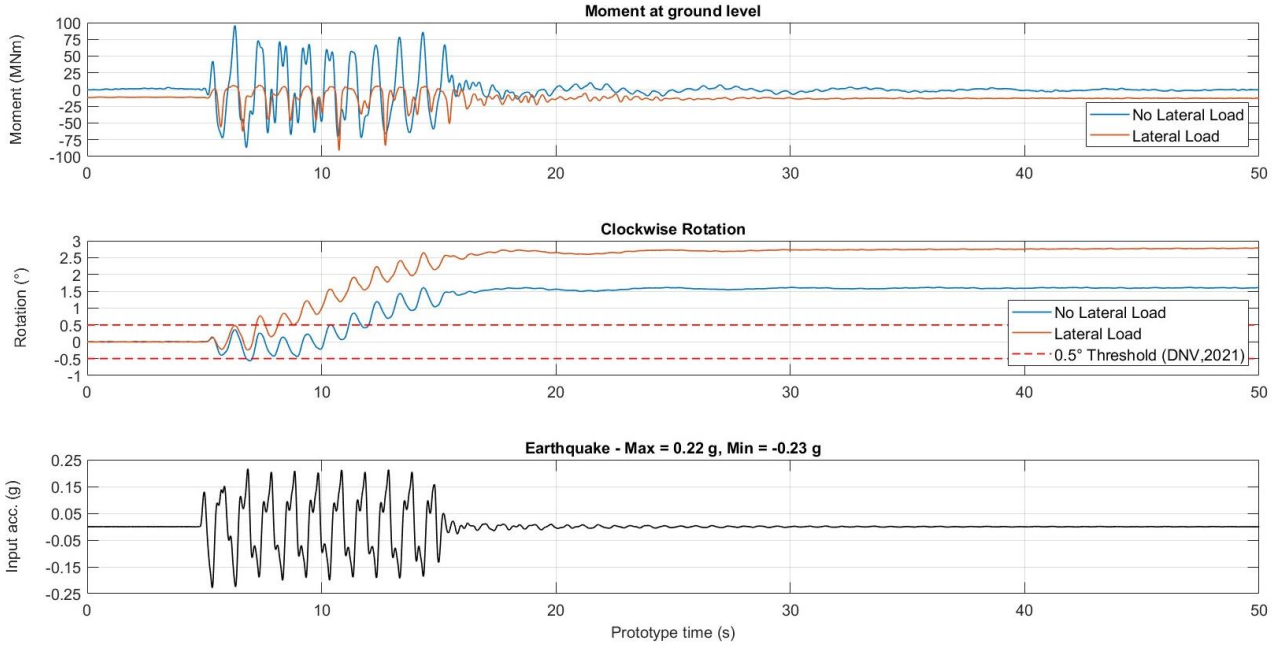

Figure 3. Static and dynamic moment acting at the mudline and resulting rotation of the OWT (Espanol-Espinel et al., 2024).

References

DNV.2021.Support structures for wind turbines. Standard DNV-ST-0126. 2021.

Español-Espinel, C., Haigh, S.K., Madabhushi, S.P.G., Abadie, C.N., Go, J.E., Morrison, P.R.J. 2024. Evolution of excess pore water pressures around monopiles subjected to moderate seismic loading. Soil Dynamics and Earthquake Engineering. **176**:108316.

Madabhushi, S.P.G., Haigh, S.K., Houghton N.E., Gould E. Development of a servo-hydraulic earthquake actuator for the Cambridge Turner beam centrifuge. International Journal of Physical Modelling in Geotechnics 2015;12(**2**):77–88.

Madabhushi, S.P.G. 2017. Centrifuge modelling for civil engineers. CRC press.

Shaofeng, W., Torben, J.L., Bredmose, H. 2021. Ultimate load analysis of a 10 MW offshore monopile wind turbine incorporating fully nonlinear irregular wave kinematics. Marine Structures, **76**:102922.

17th BGA YGES
University of Cambridge
1-3 July, 2024

Centrifuge modelling of a deep screw pile for floating wind with varying rate of installation

T. Jawid*

*Correspondence: 160010707@dundee.ac.uk

School of science and engineering, The University of Dundee, Nethergate, Dundee, DD1 4HN, UK

Abstract

To anchor floating offshore wind turbines (FOWTs), innovative anchor technologies are required as the current anchors present limitations in efficiency and anchor sharing. Installing smaller, deeper screw piles in groups (i.e., screw pile groups) has been proposed as alternatives to larger single screw piles as they can be installed with equipment readily available in the industry. This study looks to investigate the installation requirements and uplift performance of a deep screw pile designed to be part of group whilst varying the advancement ratio (AR). The results indicate that by reducing the AR the installation force reduced and the uplift capacity increased. Further physical centrifuge modelling has been proposed to determine the optimum group spacing and AR for a screw pile group.

Introduction

Deep screw piles, which have larger helix embedment ($H_{D_h}/D_h > 10$), installed in groups (i.e., screw pile groups) have been proposed to anchor Floating Offshore Wind Turbines (FOWTs) (Bradshaw et al., 2022; Davidson et al., 2022) as an alternative to current anchors as they are more efficient (higher resistance to anchor mass ratio) whilst also allowing for anchor sharing (Cerfontaine et al., 2023a). Another benefit of screw piles is that by reducing the rate at which the helix advances (i.e., advancement ratio, AR) to less than the industrial guidance in BSI (2015) of 1, the installation force (F_z) reduces, and the soil relative density (D_r) and the vertical stress (σ') above the helix significantly increases leading to an increase in subsequent uplift performance (F_u) (Cerfontaine et al., 2023b; Sharif et al., 2021). There is, however, limited research on deeper screw piles for FOWTs and more work is required to ascertain whether the AR influences the installation F_z and peak F_u. Therefore, this study investigates influence of AR on the installation F_z, torque (T) and the peak F_u of a deep screw pile designed to be part of a group of nine piles in medium dense sand by utilising a geotechnical beam centrifuge.

Methodology

The Dundee Actidyn C67-2 3m radius geotechnical beam centrifuge was used to perform each test. Pluviation of dry sand (HST95) was conducted in a 500mm × 800mm × 550mm strongbox to achieve $D_r = 55\%$. The prototype dimensions of the deep screw pile were designed using a semi-analytical method, and the model scale dimensions were calculated using a scaling factor of 1:30. The installation and testing equipment used was designed specifically to install and load a screw pile in one flight (Al-Baghdadi, 2018; Davidson et al., 2018). Differing ARs (1.0, 0.5 and 0.25) were investigated and a vertical force at a constant rate of 1mm/min was applied to test each pile. Each test was conducted in dry sand at $19g$ which exhibited the same effective stress of saturated sand at $30g$.

Results and Discussion

Figure 1. shows that the influence of reducing the AR reduces the installation F_z such that the direction of the force changes from downward (compressive or push-in) to upward (tensile or pull-in). This aligns with the observations made by Cerfontaine et al. (2023b) who suggested that the installation behaviour changes when AR < 1, as the reaction compressive crowd force applied at the top of pile is less than the pull-in force generated at the helix when the surrounding soil is compressed/squeezed during installation, resulting in a resultant force (F_z) that is in tension. There was little variation in the installation T when compared with the installation F_z, however, a slight increase in the

installation T was seen when the AR was reduced.

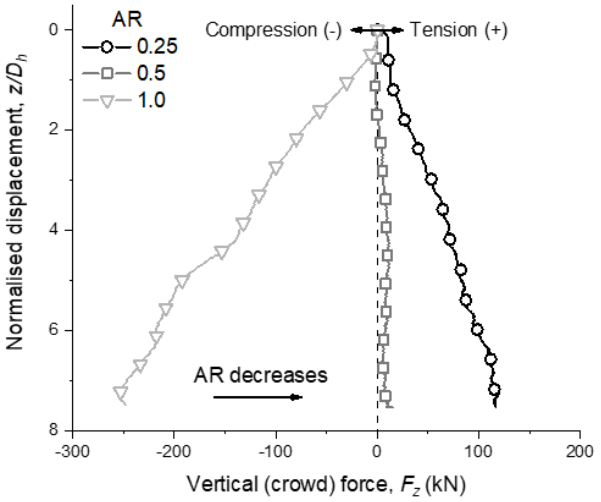

Figure 1. Measured vertical (crowd) force during installation in medium dense sand as a function of AR

Figure 2. shows that reducing the AR resulted in improved peak F_u (or uplift capacity) of the pile with respect to the industry recommeded installation mode of AR = 1.0. The peak F_u of the pile installed at AR = 1.0 was 305kN. Whereas, when AR = 0.5 and 0.25, the peak F_u was 467kN and 416kN, indicating that the reduction of AR increased the peak F_u increased by 53% and 40% respectively.

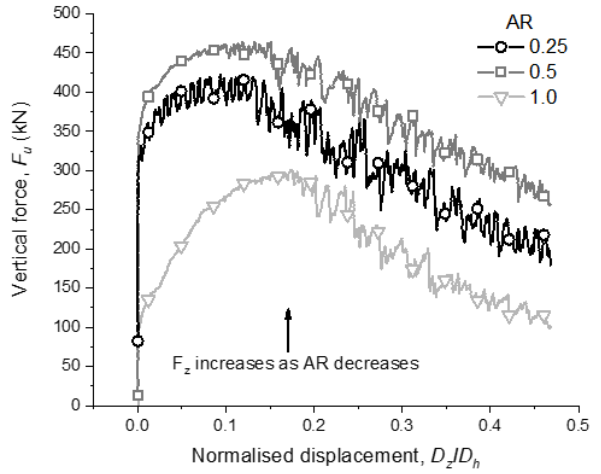

Figure 2. Measured vertical (uplift) force over normalised displacement in medium dense sand as a function of AR

Conclusions and Future Work

This study shows that the infuence of AR has a postive effect on the installation F_z and the peak F_u of deep screw piles, and therefore, the AR should be considered for the design and the future deployment of screw pile groups to anchor FOWTs. Further physical centrifuge modelling is planned to investigate the optimum spacing and AR in a screw pile group.

Acknowledgements

The author is grateful for the financial support provided by the University of Dundee, the Energy Technology Partnership (ETP) and Geowynd.

References

Al-Baghdadi. (2018). Screw piles as offshore foundations: Numerical and physical modelling. PhD thesis, University of Dundee, Dundee, UK.

Bradshaw A., Cullen L. & Miller Z. (2022). Field study of group effects on the pullout capacity of “deep” helical piles in sand. *Canadian Geotechnical Journal* **59**, No. 4, 538-545. https://doi.org/10.1139/cgj-2021-0072.

BSI, (2015). BS 8004:2015: Code of Practice for Foundations. BSI Standards Limited.

Cerfontaine, B., Brown, M. J., Knappett, J. A., Davidson, C., Sharif, Y. U., Huisman, M., Ottolini, M., & Ball, J. D. (2023b). Control of screw pile installation to optimise performance for offshore energy applications. Geotechnique, 73(3), 234–249. http://doi.org/10.1680/jgeot.21.00118.

Cerfontaine, B., White, D., Kwa, K., Gourvenec, S., Knappett, J., & Brown, M. (2023a). Anchor geotechnics for floating offshore wind: Current technologies and future innovations. Ocean Engineering, 279, 114327. https://doi.org/10.1016/j.oceaneng.2023.114327

Davidson, C., Brown, M. J., Cerfontaine, B., Al-Baghdadi, T., Knappett, J., B rennan, A., Augarde, C., Coombs, W., Wang, L., Blake, A., Richards, D., & Ball, J. D. (2022). Physical modelling to demonstrate the feasibility of screw piles for offshore jacket-supported wind energy structures. Geotechnique, 72(2), 108–126. https://doi.org/10.1680/ jgeot.18.P.311.

Sharif, Y. U., Brown, M. J., Cerfontaine, B., Davidson, C., Ciantia, M. O., Knappett, J. A., Ball, J. D., Brennan, A., Augarde, C., Coombs, W., Blake, A., Richards, D., White, D., Huisman, M., & Ottolini, M. (2021). Effects of screw pile installation on installation requirements and in-service performance using the discrete element method. Canadian Geotechnical Journal, 58(9), 1334–1350. https://doi.org/10.1139/cgj-2020-0241.

Developing a geotechnical plasticity framework for cable-seabed interaction modelling

M. Chalakatevaki*[1], and S.A. Stanier[1]

*Correspondence: mc2136@cam.ac.uk

[1] *Department of Engineering, University of Cambridge, Trumpington St, Cambridge CB2 1PZ, UK*

Abstract

Offshore wind power connectivity is reliant on networks of arrays of buried subsea cables connecting turbines and substations. The cable performance is dependent on seabed interaction, which is often modelled numerically with simple Coulomb friction or models derived from experience gained with the stability of on-bottom pipelines. A refined "macro-element" plasticity model representing the cable-seabed interaction could facilitate more sophisticated coupled hydro-soil-structure analyses.

Background

Static subsea power cables play the critical connectivity role in fixed-bottom offshore wind farms. Laid or buried within the seabed, they are connected to the offshore units (e.g. a monopile) through transitions where an unsupported section of the cable can be exposed to combined loading influenced by the local hydrodynamic regime and the seabed conditions. Assessing cable stability, which is greatly influenced by the soil bearing capacity, is essential for ensuring resilience to excessive displacements, embedment loss and fatigue risk.

Current analyses are typically based on simple Coulomb friction models or knowledge transfer from on-bottom pipeline design (DNVGL, 2021a, 2021b). These models not only are limited by empiricism, but also do not take into account the cable-specific issues such as differences in geometry/rigidity, and embedment.

Plasticity theory has been applied to material constitutive modelling for a long time. For soil-structure interaction, models have been developed for shallow foundations and pipes (e.g. Zhang, Stewart & Randolph, 2002, Tian & Cassidy, 2008, Hodder & Cassidy, 2010).

Force-resultant plasticity models can relate the forces to the corresponding displacements and model the cable-soil interaction in a concise way, consistent with structural mechanics. Such "macro-element" models are incorporated into coupled analyses (Tian & Cassidy, 2008) while representing the cable-seabed as a series of nodes with refined force-displacement relations and equivalent seabed stiffness estimates useful for fatigue assessments.

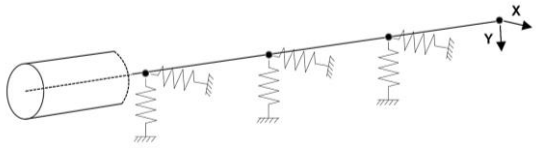

Figure 1. Cable nodes in a force-resultant model.

Although more sophisticated parabolic bearing capacity envelope models (e.g. Martin & White, 2012) exist in literature, there is little information to facilitate the development of a fully featured force-resultant model due to a lack of data regarding the kinematic behaviour over changing embedment and loading direction.

Model development

A framework for embedded cable-seabed interaction is presented here. It consists of a simple undrained elastoplastic model in plane strain space formulated via a series of yield surfaces, a hardening law, an elastic response matrix, and a non-associative flow rule. The parameters considered include the cable effective embedment, the cable-soil interface (roughness, tensile capacity), the soil weight-to-strength ratio, and the evolution of the yield surface with embedment and displacement. Their influence was investigated via multiple series of 2D finite element limit analyses (Optum G2, 2021) with various interface conditions in uniform Tresca soil.

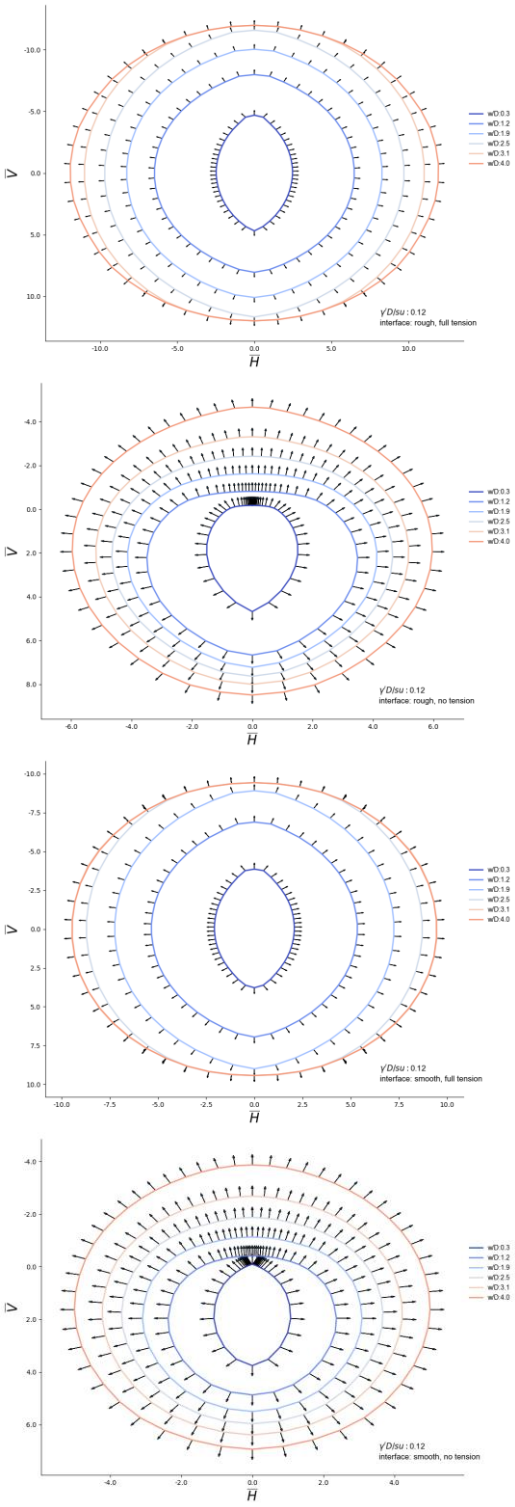

Figure 2. Interpolated yield surfaces and displacement vectors for different effective embedments (w/D) and cable-soil interface conditions.

The diversity of the data is such that curve fitting (typically parabolic) functions for the formulation of the yield and plastic potential surfaces cannot capture all the intricacies of the underlying data. These difficulties are addressed by implementing a tricubic interpolation scheme (Lekien & Marsden, 2005). This framework allows the derivation of the yield surface, derivatives, and plastic potential vectors for any scenario within a pre-determined non-dimensional parameter space and can be incorporated into structural analyses to simulate the cable-soil interaction when subjected to arbitrary displacement paths. This framework can potentially be extended to any number of additional parameters, such as variant undrained shear strength and cable weight, simply by expanding the number of variables considered by the interpolant framework.

The presentation associated with this abstract will introduce the aforementioned framework and demonstrate the implementation of a simple model for buried cables in a uniform undrained clay with various interface conditions.

References

DNVGL. 2021a. Recommended Practice DNVGL-RP-F109: On-bottom stability design of submarine pipelines. (tech. rep.).

DNVGL. 2021b. Recommended Practice DNVGL-RP-F114: Pipe-soil interaction for submarine pipelines. (tech. rep.).

Hodder, M.S., Cassidy, M.J. 2010. A plasticity model for predicting the vertical and lateral behavior of pipelines in clay soil. *Géotechnique* **60**(4): 247–263.

Lekien, F., Marsden, J. 2005. Tricubic interpolation in three dimensions. *International Journal for Numerical Methods in Engineering* **63**(3): 455-471.

Martin, C., White, D. 2012. Limit analysis of the undrained bearing capacity of offshore pipelines. *Géeotechnique* **62**(9), 847–863.

Optum G2. 2021. Optum computational engineering.

Tian, Y., Cassidy, M. 2008. Modeling of pipe-soil interaction and its application in numerical simulation. *International Journal of Geomechanics* **8**(4): 213-229.

Zhang, J., Stewart, D.P. and Randolph, M.F., 2002. Modeling of shallowly embedded offshore pipelines in calcareous sand. *Journal of geotechnical and geoenvironmental engineering* **128**(5): 363-371.

Optimized vibratory installation of Offshore Monopiles in sand: Physical and Numerical Modelling Investigation

Liqun Fang*[1], Michael Brown[1], and Matteo Ciantia[1, 2]

*Correspondence: 2497353@dundee.ac.uk

[1] *University of Dundee, Dundee, Scotland, UK*
[2] *University Milano Bicocca, Milan, Italy*

Abstract

Monopiles are a common foundation type for offshore wind turbines. Compared with the traditional impact driving installation methods for monopiles, vibratory driving is a promising alternative with advantages of rapid installation, low acoustic noise emission and limitation of stresses during driving. However, uncertainties over driving performance and bearing capacities may prove barriers to widespread adoption of purely vibration based installation. This PhD project aims to investigate the effects of driving variables on pile installation and pile performance and optimize both the vibratory driving process and post installation capabilities. Physical model tests and numerical simulations will be used in this research. A vibratory pile driving system will be developed for 1g and centrifuge model tests and pile installation and bearing capacities will be tested at both 1g and high-g level. The discrete element method (DEM) will be employed to simulate the installation process and bearing performance. The aim of this study is to develop a reliable prediction method for vibro driveability and determine the optimal driving method for installation and in-service performance. This paper presents a brief introduction of the PhD project.

Introduction

The global offshore renewable energy provision is expected to grow from 8.8GW in 2022 to 35.5GW in 2027(GWEC, 2023). To date, most of the foundations for offshore wind turbines haven been monopiles in shallow water (Bienen et al., 2023). The conventional installation method for monopiles is impact-driving where hammer blows are applied to the pile top periodically. This dynamic process may cause significant noise emissions and steel fatigue. Vibratory driving provides a promising alternative for monopile installation with much lower underwater noise emission (Molenkamp et al., 2024) and potentially more rapid installation than impact driving. However, uncertainties over driveability and post installation performance may lead to pile refusal before reaching target depth and low bearing capacities. This knowledge gap may prove a barrier to widespread adoption of purely vibration based installation. Further investigations are required to gain insights into the vibratory monopile installation and post installation performance. Physical and numerical modelling will be used in this project. For physical model tests, 1g and centrifuge tests will be conducted using a vibratory pile driving system. 3D DEM will be employed to simulate the installation process and bearing performance and the microscopic soil particle interaction will be studied. A reliable prediction method for vibro driveability will be developed and the optimal driving method will be proposed.

General Specifications

1g and centrifuge vibratory driving and loading tests will be conducted in sand. HST95 standard test sand will used in this project as this has been widely used and characterised at the University of Dundee (Davidson et al., 2022). The influence of frequency, acceleration, driving force and displacement per cycle on vibratory driving will be investigated in both 1g and high-g levels. Resonant vibration after pile installation has been shown to improve the bearing capacity after installation (Massarsch et al., 2022). The vertical bearing capacity and pull-out resistance of monopiles with and without a resonance approach will be compared. To date, 1g installation tests have been completed and the effects of driving frequency and force investigated (Fang et al., 2024). The results show that the driving frequency has a significant effect on

the driving performance compared to driving force. The setup of 1g tests is shown in Figure 1. For centrifuge tests, significantly higher driving frequency and force will be required to achieve the pile installation. A new centrifuge vibratory system is currently being developed at the University of Dundee to achieve this.

The particle flow in DEM makes it an ideal method to simulate a cohesionless geotechnical material like sand. In this project, DEM will be used to simulate the vibratory installation and investigate load capacity. The particle flow in DEM can be used to investigate the sand particle movement, stress and density development during pile installation and in-service loading, which can be used to interpret the interaction between pile and sand from a microscopic perspective. In this project, 3D DEM models in PFC will be established to investigate the vibratory installation and post installation performance. Element tests including triaxial tests and cyclic simple shearing tests will be used for material calibration before dynamic pile installation. A parametric investigation will be conducted into dynamic installation and the soil status will be monitored at the same time. Resonance processes simulation will also be attempted to allow investigation of the effects on in-service performance. It is hoped using DEM will give a more fundamental understanding of the controlling factors on vibro installation and driveability and allow these insights to optimise the full-scale process. To date, the triaxial tests in 3D DEM for material calibration have been undertaken, the selected model is shown in Figure 2.

Figures

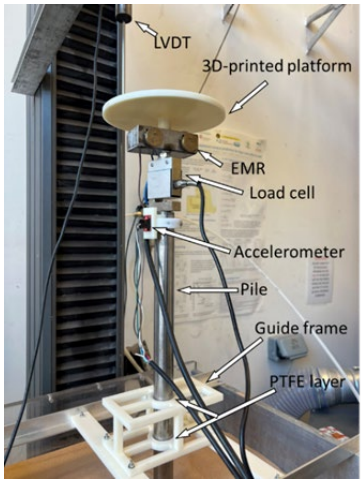

Figure 1. Experimental setup used for pile installation.

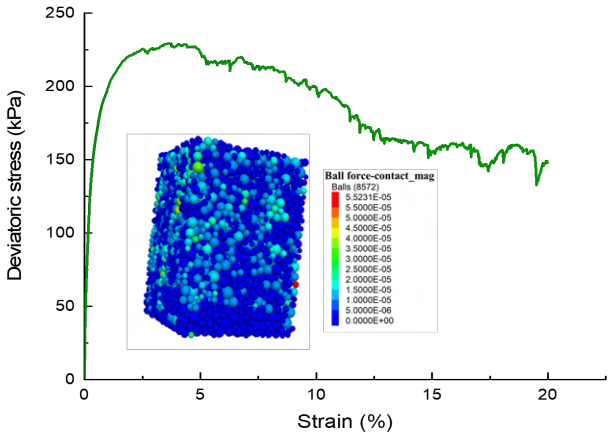

Figure 2. Deviatoric stress – strain results and test sample of DEM triaxial simulation (shown inset).

References

Bienen, B., Mazutti, J. H., Bransby, F., Esfeh, P. K., & Randolph, M. 2023. Investigating installation and post-installation performance of vibro-driven monopiles in sand: Centrifuge modelling and numerical analysis. *9th International SUT OSIG Conference "Innovative Geotechnologies for Energy Transition".* London, UK.

Davidson, C., Brown, M. J., Cerfontaine, B., Al-Baghdadi, T., Knappett, J., Brennan, A., Augarde, C., Coombs, W., Wang, L., Blake, A., Richards, D., & Ball, J. D. 2022. Physical modelling to demonstrate the feasibility of screw piles for offshore jacket-supported wind energy structures. Géotechnique, 72(2), 108–126.

Fang, L., Brown, M. J., Davidson, C., Wang, W., Sharif, Y. 2024. A 1g model experimental study on the effects of installation parameters on vibratory driving performance of monopiles. Proceedings of the 5th ECPMG 2024 (In press).

GWEC. 2023. Global Wind Report 2023. *Global Wind Energy Council*. Sao Paulo, Brazil.

Massarsch, K. R., Wersäll, C., & Fellenius, B. H. 2022. Vibratory driving of piles and sheet piles–state of practice. *Proceedings of the Institution of Civil Engineers-Geotechnical Engineering* 175(1), 31–48.

Molenkamp, T., Tsetas, A., Tsouvalas, A., & Metrikine, A. 2024. Underwater noise from vibratory pile driving with non-linear frictional pile-soil interaction. *Journal of Sound and Vibration* 118298.

Design Optimisation for Driveability of Offshore Wind Jacket Piles

M. J. Davies*[1], P. Houlston[1]

*Correspondence: miriam.davies@ramboll.co.uk

[1] *Ramboll, 240 Blackfriars Road, London, SE1 8NW, UK*

Abstract

With many offshore windfarms being constructed worldwide, there is demand for pile design with minimised installation risks. A common foundation type for offshore wind turbines is a jacket structure supported by pin-piles. This study highlights the effects of pile geometry on the driveability prediction for jacket piles. The wall thickness of a jacket pile has a potential ideal value for pile driving due to the interplay between several factors including end bearing, shaft friction and soil damping. For sites with onerous driving conditions, reducing driving risk is beneficial as delays and interventions are costly in time and resources.

Introduction

When designing a jacket pile, certain design criteria are more critical than others depending on the constraints of the project. These criteria include axial capacity, stiffness, buckling, fatigue and installation. Sites exist for which installation is a key consideration due to presence of dense sands, gravels or high strength clay. Hard driving can lead to risk of refusal or excessive fatigue damage, which must be limited to retain pile integrity. The aim of this work is to investigate a potential method of reducing the energy required for impact driving through varying pile wall thickness. This could decrease risk and save cost on offshore jacket installations.

Methodology

An example North Sea soil profile, Tab. 1, was taken comprising mixed sand and clay layers. A pile geometry was assumed with constant wall thickness over the penetration. A diameter of 3 m with a pile penetration of 40 m was used with varying wall thicknesses between runs. Driveability predictions were made in the GRL-WEAP 2010 software (Pile Dynamics Inc. 2010) with an 800kJ hammer. This software uses the wave equation approach to model the driving dynamics. Ramboll's in-house method was used to calculate the Static Resistance to Driving (SRD). This is based on a method suggested by Stevens (Stevens et al. 1982), with amendments based on back-calculations.

Table 1. Soil Profile

Soil	Depth (m)	Unit Weight (kN/m^3)	Friction Angle (º)	Undrained Shear Strength (kPa)
SAND	0	11.1	31.4	
CLAY	0.8	10.1		45.3
SAND	2.5	10.9	33.7-38.1	
CLAY	12.3	11.1		180-300
SAND	15.3	11.1	36.8-37.9	
CLAY	22.4	11.1		900
SAND	23	10.9	33.1-36.7	
CLAY	46	11.1		900

Results and Discussion

Fig. 1 presents the predicted blow count with pile penetration for three wall thicknesses. An increased end-bearing occurs for the thicker-walled pile, so more blows are required to drive it. Reduced wall thickness leads to a marginally increased shaft resistance due to decreased inner-wall area, but the reduction in end-bearing governs. Therefore, on this basis a reduction in blow-count would be expected. However, when the wall thickness is reduced past a critical point, it can be observed that the blow count at final penetration increases. For this analysis, the critical wall

thickness is about 75 mm, shown in Fig. 2, where final blow-count is shown against wall-thickness and a clear optimum is seen.

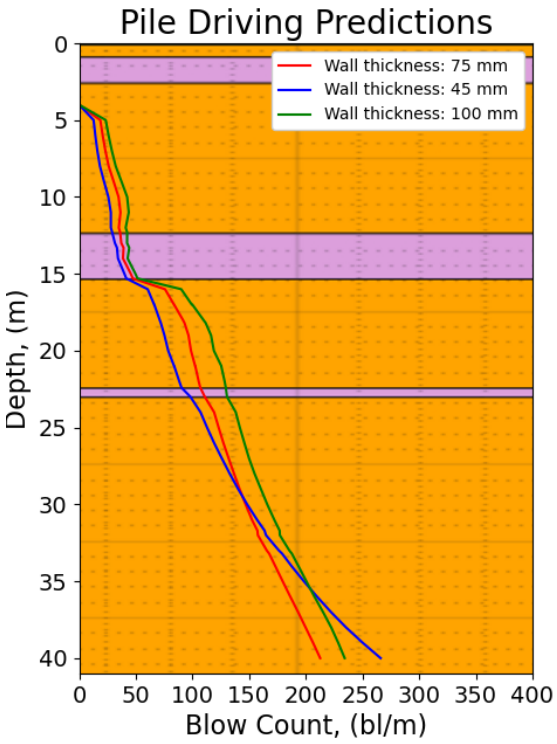

Figure 1. Blow Count Predictions with Wall Thickness

The blow-count increase for the thinner piles is a result of soil damping altering the stress wave propagation within the pile during driving. The lower cross-sectional area of the thinner pile results in more compressibility, leading to greater energy loss in soil damping. This attenuates the stress-wave propagation down the pile, which can be observed by a greater relative reduction in peak force predicted at the pile toe compared to the peak force at the pile top, which can be observed in Fig. 3.

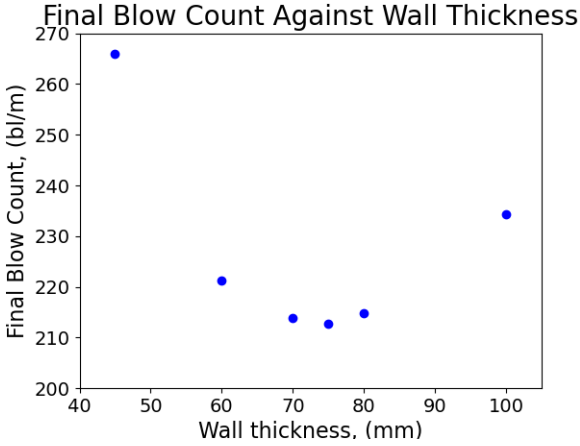

Figure 2. Final Blow Count Against Wall Thickness

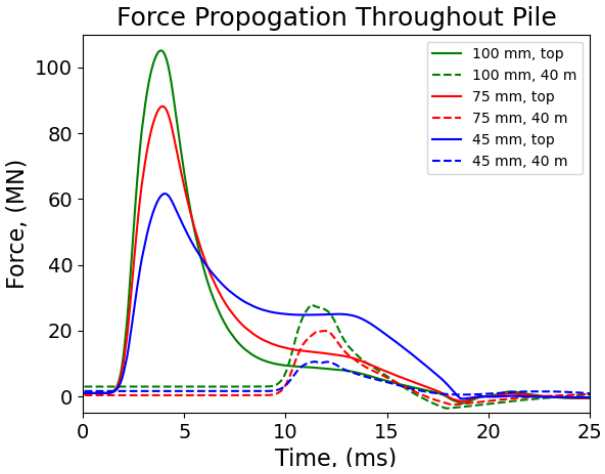

Figure 3. Predicted Force Against Time at Top and Bottom of Pile for a Single Hammer Blow at Penetration

In Fig. 1. the relative increase in blow-count for the thinner pile only occurs some distance into the pile penetration. This is due to the attenuation of the peak force seen within the pile. Greater energy loss occurs as the embedment increases, at the same time the SRD increases with depth. Therefore, the optimum pile wall thickness is sensitive to pile penetration.

Conclusions and Future Work

This study showed that for a given soil profile there is an optimum pile wall thickness that requires the least number of blows to drive. It was seen that the optimum varies with depth of penetration.

Further work could include optimisation of pile wall thickness considering this effect in combination with fabrication restraints, cost, weight, capacity, fatigue and buckling considerations. More realistic, complex geometries could be modelled accounting for varying wall thicknesses in the upper parts of the pile as is common for jacket pin-piles. The effects of different soil profiles could be studied, with especial thought to stress wave propagation and its interaction with skin friction.

References

Stevens, R. S., Wiltsie, E. A., Turton, T. H. 1982. Evaluating Pile Drivability for Hard Clay, Very Dense Sand, and Rock. *14th Annual Offshore Technology Conference in Houston, Texas, May 3-6, 1982*: 465-469.

Pile Dynamics Inc. 2010. GRLWEAP 2010 Background Report. *www.pile.com*

Impact of Kinematic Interaction on foundations for offshore wind turbines using FE analysis

F. Ortiz Wall*[1], D.M.G. Taborda[1], S. Kontoe[1], J. Möller[1]

*Correspondence: f.ortiz-wall23@imperial.ac.uk

[1] *Imperial College London, Exhibition Rd, South Kensington, London, UK (SW7 2AZ)*

Abstract

Foundations are key to structural integrity and serviceability of offshore wind turbines (OWTs) subjected to seismic loading conditions, and the understanding of the effects of soil-structure interaction (SSI) is essential to get an efficient and reliable design. Simplified methods used to address SSI often consider seismic motions recorded at the free field as the input signal imposed to the tower, but this could be a non-conservative approach as the initial motion could suffer important modifications due to kinematic interaction between the soil deposit and the OWT foundation. This study aims to evaluate different scenarios using finite element analyses in order to explore the conditions under which kinematic interaction can play an important role in the response of the tower.

Introduction

Offshore wind energy is one of the world's fastest growing and most developed sources of clean energy. OWTs are increasing in size and being installed in harsher environments than before and are subjected to complex loading conditions, including that arising from seismic events, adding a further level of complexity to their design.

OWTs foundation systems are essential to ensure the integrity and serviceability of the OWT during its lifetime. In this regard, monopiles, large-diameter steel tube piles, are the most widely installed type of foundations due to their relatively simple design, fabrication, and installation process (Hou et al., 2022).

The interaction between the foundation and the surrounding supporting soil (SSI) will affect the behaviour of the system, by influencing the overturning moment and loads, modes of vibration, and even altering some properties of the foundation and soil due to repeated cyclic or dynamic loads (Bhattacharya, 2019).

There are different methods for simulating SSI on monopiles: (a) simplified approaches where the foundation is replaced by springs explicitly defining the stiffness of monopiles for different soil profiles; (b) beam-on-spring methods where the SSI along the entire length of the monopile is modelled using non-linear springs associated with given "p-y" curves defining the relationship between the soil rection and corresponding displacement; (c) numerical finite-element analysis that discretize the medium and can represent complex soil and structural behaviour. While the latter method is clearly the most accurate, it is computationally expensive, resulting in simpler methods being the most widely used in industry.

In simpler methods, a seismic motion recorded in the free field is usually employed as input signal for the design of the monopiles. However, kinematic interaction can modify the motion reaching the surface, leading to potentially nonconservative results.

Kinematic interaction is the component of the system response that considers the influence of the presence of the foundation on the soil due to differences in the stiffness of the materials, modifying the movement of the monopile with respect to that of the free field. Some studies, such as Kaynia (2021) have shown that the tower response and bending moments are larger when considering kinematic interaction, and its effect should not be ignored.

Finite Element Analysis

A 3D model of the IEA 15-MW Reference OWT (Gaertner et al., 2020) is created in PLAXIS3D (Figure 1). The tower is supported by a fixed-bottom 45m long and 10m diameter monopile. The tower and the monopile were modelled as

a series of hollow steel cylinders of different diameter and wall thickness following the description in Gaertner et al. (2020). The rotor-nacelle assembly (RNA) is modelled as a volume of equivalent mass at the top of the tower.

To study the kinematic effect on the system, three steps are followed: firstly, an analysis of a 100m 1D soil column model subjected to a 30s harmonic sinusoidal motion is carried out to obtain the motion at surface level due only to wave propagation, without the interaction with the monopile. Secondly, the full 200x200x100m 3D model (see Figure 1) with the structure included is subjected to the same motion used in the 1D analysis. The weight of all structural elements must be set to zero to consider solely kinematic interaction. Thus, the only factor impacting the response is the stiffness of the elements. Lastly, the results from the 3D model are normalised by the results from the 1D model, in terms of the maximum displacements at the top of the monopile.

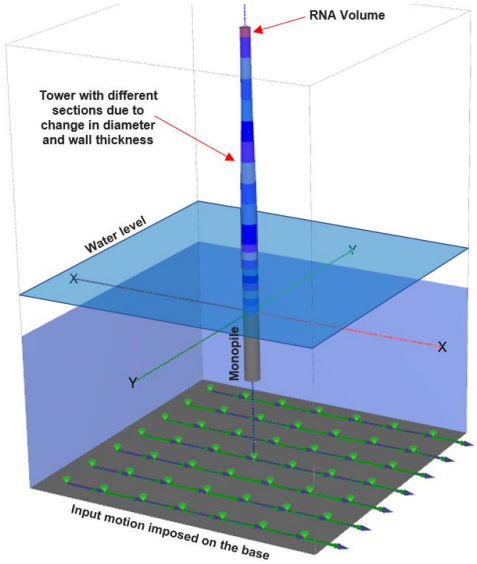

Figure 1. 3D model of the IEA 15-MW Reference OWT

Two types of soil profile are studied considering a single layer of a linear elastic material with 5% Rayleigh ramping: constant stiffness and linearly increasing stiffness with depth. The unit weight and Poisson's ratio adopted are 17.66 kN/m^3 and 0.4, respectively, while the Young's modulus is 154E3 kN/m^2 for the soil profile with constant stiffness and $10^4 \cdot z$ kN/m^2/m for the soil profile with linear increment of stiffness, where z denotes the depth below ground level. These properties match two of the scenarios considered in Kaynia (2021).

The results for all the considered frequencies are shown in Figure 2. Clearly, for most of the cases considered, the movement of the top of the monopile is greatly affected by the kinematic interaction, registering values below those obtained in the site response analyses. However, there seems to be a frequency range between 1.25 – 2 Hz for the uniform soil profile where the displacements of the monopile head are considerably larger than that of the surface. Further research is clearly needed to assess the impact of nonlinearity of soil behaviour, as well as that of other ground conditions.

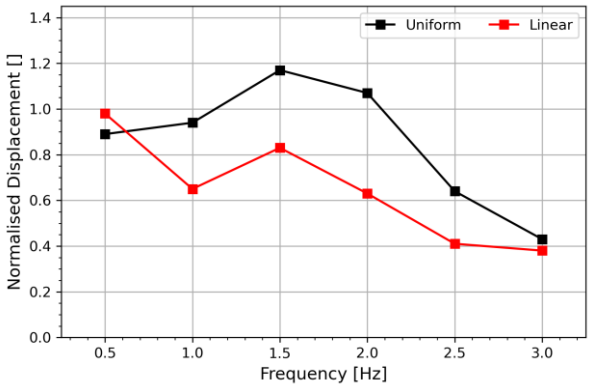

Figure 2: Kinematic interaction response for the IEA 15-MW Reference OWT in two soil profiles

Support for this research was provided by the Agencia Nacional de Investigación y Desarrollo (ANID) and its overseas doctoral programme Becas Chile.

References

Bhattacharya, S. 2019. Design of foundations for offshore wind turbines. John Wiley & Sons.

Gaertner, E., Rinker, J., Sethuraman, L., Zahle, F., Anderson, B., Barter, G., Abbas, N., Meng, F., Bortolotti, P., & Skrzypinski, W. 2020. IEA Wind TCP Task 37: Definition of the IEA 15-megawatt offshore reference wind turbine.

Hou, G., Xu, K., & Lian, J. 2022. A review on recent risk assessment methodologies of offshore wind turbine foundations. Ocean Engineering, **264**.

Kaynia, A. M. (2021). Effect of kinematic interaction on seismic response of offshore wind turbines on monopiles. Earthquake Engineering and Structural Dynamics, **50** (3), 777–790.

Offshore wind monopile foundation interaction with scour protection rock berm: centrifuge testing

D.M. Xu*[1], S.P.G. Madabhushi[2], J.M. Harris[3] and R.J.S. Whitehouse[4]

*Correspondence: dmx20@cam.ac.uk

[1] *Student (Department of Engineering, University of Cambridge, Trumpington Street, Cambridge, CB2 1PZ, UK)*
[2] *Professor (Department of Engineering, University of Cambridge, Trumpington Street, Cambridge, CB2 1PZ, UK)*
[3] *Research and Innovation Director (HR Wallingford, Howbery Park, Wallingford, OX10 8BA, UK)*
[4] *Technical Director (HR Wallingford, Howbery Park, Wallingford, OX10 8BA, UK)*

Abstract

Offshore wind is a key growing industry that will form a large proportion of the energy generation of the future as we move towards renewable sources. The most common foundation used is the mono-pile, which are large diameter steel tubes. Newly built and planned windfarms in places such as North America and South East Asia have the potential to fall on areas which are both seismically active and prone to scour. A common method to prevent or remediate scour is rock dumping, but currently, there is little data or research on the behaviour of these scour protection rock berms on liquefied sand, or indeed the interaction, if any, between the monopile and rock berm. This paper presents the results of a dynamic, saturated, centrifuge test, in which two model monopiles sit within the same rock berm. Lateral push over tests are performed pre and post-earthquake to compare the pile lateral capacity, along with surface settlements, pore pressure and acceleration data are recorded. The results are also compared with a previous study to show that there is little rock-monopile interaction, which is what was theorised, as the thickness of the rock berm is an order of magnitude smaller than the pile embedded depth. This work forms part of a PhD project with the aim of better understanding the behaviour of scour protection rock under seismic liquefaction.

Introduction

Scour is a phenomenon where the foundation redirects currents that form vortices, which then remove sediment around the structure, overtime reducing its embedded depth. To combat or remediate against scour, a method often used is rock dump.

Past studies have shown that full liquefaction is not required for significant rock settlement to occur and that the presence of rock will delay the onset of liquefaction (Xu *et al.*, 2022), there is a small effect of rock density on rock settlement, split by small and large input motions (Xu *et al.*, 2023a), and that the model rock berm cannot be modelled by a shallow foundation or plate (Xu *et al.*, 2024). The rock settlement data from this series of centrifuge tests are summarised and compared in (Xu *et al.*, 2023b).

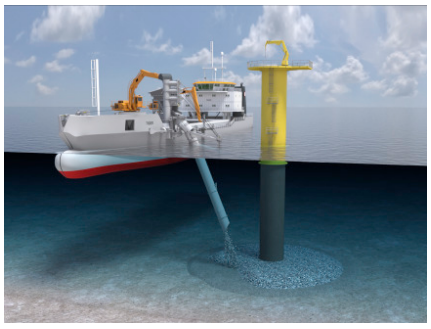

Figure 1. Rock dump to prevent scour for an offshore wind turbine monopile foundation from Offshore Wind Farms - Technologies, Design and Operation (2016)

Experimental testing

Centrifuge modelling was used to enable “scale” testing of the interaction of a rock berm and monopile foundations. Figure 2 presents a cross section schematic of the test; the two piles enable a pre-earthquake and post push over test to measure the lateral capacity of the pile. The results are compared with that from (Seong *et al.*, 2022) which has the same setup,

but without the rock berm. Pore pressure sensors and accelerometers are buried in the sand, displacement sensors are set on the monopiles and rock berm, and finally load cells are attached between the actuators and piles.

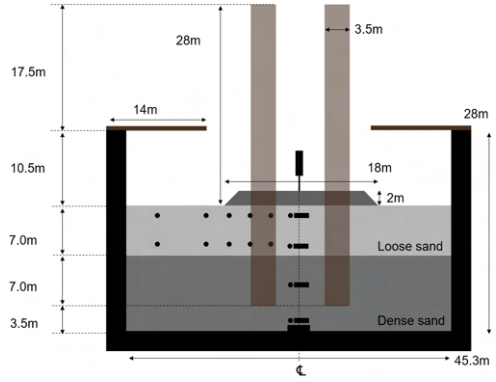

Figure 2. Test schematic diagram

Table 1 summarises the earthquake sequence and berm settlements. The sand was saturated with methylcellulose at 70cSt (70*g* test). Both the piles and rocks (0.45m diameter limestone) were wished into place at 1*g*.

Table 1. Earthquake sequence and resulting rock berm settlements

ID	Earthquake	PGA (g)	Settlement (m)
EQ1	Kobe 0.15V	0.01	0.002
EQ2	Sine wave, 70Hz, 15 cycles, 2.50V	0.03	0.569
EQ3	Sine wave, 70Hz, 15 cycles, 3.00V	0.04	0.298
EQ4	Sine wave, 70Hz, 15 cycles, 0.75V	0.01	0.014

Results

Figure 3 shows a plot comparing pre and post-earthquake push over tests, for cases with and without rock.

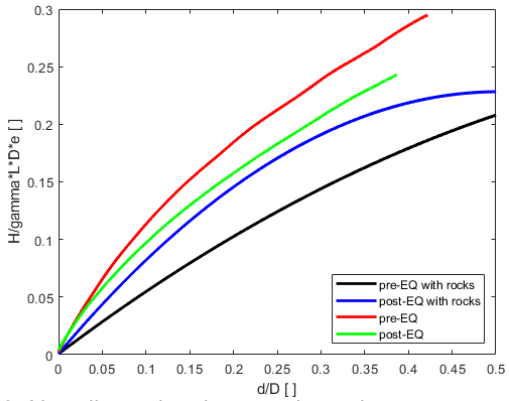

Figure 3. Non-dimensional comparison plot

The load (*H*) has been normalised by the unit weight of sand, the load eccentricity, and pile embedded depth and diameter. The pile top mass displacement (*d*) has been normalised by the pile diameter. It can be seen that there is no significant difference between the curves. From the test with piles, the post-earthquake lateral pile resistance is greater, this is expected due to the densification of the sand from previous earthquakes.

Conclusions

This paper has shown that there is no interaction between the pile and rocks. This makes sense because the depth of the rock berm is an order of magnitude smaller than the embedded depth of the pile, in addition, the design of the pile does not take into account the presence of any scour protection rocks.

References

Seong, J., Abadie, C.N., Madabhushi, G.S.P., and Haigh, S.K. 2022. Dynamic and monotonic response of Monopile Foundations for Offshore wind turbines using centrifuge testing. *Bulletin of Earthquake Engineering.* (21): 1303-1323.

Xu, D.M., Abadie, C.N., Madabhushi, G.S.P., Harris, J. M., and Whitehouse, R.J.S. 2022. Response of armour rock-scour protection to earthquake-induced liquefaction for offshore wind applications. 10th ICPMG 2022. pp. 500-503.

Xu, D.M., Madabhushi, G.S.P., Abadie, C.N., Harris, J. M., and Whitehouse, R.J.S. 2023a. Effect of rock density on the response of scour protection to earthquake-induced liquefaction for offshore wind applications. 9th International Offshore Site Investigation and Geotechnics Conference. pp. 1451-1456.

Xu, D.M., Madabhushi, G.S.P., Harris, J. M., and Whitehouse, R.J.S. 2023b. Rock-scour protection of offshore foundations subjected to earthquake-induced liquefaction. Ground Engineering Dec 2023 issue, BGA Cooling Prize 2023. pp. 29-33.

Xu, D.M., Madabhushi, G.S.P., Harris, J. M., and Whitehouse, R.J.S. 2024. Comparison of rock-scour protection berm with a shallow foundation under seismic liquefaction. 8th International Conference on Earthquake Geotechnical Engineering. OS-28-03.

Evaluating the Resilience of Monopile-Supported Wind Turbines: A Multifactorial Analysis Across Capacities, Soil Types, and Water Depths

S. Bhattacharyya*[1], S. Biswal[1]

*Correspondence: sayan.bhattacharyya@surrey.ac.uk

[1] *University of Surrey, (School of Sustainability, Civil and Environmental Engineering, GU2 7XH, UK)*

Abstract

The surge in renewable energy initiatives marks a pivotal shift toward sustainable electricity generation, with offshore wind farms at the forefront due to their minimal carbon footprint. Originally spearheaded in Europe, this technology is now expanding globally, embraced by nations facing diverse environmental hazards such as earthquakes and cyclones. This paper proposes a comprehensive modelling strategy tailored for a variety of turbine types, soil conditions, and hazard scenarios to effectively predict and analyse failure patterns in offshore wind turbines. By integrating diverse data sets and employing robust simulation techniques, this study aims to enhance the resilience and efficiency of offshore wind energy systems, ensuring their viability and safety in adverse conditions.

Introduction

Offshore wind farms are widely spreading across Taiwan, China and Japan where the soil conditions are quite different than that of North Sea and Irish Sea. These eastern parts of the world has witnessed several earthquakes, from 2011 – Fukushima Daichii (S. Bhattacharya, K. Goda, 2016) to the recent one on 3rd April 2024 in Taiwan. An extensive study of wind turbines and their performance has been validated by experimental and numerical study by Prowell, 2011. Owing to it's being a comparative new technology the affect of multi-hazards on these turbines needs a thorough assessment (Bhattacharya et, al. 2021). Thus, a wide range of met-ocean data along with soil-profile and turbine properties are collected, which has been exhaustively used for the analysis. This study will not only provide an overview of the performance of the structure but also can estimate the damage state.

Methodology and Modelling

Wind turbine properties are collected from the available data ranging from 3MW to 15MW. The properties that are considered are tower height, RNA mass, blade size, thicknesses, pile length, water depth. The wind has been considered only for the rated wind speed, which is used to calculate the thrust force. The wave height and time period of wave has been calculated for their corresponding wind speed. As per the code BS EN ISO 19901-2:2002, the soil properties and the shear velocity of soil has been derived. A dictionary of earthquake has been created and considering return period of 475 years, the amplitude of the time history is amplified to increase the PGA from 0.2g to 1g.

A Monte-Carlo simulation (S. Biswal, A. Ramaswamy, 2017) has been conducted to create a set of random samples varying all the ranges of wind turbine properties along with their soil-types and water depth.

Analytical study is carried out using FEM software Abaqus, where all the components are modelled as beam element. The blades along with RNA is connected to the tower using rigid link. The boundary conditions which is also soil, modelled as modified p-y springs (Patra et.al, 2022) as per API code. Site specific response analysis for the layered soils is conducted in Opensees, where the bed rock motion is used. As an output the ground motion response at the ends of each p-y springs are collected which on return is used for non-linear time history analysis in Abaqus. A flowchart of the methodology is shown in Figure-1.

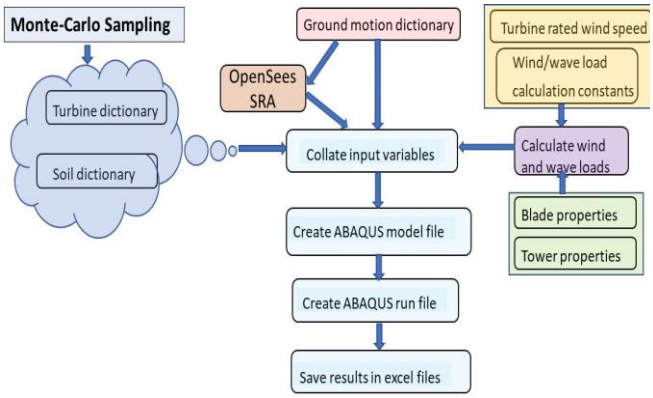

Figure 1- Flowchart for the methodology

Output and Results

The models are verified by their natural frequency. The following results are taken for estimating failure (i) pile head rotation, (ii) hub displacement, (iii) hub acceleration, and (iv) tower stress. Pile head rotation is an important criterion to define because it can create a permanent tilt which on contrary put the gears of Nacelle fail or bring to reduced power generation. Similarly, large hub displacement can introduce large eccentricity of the RNA mass which may lead to bending or buckling failure of the turbines. Large hub acceleration can create an imbalance to the assembly of the rotor and damage the gearbox. Large stresses in the tower can lead to failure of the towers which in turn result in failure of the turbines. It can be seen From Figure-2 that turbines with lower capacity possess higher acceleration at increasing PGA's and from Figure-3 larger turbines have higher hub displacements. It's evident that the lower turbines are more rigid than their higher counterparts.

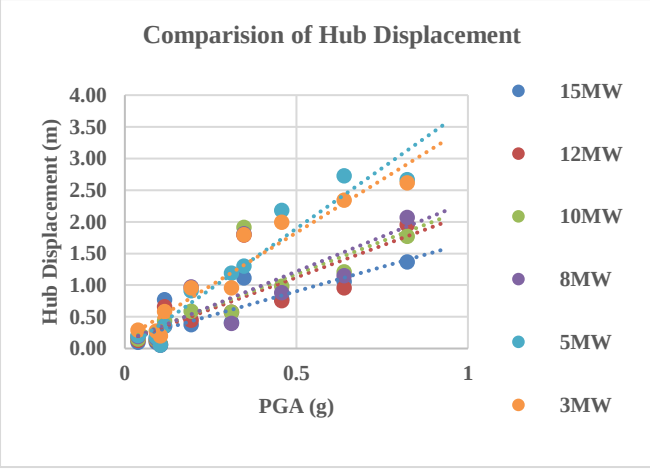

Figure-2 – Hub Displacement

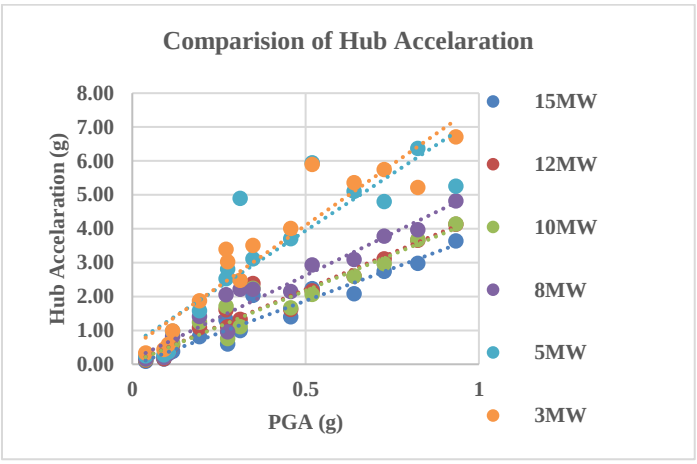

Figure-3 – Hub Acceleration

References

S. Biswal, A. Ramaswamy, Finite element model updating of concrete structures based on imprecise probability, Mechanical Systems and Signal Processing, Volume 94,2017, Pages 165-179, ISSN 08883270, https://doi.org/10.1016/j.ymssp.2017.02.042.

Bhattacharya S, Biswal S, Aleem M, Amani S, Prabhakaran A, Prakhya G, Lombardi D, Mistry HK. Seismic Design of Offshore Wind Turbines: Good, Bad and Unknowns. Energies. 2021; 14(12):3496. https://doi.org/10.3390/en14123496

Sangeet Kumar Patra, Sumanta Haldar, Subhamoy Bhattacharya, Predicting tilting of monopile supported wind turbines during seismic liquefaction, Ocean Engineering, Volume 252, 2022, 111145, ISSN 0029-8018, https://doi.org/10.1016/j.oceaneng.2022.111145.

Prowell I. An experimental and numerical study of wind turbine seismic behavior. University of California, San Diego; 2011.

S. Bhattacharya, K. Goda, Use of offshore wind farms to increase seismic resilience of Nuclear Power Plants, Soil Dynamics and Earthquake Engineering, Volume 80, 2016, Pages 65-68, ISSN 0267-7261, https://doi.org/10.1016/j.soildyn.2015.10.001

17th BGA YGES
University of Cambridge
1-3 July, 2024

Smart characterisation of geo-materials

T. Zheng*[1], R. Buckley[1], and E. Febrianto[1]

*Correspondence: t.zheng.1@research.gla.ac.uk

[1] *James Watt School of Engineering, University of Glasgow (Glasgow, UK)*

Abstract

The UK has set an ambitious goal of net-zero carbon emissions by 2050, requiring rapid and cost-effective deployment of technology including offshore wind farms (OWF). Site investigation (SI) campaigns for OWF require substantial time, carbon footprint, and cost (£10s of millions). They typically cover 100 km^2 areas, comprising geophysical, intrusive, and laboratory testing in a multi-stage process, planned heuristically. Interpretation/integration of data is still relatively manual, subjective, and time-consuming. The *Smart* project, a joint industry–funded PhD (University of Glasgow, Scottish Power Renewables, Geowynd), aims to refine and accelerate SI approaches through development of a large, worldwide geotechnical database and application of data-driven modelling techniques. This abstract introduces the completed and planned phases of the project including database generation, pre-processing, and describes the preliminary development of two characterisation models.

Background and objectives

To date, data-driven techniques have been largely absent from geotechnical engineering practice. This is partly for good reason. Geo-materials can be associated with high levels of uncertainty, variability, and local specificity, which can compromise the success of generalised, numerically-derived models. In other words, engineering judgement is paramount. However, this does not rule out all potential advances through data-driven approaches.

The objectives of the project are to: (i) curate an extensive, unified database of geotechnical data; (ii) identify key areas where data-driven approaches can provide added value; (iii) develop new correlations/models/frameworks which deal with uncertainty effectively and transparently; and (iv) use the findings to recommend best practice for data acquisition with regards to optimising survey/design timelines.

Database development

A database has been collated, curated and standardised from detailed geotechnical surveys for 20 OWF sites worldwide. It comprises data tables corresponding to: borehole location, layer descriptions, and each acquisition/test type. From here, development of any future models can take advantage of data from a large number of projects seamlessly.

Probabilistic framework

The database is being used to develop advanced probabilistic models which, crucially, reflect the underlying physics of each case, allowing for (i) wider consideration of input data than humans are capable of, (ii) more rigorous handling of uncertainty than traditional approaches, and (iii) reasonable generalisation across soil types due to the physical principles imbued in the models. A Bayesian framework is adopted and for each given characterisation problem, the nature of the relationship is first proposed in line with physical understanding. The benefits of this framework are that: (i) judgement can be applied in addition to numerical inference via prior likelihood functions; (ii) results are easily interpretable as probabilities; and (iii) separate models can be combined, within the same universal, probabilistic framework.

Pre-processing

Data must first be pre-processed to ensure they are physically representative. Crucially, cone penetration test (CPT) data must be filtered to remove misleading features, e.g., low resistance at the start of a new downhole push following a drill out (Fig. 1). The scale of the database dictates that automated solutions must be found. A solution has been devised based on physical model equations for the attenuation at the start of a push from true to measured q_c subject to several tuning parame-

ters μ_i. For each push, an optimisation algorithm is run to determine the most effective parameters. The physical basis ensures that while the final result is numerically derived out-of-sight from thousands of simulations, it generalises well across different soil conditions.

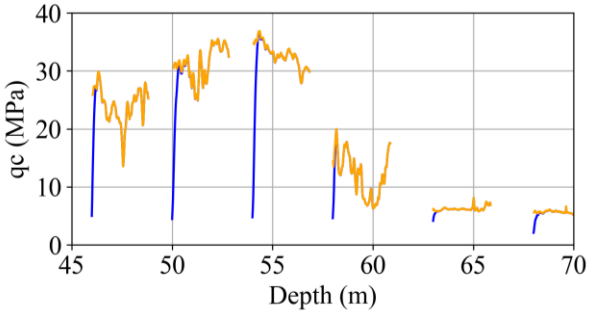

Figure 1. Example of automated pre-processing to convert unrepresentative measurements to true q_c profile; similar solutions have been developed for f_s and u_2.

Case Study 1: Soil type from CPT

A unified, probabilistic soil classification model for CPT data is being developed as an alternative to the traditional Robertson SBT charts (Robertson, 2016). This model takes the form of a series of Bayesian networks (joint probability distributions over several variables). Each network corresponds to a soil type and contains the three CPT measurements as well as hidden variables representing unknown characteristics (e.g., strength) and the joint pdfs are learned using a large training dataset. With the networks for each soil type trained, for given CPT data, the relative likelihoods of each soil type can be inferred (e.g., 10% sand, 60% silt, 30% clay). The above approach allows for all three CPT parameters to be considered together rather than needing separate *q-f* and *q-u* analyses. Furthermore, the probabilistic nature of the results delivers more information than a single, deterministic output soil type.

Case Study 2: SCPT interpretation

To interpret a given seismic CPT location, a Bayesian inversion model has also been developed, which considers the set of all available travel times between receivers to deliver the most likely profile of V_s, complete with uncertainty bounds. The full details can be found in Zheng et al., 2024. In summary, it uses a physical model to propagate uncertainty in travel times through to derived V_s. The model explicitly includes potential measurement errors as unknowns (as opposed to ignoring them in the mathematical formulation and assessing the uncertainty separately). As a result, the model is physically representative, and the magnitude of/uncertainty due to the errors is quantified. The inclusion of these error terms followed review of a large number of SCPTs within the database: certain features were found to be widespread, warranting detailed investigation. An example of a V_s profile is shown along with a traditional interval analysis is shown in Fig. 2.

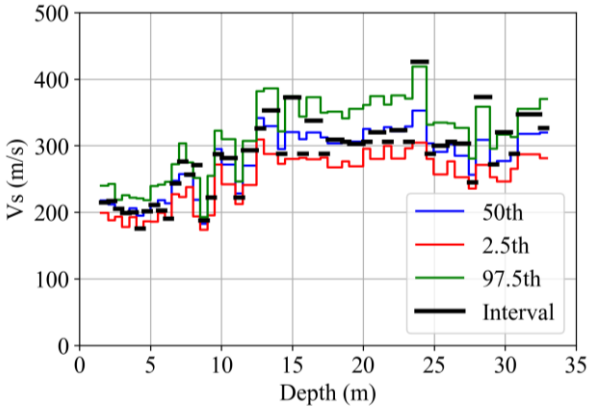

Figure 2. 2.5th, 50th, 97.5th percentile V_s derived via new method against traditional interval analysis.

Future direction

As discussed, a key benefit of the Bayesian approach relates to the ease of combining multiple models. Therefore, as the project progresses, more models will be developed related to various site characterisation problems, and eventually, these models will be converged into a unified, cohesive framework.

The next phase of the project will focus on consideration of laboratory test data, and subsequently correlation with CPT data. Eventually, the aim will be to develop and train a framework in which the following question can be answered: Given a set of geotechnical data, comprising some combination of in situ and laboratory testing, can we consider all data together, via a unified framework, in order to maximise the value of the data and best inform probabilistic estimates of key parameters?

References

Zheng, T., Buckley, M., Febrianto, E. 2024. Development of a framework for automatic quantification of uncertainty in seismic cone penetration testing. In *Proc 7th Intl Conf Geotechnical and Geophysical Site Characterization (ISC7)*, Barcelona. *In press.*

Robertson, P.K. 2016. Cone penetration test (CPT)-based soil behaviour type (SBT) classification system — an update. *Can. Geotech. J* **53** (12): 1910–1927.

Will Skynet go submarine? Three key use cases for machine learning in offshore foundation design

J.S. Alexander*[1]

*Correspondence: jal@geowynd.com

[1] *Geowynd, Glasgow, United Kingdom*

Abstract

Over the last few years Machine Learning (ML) and Artificial Intelligence (AI) have been making increasingly dramatic steps in improving productivity across a wide range of sectors and industries. ML is a promising field for geotechnical engineering as the algorithms can be trained to learn complex relationships between input parameters and the target parameter. Thanks to this characteristic, ML techniques have the potential to produce more accurate and/or faster results and be more consistent with respect to empirical correlations based on limited and regional case histories.

Introduction

This paper aims to provide insight and ideas across three distinct stages of offshore foundation design that would be suitable for employing ML models, highlighting selected benefits and drawbacks of each with some worked examples. Three case studies are presented and selected results are presented in Fig. 1:

A. ML to develop site investigation-parameter models;
B. ML to develop FEA Surrogate models;
C. ML to develop installation models, calibrated to field data.

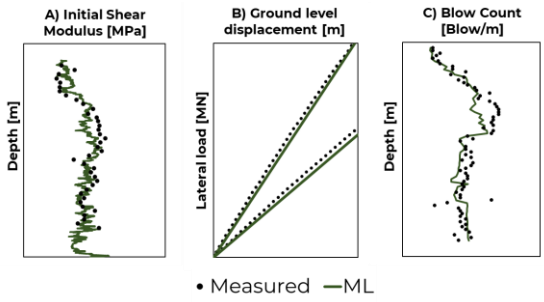

Figure 1. Example application of ML models for each case study presented.

Machine Learning Overview

Many attempts have been made over the last few years to build upon existing geotechnical engineering design and interpretation methods using ML. Most methods based on conceptually simple decision trees have been shown to be the most effective (Rauter & Tschuchnigg, 2021; Kardani et al., 2020). Neural Networks typically require large amounts of data (millions of datapoints) to unlock their full potential, making it potentially less applicable to many problems in geotechnics (Stuyts, 2020).

Using Data from Site Investigations

An essential aspect of offshore foundation design is the interpretation of in situ or laboratory tests to derive required soil properties. The key idea of using ML at this design stage is to minimise the number of expensive tests by utilising ML models to produce similar results from more affordable 'proxy data. Table 1 highlights some examples.

Table 1. Example uses of ML with site investigation data

Test	Target parameter	Proxy data
Triaxial, DSS	Undrained shear strength	CPT
SCPT*	**Initial shear modulus**	**CPT**
PSD	Gravel, sand, fines content	Imagery of cored samples

Notes: *Example in **bold** presented in Fig. 1 A).

An important advantage is that the highlighted proxy tests enable the generation of near-continuous profiles of the desired parameter, potentially reducing uncertainty compared to using lab tests at discrete intervals. An alternative option can be to use empirical correlations,

however, in many cases these are only applicable for certain soil types on which they were calibrated, whereas an ML model can be continuously retrained and updated whenever new data becomes available.

Using Numerical Methods

A second, but so far less explored application of ML to offshore foundation design is the use of 'surrogate' ML models to speed up computationally expensive tasks such as 3D FEA, which can easily take hours or days to run. If a surrogate model can be proven to output results with accuracy close to 3D FEA, then ML could provide great value for designers and developers at the concept design stage. This would enable rapid estimation of dimensions and cost for a specific foundation type in seconds, rather than days, streamlining the early-stage design process significantly. It should be noted that generating the training data for a surrogate ML model can be time consuming and complex data engineering could be required if interested in predicting outputs such as load displacement curves.

One example use of a surrogate model is predicting the initial stiffness of a monopile foundation subjected to a lateral load. Fig. 1 B) shows a good match of predictions of a surrogate model trained on 2000 linear elastic FEA simulations compared to 2 analyses conducted within the PISA JIP as presented in Byrne et al. (2020), which serves as the basis for industry-standard design methods.

Using Field Data

The area in which ML models could have the most impact over conventional design methods is by exploiting training data taken directly from measurements of real foundations during construction or operation. However, this can involve additional cost to developers, such as remote sensors or surveys, so it is crucial that the benefits and drawback are clearly defined. Table 2 highlights some examples.

Table 2. Example uses of ML with field data

Action	Target parameter	Training inputs
Monopile installation*	**Hammer blowcount**	**Monopile geometry, CPT and operative parameters**
Scour prediction	Scour depth	Flow conditions and foundation geometry
Pile design	Pile bearing capacity	Soil properties and pile dimensions

Notes: *Example in **bold** presented in Fig. 1 C).

Using real field foundation data to train ML models can allow a more 'end-to-end' approach to be taken to design. Although this reduces interpretability of the design process, it ensures that the model maintains accuracy by not predicting redundant parameters at intermediate steps. Furthermore, it is important to note that many ML models are not well-suited for extrapolation, so caution is needed when applying these models to new sites and foundation geometries.

Conclusions

Machine learning is a rapidly maturing branch of data science that lends itself well to discovering complex interplay between different soil properties and their effects on foundations. It can be applied at various stages of design, with three key areas outlined and examples presented. It is anticipated that this paper serves as inspiration for engineers to think about where ML could provide benefits compared to current methods of offshore foundation design.

References

Byrne, B. W., Houlsby, G. T., Burd, H. J., Gavin, K. G., Igoe, D. J., Jardine, R. J., & Zdravković, L. 2020. PISA design model for monopiles for offshore wind turbines: application to a stiff glacial clay till. Géotechnique **70**(11): 1030-1047.

Kardani, N., Zhou, A., Nazem, M., & Shen, S. L. 2020. Estimation of bearing capacity of piles in cohesionless soil using optimised machine learning approaches. Geotechnical and Geological Engineering **38**(2): 2271-2291.

Rauter, S. and Tschuchnigg, F. 2021. CPT data interpretation employing different machine learning techniques. Geosciences ***11***(7): 265.

Stuyts, B. 2020. Data science applications in geo-intelligence. 4th International Symposium Frontiers in Offshore Geotechnics: 120-149.

Development of a Data-driven Machine Learning Software for Geotechnical Subsurface Characterisation

Z.Z. Wang*[1], X.F. Guo[2], and Y. Hu[3]

*Correspondence: zw437@cam.ac.uk

[1] *University of Cambridge, 7a JJ Thomson Ave, Cambridge, CB3 0FA, United Kingdom*
[2] *South China University of Technology, 777 Xingye Street East, Guangzhou 511442, China*
[2] *Leibniz Universität Hannover, Callinstr. 34, Hannover 30167, Germany*

Abstract

We present a software developed for data-driven geotechnical subsurface stratigraphy characterisation. This software incorporates two novel machine-learning architectures we have developed in-house, based on data from more than 20,000 boreholes in Singapore. It allows for explicit 1D to 3D modelling, uncertainty quantification, and associated visualisation. In addition, this software is designed to be amenable to new geotechnical data, thereby permitting continuous refinement and updating of the algorithms. Selected key functionalities of the software, including the two novel machine learning algorithms, data entry, data visualisation, model calculation, and result and uncertainty visualization, are described. Advantages of the software over some existing techniques are discussed. Notably, this software has already been employed in Singapore for ongoing underground constructions and holds the potential to facilitate various geotechnical engineering applications.

Introduction

In geotechnical engineering, it is widely recognised that subsurface soils and rocks exhibit spatial variability in stratigraphy. However, accurate and reliable characterisation of subsurface stratigraphy, which is of great importance to engineers, is a challenging task due to the highly heterogeneous properties of subsurface stratigraphy. In this work, we present a software developed based on more than 20,000 boreholes sourced from the National Geotechnical Properties Database in Singapore and two novel, in-house developed machine-learning architectures. Key functionalities of the software are described, followed by a brief discussion on its contributions and advantages compared to some existing techniques.

GeoMap

The software, *GeoMap*, was developed at the National University of Singapore and consists of several key features as shown in Fig. 1:

(i) Two machine learning (ML) algorithms: The first algorithm utilises stacking ensemble learning to aggregate multiple geostatic techniques, including the multivariate adaptive regression spline, radial basis function, and kriging and their variants in making predictions (Wang et al., 2023). This algorithm is responsible for predicting individual geological interfaces, such as the soil-rock interfaces, within the software. The second algorithm is developed based on the concept of neighbourhood aggregation (Hu et al., 2024). For a given spatial location, the geological information in the neighbouring spatial locations is aggregated to allow the ML model to learn the consistency between the target spatial location and these neighbours. In the software, this algorithm handles heterogeneous stratigraphy, such as that observed in the Kallang Formation in Singapore. Finally, a geology rule-based algorithm is developed to harmonise the two algorithms.

(ii) Data entry: The software reads Excel spreadsheets following the industry format in Singapore. The National Geotechnical Properties Database, which has been pre-programmed into the software is automatically accessed to enhance sparse input data.

(iii) Data visualisation: Utilising data from more than 20,000 boreholes in Singapore, we have produced comprehensive maps displaying fault lines, folds, boulders, cavities, sandstones, and limestones, as shown in Fig. 1(b). Users can visualise the input data relative to these features for enhanced decision-making.

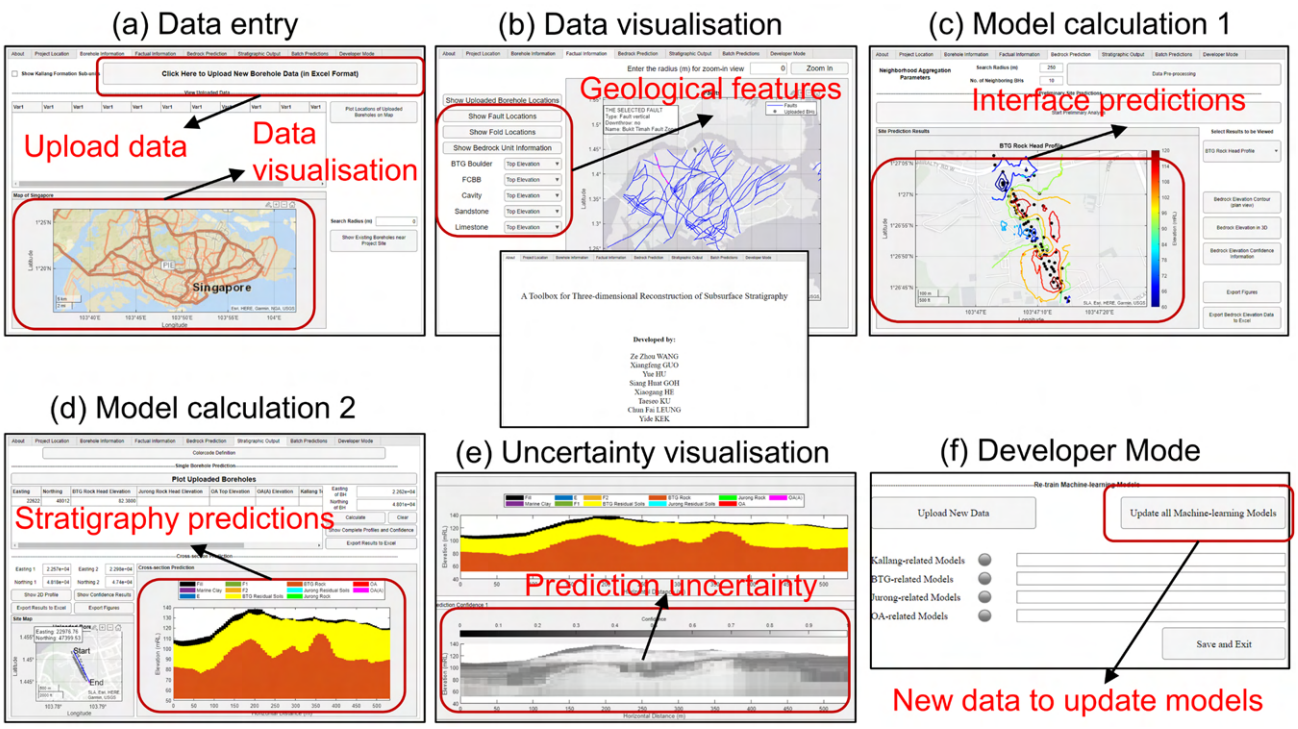

Figure 1. Selected key features of the software.

(iv) Predictions and visualisation: We enable users to predict and visualise both individual stratigraphy interfaces and the full stratigraphy. For example, Fig. 1(c) and (d) respectively show the soil-rock interface predictions and the predicted cross-sectional stratigraphy at a project site in Singapore. Users can visualise both the mean predictions and the associated uncertainties as shown in Fig. 1(e).

(v) Developer mode: Through this advanced feature, users can combine the Singapore Geotechnical Properties Database with their own borehole database to retrain and update all ML algorithms in the software.

Discussion

This software offers several advantages. First, it provides a unified and consistent approach for reconstructing 1D to 3D subsurface stratigraphy. Second, by leveraging a nationwide dataset, predictions made by this software incorporate both site-specific information and generic information, and knowledge transfer across multiple sites with different stratigraphy patterns is permitted. These features represent advancements over some existing techniques (e.g., Li et al., 2016; Gong et al., 2020) that can only handle project-level data and may not be conveniently extended to make predictions in three-dimensional space.

Conclusions

A software developed at the National University of Singapore for data-driven subsurface characterisation is presented. Key advantages of the software are also highlighted. Interested readers can refer to Wang et al. (2023) and Hu et al. (2024) for more information.

References

Gong, W., Zhao, C., Juang, C.H., Tang, H., Wang, H. and Hu, X., 2020. Stratigraphic uncertainty modelling with random field approach. *Computers and Geotechnics*, *125*, p.103681.

Hu, Y., Wang, Z.Z., Guo, X., Kek, H.Y., Ku, T., Goh, S.H., Leung, C.F., Tan, E. and Zhang, Y., 2024. Three-dimensional reconstruction of subsurface stratigraphy using machine learning with neighborhood aggregation. *Engineering Geology*. 107588.

Li, Z., Wang, X., Wang, H. and Liang, R.Y., 2016. Quantifying stratigraphic uncertainties by stochastic simulation techniques based on Markov random field. *Engineering geology*, *201*, pp.106-122.

Wang, Z.Z., Hu, Y., Guo, X., He, X., Kek, H.Y., Ku, T., Goh, S.H. and Leung, C.F., 2023. Predicting geological interfaces using stacking ensemble learning with multi-scale features. *Canadian Geotechnical Journal*, *60*(7), pp.1036-1054.

17th BGA YGES
University of Cambridge
1-3 July, 2024

Digital twin for complex underground infrastructure

Tao Li[1], Harvey J. Burd*[1]

*Correspondence: harvey.burd@eng.ox.ac.uk

[1] *Department of Engineering science, University of Oxford, OX13PJ, UK*

Abstract

The inherent complexity and uncertainty of infrastructure system (IS) calls higher requirements for enhanced decision-making, especially when conventional methods struggle to provide timely and precise suggestions. The ability of Digital Twins (DT) to capture real-time status and provide insightful overview into complex relationships empowers stakeholders to effectively evaluate the performance and expedite the decision-making process. This paper proposes a novel DT implementation workflow from a broad modelling perspective, incorporating adaptive sense, bidirectional connection, modelling, and knowledge graph-based data-model fusion. A multi-scale, multi-stage, and transdisciplinary case study, which comprises of large-scale supported excavation, adjacent subway tunnels, and utility pipelines, demonstrates the effectiveness of proposed modelling method. The results showcase the promising potential of DT in enhancing informed decision-making by effectively addressing the uncertain, complex, and dynamic features of infrastructure.

Introduction

For the highly complex infrastructure systems (IS), where uncertain mechanisms and interactions present new challenges: digitalisation and data-driven digital twins (DT) are seen as a promising way to optimise safety and efficiency of IS management (Naderi and Shojaei, 2023). By employing remote and real-time sensing, close-loop control, and optimised decision, DT offers insight into the actual status and performance of IS (Li et al., 2024). This paper introduces a knowledge graph (KG) based DT modelling method tailored for infrastructure.

Methods

Considering the characteristics of IS, e.g., interactions across disciplines, multi-stages, multi-scale, and heterogeneous data formats (Ramonell et al., 2023), DT modelling incorporates scenario definition, sensor integration, and KG-based data-model fusion. Ontologies are designed to guide the modelling process while ensuring interoperability. The superclass includes scenario (defined as context such as scale, stage, and coordinate system, Fig 1b), virtual entity (comprising attributes of physical entities, Fig 1c, e, f), and relationships (describes interactions and system hierarchy). Given this, DT utilises node-relation-node triples (property graph) as basic elements to create a KG in Neo4j (a graph database). Tags are introduced to identify the domain of ontology classes as show in Fig.1. Lastly, the DT utilises node properties to describe existing physical and data assets, e.g., sensors, data, geometry, and attributes, with metadata serving as contextual identification (Technical attribute in Fig 1f).

Results and discussion

This paper describes the DT of a complex IS, as shown in Fig. 2. It comprises a new 63,805 m^2 and 22 m deep supported excavation, four adjacent existing subway tunnels within 10 m, and six sets of existing utility pipes. Data from sensors, such as ground settlement, excavation progress, tunnel horizontal diameter and settlement, and water levels are collected and integrated into KG, driving the update of the DT.

The performance of tunnel and excavation is tracked as shown in Fig. 1 and 2. KG serves as the information centre to track the status of IS. The excavation began in Sep 2021, significant convergence of the tunnels occurred when zones 2b and 1c were excavated to a depth of -20.3 m in July 2022. Fig. 2 illustrates the convergence caused by the excavation processes. Significant cross section expansion in tunnel A1 and contraction in B1 have been identified, posing potential risks to subway operation. Discrepancies were identified between the original

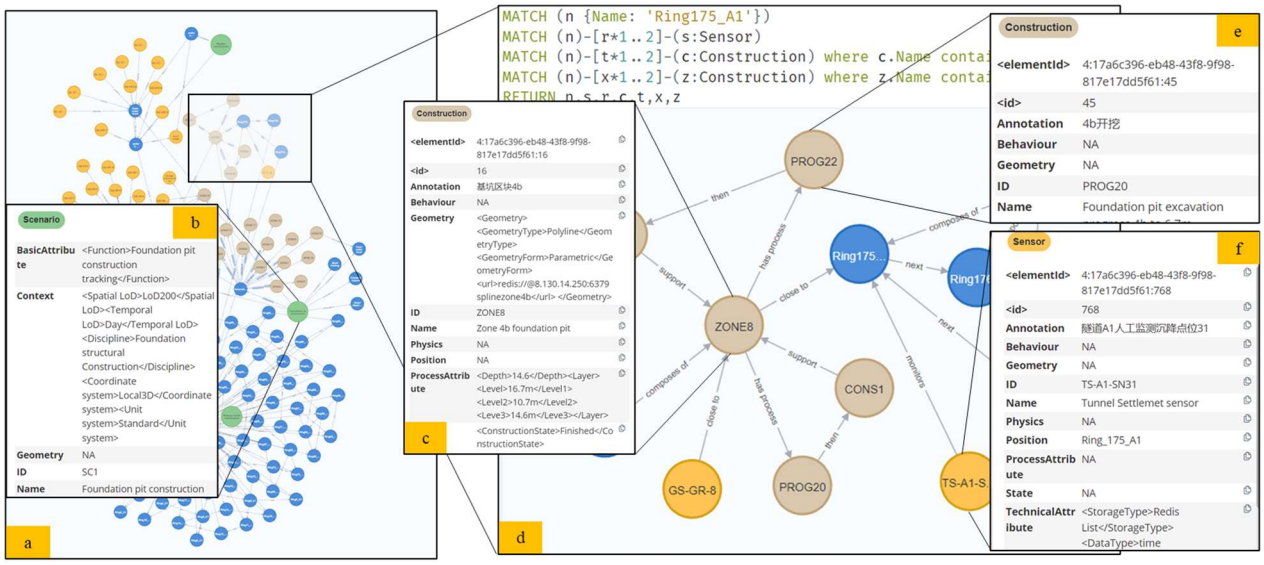

Figure 1. The established knowledge graph for DT of infrastructure system

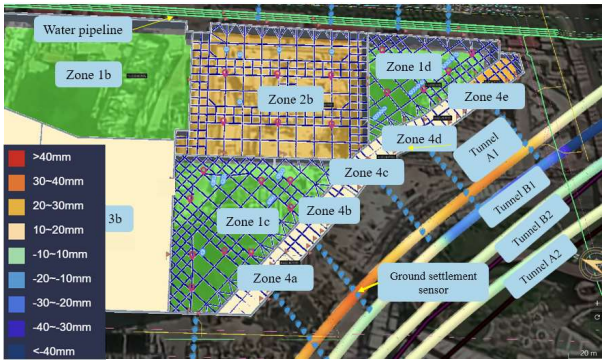

Figure 2. Environmental impact induced by foundation pit excavation on July 15, 2022 (Zone 1c to -20.3 m, the bar shows convergence of tunnel section by mm)

numerical models predicting a 6 mm settlement and the nearly 20 mm settlement observed on site.

In addition to tracking the construction progress, DT enables KG-based reasoning to identify disaster chains and provide corresponding decision-making recommendations. To address the unforeseen hazards identified by DT and to ensure continued safe subway operation, a 200 m long cross-sectional steel frame reinforcement was implemented in tunnel A1. Adjustments to excavation sequence and external pit drainage plans were made to mitigate impacts caused by drainage.

Conclusions

The DT implementation and case study demonstrate significant potential in supporting informed decision-making, particularly under uncertain conditions involving complex interactions in infrastructure management. Further research includes the introduction of rule and artificial intelligence into KG to enhance reasoning and analysing capabilities.

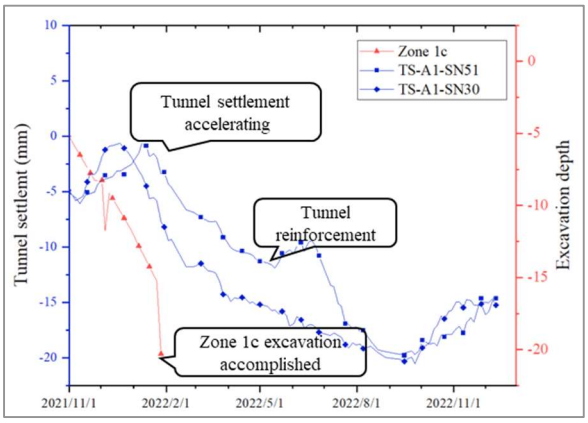

Figure 3. Data of tunnel structural performance extracted from KG

References

Li, T., Li, X., Rui, Y., Ling, J., Zhao, S., Zhu, H., 2024. Digital twin for intelligent tunnel construction. Automation in Construction 158, 105210.

Naderi, H., Shojaei, A., 2023. Digital twinning of civil infrastructures: Current state of model architectures, interoperability solutions, and future prospects. Automation in Construction 149, 104785.

Ramonell, C., Chacón, R., Posada, H., 2023. Knowledge graph-based data integration system for digital twins of built assets. Automation in Construction 156.

Pore network modelling of unsaturated soils: a digital soil twin serving environmental and energy geotechnics

Rasoul Mirghafari[1], Ehsan Nikooee*[2], and Amir Raoof[3], Ghassem Habibagahi[2], Martinus Theodorus van Genuchten[3,4]

*Correspondence: enikooee@shirazu.ac.ir

[1]*School of Engineering, Computing and Mathematics, Oxford Brookes University, Oxford, UK.*
[2]*Department of Civil and Environmental Engineering, Shiraz University, Shiraz, Iran.*
[3]*Department of Earth Sciences, Utrecht University, Utrecht, Netherlands.*
[4]*Department of Nuclear Engineering, Federal University of Rio de Janeiro, Rio de Janeiro, Brazil*

Abstract

Despite advancements in pore network modelling (PNM) in hydrogeology and petroleum engineering, it has been left as an uncovered cosset to the energy and environmental geotechnics communities. Modelling unsaturated soils necessitates detailed information on fluid phases, their interfaces, and capillary pressure, which govern fluid flow and energy transport processes. PNMs can effectively capture soil porous structures and model multiphase flow within unsaturated soils; however, they involve mathematical and geometrical simplifications that may impact the simulations. This study presents recent advancements in PNMs for predicting the thermal and hydraulic properties.

Introduction

The fate and transport of hazardous materials in unsaturated soils, including per- and polyfluoroalkyl substances, microorganisms, and microplastics, are significantly influenced by their interaction with the air-water interface. The specific air-water interfacial area (SAWIA) depends on the capillary pressure and saturation. PNMs capture the structural parameters of the porous skeleton in unsaturated soils (Rostami et al. 2015), enabling the modelling of multiphase flow within soil void spaces. They can be used to predict SAWIAs at various hydraulic branches and estimate soil thermal and hydraulic properties, which are crucial for energy and environmental geotechnics applications (Mirghafari et al., 2024a,b).

Pore Network model generation

PNMs represent the soil's porous structure using a three-dimensional cubic lattice with cylindrical throats and spherical pore bodies. In our study, the PNM is connected to a bottom wetting phase reservoir and a top non-wetting fluid reservoir, with lateral no-flow conditions. Fig. 1 illustrates a schematic of the PNM cross-section.

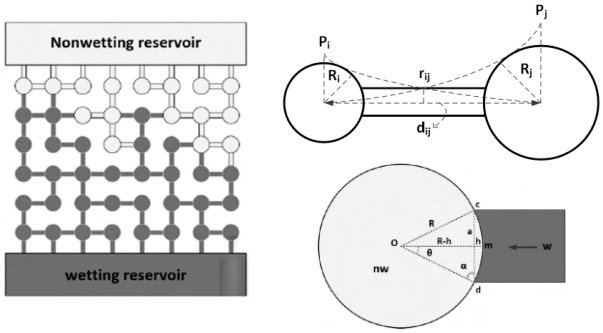

Figure 1. A schematic PNM cross-section (left) and the pore-to-pore connection description (right).

Pore body radii are generated using the lognormal distribution function. The pore size distribution function reads as (Daneshian et al., 2021; Mirghafari et al., 2024a,b):

$$f(x\,|\,\mu,\sigma)=\frac{1}{x\sigma\sqrt{2\pi}}\exp\left(-\frac{(\ln(x)-\mu)^2}{2\sigma^2}\right) \tag{1}$$

where μ is the mean and σ is the standard deviation. The next step is to determine the radius of the throat connecting two pores, as described in Fig. 1

$$\begin{gathered} r'_{ij}=p_i p_j\left(p_i^{(1/n)}+p_j^{(1/n)}\right)^{(-n)} \\ p_i=\frac{R'_i\sin(\pi/4)}{(1-R'_i\cos(\pi/4))^n} \\ p_j=\frac{R'_j\sin(\pi/4)}{(1-R'_j\cos(\pi/4))^n} \\ n>0,\ R'_i=R_i/d_{ij},\ R'_j=R_j/d_{ij},\ r'_{ij}=r_{ij}/d_{ij} \end{gathered} \tag{2}$$

where R_i and R_j denote the radii of two adjacent spherical pores, r_{ij} represents the throat radius, d_{ij} is the pore-to-pore distance, and n is the aspect ratio controlling the throat radius.

Specific air-water interfacial area

To calculate the SAWIA, the air-water interface location is assumed to be at the entrance of an empty pore (see Fig. 1). The curvature of the water meniscus at each suction is calculated as follows:

$$A^{nw} = \pi \left\lfloor (r_{throat})^2 + \left(\frac{r_{throat}}{\sin\theta_e}(1-\cos\theta_e)\right)^2 \right\rfloor$$
$$V_T = \frac{V_V}{n},\ a^{nw} = \frac{\sum A^{nw}}{V_T} \quad (3)$$

where θ_e is the contact angle at an imposed equilibrium suction state, with θ_{rec} and θ_{adv} denoting drying and wetting processes, respectively. The A^{nw} values, to be calculated for all throats, are divided by the total volume V_T to obtain SAWIA, denoted by a^{nw} (Fig. 2).

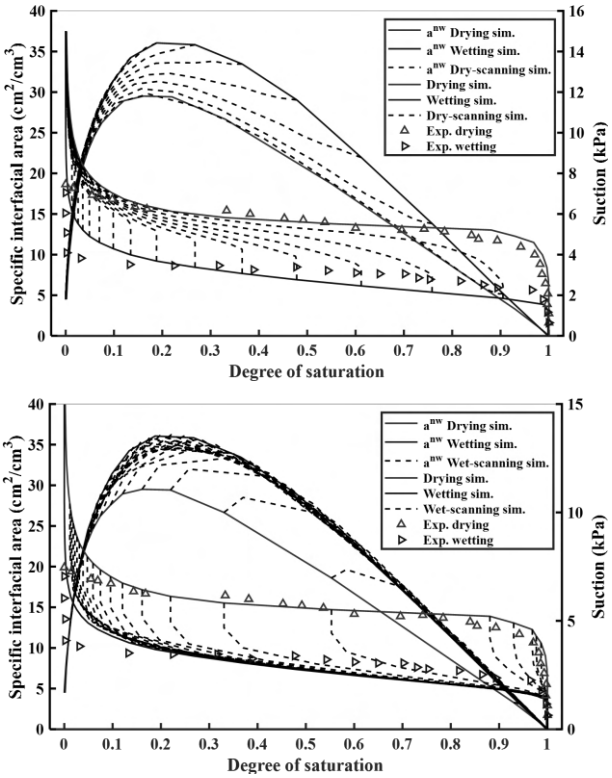

Figure 2. SAWIA results of the soil NEII (dry-scanning at the top and wet-scanning at the bottom); refer to Mirghafari et al. (2024a) for more details.

Soil thermal conductivity drying curve

We next estimate the soil thermal conductivity drying curve (TCDC); Eq. (4) is introduced to calculate the pore scale thermal conductivity (of a soil unit embracing one pore), whose upscaling results in TCDC.

$$\lambda(S) = \left\lfloor \frac{\kappa S}{1+(\kappa-1)S} \right\rfloor (\lambda_{sat} - \lambda_{dry}) + \lambda_{dry},\quad \kappa = 13 \quad (4)$$

where λ_{sat} and λ_{dry} are the fully saturated and dry state thermal conductivity values, and κ is a soil structural parameter having a value of 13 for sandy soils. The average λ derived from local saturations can substantially deviate from the thermal conductivity estimated directly at a single network saturation, indicating the critical role of PNMs in upscaling.

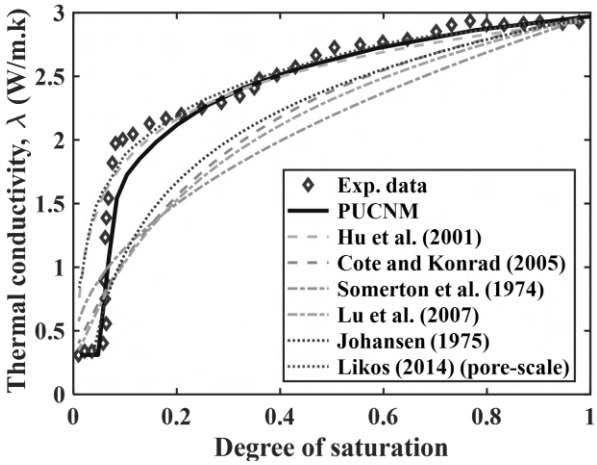

Figure 3. Soil thermal conductivity of the soil 12/20 sand; refer to Mirghafari et al. (2024b) for more details.

References

Mirghafari, R., Nikooee, E., Raoof, A., & Habibagahi, G. 2024a. Determination of a pedotransfer function for specific air–water interfacial area in sandy soils: A pore network-informed multigene genetic programming approach. *Vadose Zone Journal*, **e20352**.

Mirghafari, R., Helforoosh, A. H., Nikooee, E., Habibagahi, G., Raoof, A., & van Genuchten, M. T. 2024b. Pore unit cell network modeling of the thermal conductivity dynamics in unsaturated sandy soils: Unveiling the role of spanning-wetting phase cluster. *Vadose Zone Journal*, **e20350**.

Daneshian, B., Habibagahi, G., & Nikooee, E. 2021. Determination of unsaturated hydraulic conductivity of sandy soils: A new pore network approach. *Acta Geotechnica*, **16**, 449–466.

Rostami, A., Habibagahi, G., Ajdari, M., & Nikooee, E. 2015. Pore network investigation on hysteresis phenomena and influence of stress state on the SWRC. International Journal of Geomechanics, **15**(5), 04014072.

Dynamic behaviour of tree roots during windstorms

V.K. Rugamba*[1], N. Metje[1], M. Sterling[2], and N. Farrelly[3]

*Correspondence: vxr222@student.bham.ac.uk

[1] *National Buried Infrastructure Facility, University of Birmingham, B15 2TT, U.K.*
[2] *Faculty of Science and Engineering, Manchester Metropolitan University, M15 6BH, U.K.*
[3] *Teagasc – the Agriculture and Food Development Authority, H91 TK33 Galway, Ireland*

Abstract

Trees are an important asset in the mitigation of the adverse effects of climate change; they have the potential to sequester carbon from the atmosphere, store it in their biomass and the soil and stabilise the ground, e.g., in slopes. However, recent extreme weather conditions in Europe characterised by large and violent windstorms have caused considerable damage across European forests. Current methods to assess the likelihood of windthrow in trees are limited to visual assessments and empirical models based on relationships of tree height, stem diameter, soil type and wind speed needed to overturn a tree. Limited work has been done to incorporate geotechnical properties such as clay content, moisture content and shear strength of the soil, when determining overturning resistance of trees. As a result, this research will consider *1g* models (1:20 scale) of tree-root systems and test them for their overturning resistance under different soil water and clay contents during dynamic loading.

Introduction

Forests are facing an increased threat from climate change. The study by Schelhaas et al. (2003) found an increase in the volume of annual wood damaged in European forests due to windstorms in the years succeeding 1950. In total, 50% of all tree damage in Europe between 1950-2000 was due to windstorms.

Tree overturning (windthrow, **Figure 1**) is the most common form of tree failure during windstorms and occurs when the total turning moment at the base of the stem exceeds the tree's anchorage strength (Nicoll et al., 2006).

Currently, tree stability can be assessed through a range of observational techniques, e.g., Visual Tree Assessment (Mattheck & Breloer, 1994), which are highly subjective to personal experience and do not sufficiently link tree attributes and soil strength to wind damage. Empirical models relating tree properties such as stem diameter and tree height to critical wind speed needed to cause tree overturning, have also been developed (Scott & Mitchell, 2005). These statistical models, however, do not consider the soil in detail and are location-specific and have limited success for trees in other locations (Gardiner et al., 2008).

Mechanistic models that are based on physics to describe the uprooting process have been developed by Peltola et al. (1999) and Gardiner et al. (2000). Such mechanistic models have benefited from advancements in the understanding of the above-ground tree structure's response to wind loading, however, the below-ground response has not been sufficiently modelled. This is partly due to the inaccessibility of the tree-root-soil system and the interrelation of root and soil properties.

This research aims to improve the understanding of the impact of the clay and water contents of soil and root morphology on the response of shallowly rooted tree roots to dynamic load.

Figure 1. Tree overturned after a windstorm.

Methodology and Future Work

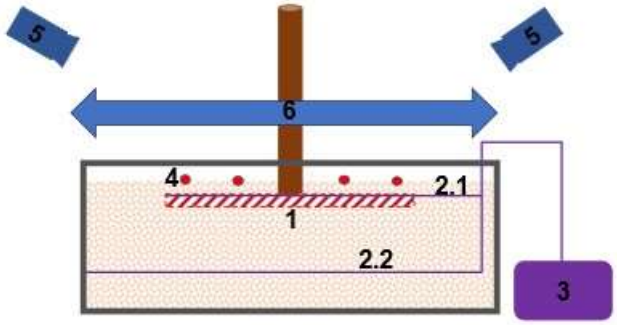

Figure 2. Schematic section view of the proposed methodology, showing **(1)** a 3D printed root model buried in soil, **(2.1)** distributed fibre optic sensors (DFOS) instrumenting the root model, **(2.2)** the soil just below the root model is also instrumented with DFOS and then connected to **(3)** a DFOS interrogator. **(4)** A grid of point targets is placed on the soil-surface above the root model to enable 3D Particle Tracking Velocimetry (PTV) to be conducted using **(5)** two high-speed cameras. **(6)** A linear actuator is attached to the stem slightly above the soil surface with a tension/compression load cell attached and is extended and retracted to mimic wind loading until failure.

Figure 3. Schematic plan view of **(7)** idealised root structures, which will be further defined as the project evolves.

The proposed methodology depicted in **Figure 2** will employ 3D printed shallow root systems using Thermoplastic polyurethane scaled down to 1:20 shown in **Figure 3**. The experiment will be conducted under *1g* conditions. Distributed fibre optic sensors (DFOS) will be used to instrument the dominant leeward and windward sides of the root model; and the soil beneath the root structure placed in a box. Point tracking pins will be placed at the soil surface to cover the area above the root system. Two high-speed cameras will track the motion of the pins and the subsequent soil-surface deformations using 3D Particle Tracking Velocimetry (PTV). A linear actuator attached to the stem will then be extended and retracted to cause an overturning moment in the model root system, which will be measured by the connected load cell.

Soil water and clay contents will be varied to understand their influence on the overturning resistance of the root models. Tree roots in soils with higher water content have been observed to exhibit lower overturning resistance presumably due to a reduction in soil shear strength (Zhang et al., 2022). While tree roots in soils with a high clay content and therefore low permeability, have been observed to fail through soil liquefaction during dynamic loading (Rodgers et al., 2006). Understanding the role that soil water and clay contents play in overturning failure of shallowly rooted trees during dynamic loading will enable foresters to better predict windthrow events and develop modified forest management approaches.

Acknowledgements

The authors would like to thank Teagasc — the Agriculture and Food Development Authority in Ireland and the University of Birmingham, for funding this PhD project.

References

Gardiner, B., Peltola, H., & Kellomäki, S. (2000). Comparison of two models for predicting the critical wind speeds required to damage coniferous trees. Ecological modelling, **129**(1), 1-23.

Gardiner, B., Byrne, K., Hale, S., Kamimura, K., Mitchell, S. J., Peltola, H., & Ruel, J.-C. (2008). A review of mechanistic modelling of wind damage risk to forests. Forestry, **81**(3), 447-463.

Mattheck, C., & Breloer, H. (1994). Field guide for visual tree assessment (VTA). Arboricultural Journal, **18**(1), 1-23.

Nicoll, B. C., Gardiner, B. A., Rayner, B., & Peace, A. J. (2006). Anchorage of coniferous trees in relation to species, soil type, and rooting depth. Canadian Journal of Forest Research, **36**(7), 1871-1883.

Peltola, H., Kellomäki, S., Väisänen, H., & Ikonen, V.-P. (1999). A mechanistic model for assessing the risk of wind and snow damage to single trees and stands of Scots pine, Norway spruce, and birch. Canadian Journal of Forest Research, **29**(6), 647-661.

Rodgers, M., McHale, J., & Mulqueen, J. (2006). Stability of Sitka spruce on mole-drained and ploughed surface water gley soil. Irish forestry.

Schelhaas, M. J., Nabuurs, G. J., & Schuck, A. (2003). Natural disturbances in the European forests in the 19th and 20th centuries. Global Change Biology, **9**(11), 1620-1633.

Scott, R. E., & Mitchell, S. J. (2005). Empirical modelling of windthrow risk in partially harvested stands using tree, neighbourhood, and stand attributes. Forest Ecology and Management, **218**(1), 193-209.

Zhang, X., Knappett, J. A., Leung, A. K., Ciantia, M. O., Liang, T., & Nicoll, B. C. (2022). Centrifuge modelling of root–soil interaction of laterally loaded trees under different loading conditions. Géotechnique, **73**(9), 766-780.

Effect of vegetable fibres on the geo-mechanical properties of soil in Chilean adobe blocks

J. Concha-Riedel*[1], and S. López-Queról[1], and D. Boldrin[2]

*Correspondence: jose.riedel.20@ucl.ac.uk

[1] *University College London, Gower Street London WC1E 6BT, United Kingdom*
[2] *James Hutton Institute, Invergowrie, Dundee DD2 5DA, United Kingdom*

Abstract

This study measured the effect of reinforcement using fodder fibres on the geo-mechanical and biochemical properties of soil used for adobe block manufacture in Chile. The main objective of the research is to observe the role of organic matter, obtained both from the soil and the decay of the fibres, on the mechanical strength parameters of the soil. Results show that the addition of fibres causes a higher friction angle under all tested conditions and that the organic content increases, even though the fibres have already decayed at that stage. This study shows that the organic matter, and its transfer from the fibres, have an important effect on the mechanical strength of soil used in adobe block manufacture.

Introduction

The use of earth as a construction material has a long tradition in human history, spreading since the first civilisations until the 18th century, only to resurface in the last years (Jaquin, 2012). Although spread all over the world, earth construction has very different methodologies and construction techniques depending on the location, and thus should be studied as such (Duarte et al., 2017). Most current research has focused on the effect of small size particles, especially clays, on the mechanical properties of earth bricks and rammed earth. Cohesion and suction are the driving factors on the compressive strength of the material. However, several studies have tested bricks from other parts of the world and showed that little to no amount of clay is present in them, rendering it impossible for cohesion and suction to report such an effect on the blocks (Duarte et al., 2017). The aim of this study is to measure the geo-mechanical properties of soil, used for adobe block manufacture in Chile, with and without reinforcement, and compare the results to the available research.

Methodology

The soil used in this study was collected from an adobe manufacturing pit in Putaendo, Chile, and shipped to London, United Kingdom. Index properties are listed in Table 1, and the organic matter content (OMC) was measured using the loss on ignition (LOI) and thermogravimetric analysis (TGA) techniques. Under the USCS classification, the soil is an ML-SM or OL-SM type.

Table 1. Soil index properties

Property	Measurement	Unit
Sand Fraction	46.08	%
Silt Fraction	43.55	%
Clay Fraction	10.37	%
Liquid Limit	45	%
Plastic Limit	34	%
OMC	9.2	%
Specific Gravity	2.62	Mg/m^3

To assess the effect of fibres, cattle fodder fibres were also shipped from Chile. They were then cut to a length of 10 mm and were mixed with the soil in 0.5 and 2.0% contents per dry weight of soil. Fibres were also tested for tensile strength at 0, 7 and 30 days of decay, which meant leaving the fibres inside a slurry soil sample for those respective periods of time. For each condition, 30 samples were tested. Soil samples were pre-consolidated using a 38 mm consolidometer from a slurry state at 43 kPa and were then tested in a conventional triaxial apparatus, with both axial and radial local instrumentations. After triaxial testing,

some samples were tested for SEM and TGA analysis to observe changes in the soil structure. TGA tests were only performed on the soil matrix avoiding any fibres.

Results and Discussion

Table 2 shows the results obtained for the tensile strength test at different ages of the fibres, placed inside a saturated soil medium. The highest strength (σ_f) is obtained by the 7 days fibres, however, a statistical analysis showed that due to the high variability, there is no evidence to show a significant difference between the mean values. On the other hand, the 30 days condition had a roughly 60% reduction. A similar effect was observed for the Young modulus (E_f), where dry and 7 days fibres have no statistical difference, but 30 days samples have the lowest value (47% reduction). The failure strain (ε_f) had no statistical difference for any treatment and was roughly 1%.

Table 2. Fibre tensile strength results

Condition	E_f GPa	σ_f MPa	ε_f %
Dry	3.27±1.33	31.80±15.54	1.03±0.44
7 Days	2.71±1.03	34.46±9.68	1.33±0.40
30 Days	1.74±1.20	13.35±5.66	0.97±0.51

Triaxial tests on the soil, with and without reinforcement, showed a strain hardening behaviour, without any evident peaks. The critical state was reached after 15, 25 and 30% of axial strain for 0, 0.5 and 2% reinforcement respectively. Table 3 shows the strength parameters at the critical state of the soil, from which the highest value was obtained by the 2% reinforced sample. Not much difference was observed between the 0 and 0.5% samples, although there is a slight increment. It is worth mentioning that at the time of shearing, all samples were at least 25 days old, which is comparable with the 30 day old fibre condition.

Table 3. Soil strength parameters

Sample	ϕ_{cr}°	M
0%	39.00	1.59
0.5%	39.93	1.63
2%	46.15	1.90

TGA tests performed at the end of the triaxial tests showed an OMC increase of 0.62 and 3.13% for the 0.5 and 2% samples, whereas SEM images showed a complete decomposition of the fibres into the soil matrix.

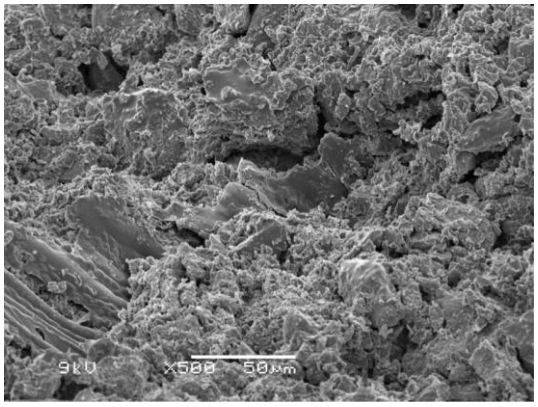

Figure 1. SEM image from 2% sample after shearing

Conclusions and Future Work

This study showed the effect of fibres on the geo-mechanical properties of Chilean soil used in the production of adobe blocks. Tensile strength results showed that 30-day fibres have a reduction in strength of approximately 60% when compared to dry fibres, which leaves them in a similar range as the strength of soil matrices. It was also observed that the fibres increase the friction angle of the soil, however, no cohesion increase was recorded. This effect was attributed not only to the mechanical friction but also to organic matter decomposed from the fibres, as TGA measurements showed an increase in OMC. Future tests contemplate the measurement of suction during shearing, to assess its effect in the shear strength of the soil.

Acknowledgements

The authors thank the Chilean National Agency for Research and Development (ANID) / Scholarship Program / DOCTORADO BECAS CHILE / 2020 – 72210077 for the founding of this research.

References

Duarte, I., Pedro, E., Varum, H., Mirão, J., & Pinho, A. 2017. Soil mineralogical composition effects on the durability of adobe blocks from the Huambo region, Angola. *Bulletin of Engineering Geology and the Environment*, *76*(1), 125–132.

Jaquin, P. 2012. History of earth building techniques. *Modern Earth Buildings: Materials, Engineering, Constructions and Applications*, 307–323.

Quantification of 3D Particle Morphologies of Crushed Glass and Sand and Their Application in Discrete Element Method (DEM) Simulations

X.R.Zhang*[1] and Y.P.Cheng[2]

*Correspondence: xinran.zhang.20@ucl.ac.uk

[1]*PhD student (Department of Civil, Environmental and Geomatic Engineering, University College London, London WC1E 6BT, UK)*
[2]*Associate professor (Department of Civil, Environmental and Geomatic Engineering, University College London, London WC1E 6BT, UK)*

Abstract

Developing sustainable and cost-effective alternatives to construction sand has become necessary due to rising costs and dwindling reserves. Waste glass is a derivative of natural sand and has the potential to exhibit similar geotechnical behaviour. This study first investigated the morphology of natural sand (NS) and crushed waste glass (CWG) using X-ray computed tomography scans. Morphological analysis shows that NS particles are more rounded, while the shape variability of small-sized CWGs is greater. The 3D images provided by the scans were simplified and imported into PDC3D for modelling. These models are then used in the simulation of direct shear tests to discuss the shear behaviour of materials at the microscale based on real particle morphology and gradation.

Background

In recent decades, the heavy use of natural aggregates and their overexploitation have led to environmental damage and sand shortages. For this situation, it is important to develop sustainable natural aggregate alternatives (Ismail *et al*., 2013). Crush wasted glass (CWG) is a potential substitute for natural sand in geotechnical construction due to its similar chemical composition and specific gravity to sand (Arulrajah *et al*., 2012).

Kazmi *et al.*, (2021) conducted pure material direct shear tests on CWG and natural sand (NS) under dry conditions. Experimental results show that CWG with medium particle size range (0.6–2 mm) is similar to natural sand (NS) in shear strength behaviour.

Based on the above research results, this study will further conduct a detailed 3D morphological analysis of the test materials through X ray CT scanning, and use the discrete element method to simulate the mechanical behaviour from the microscopic scale.

Material and Methodology

This study used natural sand (NS) from Pine River Beach, Queensland, Australia, and crushed wasted glass (CWG) from commercial supplier Enviro sand in Brisbane.

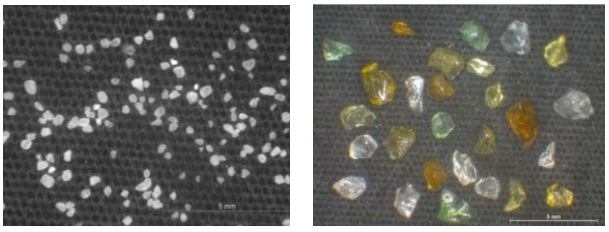

(a) (b)

Figure 1: (a) Micrograph of NS particles; (b) Micrograph of CWG particles (Kazmi *et al*., 2021)

In this study, a sieving machine was used to classify CWG samples into five different size ranges: <0.6mm, 0.6-1.18mm, 1.18-2mm, 2-3.35mm, and >3.35mm.

X-ray CT scans were performed on these samples. AVIZO software was used to process the obtained high-resolution 2D slice images, extract the morphology of individual particles, generate the stl. file of the particles, and obtain the particle size data (Zheng *et al*, 2020). The elongation (EL), flatness (FL) and

sphericity, (S) of the particles are calculated based on Eq.(1)-Eq.(3).

$$EL = \frac{Breadth}{Length} \quad (1)$$

$$FL = \frac{Width}{Breadth} \quad (2)$$

$$S = \sqrt[3]{\frac{36\pi V^2}{A^3}} \quad (3)$$

The spherical harmonics method was used to simplify the particle surface mesh. This method could reconstruct smooth continuous triangular surface meshes and reproduce the irregular shapes and surface textures of particle morphology (Zhou *et al*., 2014). Then, import the new stl. file into PFC3D as the geometry of clump or rblock.

Finally, based on the pure material direct shear experiment (Kazmi *et al*., 2021), the experiment will be simulated and calibrated by considering the realistic shape and gradation of the samples.

Results

For morphological analysis, small-sized CWG samples exhibit significantly smaller elongation, flatness, and greater variability. NS particles are more rounded.

For 3D modelling, five particles were selected for each sample that could represent the morphological characteristics, such as Fig. 2. Adjusting the built-in parameters, a series of 3D models were built, as shown in Fig. 3.

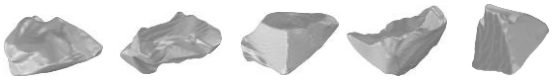

Figure 2: Five selected particles for CWG 0.6-1.18mm

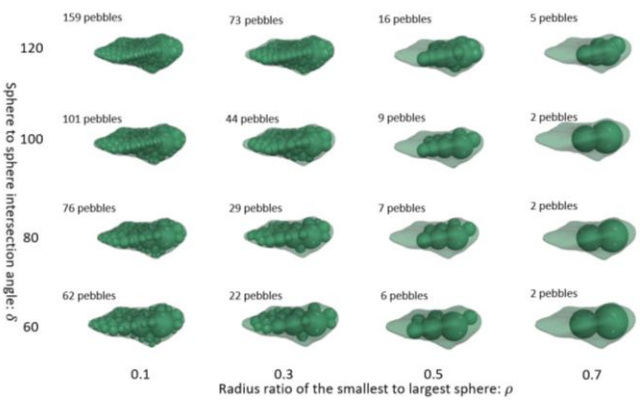

Figure 3: Comparison of clump template and geometry under different built-in parameters

The simulation and calibration of the direct shear test are still in progress, Will be discussed after calibration.

Future Work

The study will also include the use of CWG as a sustainable alternative to NS for use as granular column backfill. Future studies include modelling the shear strength behaviour of kaolin reinforced with CWG columns in different size ranges. By integrating computational modelling techniques with experimental results, further research will be conducted on the impact of using CWG as a composite material on its performance in practical engineering applications. This helps provide sensible, environmentally friendly and cost-effective solutions and also contributes to the wider use of recycled materials in civil engineering projects.

References

Arulrajah, A., Ali, M., Disfani, M., Piratheepan, J., Bo, M., 2012. Geotechnical performance of recycled glass-waste rock blends in footpath bases. J. Mater. Civ.Eng. **25** (5): 653-661.

Ismail, S., Hoe, K. W., & Ramli, M., 2013, Sustainable aggregates: The potential and challenge for natural resources conservation. AicQoL 2013 Langkawi AMER International Conference on Quality of Life "*Quality of Life in the Built and Natural Environment*", Procedia-Spcial and Behavioral Sciences **101**: 101-109.

Kazmi, D., Serati, M., Williams, D. J., Qasim, S., and Cheng, Y. P. 2021. The potential use of crushed waste glass as a sustainable alternative to natural and manufactured sand in geotechnical applications. *Journal of Cleaner Production* **284** 124762.

Zheng, W., Hu, X. and Tannant, D. D. 2020. Shape Characterization of Fragmented Sand Grains via X-Ray Computed Tomography Imaging. *International Journal of Geomechanics* **20** 04020003.

Zhou, B., Wang, J., and Zhao, B. 2014. Micromorphology characterization and reconstruction of sand particles using micro X-ray tomography and spherical harmonics. Engineering Geology **184**: 126–137.

The contact behaviour of railway ballast particles under different normal loading conditions

Aziz U Hakimi[1],

*Correspondence: aziz.hakimi.20@ucl.ac.uk

[1] *University College London, WC1E 6BT, UK)*

Abstract

The micromechanical behaviour of basalt ballasts was investigated by subjecting them to normal loading under varying loads. Notably, when responding to a low normal load, natural ballast particle pairs exhibit a softer response than predicted by Hertz's theory (1882). Additionally, roughness measurements before and after testing reveal that asperities undergo plastic deformation and the contact area is increasing as the load increases.

Introduction

Incentives to reduce maintenance of railway ballast has underscored the need for fundamental research into their behaviour. Ballast, composed of discrete particles, has been a subject of study using the Discrete Element Method (DEM), in which recent advancements involve incorporating more realistic ballast shapes into simulations (e.g., Tolomeo & McDowell, 2022). However, experimental evidence suggests that the contact laws used in DEM may not accurately represent ballast behaviour, especially for certain types of granitic ballast (e.g., Wong et al., 2019; Altuhafi et al., 2023).

This paper presents unique experimental data obtained from pairs of basalt ballast sourced from Australia. These ballast samples were subjected to normal loading in a bespoke particle-to-particle apparatus. The insights gained from this research will inform discrete element modellers, enabling them to enhance existing numerical models. Specifically, hence, we explore the normal load-displacement response and the evolution of particle surface roughness.

Methodology

Innovative experimental methods were employed to investigate the micro-mechanical behavior, utilising the inter-particle apparatus developed at UCL (Wong et al., 2019). Loading was applied in three orthogonal directions, with 0.01-0.02 N accuracy, while deformations were monitored using transducers with an accuracy of approximately 10^{-2} µm. The experiments were carried out on pairs of basalt railway ballast particles with a natural angular to flat contact, where the apex of the natural ballast serving as the contact point (Figure 1). Normal loading was controlled by load and by force displacement to move slowly and avoid breaking the asperities. The top and bottom particles were also examined using optical microscopy. This examination took place both before and after the test. The focus was on assessing the roughness within the contact area. To achieve this, a technique called z-stacking was employed, with the thickness of slices equal to 6 µm.

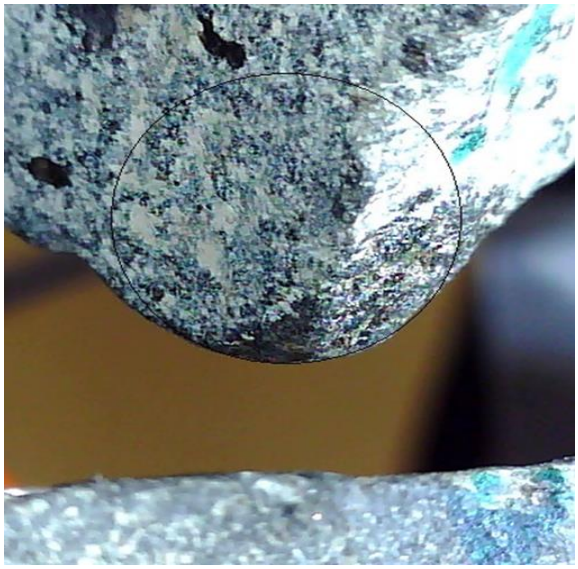

Figure.1 A natural angular to flat contact of Basalt ballast particles before the test

The measurements were performed using optical microscopy (Stereo-Discovery V8 microscope by Zeiss) with an accuracy of 0.63 µm, at a magnification of 80, covering a total viewing area of 1.62 mm x 1.34 mm which was kept

the same for all measurements, as shown in Figure 2 .

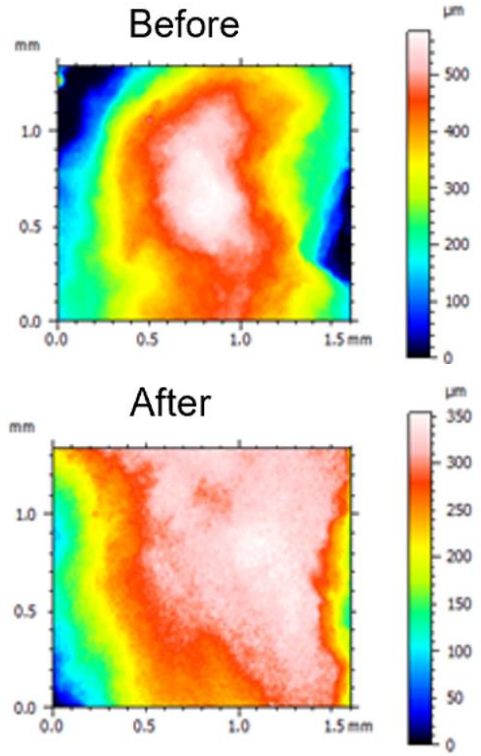

Figure 2. Surface analysis before and after normal loading (angular top particle, 100N)

Surface characteristics were analysed using ConfoMap7 software (Mountains 7), providing a detailed examination of topography, including fractal and peak analyses. The fractal dimension (Df), indicating asperity frequency, was determined using boxing method. Root-mean-square roughness (Sq) was calculated after applying noise and form removal filters. Changes in surface roughness during normal testing were evaluated by correlating the apex of angular particles with the contact area against the flatter surface.

Results and Discussion

In the monotonic normal loading, the load-displacement response of the contact is initially soft (0.01-0.5 N/μm) and with increase in the load, response gets stiffer (5-10 N/μm). This behaviour is often attributed to increase in true area of contact; however, the experimental response does not follow existing models such as Hertz (1882), Modified Hertz (Yimsiri and Soga, 2001) here called RMS (Figure 3). It is worth noting that observable deformation of the bulk is negligible in comparison to deformation of the contact asperities. The measurements of the surface roughness suggest that S_q decreases during normal loading, which was attributed to flattening of the asperities. The value of D_f nonetheless was found to increase, indicative of a more irregular surface, suggesting that the peak count might have increased while the height of the peaks decreased.

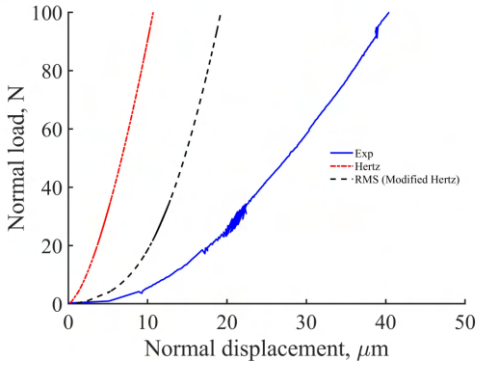

Figure 3. Comparison of experimental and predicted normal loading data

Conclusion

Basalt ballast subjected to normal loading shows a softer behaviour than that predicted by Hertz and modified Hertz, as was found in previous work on granitic ballast. Roughness measurements before and after testing reveal that asperities undergo plastic deformation during normal compression.

References

Altuhafi, F.N., Baudet, B.A. & Coop, M.R. (2023). An investigation of the applicability of contact models to the normal load-deflection behaviour of artificially shaped granite. Acta Geotechnica [doi 10.1007/s11440-023-02123-9].

Tolomeo, M. & McDowell, G.R. (2022). Modelling real particle shape in DEM: a comparison of two methods with application to railway ballast. International Journal of Rock Mechanics and Mining Sciences 159.

Wong, C.P.Y., Boorman, B. & Coop, M. R. (2019). The construction and commissioning of a new inter-particle loading apparatus for the micromechanical behaviour of railway ballast. In Atlanta, USA, IS Atlanta 2018, a symposium on geomechanics from micro to macro in research and practice.

Evolution of clay microstructure

R. Tiwari*[1]

*Correspondence: rishabh.tiwari.21@ucl.ac.uk

[1] *Ph.D Student (University College London, WC1E6BT, United Kingdom)*

Abstract

The evolution of clay micro-structure has been studied by many researchers to develop an understanding about microstructural response to macroscale mechanical loading. With the advancement in modern microstructural observation techniques and microstructure based constitutive models, the microstructural characterisation of soils is a way forward for interpreting soil behaviour. The details of these techniques, their advantages, and limitations must be studied to perform precise studies.

Introduction

Micro, size below 2 nm and mesostructural, between 2 and 50 nm, studies are increasingly used to improve understanding of the macroscopic behaviour and physical properties of compacted and natural soils, micropores are pores of size below 2 nm; mesopores have sizes and macropores have sizes greater than 50 nm. Microstructural studies involve the use of techniques at particle aggregation scale (<100 μm) to analyse the arrangement and distribution of particles, particle assemblies, micropores-macropores and their contacts and connectivity in different soils (Collins and McGowan 1974; Delage and Lefebvre 1984; Mitchell and Soga 2005). The increasing use of microstructural studies have led to improved techniques and their interpretations.

The microstructure of soil is the fundamental key to resolving many unexplained behaviours of soil, but it is challenging to examine during loading. Typically, microstructure analyses are done at specific states, on samples retrieved from the loading tests (Delage and Lefebvre, 1984). The mechanical testing typically involves the specimen consolidation with or without shearing in oedometer and triaxial testing system. After test completion, the specimen is carefully unmounted and preserved small soil samples (about 1 cm^3) are then freeze-dried to retain the soil structure as scanning electron microscopy (SEM) and the mercury intrusion porosimetry (MIP) are some of the techniques that require the use of thoroughly dried samples. A standard air or oven-drying is not convenient for high water content clays due to significant volume shrinkage. Therefore, other methods like critical-point-drying and freeze-drying are used. The freeze-drying method, also known as lyophilization, introduced by (Delage *et al*., 1984), is applied to dehydrate samples. The microscopic testing can involve the analysis on SEM, gas adsorption technique, MIP, transmission electron microscopy (TEM) and X-ray microtomography (XR-μCT). The physical observations and interpretations are carried out to analyse such as particles and micropore microstructure from the microscopic images. The final stage of the analysis is the interpretation of post-processed results. This projects focuses on microporosity. The voids are classified as interparticle intraparticle and interlayer voids. The size and orientation of the pores are extracted by post-processing the outcomes to get the final results in analysing variation in parameters like: pore size distribution, pore orientation, aspect ratio, coefficient of compression, void ratio and coefficient of uniformity and specific volume subjected to different stress path and initial state.

Methodology

The scanning electron microscope, SEM is a direct method for observing soil microstructures from aggregate scales down to particle scales or even smaller. Images of a soil sample are obtained by scanning the surface with a focused electron beam. The primary electrons interact with the sample, producing various signals containing information about the surface's topography and composition. Combined with the image processing method, this technique allows for quantitatively characterizing pore

morphology, void ratio, and soil pore size distribution. The SEM-based image analysis method can measure soil pores of size 0.1–100 μm as shown in Fig.1. In MIP analysis a non-wetting fluid is forced to ingress porous medium placed into a vacuum by being submitted to increasing pressure. During this test, mercury pressure is very progressively increased by steps to let mercury intrude each pore that correspond to the applied pressure step. The equation Eq.(1). (Washburn, 1921) applies to pores of cylindrical shape and parallel infinite plates (fissure-like microstructure) here σ_{Hg} is the surface tension of mercury, θ_{nw} the contact angle between mercury and the pore wall, (σ_{Hg} = 0.484 N/m at 25°C and θ_{nw} = 147°) (Diamond, 1970) and x the entrance pore diameter.

A well-known limitation of MIP is that the pore volumes of ink-bottle pores that have an entrance radius smaller than their real radius are qualified by the smaller radius of the pore access. (Delage et al., 1984) described after releasing pressure, the volume of mercury remaining inside the sample corresponds to entrapped porosity. They found that in sensitive clay the compression is due to the large inter-aggregate pores collapsing orderly. Small pore sizes require higher mercury pressures to be intruded, but generally, the mercury pressure used for MIP has an upper limit of 210 MPa. Therefore, some intra-aggregate pores below 5 nm, cannot be detected and gas adsorption maybe used. Using scans from the SEM, XR-μCT, TEM, interpretation requires image processing steps: a) pre-processing, b) thresholding, c) separation, d) ellipses fitting shown in Fig.2. and Fig.3. sometimes the micropore shape and orientation are investigated.

Conclusion

Commonly used analysis techniques involving SEM and MIP can provide reasonably accurate results for studying micromechanics of clayey soil within their range of applicability in terms of the pore size distribution (PSD) and orientation analysis.

Using those techniques, variations of PSD and orientation with stress state of soil under different conditions of drainage can be analysed and compared. Observations can provide an insight in the physical laws governing micro-macro relationships.

Equations

$$p = -\frac{n\sigma_{\mathrm{Hg}}\cos\theta_{\mathrm{nwx}}}{x} \qquad (1)$$

Figures

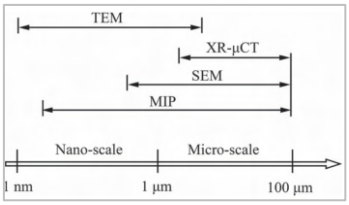

Figure 1. Pore scale Gao *et al*., (2020)

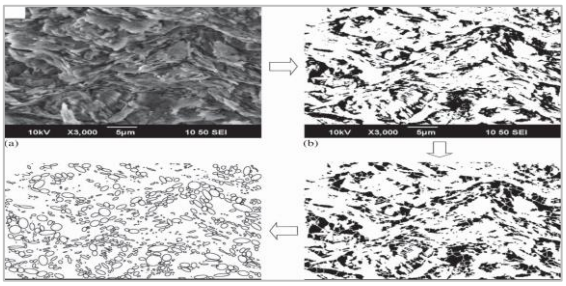

Figure 2. Analysis using image rostering technique (Gao *et al*., 2020)

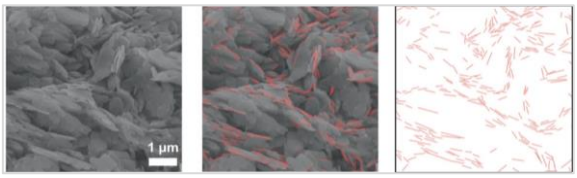

Figure 3. Hand tracing method (Gao *et al*., 2020)

References

Collins, K. and A. McGown 1974. *The form and function of microfabric features in a variety of natural soils.* Géotechnique. **24**(2): 223-254.

Delage, P. and G. Lefebvre 1984. *Study of the structure of a sensitive Champlain clay and of its evolution during consolidation.* Canadian Geotechnical Journal. **21**(1): 21-35.

Diamond, S. 1970. *Pore Size Distributions in Clays.* Clays and Clay Minerals. **18**(1): 7-23.

Gao, Q.-F., et al. 2020 *Microstructural organization of remoulded clays in relation with dilatancy/contractancy phenomena.* Acta Geotechnica. **15**(1): 223-243

Mitchell, J.K. and K. Soga 2005. *Fundamentals of soil behavior*. Vol. 3.: John Wiley & Sons New York.

Washburn, E.W. 1921. *The Dynamics of Capillary Flow.* Physical Review. **17**(3): 273-283.

A DEM model of hydrate bearing sediments in the South China Sea with carbonate sand and silt mixtures

Huajie Guo[1]*, Yi Pik Cheng[1], Yuedong Wu[2] Yuzhe Ren[2], Yan Qian[2], Abraham Chung Fai Chiu[3]

*Correspondence: uceshg1@ucl.ac.uk, +44-7902311610
[1] *UCL (UCL, Gower St, London WC1E 6BT, UK)*
[2] *Key Laboratory of Ministry of Education for Geomechanics and Embankment Engineering, Hohai University, Nanjing 210098, China*
[3]*Guangdong Engineering centre for structure safety and health monitoring, Shantou University, Shantou 515063, China.*

Abstract

High gas hydrate content has been found in the fine-grained sediments containing substantial amount of foraminifera in the South China sea. One of the possible hydrate accumulation habits is filling the intra- particle voids in the carbonate sand (CS) particles. To understand the mechanical behaviour of these hydrate bearing fine-grained dominated sediments, a particle-based model of hydrate bearing sediments of the CS-silt mixtures has been created using the discrete element Method (DEM) in this study. Realistic particle shape and correct amount of internal void of the CS particles were simulated using the Itasca PFC3D before adding the fines particles and hydrate particles. This should mimic hydrate formation and growth in the intra-particle voids before calibrating with laboratory testing data.

1. Introduction

Gas hydrates, primarily methane trapped in water molecule cages, form under low temperature and high pressure in deep ocean areas. Past explorations in the South China Sea showed that hydrates are abundant in fine sediments rich in foraminifera: tiny carbonate-shelled organisms. This suggests that hydrates may grow from intra- and inter-particle pores, very different from typical formations in coarse-grained soils (Wang et al, 2011; Liu et al, 2012). CS also differs from silica sand due to variations in particle shape, mineral composition, and structure. The micromechanical impact of hydrate distributions on stiffness and strength of carbonate sand-silt mixtures will be explored.

2. Materials from Laboratory Tests

To ensure consistency between the numerical study and laboratory tests, this study includes data from Hohai University (Ma et al, 2021; Ren et al., 2022). Figure 1 shows the particle size distribution (PSD) for CS and silt, along with PSDs from South China Sea samples (Liu et al., 2012). The tested CS was marine sediment, and the fines were crushed quartz from a quarry. The CS is uniformly graded sand with grain size d_{50} of 0.75 mm, and the fines are smaller than 75 μm. X-ray computed tomography (CT) scans revealed three types of carbonate particles: solid, coral, and spiral. Their average internal void ratios are 0.035, 0.175, and 0.605, respectively.

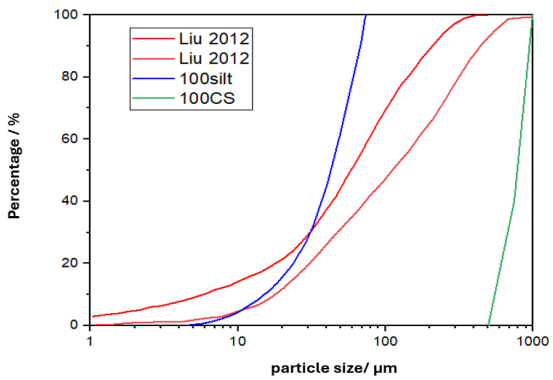

Figure 1. particle size distribution CS, silt (Ma et al 2021) and sediment sample from SCS (Liu et al 2012)

3. Numerical simulation process

3.1 Carbonate sand models with realistic shapes

Numerical cubical sample was created using the DEM PFC3D program to simulate carbonate sand with realistic shapes, inspired by the methodology of Dong et al. (2024). Sixty carbonate sand particles, representing three different types, were selected and scanned with a Nikon 3D X-ray CT scanner. The scanned files were saved in STL format. An improved subdivision method was developed to handle complex particle shapes, as shown in Fig. 2. The process involves Voronoi subdivision using Neper, importing particle surface into PFC 3D 7.0, filling surface with balls of various radii to create rblocks, and finally cutting each rblock to match particle shape profile.

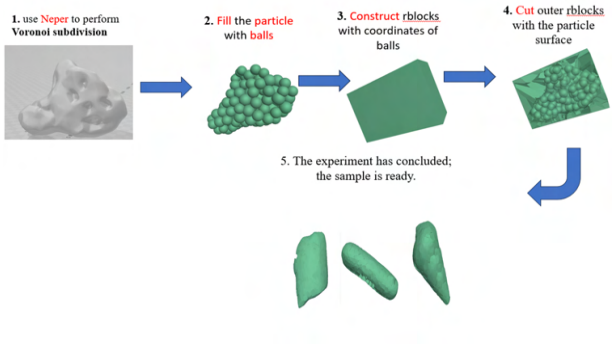

Figure 2 Creation of a realistic CS particle model.

3.2 Isotropic and true triaxial loadings

Two synthetic samples were used by Brugada et al.(2010), 'hydrate + soil' and 'hydrate → soil'. The first involves mixing hydrates directly with soil and then consolidating, while the second consolidates the soil first, then introduces methane to form hydrates. This study uses the 'hydrate → soil' method for its closer resemblance to natural formation.

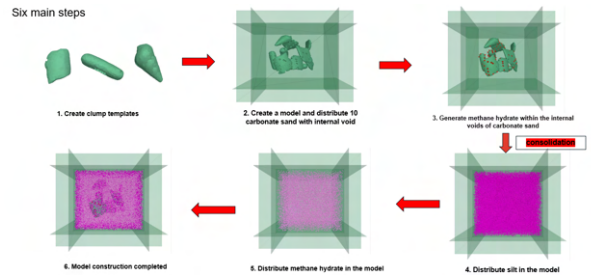

Figure 3. DEM sample preparation procedure of the hydrate-bearing CS and silt mixture.

As can been seen from the figure 3. Initial model creation procedure involves: 1) creating clump templates for carbonate sand (CS) particles; 2) generating a model with 10 CS particles with voids; 3) synthesizing methane hydrate particles in intra-particles voids; 4) distributing silt around CS particles and consolidating the sample; 5) synthesizing hydrate to inter-particles voids; and 6) completing the model construction.

4 . Conclusion and further works

In this study, the Discrete Element Method (DEM) was adopted to simulate carbonate sand (CS) and silt mixtures with plan to add various percentages of hydrate particles later. Three materials were modelled: CS particles, silt particles, and hydrate particles. An average internal void ratio of 0.2 was adopted for CS particles. The initial DEM model for CS was based on typical shapes. For efficiency, silt and hydrate particles were assumed spherical. Future simulations will add different amount of hydrate particles in the mixture before triaxial compression and shearing to investigate how different hydrate morphologies affect the mechanical behavior of hydrate-bearing sediments.

References

Brugada, J., Cheng, Y. P., Soga, K., and Santamarina, J. C. (2010). Discrete element modelling of geomechanical behaviour of methane hydrate soils with pore-filling hydrate distribution, *Granular Matter*, 2010, vol. 12, no. 5, pp. 517-525.

Dong, Z., Cheng, Y. P., Tong, C.*, Liu, H., Zhang, S., & Sheng, D. (2024). DEM simulation of single particle crushing of carbonate particles. *Powder Technology* (under review).

Liu, C. *et al.* (2012) 'The characteristics of gas hydrates recovered from shenhu area in the South China Sea', *Marine Geology*, 307–310, pp. 22–27.

Ma, L., Chiu, C.F., Cheng, Y.P., Ren, Y.Z. (2021). 'Effects of particle breakage on the compression behaviour of gap graded carbonate sand–silt mixtures', *Géotechnique Letters*, 11(1), pp. 1–17.

Ren, Y. *et al*. (2022) 'Shear modulus of a carbonate sand–silt mixture with THF hydrate', Journal of Marine Science and Engineering, 10(10), p. 1519.

Wang, X., Hutchinson, D.,R., Wu, S., Yang S., Guo Y. (2011) Elevated gas hydrate saturation within silt and silty clay sediments in the shenhu area, south

china sea. J. Geophy. Res.: Solid Earth 116, B05102.

Contact behaviour of lentils under normal loading

S. Singh*[1], B.A. Baudet[1], and M.R. Coop[1]

*Correspondence: saurabh-singh@ucl.ac.uk

[1] *University College London, London WC1E 6BT, UK*

Abstract

A set of experiments was performed to understand the particle and contact behaviour of lentil particles. This study was conducted in conjunction with an in-situ X-ray computed tomography study on lentils subjected to a conventional triaxial compression stress path, performed by Pinzon et al, 2023. The primary objective was to develop a comprehensive dataset on a model granular material to calibrate discrete element simulation algorithms. Two types of particle-scale tests were performed: single particle crushing tests and inter-particle contact behaviour tests. Lentils have a thin outer cover (shell) and a strong inner core. The shell exhibits a linear load-displacement response, while the core follows a power law relationship in load-displacement. The shell has low stiffness and ruptures under very small loads, whereas the stiffness of the core increases with load.

Introduction

Traditionally, granular materials have been studied as a continuum, ignoring their particulate nature. To accommodate newly discovered experimental behaviours, continuum-based constitutive models for granular materials have become increasingly complex and cumbersome to use in engineering design. Discrete element simulations offer an alternative that leverages the particulate nature of the materials (Tolomeo & McDowell, 2023). The objective of this study is to provide particle- and contact-level insights into the micromechanical behaviour of lentils.

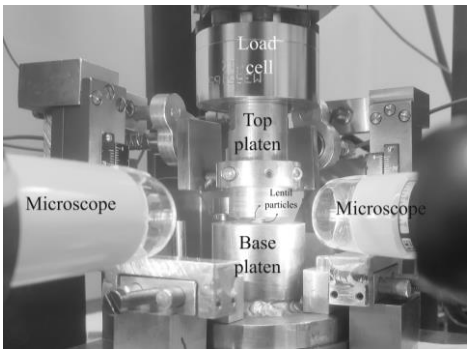

Figure 1. Inter-particle test on lentils

Material tested, experimental equipment and specimen preparation

Oblate (ellipsoidal) lentil particles were studied for single particle crushing and inter-particle contact behaviour. On average, lentil particles have a major/intermediate diameter of 6.30 mm and a minor diameter of 2.40 mm. The outer cover of the lentil (shell) has an average thickness of 65 µm.

The inter-particle apparatus (Fig. 1), equipped with three linear actuators (along a vertical and two orthogonal horizontal directions), three capacitive displacement transducers, and three load cells, was used to carry out the particle-particle and single particle tests. Details of the inter-particle test can be found in Wong & Coop, 2023.

In the inter-particle test, lentil particles were glued on the top and base platen using standard Araldite epoxy resin and hardener. The particles were then kept under a load of 5 N for 12 hours to set on the platen. The platens were then screwed into the apparatus, and both particles were brought into proximity to start the test. To bring the particles into contact, the vertical arm of the apparatus was moved downward at a speed of 0.05 mm per hour.

In the single particle crushing test, the particle was placed between the platens, and the vertical arm was brought down at a speed of 1.2 mm per hour. The vertical and horizontal loads, along with the corresponding displacement, were recorded for analysis.

Result

Fig. 2 and Fig. 3 present the response of lentil in crushing and inter-particle test, respectively.

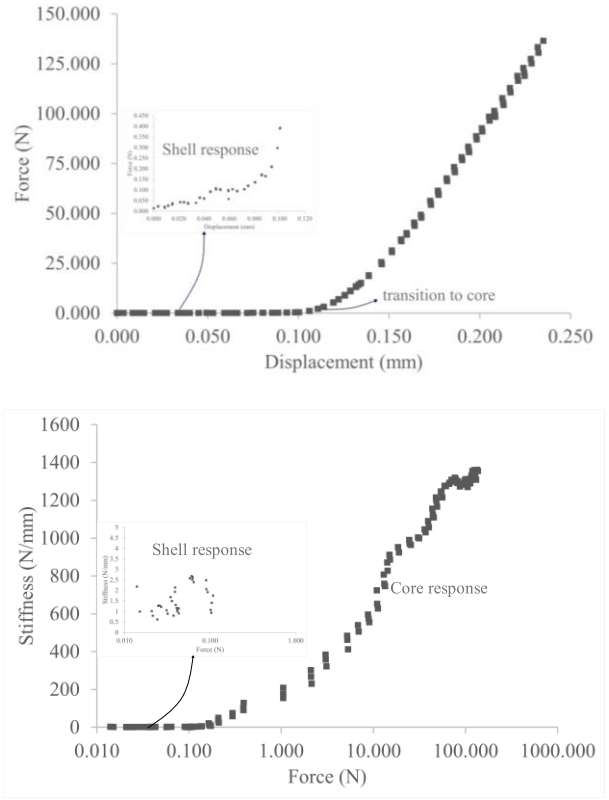

Figure 2. Response of a lentil in crushing test

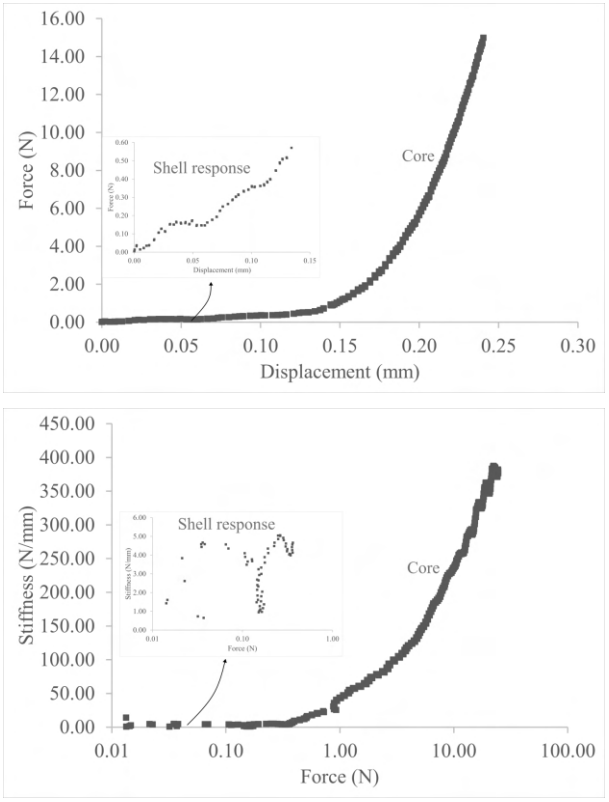

Figure 3. Response of lentils in inter-particle test

From Fig. 2, as the particle deforms, the force increases linearly to 0.15-0.20 N with a deformation of 80 microns (which is nearly half of the thickness of shell on two sides of lentil). Further deformation of the lentil particle results in an exponential rise in force, primarily because of the core. The lentil core is very stiff in comparison to the shell. The stiffness of the shell was nearly constant at 2 N/mm; and after transition, stiffness of core increases steadily to 1300 N/mm and remains constant afterwards.

A similar response is observed in inter-particle normal loading (Fig. 3). Force increases linearly with displacement till 140 microns and 0.60 N with a constant stiffness of 4 N/mm. The core of lentils shows a stiff response; however, single lentil core in particle crushing test shows stiffer response in comparison to core-core response in inter-particle test.

Conclusions

The lentil particle shows a linear force-displacement response at small loads and a power law relation with increase in the load. This behaviour can be attributed to the presence of cover (shell) on the surface of the particle. The stiffness of shell was found to be 2 N/mm and stiffness of core increases till particle failure. Further, stiffness of shell in particle-particle contact was found to be 4 N/mm and stiffness of core-core increases with power law relation however the exponent was found to be less than single particle crushing test.

References

Pinzón, G., Andò, E., Desrues, J. and Viggiani, G., 2023. Fabric evolution and strain localisation in inherently anisotropic specimens of anisometric particles (lentils) under triaxial compression. *Granular Matter*, *25*(1), p.15.

Tolomeo, M. and McDowell, G.R., 2023. DEM study of an “avatar” railway ballast with real particle shape, fabric and contact mechanics. *Granular Matter*, *25*(2), p.32.

Wong, C.P. and Coop, M.R., 2023. The contact mechanics of a UK railway ballast. *Géotechnique*, pp.1-13.

Effects of episodic cycling and reconsolidation on an offshore monopile in clay

I. Aghedo*[1], M. Rouainia[1] and T. Charlton[1]

*Correspondence: i.o.aghedo2@newcastle.ac.uk

[1] *School of Engineering, Newcastle University, Newcastle upon Tyne, NE1 7RU, UK*

Abstract

This study investigates the behaviour of a 6m diameter monopile in a normally consolidated clay, subjected to multiple episodes of cyclic loading and reconsolidation. Three-dimensional (3D) finite element (FE) simulations accounting for pile-soil interaction have been undertaken. The monopile was subjected to three one-way cyclic episodes, consisting of 100 cycles each, with intervening periods of reconsolidation between each cyclic episode. The cyclic behaviour of the clay was simulated with an effective stress kinematic hardening constitutive model. The numerical predictions provide a very close match to the centrifuge measurements in terms of accumulated displacement during each loading episode.

Introduction

Offshore monopiles are subjected to a series of high amplitude cyclic loads during extreme weather conditions, which can cause excess pore water pressure (pwp) to build up, leading to soil stiffness degradation and reduction in strength. These extreme weather conditions are followed by calm conditions typified by low-amplitude load cycles, during which the soil undergoes consolidation and dissipates any excess pwp generated, potentially leading to a regain in stiffness and strength of the soil. Experimental tests (Zhang et al., 2011, Lai et al., 2020, Laham et al., 2023) have shown the beneficial effects on pile performance of reconsolidation amidst cyclic episodes.

In this paper, a kinematic hardening model was calibrated against stress-controlled undrained cyclic triaxial tests on kaolin and used to perform numerical predictions of centrifuge tests to investigate the performance of a 6m diameter monopile under episodic cyclic reconsolidation periods.

Methodology

The numerical prediction is carried out using the kinematic hardening soil constitutive model proposed by Rouainia and Muir Wood (2000), formulated within the critical state framework with elements of bounding surface plasticity. The model has three surfaces namely, a reference surface which controls the state of the reconstituted soil, a structure surface and a bubble which acts as the true yield surface and moves around following a kinematic hardening rule. The model was calibrated against stress-controlled undrained cyclic triaxial tests (UCT) on kaolin carried out by Duque et al. (2021). Figure 1 presents the simulations for the cyclic undrained compression behaviour of kaolin with an isotropic consolidation pressure of 200kPa.

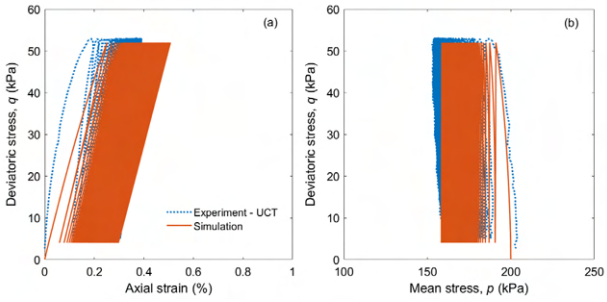

Figure 1. Comparison of model predictions and experimental results for cyclic undrained triaxial tests: (a) stress-strain response and (b) effective stress paths.

The model simulations are in good agreement with the experimental data in terms of the effective stress path and stress-strain response. A 3D finite element (FE) model (Plaxis 3D, 2023) was developed and validated against centrifuge test results by Lai et al. (2020), who investigated reconsolidation effects on a monopile installed in kaolin clay. The dimensions of the pile are shown in Figure

2, with the mesh consisting of 7034 10-node tetrahedral elements.

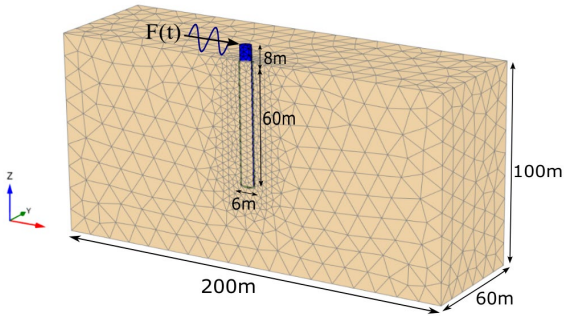

Figure 2. 3D finite element model.

The monopile is modelled as a plate with Young's modulus E_p = 210GPa and Poisson's ratio ν = 0.3. To minimise computational time, only half of the pile is modelled, and installation effects are ignored, with the monopile being wished-in-place. The cyclic loading magnitude is defined as ζ_b = 25% of the ultimate lateral capacity of the monopile, F_u= 54MN (obtained by a static pushover test both in the centrifuge and FE model). Three loading episodes of one-way cycling, consisting of 100 cycles each, are applied to the head of the pile, with reconsolidation between each episode.

Results and Discussion

The centrifuge test results and the model predictions for the first and third loading episodes are presented in Figure 3. The model shows a good prediction of the evolution of lateral displacement under cyclic loading. The accumulated displacement is much lower in the third episode compared to the first, which is captured by the model.

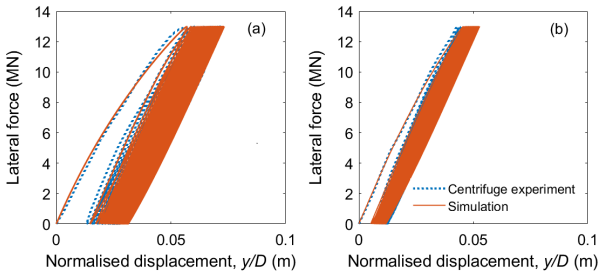

Figure 3. Load-displacement response of the monopile during the first and third episode of cyclic loading: (a) 1st episode; (b) 3rd episode.

Figure 4 shows the decrease in the cumulative displacement in each subsequent loading episode. It can be seen that the model is able to describe the strength gain in the clay due to the effect of the intervening reconsolidation periods, which reduces the accumulation of plastic strains.

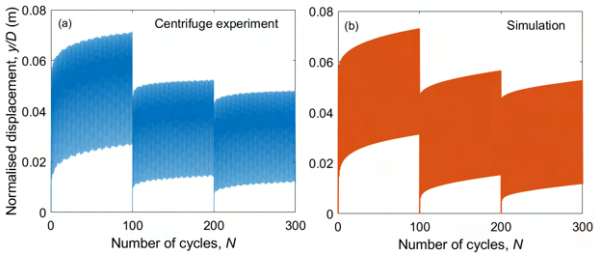

Figure 4. Evolution of accumulated displacement with cycle number for each cyclic episode: (a) centrifuge experiment and (b) simulation.

Conclusion

The study demonstrates that the numerical model is able to accurately reproduce the results from the centrifuge tests in terms of the cumulative displacement. Further investigations will be carried out to assess the recovery of pile-soil strength and stiffness under conditions of high cyclic stress amplitudes near failure, in severe sea states, and with varying overconsolidation ratios in different soil types.

Acknowledgements

The first author is funded by the Petroleum Technology Development Fund (PTDF). This funding is gratefully acknowledged. The first author is grateful to Dr. Yongquing Lai and Dr. Lizhong Wang for providing the triaxial and centrifuge test data.

References

Duque J., Ochmański M., Mašín D., Hong, Y., Wang, L. On the behavior of monopiles subjected to multiple episodes of cyclic loading and reconsolidation in cohesive soils. *Comput. Geotech.*,134, 2021.

Lai Y., Wang L., Hong Y., and He B. Centrifuge modeling of the cyclic lateral behaviour of large diameter monopiles in soft clay: Effects of episodic cycling and reconsolidation. *Ocean Eng.*, 200, 2020.

Laham N., Kwa K., Deeks A., Suzuki Y., White D., and Gourvenec S. Changing soil response during episodic cyclic loading in direct simple shear tests. *Int. J. Offshore Polar*, 33(1), 54-61, 2023.

Plaxis. PLAXIS 3D 2023: Reference Manual, Delft, Plaxis bv, 2023.

Rouainia M. and Muir Wood D. A kinematic hardening constitutive model for natural clays with loss of structure. *Géotechnique*, 50, 153-164, 2000.

Zhang C., White D., and Randolph M. Centrifuge modeling of the cyclic lateral response of a rigid pile in soft clay. *J. Geotech. Geoenviron. Eng.,* 137(7), 717-729, 2011.

Rock-socketed tension pile design: with parametric modelling and automated workflow

C.F. Foo*[1]

*Correspondence: David.Foo@arup.com

[1] *Arup, 8 Fitzroy Street, W1T 4BJ, London, United Kingdom*

Abstract

Different failure mechanisms have been considered in the tension pile design for a 200m long, 26m deep and 24m wide underground station box founded on rock. Parametric modelling was adopted for precise calculation of mobilised group rock cone volume and side shear area. This allowed the cone side shear to be accurately quantified and considered in uplift resistance. In order to improve design efficiency for long linear infrastructure, an automated workflow has been developed to cut analysis time allowing further optimisation of the tension pile solution. Approximately 21% total pile concrete volume savings was achieved by considering group cone side shear. Potential time savings from using the automated workflow is estimated to be around 85%.

Introduction

Tension piles are commonly used to provide additional uplift resistance for structures subject to large hydrostatic and/ or ground swelling pressures. In practice, rock-socketed tension piles are typically arranged in regular grids with the same pile length for ease of calculating overlapping rock cone volume with guidance in the literature (e.g. Tomlinson & Woodward, 2015; Structural Division The Hong Kong Institution of Engineers, 2019). However, calculating mobilised group cone side shear area is more complicated and limited guidance is available in the literature. This often leads to the omittance of beneficial contribution of cone side shear in resisting uplift.

This paper presents how design efficiency of rock-socketed tension piles can be improved using parametric modelling and an automated workflow. The design of tension piles for a 200m long, 26m deep, 24m wide underground station box founded on rock has been undertaken using parametric modelling to calculate mobilised rock cone geometry. An automated workflow was developed to accelerate the design process and optimise pile lengths and arrangement.

Rock-socketed tension pile design

Four main failure mechanisms have been considered in design: (1) piston pull-out; (2) single cone pull-out; (3) group cone pull-out with conical failure; (4) group cone pull-out with conical and block failure (Hong Kong Buildings Department, 2017). Refer to Figure 1 for group cone pull-out mechanisms.

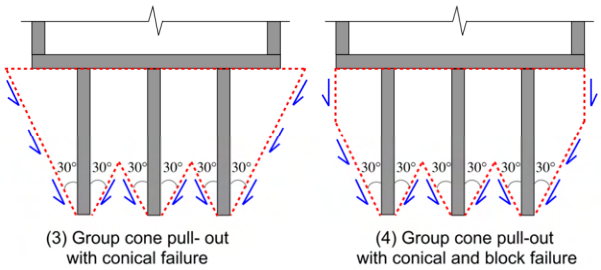

Figure 1. Group cone pull-out failure mechanisms

Piston pull-out resistance is provided by shaft adhesion and effective pile weight. Single and group cone pull-out resistance are derived from vertical component of cone side shear, vertical side shear (if any), and effective weight of pile and mobilised rock cone. For group cone pull-out with block failure, mobilised rock cone extent is limited to within the station box boundary. Rock cone angle has been conservatively limited to 60°, which represents the conditions for a heavily jointed or shattered rock. Mobilised rock cone side shear is limited to between

5% and 10% depending on weathering state (Pells et al., 1998).

Parametric Modelling

Parametric modelling of mobilised rock cone was undertaken using Rhino 7 software. Grasshopper scripting was used to automate the simulation and carry out precise calculation of mobilised rock cone geometry for different pile arrangement at each design section. This capability allowed refinement of internal and external pile lengths, and repositioning of piles locally (with irregular grid) to accommodate deepened sumps (see example in Figure 2).

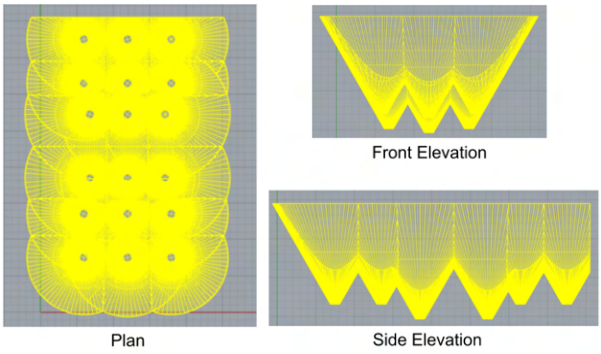

Figure 2. Parametric modelling of mobilised group cone (conical failure) for irregular pile lengths and layout.

Automated Design Workflow

The station box was divided into six design sections primarily based on ground conditions and structural sections. An automated workflow was developed such that design calculations can be iterated for different combinations of pile diameters, pile arrangement, internal/ external pile lengths, rock cone angle, ground model, applied internal/ external pile forces and total uplift force. Each design section can be specified as 'end' or 'intermediate' section for group cone pull-out resistance calculation. The design workflow involves the integration of Excel spreadsheets, Python and Grasshopper scripts, as shown in Figure 3.

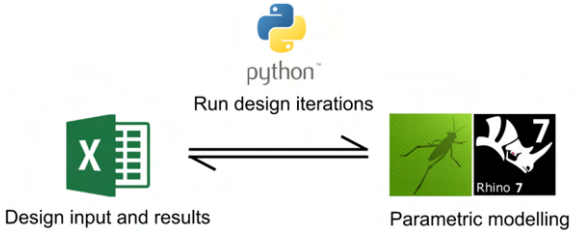

Figure 3. Simplified automated design workflow

A comparison study of similar pile arrangements for the station box showed that by considering mobilised group cone side shear in uplift resistance, a reduction of approximately 21% in total pile concrete volume was achieved due to shorter required pile lengths.

The automated design workflow was estimated to have provided time savings of approximately 85% per design iteration, when compared to the manual process of carrying out parametric modelling, extracting geometry results and running Excel spreadsheet calculations. This provides further opportunity to explore different pile arrangements with structural engineers to minimise base slab bending moments.

Conclusions

This paper presents an innovative approach to rock-socketed tension pile design using parametric modelling and an automated workflow. Parametric modelling allows precise calculation of mobilised group rock cone volume and shear surface area. By considering mobilised group rock cone side shear in uplift resistance calculation, a significant reduction of around 21% in total pile concrete volume was achieved for the underground station box design. The automated workflow also resulted in substantial time savings of 85% per design iteration.

Acknowledgements

The author would like to thank Arup and colleagues for their guidance, support, and constructive feedback.

References

Hong Kong Buildings Department (2017) *Code of Practice for Foundations*. Hong Kong, Buildings Department.

Pells, P. J. N., Mostyn, G. and Walker, B. F. (1998) Foundations on sandstone and shale in the Sydney Region. *Australian Geomechanics*.

Structural Division The Hong Kong Institution of Engineers (2019) *An Explanatory Handbook to the Code of Practice for Foundations 2017*. Hong Kong, Structural Division The Hong Kong Institution of Engineers.

Tomlinson and Woodward (2015) Pile Design and Construction Practice, Sixth Edition.

17th BGA YGES
University of Cambridge
1-3 July, 2024

Effects of pile stiffness on pile behaviour

G. Sabaliauskaite*, S. Divall, and A. M. McNamara

*Correspondence: greta.sabaliauskaite@city.ac.uk

Department of Civil Engineering, City, University of London, UK

Abstract

The load settlement behaviour of piles with a reduced stiffness is being investigated using geotechnical centrifuge modelling techniques. The tests are modelling bored cast in situ piles constructed in overconsolidated clay. The reduction in pile stiffness has been achieved by creating model piles with hollow cores of varying sizes.

Background

Bored cast in situ piles in clay soils mobilise resistance when loaded from the undrained response of the soil-pile interface at the shaft and base of the pile. However, the settlements necessary to mobilise the end bearing capacity of the piles occur at applied loads which typically exceed the safe working capacity of the pile (Burland, 2023). Thus at working loads the resistance at the shaft of the pile is critical. McNamara *et al*., (2014) found that this resistance was mobilised more effectively by a less stiff hollow pile than a stiffer solid pile when undertaking a field test in London clay.

In addition, in a physical model test conducted by Panchal *et al.,* (2019), it was reported that a reduction in the stiffness of a model pile had resulted in higher displacements. Therefore, reducing the stiffness of a piled foundation has the potential to improve the pile load displacement response and with the advent of hollow piles varying the pile stiffness is possible in practice.

This research aims to investigate how the behaviour of piled foundations are affected when the stiffness of piled foundations is varied, and to establish a framework which allows the prediction of this behaviour. In order to do this it was key to have a consistent model soil pile interface and a reproducible method of varying the pile stiffness as described below.

Model Piles

3D Printed Piles

Three piles were drawn using SolidWorks 3D modelling software for the preliminary tests. Each pile was printed in two halves with a Markforged Onyx One Fused Filament Fabrication 3D printer. A micro carbon fibre filled nylon filament, known as Markforged Onyx, was used for the piles. The two printed pile halves of each pile were then fixed together by applying Araldite epoxy resin to specially designed channels in the annulus of the piles. The tops of the bonded piles are shown in Figure 1.

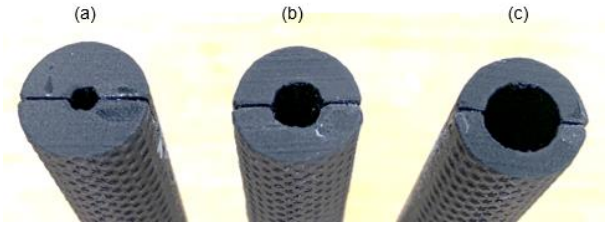

Figure 1: Novel 3D printed piles with hollow cores of (a) 3mmOD (b) 6mmOD (c) 9mmOD

The piles were designed to be 200mm long with an external diameter of 16mm at model scale. When accelerated to 50*g*, this corresponds to a pile 8.0m in length, with a diameter of 0.8m at prototype scale.

The hollow core outer diameters (*OD*) of the model piles were chosen to be 3, 6, and 9mm, with corresponding axial stiffness values of 2.33, 2.09, and 1.68 kN/mm, respectively.

3D Printed Roughness

As it is extremely difficult to replicate the exact roughness profile on the surface of model piles using traditional methods such as sandblasting, machining, or gluing sand to the outside of model piles, 3D printed model piles were chosen for this series of centrifuge tests. This method made it possible to accurately repeat the surface roughness profile for each model pile.

In order to apply the roughness on the model piles, a built-in 3D texture, the polyhedron pattern, from the SolidWorks Appearances library was used. It was first applied to the surface of the pile halves as a 2D pattern, allowing the pattern size to be scaled. A mesh was then applied to the pile, which allowed selection of the necessary offset distance for the white areas of the pattern, thus creating the rough surface profile (Figure 2).

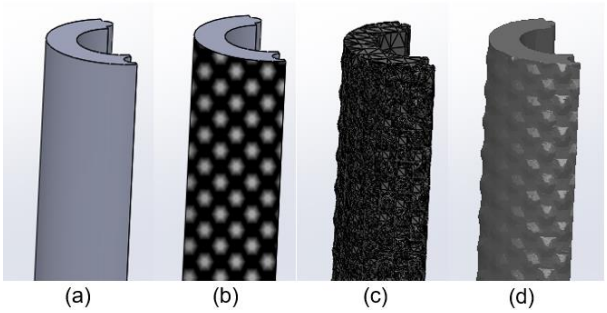

Figure 2: Application of surface roughness to 3D printed piles using SolidWorks. (a) Plain pile face (b) Pile face with applied and scaled 2D Polyhedron Pattern (c) Pile face with applied mesh (d) Pile face with applied mesh, contours removed for clarity

A texture offset distance of 0.25mm was chosen through comparison of roughness measurements taken on sample gauge blocks with varying offset distances applied, and a 100x100x100mm concrete block using a Mitutoyo Surftest SJ-210 surface roughness measurement instrument.

Model Making

A preliminary test was conducted in a 375mm deep strongbox with an internal area of 550x220mm, containing a bed of overconsolidated Speswhite kaolin prepared from a slurry in a consolidation press.

The model was made under 1*g* conditions using a pile bore cutter, and pile bore guide to ensure exact positions of the model piles within the soil sample. Once the piles were installed into their respective bores, an instrumented load frame with 6 LVDTs (Linear Variable Differential Transformers), and 9 load cells, was attached to the strongbox (Figure 3).

The model was then placed on the centrifuge swing, accelerated to 50g, and left to consolidate for 48 hours.

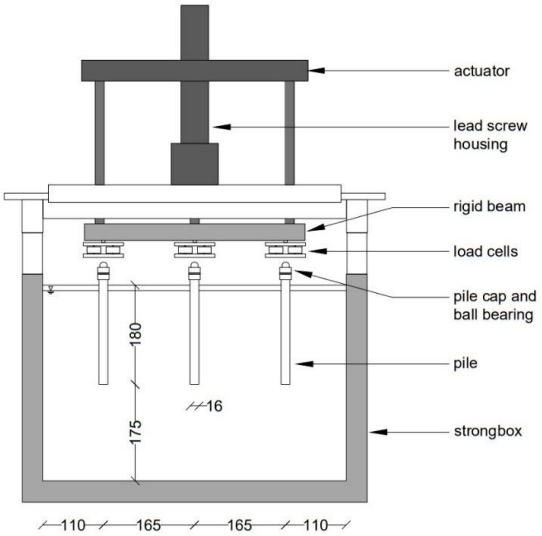

Figure 3: Schematic diagram of model layout

Test Results

Figure 4 shows the load-normalised settlement response for the three model piles. A considerable difference can be observed for pile capacity at working load (taken as 1% normalised settlement) between the three piles. These results confirm larger strains and an increased adhesion between the pile and the soil when the axial stiffness of a pile was reduced.

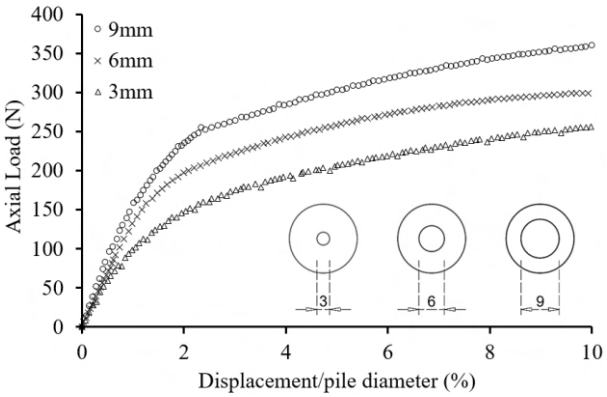

Figure 4: Settlement response for model piles under applied axial load

References

Burland, J.B., 2023. Behaviour of single piles under vertical loads. In *ICE Manual of Geo. Eng., II edition, Vol. I: Geotechnical engineering principles, problematic soils and site investigation* (pp. 257-272). Emerald Publishing Limited.

Panchal, J.P., McNamara, A.M., Halai, H. and Divall, S., 2019, September. Centrifuge modelling to determine the influence of pile stiffness on pile capacity. In *Proc XVII ECSMGE*. ISSMGE.

McNamara, A.M., Suckling, T.P., McKinley, B. and Stallebrass, S.E., 2014. A field trial of a reusable, hollow, cast-in-situ pile. *Proc of the ICE*, *167*(4), pp.390-401.

Coupled DEM-FDM analysis of OE piles in chalk

J. Zheng*[1] & M.O. Ciantia[1,2]

*Correspondence: 180026675@dundee.ac.uk

[1] University of Dundee, School of Science and Engineering, Dundee, United Kingdom
[2] University of Milano Bicocca, Department of Erath and Environmetal Sciences, Milan, Italy

Abstract

To investigate open ended pile-chalk interaction and axial load transfer mechanisms during installation, a coupled DEM (discrete element method) – FDM (finite differential method) model is used. To capture the complex behaviour of chalk a newly developed DEM bond damage contact model for highly porous soft rocks is used. The DEM model is calibrated to capture experimental data of St Nicholas-at-Wade (SNW) chalk from the literature. The model is then used to simulate model pile installation experiments on the same chalk.

Introduction

Chalk is widely distributed across the seabed of the North Sea in the UK and the Baltic Sea, which are currently the primary sites for offshore wind farms. Monopiles are typically driven into the chalk to support the overlying offshore wind turbines. During monopile installation, the chalk close to the pile tip undergoes bond breakage and particle crushing, eventually degrading into chalk putty (Ciantia, 2021). This soil-structure interaction complexity has led to overly conservative monopile designs in chalk, with recommended shaft resistance for driven piles in low-to-medium density chalk being only 20 kPa (Lord et al., 2002). Given that monopile foundations account for 20-30% of the project budget, improving pile design from an economic perspective is essential. The drivability of the piles, as well as subsequent axial and lateral load responses, depend on the stiffness and strength of the chalk putty annulus and the chalk stress field. To obtain a realistic response of the chalk putty around the pile, many laboratory (Alvarez-Borges et al., 2022) and field tests (Buckley et al., 2018) have been conducted recently, yet the mechanism explaining this complex behaviour is not fully understood.

DEM modelling is a promising tool for interpreting the axial load transfer mechanism of piles from a microscopic view (Ciantia et al., 2019). However, current DEM modelling faces limitations due to the inability of existing bond damage models to reproduce the typical behaviours of highly porous soft rocks. Another restriction is the computational inefficiency of DEM modelling when simulating boundary value problems (BVPs). Therefore, a newly proposed bond damage model for highly porous soft rocks, combined with the DEM-FDM modelling technique, is employed to simulate pile installation in chalk.

DEM modelling of chalk

To model rocks using the DEM cohesive contact laws are generally employed. Existing models from the literature proved to be ineffective in replicating the highly collapsible behaviour of chalk followed by the frictional behaviour of the putty. For this reason, in this work a novel DEM contact model is used. The bonds are described using a 3D failure envelope while the crushed putty is modelled by a purely frictional contact law. More details can be found in Zheng et al. (2024; 2023).The model is calibrated to replicate St Nicholas-at-Wade chalk (Figure 1) and the contact model parameters are summarised in Table 1.

Tests results

A cylinder-shaped chalk sample is generated using a DEM-FDM coupling approach to match the model pile experiment by Alvarez-Borges et al. (2022). The DEM region is a 40 mm diameter and 60 mm height cylinder in which a pile diameter of 8mm with a wall thickness of 1mm is installed. The FDM region has the same elastic properties of intact chalk. Figure

2a shows the load-displacement curves between the simulations and the small-scale penetration test. The curves are in good agreement. In the model it was possible to identify the shaft and tip components that are also reported in the figure. To represent the extend of calk damage, in Figure 2b the DEM contacts are represented in terms of their damage variable state. The damage zones extend laterally up to 1 time the diameter and vertically up to 2 times the pile diameter below the pile tip. The thickness of the unbonded chalk on the shaft is the same as that observed by Alvarez-Borges et al. (2022).

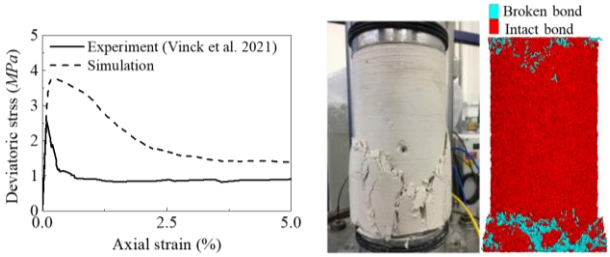

Figure 1. Calibrated triaxial results: (a) load-displacement curve; (b) failure mode.

Table 1. Calibrated model parameters

Frictional Behaviour			
Parameter	Value	Parameter	Value
E_{mod}	0.63*Gpa*	$\kappa^*(\bar{\kappa}^*)$	5
$\bar{E}_{mod}$	5.5*Gpa*	μ	0.2
Cohesive behaviour			
σ_c	6*MPa*	$u_c^n(u_c^s)$	0.03d_{00}
σ_t	1.5*MPa*	θ_c^b	0.01
C	1.5*MPa*	g_a	0.13d_{00}

Note: u_c^n=0.23d_{00} for compression.

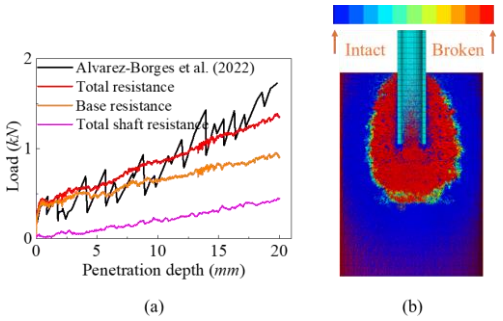

Figure 2. (a) Load-displacement curve; (b) damage zone.

Looking at the contact force distribution in Figure 2b, it can be observed that they are greater near the pile tip and present a decreasing trend along the shaft. Integration over the pile surface would lead to stress distributions similar to what observed numerically by Ciantia (2021).

Conclusions

In this work, a coupled DEM-FDM modelling for OE pile installation in chalk is performed. The findings show that the novel contact model can capture SNW chalk element behaviour quite reasonably. It is also shown that thanks to the DEM-FDM coupling approach it is also possible to replicate model pile experiments and investigate the microscale mechanism underling the macroscopic response. The approach appears to be promising and may assist the interpretation of the mechanics of this complex ground structure interaction problem.

Acknowledgments

This work is part of the EPSRC funded ICE-PICK project (EP/W00013X/1).

References

Alvarez-Borges, F., Ahmed, S., Madhusudhan, B. N., et al. 2022. Investigation of pile penetration in calcareous soft rock using X-ray computed tomography. *Int. J. Phys. Model. Geotech*, **22**(1): 38–52.

Buckley, R., Jardine, RJ., Kontoe, S., et al. (2018). Ageing and cyclic behaviour of axially loaded piles driven in chalk. *Géotechnique*, **68**(2): 146-161.

Ciantia, M. O. 2021. Installation Effects on Axial Performance of Monopiles in Chalk for Offshore Renewables. In: Huynh, D.V.K., et al. (eds) VSOE2021., 424-432, Singapore.

Ciantia, M. O., O'Sullivan, C., & Jardine, R. J. (2019). Pile penetration in crushable soils: Insights from micromechanical modelling. 17th ISSMGE-ECSMGE, 298–317, Reykjavik.

Lord, J. A., Clayton, C. R. I., & Mortimore, R. N. 2002. Engineering in chalk. In *CIRIA*.

Vinck, K. (2021). Advanced geotechnical characterisation to support driven pile design at chalk sites (Ph. D. thesis, Dept. of Civil and Environmental Engineering, Imperial College London).

Zheng, J., Ciantia, M. et al. (2024). A coupled damage-plasticity DEM bond contact model for highly porous rocks. In William M. Coombs (Ed.), *Annual Conference of the UKACM.* 132–135, Durham.

Zheng, J., Previtali, M., Ciantia, M.O., et al. 2023. Micromechanical Numerical Modelling of Foundation Punching in Highly Porous Cemented Geomaterials in a Virtual Centrifuge Environment. In: Ferrari, A. et al. (eds) CNRIG 2023. 390-397, Palermo.

Design of Vibro-Installed Offshore Monopiles in Sand

S. Elliott*[1], S. Whyte[1]

*Correspondence: seb@geowynd.com

[1] *Geowynd, 17 Grosvenor Street, London, W1K 4QG, UK*

Abstract

Vibro-installation of offshore monopile foundations is now being used as an alternative to traditional, impact driven methods in sand dominated profiles; reducing installation time and noise whilst mitigating pile run risk. In dense sands, vibro-installation has been observed to alter the state of the in-situ soil, dependent on installation parameters (frequency and penetration velocity), typically loosening sands leading to a softer pile load-displacement response. This paper presents an FEA-based design approach that captures the vibro-induced degradation of monopile load-displacement response within an effective stress framework, benchmarked against published pile-load tests on paired impact-driven and vibro-installed piles, that can be adopted directly in a vibro-modified PISA approach.

Introduction

Traditionally, monopile foundations are installed under multiple thousands of blows from large hydraulic hammers in a process termed impact driving. Whilst popular, impact driving presents high noise emissions and potential for pile damage and slow installation campaigns. Vibro-installation is now being used as an alternative installation method, boasting reductions to installation noise and faster installation times. However, vibro-installation, particularly in dense sands, has been observed to alter the state of the in-situ soil, typically loosening sands leading to softer pile load-displacement response (Achmus et al., 2020) (Kirsch et al., 2021) (Spill et al., 2022).

Load-Displacement Softening

Available literature regarding the lateral response of vibro-installed monopiles is limited. Published pile-load test data for vibro-installed piles, e.g. the VIBRO Project (Achmus et al., 2020) and TANDEM Project (Spill et at., 2022), observe degradation in stiffness response of vibro-installed piles compared to those which were impact-driven, see Figure 1. This is corroborated by model testing, e.g. Kirsch et al. (2021). However, it should be noted that other authors report the contrary, i.e. no degradation in the small displacement region, e.g. LeBlanc Thilsted (2014).

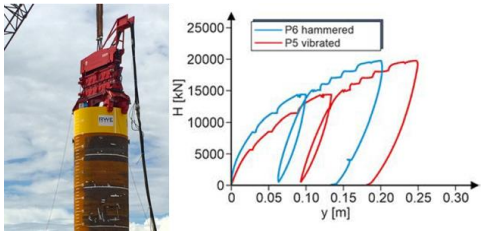

Figure 1. Softer lateral load-displacement response of a vibro-installed pile (red) compared to an impact driven pile (blue) from the VIBRO project (Achmus et al., 2020)

Soil Degradation

Soil degradation resulting from a stress relaxation loosening mechanism is postulated by several authors. Warrington (2021) highlights that the relationship between amplitude ratio and installation time during vibratory driving is a mirror of a typical stiffness degradation curve.

In terms of in-situ response, the VIBRO Project (Achmus et al., 2020) (Gavin et al., 2022) presents CPT data pre and post monopile installation for both impact-driven and vibro-installed cases at an offset of 1.2 m from the monopile. Showing typical post-installation cone tip resistance ratio, between vibro-installed and impact-driven, of ~0.7. It is important to note that both were different to the virgin CPT case.

The VIBRO Project observes a zone of influence around the monopile of ~0.7D, with D the outer diameter of the pile. Model tests performed at TU Berlin (Kirsch et al., 2021) ob-

serve a zone of influence of ~1.5D, with decreasing impact with radial distance from the pile wall.

FEA-Based Approach – Monotonic

Stiffness and strength degradation, in comparison to the impact driven case, resulting from vibro-installation can be captured directly in a 3D FEA model through inclusion of a vibro-degraded soil-volume around the monopile, Figure 2. There are many potential methods to apply this degradation (e.g. reduction in specific model parameters); however, in this study effective stress reduction (i.e. relaxation) only within the degraded zone was applied. This reduction in turn allowed for an intrinsic physically based reduction in the strength and stiffness response of the isotropic double hardening plasticity model being used (Schanz et al., 1999). The stress dependent stiffness and strength, relevant to monotonic conditions, are calculated within the model as shown below.

$$E_{50} = {E_{50}}^{ref}\left(\frac{\sigma'_{3,reduced}}{p_{ref}}\right)^{m} \quad G_{max} = {G_{max}}^{ref}\left(\frac{\sigma'_{3,reduced}}{p_{ref}}\right)^{m} \quad (1)$$

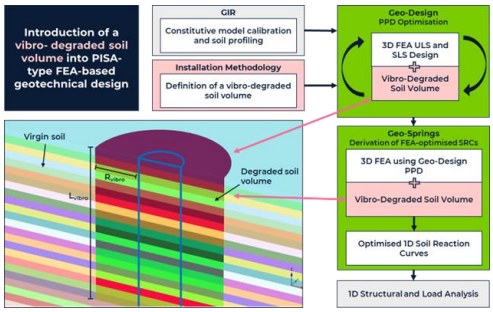

Figure 2. Vibro-degraded volume in the FEA model

In the FEA model presented in this paper, an effective stress reduction factor of 0.70 is applied, broadly congruent with the CPT reduction factor from the VIBRO Project and the findings of TU Berlin model tests (Kirsch et al., 2021). Laterally, the vibro-degraded zone extends 1.0D from the pile wall.

Performance

In double-normalised space the performance of the outlined FEA-based effective stress reduction framework for a synthetic dense sand soil profile can be compared against pile-load test results from the VIBRO Project. As evidenced in Figure 3, softening of the pile load-displacement response is captured well.

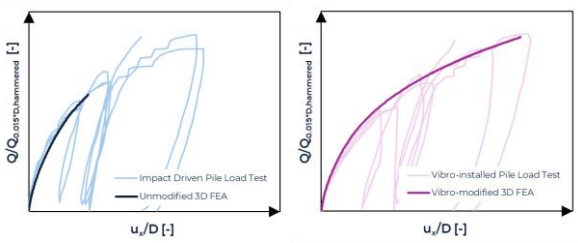

Figure 3. FEA benchmark against VIBRO project pile load tests: impact driven (left) and vibro-installed (right).

Extension to Cyclic Design

The stress regime acting on a soil element under cyclic loading is represented by the cyclic stress and average stress components of the loading, in sands normalised by a reference effective stress. The stress relaxation approach described in this paper can also be applied in a consistent manner for cyclic design scenarios, a reference effective stress reduction resulting in a cyclic strength reduction.

Conclusion

An FEA-based effective stress reduction framework, that can be embedded in state-of-the-art design methods (e.g. PISA), is proposed to represent degradation of monopile load-displacement response following vibro-installation in comparison to an impact drive case. Compared against published pile load test data for vibro-installed piles in dense sands, the approach matches softening of the load-displacement well.

References

M. Achmus., V. Herwig., S. Kirill., B. Matlock. 2020. Lateral bearing behaviour of vibro- and impact-driven large-diameter piles in dense sand. *Geotechnik* **43** (3): 147-159.

K. Gavin., S. Blok., G. Eiksund. 2022. The Impact of Installation Method on Monotonic Loading of Monopiles in Sand. *4th International Symposium on Frontiers in Offshore Geotechnics*, Austin, 2022.

F. Kirsch., F. Rackwitz., V. H. Le., K. Grivas. 2021. Design of Vibro-Driven Large Diameter Monopiles. *Vietnam Symposium on Advances in Offshore Engineering*: 246-253, Singapore, 2021.

C. LeBlanc Thilsted. 2014. Vibro-driving monopiles-A feasible installation concept for the future?. *Danish Geotechnical Society Seminar* **1,** Gentofte, Denmark, 2014.

S. Spill., A. Foglia., J. Dührkop. 2022. Comparison of p-y Methods with Large-Scale Tests of Impact- and-Vibratory-Driven Piles. *Proc. 4th Int. Symp. Frontiers in Offshore Geotechnics,* Austin, 2022.

D. C. Warrington. 2021. Reconstructing a Soviet-Era Plastic Model to Predict Vibratory Pile Driving Performance. *ReSEARCH Dialogues Conference vol.* ***2021***.

17th BGA YGES
University of Cambridge
1-3 July, 2024

Effect on pile group performance due to adjacent deep excavation in multi-layered soil

Paromeeta Bandyopadhyay*[1], Fuchen Teng[1]

*Correspondence: paromeetab@gmail.com

[1] *Affiliation (National Taiwan University of Science and Technology, Taipei, Taiwan)*

Abstract

This study examines the impacts of deep excavations adjacent to a pile group in a naturally occurring multi-layered soil profile, characterized by distinct clay and sand strata. The load-bearing capacity of the pile group in this soil profile is derived from both negative skin friction from the clay and end bearing from the sand. A detailed three-dimensional numerical finite element analysis is used in this study to determine the change in pile group capacity. This research is pivotal for risk assessment and formulating effective mitigation strategies in urban construction, ensuring the durability and stability of pile-supported structures.

Introduction

The impact of deep excavations on the capacity of in-service pile groups is a key concern in urban areas, where such excavations are often needed and situated close to these pile groups. Excavation causes ground movement and stress redistribution of the surrounding soil. This study uses a 3D numerical finite element method to analyze the change in pile group behaviour and capacity within the deep excavation's primary influence zone. Previous studies mostly focused on only one type of soil; either clay or sand (Finno et al., 1991; Liyanapathirana and Nishanthan, 2016; Ong et al., 2009). Korff et al. (2016) analyzed multi-layered soil but did not consider the effect of stress release. Bandyopadhyay and Teng (2024) studied how the position and thickness of sand and clay affect the change in behaviour of a pile group near an excavation.

Case study in Taiwan and numerical model

A group of 3 piles is placed 5m away from a 22 m wide excavation with a final excavation depth of 15 m. The length of each pile is 48 m. The piles are rigidly connected to a 1.5 m thick pile cap. The diaphragm wall is 1.2 m thick and 57 m deep. The embedded beam feature of PLAXIS 3D (2020) is used to model pile which has an in-built interface to model pile-soil interaction. 12-node interface elements of the D-wall and pile cap model the soil-structure interface. The hardening soil small strain model is used to model the small-strain non-linear behaviour of clay. The soil profile, excavation geometry, and pile group location is shown in Figure 1. For clay, undrained analysis, and for sand, drained type plastic analysis is performed to study the short-term effect of excavation on the pile group.

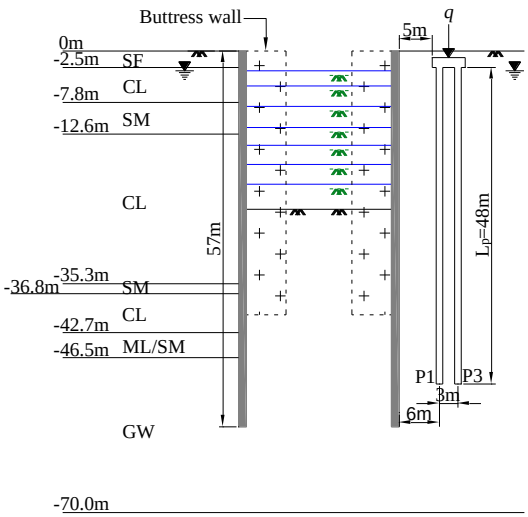

Figure 1. Soil profile, excavation, and pile group geometry

Results and discussions

When only the working load acts on the pile, the axial force curve follows a continuous decreasing trend. This is the expected behavior of an axially loaded pile. However, with excavation, initially, there is an increase in the magnitude of the axial force, followed by a subsequent decrease as shown in Figure. 2. This changed axial force curve resembles the behavior typically observed for the negative skin friction effect. Also, almost 97% of the load is taken by the pile shaft and only 3% is taken by the pile toe when only the working load is acting. The maximum length of the pile considered in this study is in clay the majority of the load is taken by skin friction. However, after the completion of the excavation, around 73% of the maximum load is taken by the pile shaft and the pile toe takes 27%. This indicates that soil experiences higher stress at the end of excavation due to an increase in the end-bearing load as there is redistribution of the axial and excavation-induced load.

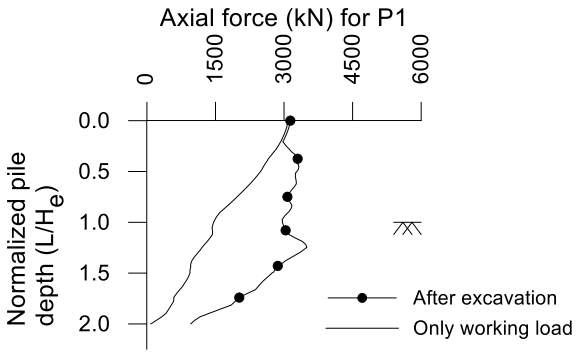

Figure 2. Axial force in pile P1

The settlement of the top of pile P1 is 8.2 mm with only working load of 523 kN/m^2 on the pile cap. The settlement however increases to 36.7 mm after the final excavation phase as shown in Figure. 3. This increase in settlement of 28.5 mm is only due to the excavation which will reduce the FOS of the pile group. The load of -523 kN/m^2 is numerically obtained for this pile group with a FOS of 2.

Future Studies

To determine the reduced factor of safety due to excavation, this study is being extended to include centrifuge model testing. This can help in numerical back analysis to obtain the FOS in other similar cases.

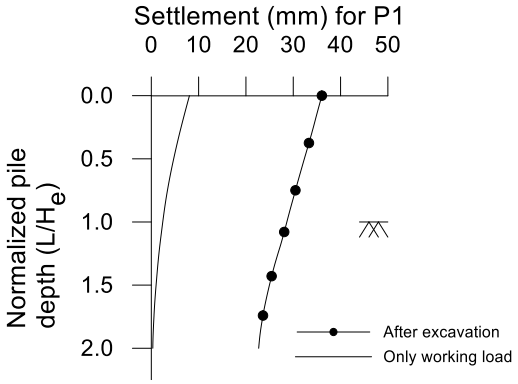

Figure 3. Settlement in pile P1

References

Bandyopadhyay, P., and Teng, F. (2024). "Analysis of pile-soil-excavation interaction and load transfer mechanism in multi-layered soil for an in-service pile group." *Computers and Geotechnics*, Elsevier Ltd, 171(December 2023), pp.106378. https://doi.org/10.1016/j.compgeo.2024.106378.

Finno, R. J., Lawrence, S. A., Allawh, N. F., and Harahap, I. S. (1991). "Analysis of performance of pile groups adjacent to deep excavations." *Journal of Geotechnical Engineering*, 117(6), pp.934–955. https://doi.org/10.1061/(ASCE)0733-9410(1991)117:6(934).

Korff, M., Mair, R. J., and Van Tol, F. A. F. (2016). "Pile-Soil Interaction and Settlement Effects Induced by Deep Excavations." *Journal of Geotechnical and Geoenvironmental Engineering*, 142(8), pp.1–14. https://doi.org/10.1061/(asce)gt.1943-5606.0001434.

Liyanapathirana, D. S., and Nishanthan, R. (2016). "Influence of deep excavation induced ground movements on adjacent piles." *Tunnelling and Underground Space Technology*, Elsevier Ltd, 52, pp.168–181. https://doi.org/10.1016/j.tust.2015.11.019.

Ong, D. E. L., Leung, C. F., and Chow, Y. K. (2009). "Behavior of Pile Groups Subject to Excavation-Induced Soil Movement in Very Soft Clay." *Journal of Geotechnical and Geoenvironmental Engineering*, 135(10), pp.1462–1474. https://doi.org/10.1061/(asce)gt.1943-5606.0000095.

PLAXIS 3D. (2020). *PLAXIS 3D Reference Manual*.

Modelling of a new CPT module for direct in-situ measurements of undrained shear strength in clay

K. Wen*

*Correspondence: k.wen@soton.ac.uk

[1] *University of Southampton, UK*

Abstract

Conventional CPTs, as one of the most widely used site-investigation tool over last 50 years, have been used to infer soil properties such as undrained shear strength through the use of empirically-derived correlations. To improve the speed of site investigation and the data quality for supporting offshore pile design, a new CPT module capable of horizontal translation within the conventional CPT shaft, referred to as a p-y module, has been implemented that allows the soil to be probed through the application of kinematic mechanism like p-y springs for laterally loaded piles. This paper presents a finite element simulation of p-y module in undrained clay and provides the guidance for converting the direct measurements of a p-y module to undrained shear strength with the use of bearing factors.

Introduction

There is an impetus to develop efficient site characterisation tools that more faithfully replicate the loading conditions of infrastructure throughout their service life (White 2022). A collaborative research project 'ROBOCONE' between University of Bristol, University of Southampton and Trinity College Dublin, sponsored by the UK and Ireland research councils, aims to integrate a short cylindrical module capable of actuating laterally into the conventional CPT shaft (Diambra et al. 2022). As seen in Figure 1, the tool can mimic the load and displacement history imposed by a laterally loaded pile element, whose measurements can be converted into soil properties, including undrained shear strength. However, there exists a need of robust methodology equivalent to the bearing factors developed for other new penetrometer tests (e.g. Yan et al. 2011).

This study adopts a 3D finite element analysis for the ROBOCONE p-y module in clay and aims to develop an interpretation framework of bearing factors for the ROBOCONE p-y module that allows the undrained shear strength to be determined from the monotonic load-displacement measurements. The numerical model described in this paper has also been used to consider stiffness factors and also drained behaviour, but these topics are beyond the scope of this short paper.

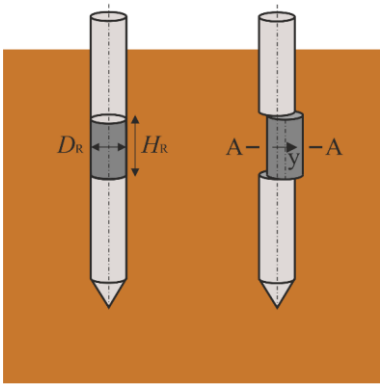

Figure 1. Illustration of the ROBOCONE p-y module (adapted from Diambra et al. 2022)

Methodology

The finite element analyses were carried out with the commercial software PLAXIS 3D V23. Figure 2 illustrates the layout of the ROBOCONE system (including shaft, rings and moveable p-y module) embedded in the soil domain. The p-y module to be modelled has an external diameter of 54 mm and a height of 200 mm, following the specification of the prototype p-y module (Creasey et al. 2023).

The soil was modelled as a weightless, homogeneous, undrained material, using linear isotropic elasticity and a Tresca failure criterion for plasticity (G = 4.6 MPa; s_u =30 kPa). The mechanical behaviour of the interface elements

for soil-structure interaction was modelled using the linearly elastic-perfectly plastic model, for which the maximum shear strength is defined as αs_u, with $0 < \alpha \leq 1.0$. Details regarding the numerical model and calculation phases are discussed in Wen et al. (2024).

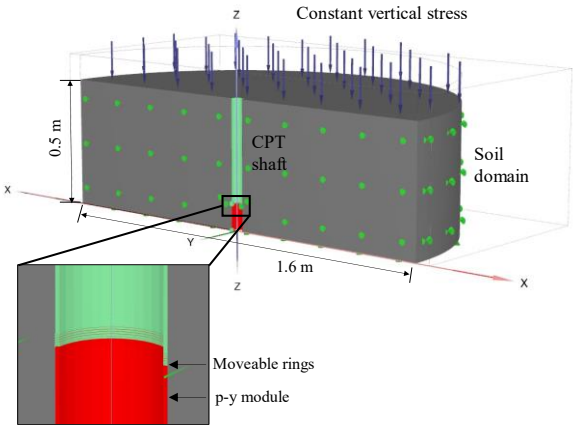

Figure 2. The layout and boundary conditions for modelling of p-y module in clay

Results and Discussions

Figure 3 shows the variation with the normalised lateral reaction forces measured on the p-y module with the normalised lateral movements, while the interface roughness factors α range from 0.01 to 1.0. All results indicate an initially linear behaviour followed by a plateau after a displacement of roughly between 2% D_R and 4%D_R. In this study, the values of the plateau are defined as the lateral bearing factor (N_{RC}) of p-y module. Results show a rise in bearing factors with an increase in the interface roughness. It is interesting to note the magnitudes of N_{RC} are consistent with those from the semi-analytical upper bound solutions developed by Wen et al. (2024). Although not presented here, for a specific interface roughness, N_{RC} is found to be enhanced by the end resistance at the top and bottom of the deforming soil zone, with this factor increasing with D_R/H_R. A simple analytical adjustment factor for this end effect is set out by Wen et al. (2024).

Conclusions

Symmetric 3D FE approach has been utilised in this study to assess the bearing factors of ROBOCONE p-y module that link the load-displacement measurements to key ground geotechnical parameters (i.e. undrained shear module). Results indicate the strong relationship between bearing factors and interface roughness. In addition to undrained shear strength, it is also feasible to provide the elastic stiffness factor that aid to convert the small displacement stiffness of p-y module to the elastic shear modulus of clay (Wen et al. 2024).

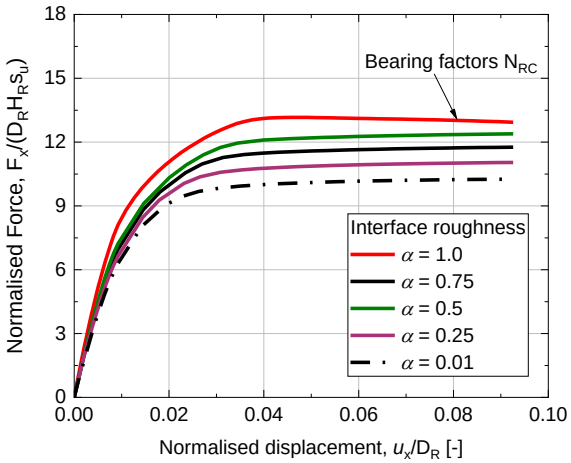

Figure 3. Impact of the interface roughness on the lateral load displacement response of p-y module prototype

Acknowledgements

Financial support from the Engineering & Physical Sciences Research Council (Ref: EP/W006235/1) and Science Foundation Ireland (Ref: 21/ EPSRC/3787) is acknowledged.

References

Creasey, J. et al. 2023. Motivation and demonstration of robotic tolling for ground characterisation: the ROBOCONE. Proceedings of the 9th Int. Conf. on Offshore Site Investigations and Geotechnics, pp: 368-375. London, UK: Soc. Underwater Tech.

Diambra, A., Creasey, J., Leonet, J., Conn, A., Ibraim, E., Mylonakis, G., White, D., Cerfontaine, B., Gourvenec, S., & Igoe, D. 2022. Concept design of a new CPT module for direct in situ measurement of py soil responses. In *Cone Penetration Testing 2022* (pp. 900-906). CRC Press.

Wen, K., White, D.J., Cerfontaine, B., Gourvenec, S., Diambra, A. 2024. Lateral bearing factors and elastic stiffness factors for robotic CPT p-y module in undrained clay. *Comp. & Geotechnics*. (in press).

White, D. J. 2022. CPT equipment: Recent advances and future perspectives. In *Cone Penetration Testing* 2022, (pp. 66-80). CRC press

Yan, Y., White, D. J., & Randolph, M. F. 2011. Penetration resistance and stiffness factors for hemispherical and toroidal penetrometers in uniform clay. *Int. J. Geomechanics*, 11(4), 263-275.

Penetration rate analysis of London Clay using MWD data with time-series method for ground characterization

Siyuan Wu[1], Wendal Victor Yue[2], and Zhongqi Quentin Yue*[3]

*Correspondence: yueqzq@hku.hk

[1] *Department of Civil Engineering, The University of Hong Kong, Hong Kong, P. R. China.*
[2] *Department of Geotechnical Engineering, College of Civil Engineering, Tongji University, Shanghai, P. R. China.*
[3] *School of Science, Harbin Institute of Technology, Shenzhen, P. R. China. (Formerly Department of Civil Engineering, The University of Hong Kong, Hong Kong, P. R. China)*

This extended abstract is republished based on the paper (Wu, S.Y., Yue, W.V., Yue, Z.Q. 2023. On drilling speed of London Clay from MWD data with time-series algorithm for ground characterization. *Géotechnique*, 1-34.)

Abstract

This study examines ground conditions surrounding an old cast iron tunnel within the London Clay strata. Previous research has explored the correlation between borehole investigation and measurement while drilling (MWD) data. However, noise leds to unsatisfactory results, necessitating further investigation. To address this issue, the time-series method is employed, converting MWD data from depth-series to time-series. This allows for a drilling depth curve against net drilling time, which can be divided into linear segments with constant penetration rates. These linear segments, representing homogeneous geomaterials, can be effectively compared with lithological units identified from rotary-cored samples. The consistent results of this study provide valuable insights for ground investigation and construction not only in London but also in other urban areas.

Introduction

Measurement While Drilling (MWD) is a typical in-situ technique employed in mining and tunnelling industries for ground investigation, aiming at collecting drilling data at pre-selected length intervals to interpret the strength of geomaterial and geological bodies based on software and several transducers. This study explores ground investigation methods for evaluating the boundary of London Clay, focusing on the innovative use of (MWD) to estimate soil and rock properties. Traditional investigation methods are expensive, technically demanding, and time-consuming. The MWD system, an external system installed on drilling machines, records drilling data to interpret the strength of geomaterial and geological bodies without disturbing the drilling process. Despite its potential, MWD analysis of London Clay has been limited due to challenges in interpreting penetration rate data, which is often affected by noise.

Various attempts have been made to filter out noise, such as step-wise normalization and data conversion from time-series to depth-series, but these methods have been unsatisfactory. Recent research has utilized Gaussian process models to clean MWD data and identify stratigraphic boundaries, but inaccuracies remain. The study highlights the time-series method for improved methods to address noise issues and interpret penetration rate data from MWD systems for better ground characterization, particularly in London Clay.

MWD data for the ground

The MWD system records drilling parameters, such as penetration rate, down-thrust pressure, rotation speed, torque, and mud pressure at 5 mm depth intervals. Fig. 1 presents the original MWD data, illustrating noise in penetration rate with respect to drill-bit depth. The MWD penetration rate is calculated using Eq.(1).

$$V_{MWD_{(t_i)}} = \frac{\Delta D_{(t_i)}}{\Delta t_i} \quad (1)$$

where $\Delta D_{(t_i)}$ is the i-th preselected depth interval of 5 mm. Δt_i is the total time used for drilling the i-th preselected depth interval.

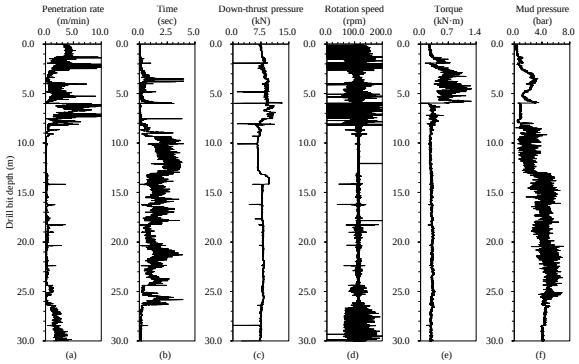

Figure 1. Original MWD (ENPASOL) data along the drill-hole of 30 depth (depth-series record by preselected depth interval of 5 mm) (modified after Gui et al., 2002).

Analysis and result of MWD data with time-series algorithm

Fig. 2a displays the variation of the drill-bit depth with the corresponding total drilling time. The data for the drill-bit depth versus the total drilling time is obtained from the MWD depth-series data in Figs. 1a-b by using the Eq.(2-3).

$$Depth_{(t_i)} = \sum_{i=1}^{I} V_{MWD_{(t_i)}} \times \Delta t_i = \sum_{i=1}^{I} \Delta D_{(t_i)} \quad (2)$$

$$t_i = \sum_{i=1}^{I} \Delta t_i \quad (3)$$

where $Depth_{(t_i)}$ represents the drill-bit depth at the i-th sampling point. t_i is the drilling time at the i-th sampling point.

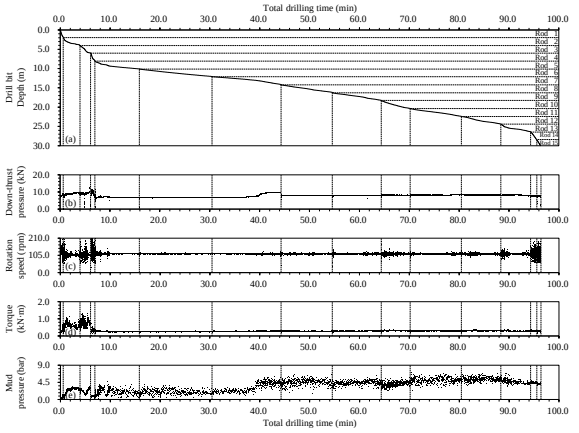

Figure 2. Variation of drill-bit depth and associated drilling parameters versus the total drilling time.

Figs. 2b-e reveal noise in drilling powers during drilling process. Unusual gaps shown at every 2m depth, due to the chuck position moving along sliding channels, indicating a 2m rod length. The unusual gaps are time for adding rod and needs to be eliminated.

Fig. 3 illustrates drill-bit depth advancement against net drilling time, comprising linear segments representing constant penetration rates for homogeneous strata. With 41 subzones ranging from 0.080-3.600m thickness, the ground features 41 homogeneous layers from surface to 30m depth.

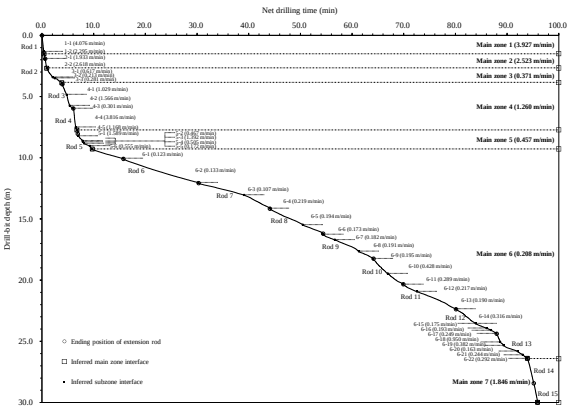

Figure 3. Curve of drill-bit depth versus net drilling time with identified linear zones and constant penetration rates along 30 m drillhole.

Gourvenec et al. (2005) presented ground lithological units and depths from samples in R1 and R2 drillholes. Fig. 3 compares these results with DPM zoning results, showing minimal differences in bottom depths of the four main units (Made Ground, River Terrace Deposits, London Clay, and Lambeth Group).

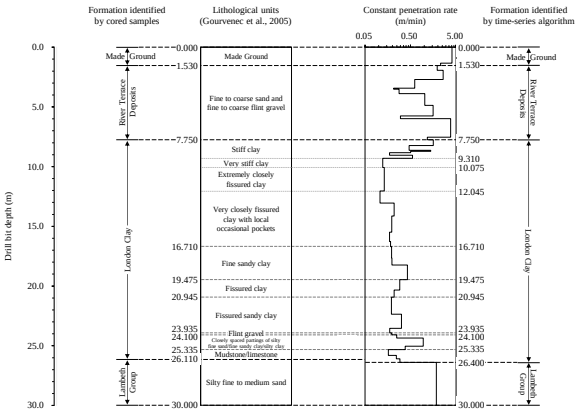

Figure 4. Comparison between the stratigraphy profile from rotary-cored samples and the zoning profile of constant penetration rate.

References

Gui, M.W., Soga, K., Bolton, M.D., Hamelin, J.P. 2002. Instrumented borehole drilling for subsurface investigation. *Journal of Geotechnical and Geoenvironmental Engineering*, 128(4), 283-291.

Gourvenec, S.M., Mair, R.J., Bolton, M.D., Soga, K. (2005). Ground conditions around an old tunnel in London Clay. *Geotechnical Engineering*, 158(1), 25-33.

Fugro AQUISENSE™

Burcin Oral

b.oral@fugro.com

Project Engineering Geologist (Fugro, Fugro House Hithercroft Road Wallingford Oxfordshire OX10 9RB, UK)

Fellow Member (The Geological Society Burlington House Piccadilly London W1J 0BG, UK)

Abstract

Infrastructure development projects face a number of uncertainties relating to the subsurface including hydrogeological conditions and the behaviour of groundwater. Urbanisation and climate change are also having an increasing impact on water as a resource, driving the need for better risk management through monitoring and prediction.

Fugro's patented, integrated and innovative technology, Aquisense™ provides a high speed and accurate approach to evaluate the hydrogeological conditions of permeable soil layers in near surface.

This new approach provides hydrogeologists and geotechnical engineers with more accurate and representative information of a site's hydraulic conductivity potential, leading to safer and more cost-effective construction.

Introduction

Effective ground risk management for infrastructure development and groundwater resource management requires characterisation of subsurface conditions. Using the patented HPT-(A) MPT® technology, Aquisense™ provides a fast and accurate approach to characterise hydraulic conductivity in near-surface permeable soil layers.

Figure 1. Fugro's patented, innovative technology, Aquisense™

Groundwater Risk Management

Managing groundwater and its flow can significantly improve the design of assets that interact with it. Accurate characterisation and representation of the subsurface hydrogeological conditions can contribute to better design and construction, leading to longer asset life and uptime.

Aquisense™ delivers absolute horizontal permeability profiles using the HPT-(A) MPT® technology with a single push ground probe, optimising and even removing the need for costly slug and pump techniques.

Aquisense™ data can contribute to a high-fidelity digital ground model to support better groundwater management decisions. This technique has been proven to deliver more targeted and optimised design of civil assets, particularly flood defence structures, that has contributed to reduction of project cost and risk to up to %50.

Our Approach

A conventional electric cone penetrometer is enhanced with an additional filter port through which water is continuously injected into the subsoil as the cone penetrates the subsurface at the standard rate of 2 cm/sec.

The flow rate and pressure of the injected water are measured and recorded. These measurements provide a continuous profile of relative permeability over the entire depth of the

probing at the same time as engineering measurements are obtained from the conventional cone sensors.

Aquisense™ real-time measurements are used to identify permeable soil zones, which are critical for engineering design that can be targeted for a mini pumping test (MPT). sensors.

The MPT provides an absolute and undisturbed measurement of horizontal permeability, conducted in situ without recovery or rerun of the tool. MPTs performed within the probing are used to calibrate the continuous relative permeability profile from the hydraulic profiling tool (HPT) measurements into absolute data.

Depth reach	40-50 m*
Permeability range	0.1 - 200 m/day ($1*10^{-6}$ - $2*10^{-4}$ m/s)
Subsoil conditions	Saturated
Probing speed	2 cm/s
Injection ratio	0.1 – 5.0 L/min
Measured soil properties	(Horizontal) permeability
	Water pressure
	Electrical conductivity
	Cone resistance
	Friction ratio
	Storage of the soil
	Temperature sensor
*Dependent of the equipment and hardness of the soil	

Figure 2. Technical Specificationso

Additionally, with the so called Anisotropic Mini-Pumping Test (AMPT) the vertical permeability can be determined by placing a second water pressure sensor next to the Aquisense™.

The Fugro Difference

Fugro's integrated and innovative approach to site investigation improves the speed and accuracy of ground risk characterisation to support optimised groundwater control design and improve management of critical structures.

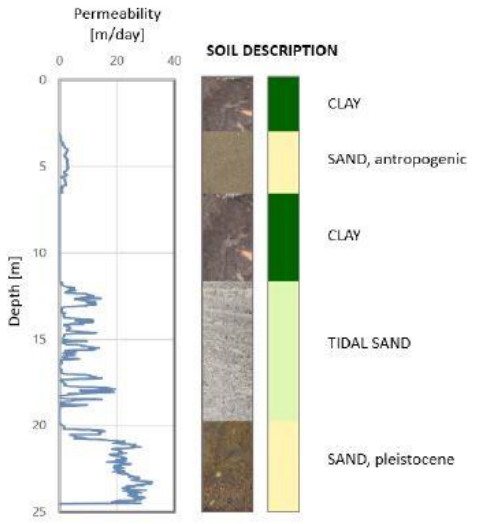

Figure 3. Readjusted and representative hydraulic conductivity soil profile acquired using Aquisense™

Benefits

- Improved asset design through high quality hydraulic conductivity.
- Less invasive single push design in contaminated or urban sites where minimal environmental impact is critical.
- Remote CPT in contaminated or isolated environments.
- Faster data acquisition compared to conventional pump tests.
- Continuous in situ permeability profiles over the entire probe depth.

Assessment on Instrument-Soil-Structure Interaction

J. Wills-Sanin*[1], J. Standing[1], L. Zdravkovic[1]

*Correspondence: jw3918@ic.ac.uk

[1] *Imperial College London, Department of Civil and Environmental Engineering, London, UK*

Abstract

A methodology to assess the interaction between monitoring instrument, soil and structure has been developed. The objective of the Instrument-Soil-Structure Interaction (ISSI) methodology is to create an environment which allows the reliability of monitoring instrument readings and verification of general mechanisms acting in specific geotechnical scenarios to be investigated. Various examples have been developed showing the influence that these three components have on each other in different contexts.

Introduction

The ISSI methodology follows the spirit of Peck's Observational Method (OM) (Peck, 1969) adding a higher level of detail to the reliability and fidelity of field observations. Quantifying the precision and bias of field instrumentation is challenging, however, processing field monitoring data without considering the interaction between a three-component system (Instrument-Soil-Structure as seen on Figure 1) could hinder the understanding of mechanisms acting in some specific geotechnical scenarios. The first ISSI assessment evaluates the influence of the datum location on the apparent observed response of the structure. A stable datum is essential for guaranteeing reliable measurements from field. A Finite Element Analysis (FEA) model has been developed to investigate the influence of tunnel construction on potential datum positions (Potts and Zdravkovic, 1999). If the datum is too close to the structure (e.g. tunnel), ground and structural interaction with the instrument could result in inaccurate readings.

A second ISSI assessment, similar to the first, studies the role of datum location but incorporates the role of the soil heterogeneity in this interaction. If the ground is highly variable it is possible that the datum could be installed within different, unrepresentative, soil conditions from the structure, thus creating variability in readings and affecting measurement reliability. Random fields (Vanmarcke, 2010) have been implemented within the FEA to investigate this effect, assessing different levels of soil heterogeneity for a tunnel excavation.

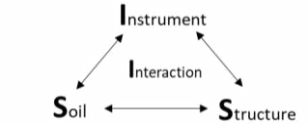

Figure 1. ISSI diagram

Lastly, the ISSI methodology is applied to a case study relating to a deep excavation in Boom Clay, the heaving at the base of the excavation was found to be influenced by inward movement of the retaining walls, showing that the heaving mechanism in this scenario is not only dependent on stress release, but is also influenced by the interaction of the structure.

ISSI on Datum Correction

If the datum location is within the zone of influence of the construction actions, absolute measurements are unreliable, as mentioned by Dunnicliff: "many benchmarks used on construction projects are not as stable as the user thinks" (Dunnicliff, 1988). The objective of this study is to attempt to quantify this statement using the ISSI methodology on a specific boundary value problem (short-term tunnel excavation) with a concise parametric study on different ground conditions (stiff clay vs soft clay). The datum correction uses FE simulations to assess the error related to different datum locations. The absolute displacements (i.e. corrected values of displacements) are computed by selecting different datum locations. As expected, as the distance of the datum from the tunnel increases, the smaller the error. Figure 2 shows the contour region for 1 mm of the

corrected vertical displacement for datum locations varying at different depths at a 10 m offset from the centre-line of the tunnel.

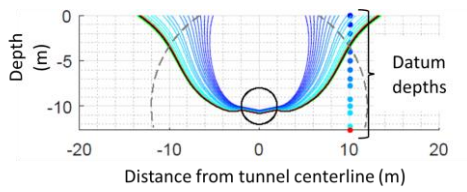

Figure 2. Datum correction for vertical contour displacement for 0.001 m

The practical purpose of this ISSI assessment is to provide guidance on a minimum distance and depth of the datum location from the structure. This approach avoids reliance on statements such as “datum should be stable” or blindly using nonspecific and un-quantitative “rules of thumb”.

ISSI on Datum & Heterogeneous Soil

The second ISSI assessment of datum selection incorporates soil heterogeneity. An extensive parametric analysis assessing the influence of the soil correlation distances (i.e. ground spatial variability) on the datum correction has been performed.

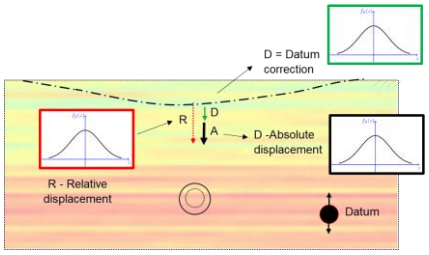

Figure 3. Schematics of heterogenous and datum

Figure 3 illustrates the essence of this ISSI assessment, which shows the soil surrounding a tunnel excavation represented by a random field with a tunnel excavation. The absolute displacements are not a deterministic value; the stochastic behaviour of the ground can be incorporated into a reliability-based design.

ISSI Case study Boom Clay

The Geotechnical division of the Flemish government (GDFG) performed a large-scale monitoring trial to assess the heaving behaviour of the Boom Clay as important engineering assets are built on this geological unit (Couck, 2015). Following the ISSI methodology FE simulations verified the field monitoring data from extensometers at the base of the excavation (Case 1 stress release excavation). Then a modified boundary value problem of the excavation was assessed using FEA (Case 2), where there was no stress release, and the known wall displacements were applied as a boundary condition of the model.

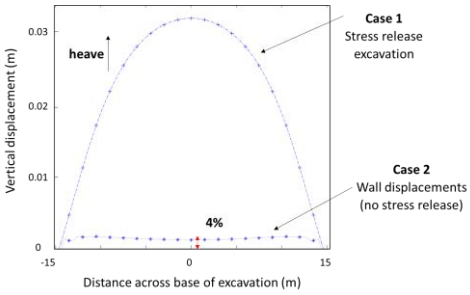

Figure 4. Heaving at base of excavation Case 1 and 2

As shown on Figure 4 the heaving at the base of the excavation was found to be triggered by stress release as well as the inward movement of the walls, the wall displacements are responsible for up 4% of the heave at the base of the excavation. Furthermore, a parametric analysis assessing the influence of the closeness of the walls was performed. The results show that the influence of heaving due to wall displacements increases as the width of the basement decreases. The ISSI methodology highlighted the role of the structure on the heaving behaviour which increased precision in the understanding of the heaving behaviour of Boom Clay and overall, a better understanding of the mechanisms acting in this specific geotechnical scenario was achieved.

References

Couck, J., van Lysebetten G., van Royen, K., Janssens, B., de Nijs, R.). 2015. Proefcampagne voor de Oosterweelverbinding in Antwerpen. Geotechniek. 12-19.

Dunnicliff, J. 1988. Geotechnical Instrumentation for Monitoring Field Performance. ISBN: 978-0-471-00546-9

Peck, R. B. 1969. Advantages and limitations of the Observational Method in applied soil mechanics. Ninth Rankine Lecture. Géotechnique 19: 171-187.

Potts DM., Zdravkovic L. 1999. Finite element analysis in geotechnical engineering: theory. Thomas Telford, London, UK.

Vanmarcke, E. 2010. Random fields: analysis and synthesis. World Scientific, USA.

A new equipment to investigate the effect of cable installation procedure on thermal properties of soil

Z. Zhou*, A. Diambra, and T. Liu

*Correspondence: zhixin.zhou@bristol.ac.uk

School of Civil, Aerospace and Design Engineering, University of Bristol, Bristol, BS8 1TR, UK

Abstract

Accurate determination of ampacity rating for high-voltage submarine cables is crucial for offshore renewable wind energy sector. A key factor influencing this rating is the thermal properties of the soils surrounding the cables. This paper focuses on developing a new laboratory experimental methodology to assess how cable trenching installation and backfilling processes alter soils' physical and thermal characteristics over the cable's short- and long-term lifecycle. The experimental set-up included a multiple thermal needle system that can measure thermal conductivities simultaneously at multiple locations and along different directions. The cable installation and backfilling process was modelled by applying jetting pressures to the soil samples and allowing subsequent re-deposition. Preliminary results are presented in this paper that demonstrate the functionality of the testing system.

Introduction

Reliable and optimised design of submarine high-voltage (HV) electrical cables is increasingly critical due to the highly non-uniform distributions of offshore renewable energy production (Wang et al., 2021). Typical ampacity rating restricts the cable operating conductor temperature to 90°C for alternating electrical current (Worzky, 2009). Therefore, accurate assessment of the rates of heat dissipation, primarily influenced by the thermal conductivities of the surrounding sediments, is crucial for designing and operating HV cables within this temperature limit. However, there are few direct measurements of post-installation soil thermal properties and relatively limited assessments of changes in geotechnical properties induced by cable installation (Carbon Trust, 2024). This study aims to close these research and application gaps through laboratory investigation applying a new experimental methodology and system.

Cable installation methods

Submarine cables require adequate burial and protection to withstand mechanical perturbations and ensure their integrity and reliability throughout project lifetime. Figure 1 provides an overview of typical installation procedures adopted for different soil types.

While all these procedures are expected to affect soils' mechanical and thermal properties (and in turn their ability to conduct heat), the initial aim of this research is to simulate the water jetting operations typically employed for sandy soils.

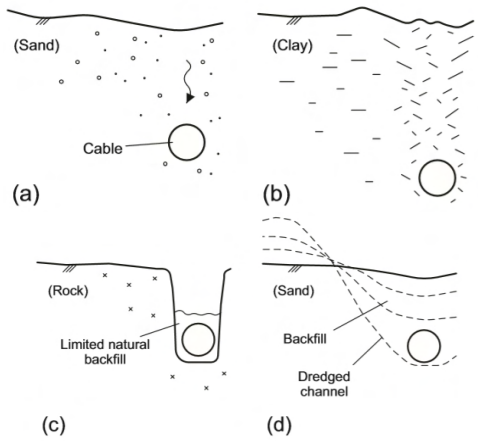

Figure 1. Cable installation methods: (a) jetting, (b) ploughing, (c) cutting, (d) dredging (DNV, 2016).

Methodology

The experimental setup developed for investigating the effects of installation processes on seabed soil properties is shown in Figure 2. A soil specimen was formed in the 140mm-diameter cylindrical model. Jetting was simulated through upward water flow, and the pressure was regulated by two water-air interfaces connected to the air pressure system. Soil thermal properties were monitored by a customised multi-needle system shown in Figure 3. The system allowed for simultaneous monitoring of thermal conductivities at different positions

within the soil sample, offering significant advantages over commercially available single-needle devices. Routine testing method using vertically penetrated needles may not fully characterise soil stratification and heterogeneity effects, which are potentially critical for HV cables typically buried within the first meter of sediments (van Landeghem et al., 2014).

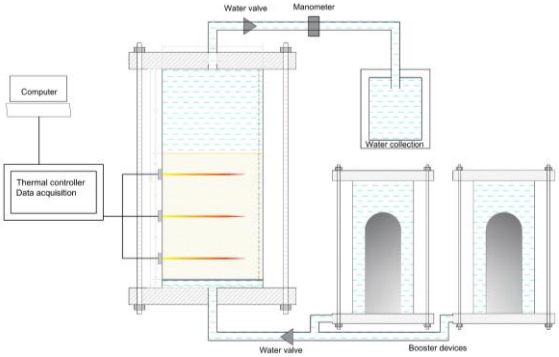

Figure 2. Setup of the customised test system.

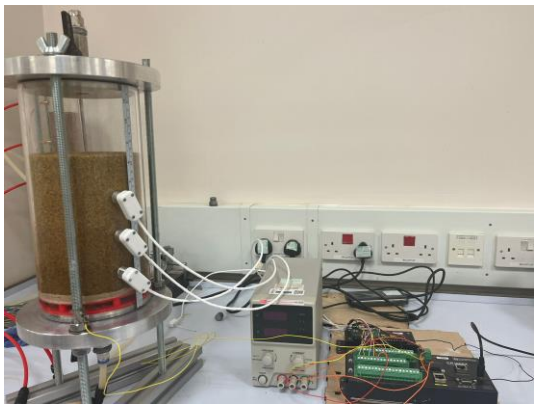

Figure 3. Multi-needle system setup.

Initial results and discussion

Initial tests were performed with a saturated Leighton buzzard 14/25 sand (d_{50} = 0.88 mm, C_c = 1, C_u = 1.88, G_s = 2.65) specimen prepared to a relative density of 77.4%. Figure 4 plots the evolution trends for thermal conductivities measured by three needles after jetting at 50 kPa pressure. Variabilities can be seen in the pre-jetting thermal conductivity measurements, which might reflect effects of boundary conditions, as the lower and upper needles were placed relatively close to the specimen ends. Measurements at the middle needle position decreased abruptly post water jetting but remained largely constant as the sand re-deposited and settled. This indicates that the jetting process loosened the specimen substantially, leading to soil states significantly differing from those 'in-situ' pre-jetting conditions.

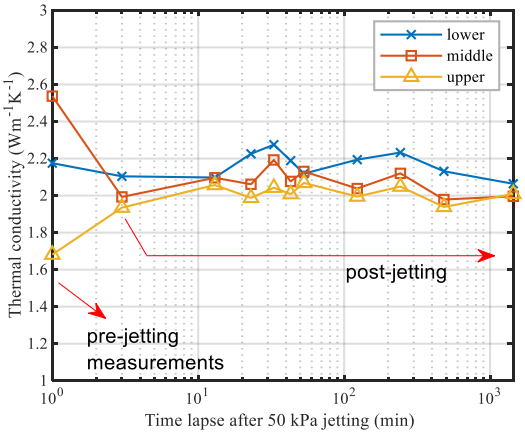

Figure 4. Evolution of thermal conductivity after jetting.

Conclusions and future work

A new laboratory procedure employing an in-house multi-needle system was proposed to assess the effects of HV electrical cable installation on the thermal properties of soils. Preliminary results show considerable changes to soil density and thermal properties due to jetting. Further studies are underway to explore the effects of varying column heights, soil mixtures and conditions, and jetting pressures, enabling optimised installation and design of HV cables.

Acknowledgement

We thank the financial support by China Scholarship Council and technical support by ScottishPower Renewables, Geoquip Marine and Prof. Justin Dix (University of Southampton).

References

DNV. 2016. Recommended Practise: Subsea power cables in shallow water. Available online: http://rules.dnvgl.com/docs/pdf/dnvgl/RP/2016-03/DNVGL-RP-0360.pdf. DNV-RP-0360

RPS. 2021. Review of cable installation, protection, mitigation and habitat recoverability. Crown Estate.

van Landeghem, K.J.J., Baas, J.H., Mitchell, N.C., Wilcockson, D. & Wheeler, A.J., 2014. Reversed sediment wave migration in the Irish Sea, NW Europe: A reappraisal of the validity of geometry-based predictive modelling and assumptions, *Marine Geology*, **295-298**, 95-112.

Wang, W., Yan, X., Li, S., Zhang, L., Ouyang, J., and Ni, X. 2021. Failure of submarine cables used in high-voltage power transmission: Characteristics, mechanisms, key issues and prospects. *IET Gener Trans Distr*, **15**(9), 1387-1402.

Worzyk, T. 2009. Submarine Power Cables: Design, Installation, Repair, Environmental Aspects. 10.1007/978-3-642-01270-9.

Experimental investigation of Rock Anchor behaviour under diverse loading conditions

A. Genco*[1], M.O. Ciantia[1], M. Brown[1], M. Previtali[1], A. Ivanovic[2], N. Cresswell[3] and V. Twomey[3]

*Correspondence: 180026675@dundee.ac.uk

[1] University of Dundee, Nethergate DD1 4HN, United Kingdom
[2] University of Aberdeen, King's College AB24 3FX, United Kingdom
[3] Schottel Marine Technologies, Commercial Quay EH6 6LX, United Kingdom

Abstract

The increasing attention toward Offshore Renewable Energy (ORE) applications require the development of cost-efficient and reliable anchoring solutions. In the context of rocky seabeds, Rock Anchors (RAs) represent a promising solution since can be applied in shallow and deep waters minimizing the relevant costs (i.e. installation, operational, and materials). These systems require novel design procedures based upon the direct observation of failure mechanisms through experimental tests. In this work a 1g physical model is presented to show the behaviour of a real groutless and self-drilling anchoring system under diverse loading conditions by means of sleeved anchor bolts installed in soft calcarenite rock. The load was applied through an Instron UTM in tension. The failure mechanisms and the load capacity were herein evaluated experimentally and compared with existing analytical methods. The main findings of this work show the underestimation of the maximum axial and lateral capacity using both analytical design methods and the formation of axisymmetric pull-out cone and shallow wedge respectively for axial and lateral failure mechanism.

Introduction

Even though many anchoring technologies exist in literature for offshore applications, a lack of systems was identified for rocky seabeds. Rocky seabeds are frequently characterized by strong current and wave conditions which require reliable solutions. Current RA design procedures are based upon conservative analytical methods, which drive up the overall cost of these systems. This requires an advanced investigation of the propagation of the failure mechanism by means of field and physical modelling tests, which can lead to the optimization of the design methods. This work presents 1g physical model testing of a novel RA designed for Offshore Renewable Energy (ORE) applications in soft rock under diverse loading conditions. The real RA was modelled using expandable anchor bolts generally adopted for installation in concrete. The results highlight the underestimation of the axial and lateral capacity using existing analytical approaches and the formation of axisymmetric pull-out cone and shallow wedge failure respectively under axial and lateral/inclined loading.

Physical modelling of a novel anchoring system

An innovative groutless and self-drilling anchoring technology was designed by SCHOTTEL Marine Technologies for rocky seabeds and ORE applications (Figure 1a) (Genco et al., 2023). This anchor was physically modelled by means of sleeve expanded anchor bolts installed in soft calcarenite rock which transfer the load mainly by friction.

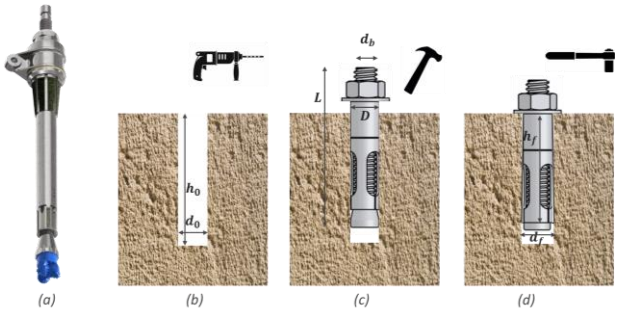

Figure 1. (a) 3D visualization of the Rock Anchor proposed by SCHOTTEL Marine Technologies and (b, c, and d) sketch representing the different installation phases of the sleeve expanded anchor bolts installed in calcarenite rock

The installation can be summarised in the following phases: hole drilling, insertion, and pretension of the sleeve anchor bolt (Figure 1b, c, and d). The main geometrical properties of the anchor bolt are listed in Table 1.

Table 1. Main geometrical properties of the anchor bolt

d_b [mm]	d_0 [mm]	d_f [mm]	h_0 [mm]	h_f [mm]	L [mm]
8.0	14.0	17.0	60.0	40.0	87.0

The soft rock used in this study is the calcarenite of Gravina (outcropping in Apulia, Southern Italy) which exhibits a softening behaviour. Further details on this rock type are available in Ciantia et al., (2015). The main physical and mechanical properties are synthesized in Table 2.

Table 2. Main physical and mechanical parameters of Calcarenite rock from Ciantia et al., (2015)

γ_{dry} $[kN/m^3]$	G_s [-]	e [-]	$\sigma_{c,dry}$ [MPa]	$\sigma_{t,dry}$ [MPa]	E_{dry} [MPa]	ν [-]
13.1	2.73	1.09	2.44	0.47	315	0.09

Tests results

Figure 2a displays the comparison between the axial, lateral, and inclined (30°) load-displacement curves. The axial loading test was conducted performing a loading phase up to 5 mm (0.35D) (Point A), followed by an unloading stage (Point B), and a final loading phase (0.57D) (Point D). Whereas lateral and inclined loading tests were conducted performing a single loading phase up to the end of the test. The axial and lateral experimental data were compared with two existing analytical methods: Kim and Cho (2012) and Yang (2006), showing that both analytical methods presented underestimate the maximum axial and lateral load capacity by 22.4% and 73.1%, respectively.
Figure 2b shows the failure mechanism exhibited for the axial loading test which presents the progressive formation of an axisymmetric pull-out cone (Point D). Whereas the lateral loading test shows the gradual spalling of the rock in front of the sleeve anchor bolt due to the propagation of a shallow failure wedge (Point H). Similar shallow wedge failure mechanism was observed for the inclined loading test (Point F) performed which shows higher load capacity than the lateral loading configuration.

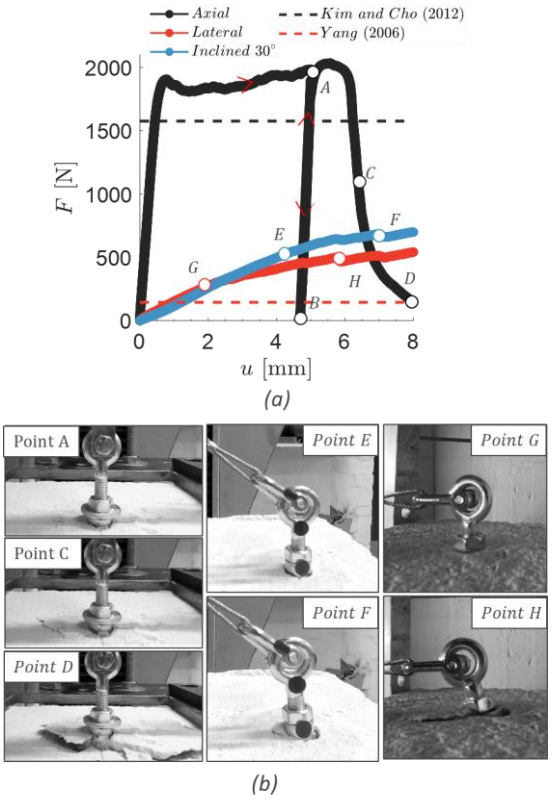

Figure 2. (a) Load-displacement curves compared with analytical methods and (b) and pictures taken at different stages of the tests (Point A, C, and D for axial, Point E and F for inclined, and Point G and H for lateral loading)

Conclusions

In this work the axial and lateral response of RAs by means 1g physical tests was evaluated. The results show:

1. The propagation of an axisymmetric pull-out cone and shallow failure wedge respectively for axial and lateral loading
2. The underestimation of maximum capacity for both axial and lateral analytical methods

References

Ciantia, M. O., Castellanza, R., & Di Prisco, C. 2015. Experimental Study on the Water-Induced Weakening of Calcarenites. Rock Mechanics and Rock Engineering, **48**(2), 441–461.

Genco, A., Ciantia, M. O., Brown, M., Previtali, M., Ivanovic, A., & Cresswell, N. 2023. Large deformation numerical analysis of rock permeability influence on anchor performance for offshore renewable applications. Proceedings of the 10th European Conference on Numerical Methods in Geotechnical Engineering, (June): 112-118

17th BGA YGES
University of Cambridge
1-3 July, 2024

The influence of drainage conditions on cyclic behaviour of cohesionless soils in the VDDCSS

K.Z. Wen*[1], R.M. Buckley[2], and B.W. Byrne[1]

*Correspondence: kathy.wen@spc.ox.ac.uk

[1] *University of Oxford, Department of Engineering science, Parks Road, Oxford OX1 3PJ, UK*
[2] *University of Glasgow, James Watt School of Engineering, G12 8QQ, UK*

Abstract

This study experimentally explores the limiting cyclic behaviour of a cohesionless soil under fully drained and fully undrained conditions using the VDDCSS. A series of cyclic tests in the two drainage conditions were conducted varying loading amplitude, ζ_b and loading asymmetry, ζ_b. The results demonstrate that cyclic loading increases the stiffness and strength of cohesionless soils in drained conditions due to densification and interlocking. Contrastingly, undrained behaviour exhibits almost no changes with cycles until liquefaction which is observed to occur instantaneously.

Introduction

Cyclic loading is known to induce several phenomena at both the soil elemental and foundation level, including densification, generation of porewater pressure, u, accumulated ratcheting, γ_{acc}, changes to stiffness, G_{sec}, and energy dissipation, η, see Fig. 1b for definitions. In drained conditions, densification has a positive relationship with loading amplitude, ζ_b and loading frequency, f and a negative relationship with relative density, D_r and vertical stress, σ'_v, see Al Tarhouni and Hawlader (2021); Nong and Park (2021). Similarly, γ_{acc} has a positive relationship with ζ_b and a negative relationship with p'_0 and D_r, see Chang and Whitman (1988); Arangelovsk and Towhata (2004).

In undrained conditions, researchers have investigated the development of u, which is positively related to ζ_b and f and negatively related to D_r (Do et al., 2023). Mele et al. (2019) demonstrates a strong correlation between η and u. Andersen (2015) presents a large set of undrained cyclic direct simple shear tests indicating that D_r is negatively correlated to γ_{acc} and number of cycles to failure, N_f, noting that N_f is a function of ζ_b and loading asymmetry, ζ_c.

For field applications, cyclic loading is likely to induce a partially drained condition, which exists between the drained and undrained conditions. This response is dependent on the drainage length, permeability of the material and loading frequency. It is therefore of interest to explore limiting behaviours of drained and undrained cyclic behaviour, to understand the mechanisms that govern each condition.

This study presents the drained and undrained cyclic behaviour of Cuxhaven sand, a fine-grained naturally occurring silica sand from the North of Germany.

Testing apparatus and definitions

This research makes use of the NGI-style Variable Direct Dynamic Cyclic Simple Shear (VDDCSS) apparatus manufactured by GDS Instruments as illustrated in Fig.1(a).

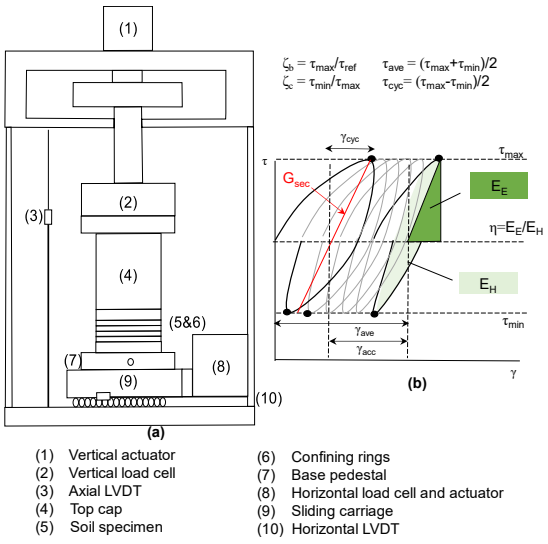

Figure 1. (a) VDDCSS schematic (b) Cyclic stress-strain behaviour and cyclic definitions, τ_{ref} refers to maximum shear stress from monotonic tests.

Stress-strain behaviour

The cyclic stress-strain response of selected drained and undrained tests is shown in Fig. 3.

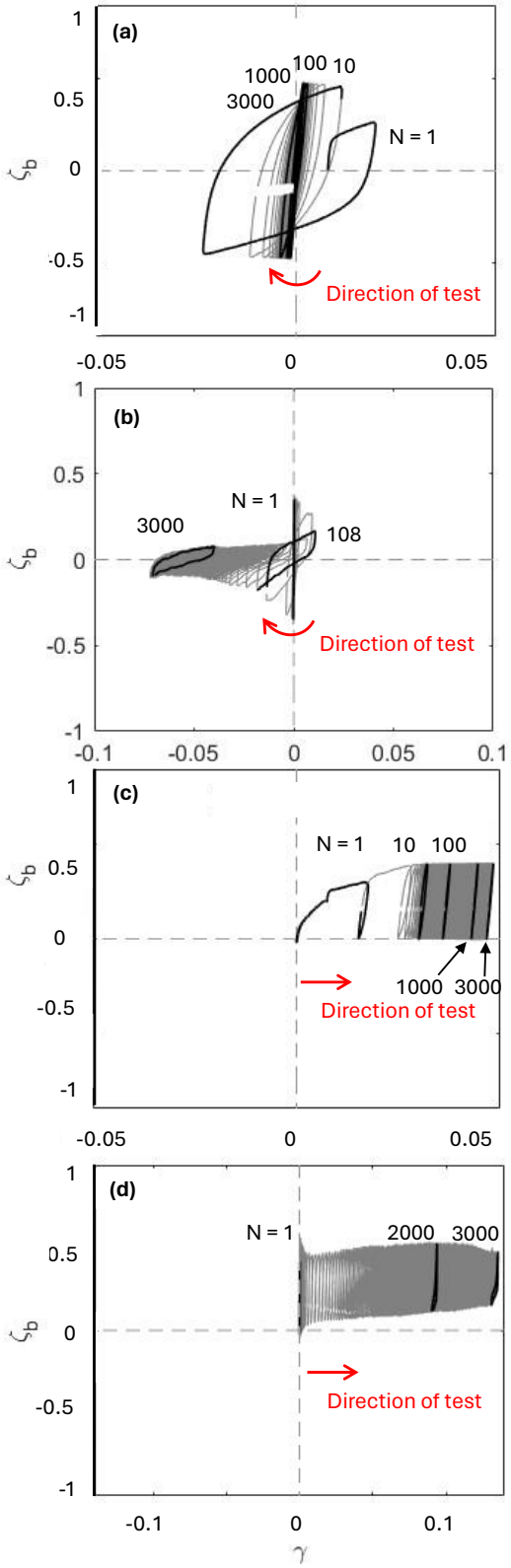

Figure 3. Cyclic stress-strain, D_r =60%, σ'_v = 36kPa (a) Drained ζ_b = 0.4, ζ_c = -1 (b) Undrained ζ_b = 0.4, ζ_c = -1 (c) Drained ζ_b = 0.4, ζ_c = 0 (b) Undrained ζ_b = 0.4, ζ_c = 0.

Idealised cyclic behaviour

The idealised cyclic behaviours based on experimental results are shown in Fig 4. The dotted red line shows N_f of undrained specimens.

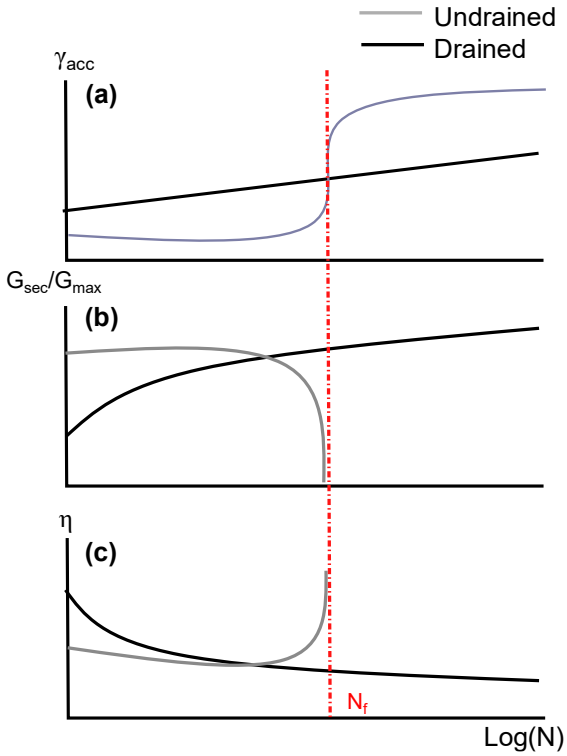

Figure 4. Idealised cyclic features (a) Accumulated ratcheting (b) Stiffness (c) Energy dissipation.

References

Arangelovsk, G., Towhata, I., 2004. Accumulated Deformation of Sand with Initial Shear Stress and Effective Stress State Lying Near Failure Conditions. *Soils and Foundations* **44** (6): 1-16

Al Tarhouni, M.A., Hawlader, B. Monotonic and cyclic behaviour of sand in direct simple shear test conditions considering low stresses. *Soil Dynamics and Earthquake Engineering* **150**

Andersen, K. 2015. Cyclic soil parameters for offshore foundation design. *Frontiers in offshore geotechnics III* **5**

Chang, C.S., Whitman, R.V. 1988. Drained Permanent Deformation of Sand Due to Cyclic Loading. Journal of Geotechnical Engineering **114** :1164-1180

Do, T.M., Laue, J., Mattson, H.,Jia, Q. 2023. Excess pore water pressure generation in fine granular materials under undrained cyclic triaxial loading. *International Journal of Geo-Engineering*

Mele, L., Lirer, S., Flora, A. 2019. The specific deviatoric energy to liquefaction in saturated cyclic triaxial tests. *Earthquake Geotechnical Engineering for Protection and Development of Environment and Constructions*: 3861-3868

Nong, Z., Park, S. 2021. Effect of Loading Frequency on Volumetric Strain Accumulation and Stiffness Improvement in Sand under Drained Cyclic Direct Simple Shear Tests. *Journal of Geotechnical and Geoenvironmental Engineering*

Design and development of apparatus for modelling a "Shaft-breakout" in clay

M. Ucur*[1], S. Divall[1], and S.E. Stallebrass[1]

*Correspondence: mayda.ucur@city.ac.uk

[1] *Affiliation (City, University of London, Northampton Square, London, UK)*

Abstract

This paper details the proof-of-concept testing of a shaft-breakout construction process. The novel geotechnical centrifuge testing comprised a model circular liner with a removable opening situated within a normally consolidated Speswhite kaolin clay sample. This standardised model approach will later be modified to simulate the short-term structural behaviour of the model shaft liner during the controlled formation of an opening in a series of centrifuge tests.

Background

Recently, there has been an increase in underground infrastructure development driven by the aim of reducing the contribution transportation and other systems have to surface congestion. The incorporation of shafts are essential for providing access to underground tunnels, for ventilation, and for material transportation. The connection between a shaft and a tunnel is achieved by a construction process known as "shaft-breakout". This construction process involves the formation of a circular opening in the sides of the vertical shaft, disturbing the loading and supporting equilibrium of the shaft.

Recent research (Challinor, 2022) highlights the limited publications and guidance available for designing the shaft break-out. The most detailed guidance published is the British Tunnelling Society's Tunnel Design (The British Tunnel Society, 2004). However, this approach is considered to lead to conservative designs regarding cost and/or material efficiency and generally restricts the size of this opening to one-third of the shaft diameter.

This paper aims to describe the physical modelling techniques used to model a circular vertical shaft break-out in clay. It focusses on the design of a repeatable and removeable opening simulating the break-out at 118 times Earth's gravity (N = 118*g*).

Introduction

The model shaft lining, Figure 1 is formed of a 1.6mm thick aluminium tube with an outer diameter of 101.6mm and depth of 254mmm. These model dimensions were chosen to represent a continuous concrete lining at prototype scale. An opening of 34mm diameter was cut into the aluminium tube 212mm from the top of the shaft to the centre of the opening. A 3D printed curved plug, using micro carbon fibre-filled nylon material known as onyx, (Figure 2) is used to fill and seal the opening.

The preliminary geotechnical centrifuge test, described herein, was conducted to provide an understanding of what would be a suitable support mechanism for the curved plug to ensure the seal between the lining and the plug would not be broken until initiated remotely at 118*g*.

Figure 1. Model shaft lining with an opening

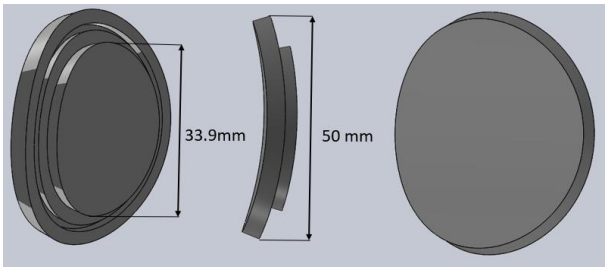

Figure 2. Render of the curved plug

Experimental Setup

The soil container used was a stainless-steel cylindrical tub with a diameter of 420mm and depth of 295mm. The tube was filled with Speswhite kaolin slurry at a water content of 120% and subsequently subjected to a vertical stress of 225kPa using a hydraulic press. After consolidation a thin-walled circular cutter was used to create a pre-bored cavity in the centre of the sample. The model shaft lining was placed within this cavity with the plug pre-installed as shown in Figure 3. The model was weighed and placed on the swing of City, University of London's geotechnical centrifuge.

The preliminary test consisted of accelerating the model up to 118 times Earth gravity in stages. An endoscope was installed facing into the model shaft lining from the top of the tub. The endoscope was used to observe the behaviour of the curved plug and any soil failure.

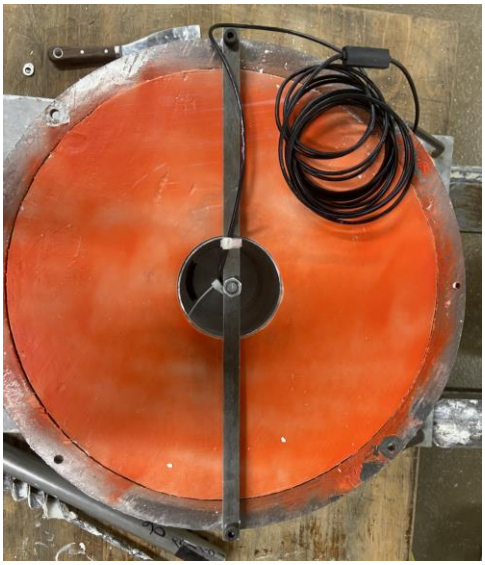

Figure 3. Photo of the top of the model

Initial Results

Images were captured at a rate of one a second during the test. During the test the images recorded were related to the current *g*-level. At 50g the plug was pushed from the opening into the centre of the model shaft lining. Subsequently, the soil slowly extruded into the model shaft lining as the g-level increased from 50 and 118 times Earth's gravity.

Figure 4. Typical image recorded by the endoscope

Conclusion

Although, the final design is not yet fully developed the preliminary test assessing the stresses from the soil acting on the plug was successful. The preliminary test indicates a mechanism will be required for the plug to be released remotely at 118g. The support mechanism will be required to hold the curved plug in place without the requirement of the plug to be "pulled out". One possible solution would be to use compressed air confined in a shaped rubber bag. To provide insight into the distribution of stresses in the shaft during the shaft-breakout, instrumentation, strain gauges, will be attached to shaft.

References

Challinor, P. (2022). Openings in shafts (in London Clay). MSc Dissertation, City, University of London, London, UK.

The British Tunnelling Society (2004) *Tunnel Lining Design Guide*

17th BGA YGES
University of Cambridge
1-3 July, 2024

Numerical analysis of tunnel-foundation interaction in London Clay

J. Liu*[1], A. Tsiampousi[1], A. Ruiz López[1], and D.M.G. Taborda[1]

*Correspondence: j.liu22@imperial.ac.uk

[1] *Imperial College London, Exhibition Rd, South Kensington Campus, London, UK (SW7 2AZ)*

Abstract

Tunnelling-induced ground movements can lead to the deformation of superstructures, which may affect their serviceability. In London, research has been carried out to understand tunnel-superstructure interactions and improve predictions of the impact of tunnelling on adjacent buildings. Existing research has focused primarily on raft foundations. As a result, the design guidelines that have been developed to tackle the problem of tunnel-structure interaction are limited to such foundations and further research is required to understand the impact of tunnelling on piled and piled raft foundations. Numerical analysis can provide an invaluable tool to bridge this gap, allowing the influence of deep foundations (e.g., piles) and the interface conditions between the building and the ground to be considered, provided that validated numerical models are used. In this research, the case study of the construction of the Elizabeth line beneath a site in Whitechapel, London, is simulated using 2D finite element (FE) analysis. A greenfield case is first considered to calibrate the FE model. The numerical results are in very good agreement with the field data. The second part of the study involves the analysis of tunnelling beneath a building founded on a piled raft. The influence of the building stiffness and the characteristics of its foundations on the shape of the settlement trough as predicted by the FE model are carefully evaluated.

Introduction

Space overuse in big cities has shifted focus to underground space usage. Tunnel induced volume loss can cause settlement of the soil, thus affecting existing superstructures. In London, many studies have been carried out to predict tunnelling effects on adjacent buildings (Potts & Addenbrooke, 1997; Franzius et al., 2004). However, most existing methods to predict the influence of tunnelling are based on studies that neglect foundations or assume them to be simple rafts rather than more complicated deep foundations (e.g., piled raft foundation). Therefore, more careful studies need to be carried out regarding the influence of tunnelling under piles.

Site Description

The site chosen for study is the Vallance Road Gardens and a nearby 3-storey building supported by a piled raft foundation along Castlemain Street. This site is located west of Whitechapel underground station in East London, undercrossed by the Elizabeth Line. Field data for the greenfield movements observed at Vallance Road Gardens are available, allowing the validation of numerical models which can then be used to investigate tunnel-structure interaction.

Numerical Model

A typical London ground profile is found at this site. Made Ground is modelled as a linear elastic-perfectly plastic material with a Mohr-Coulomb failure criterion. The remaining strata (River Terrace Gravel, London Clay, Lambeth Group Clay, Lambeth Group Sand and Thanet Sands) are modelled using a perfectly plastic Mohr-Coulomb yield surface combined with an isotropic nonlinear elastic stiffness model implemented as a user-defined model in PLAXIS (Taborda et al., 2023a, 2023b). The parameters for all layers follow those adopted by Gawecka et al. (2017).

This site has a perched aquifer above London Clay and a bottom aquifer in the Thanet Sands with the pressure head at -27 mOD (Chong, 2015).

The analyses considered coupled consolidation, with the following nonlinear anisotropic variation of permeability with depth, implemented through a user-defined flow model in PLAXIS, adopted for the clay layers (Taborda et al., 2023c):

$$log_{10}k_y = a(y - y_{LC}) + b \quad (1)$$

$$k_y > k_{y,min} \quad (2)$$

$$k_x = 2 \cdot k_y \quad (3)$$

The remaining layers were considered drained.

Results

The analysis results for the greenfield case are shown in Fig. 1. A good agreement with the field data was attained.

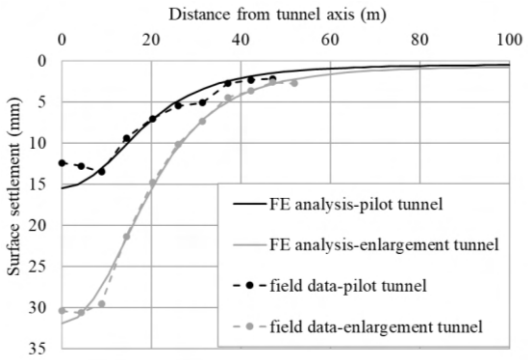

Figure 1. Greenfield settlement trough compared with field data (Chong, 2015)

Three cases are considered to study the influence of building stiffness and existence of piles, as shown in Fig. 2. The results indicate that the introduction of piles leads to settlement troughs which are narrower and deeper. Moreover, the influence of the building stiffness on the shape of the settlement trough is clear, resulting in a reduction of the maximum settlement.

Conclusions

2D Finite Element analysis has been carried out to verify the ability of the numerical model with regard to reproducing the greenfield excavation of a tunnel in London. A good agreement is obtained between measured and calculated settlements The influence of building stiffness and existence of piles are also studied. When compared to the case where a raft foundation is used, both aspects are seen to influence considerably the shape of the settlement trough. Future work will focus on the detailed three-dimensional modelling of tunnel-structure interaction.

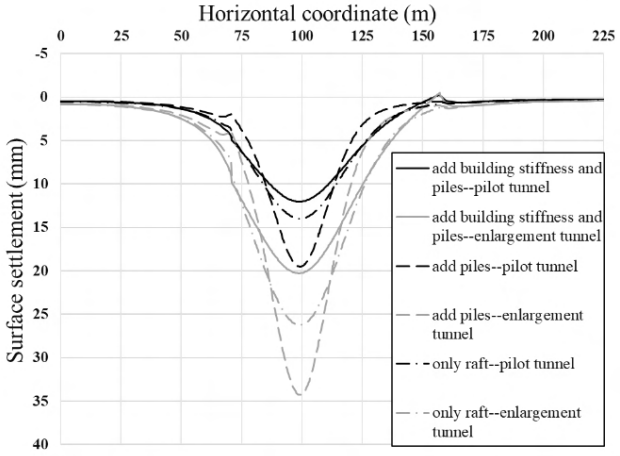

Figure 2. Influence of building stiffness and piles on settlement trough

References

Chong, H.Z. 2015. Influence of tunnelling on a piled structure-Crossrail case study. MEng thesis. Imperial College London.

Franzius, J.N., Potts, D.M., Addenbrooke, T.I., Burland, J.B. 2004. The influence of building weight on tunnelling-induced ground and building deformation. *Soils and Foundations* **44**(1): 25-38.

Gawecka, K.A., Taborda, D.M.G., Potts, D.M., Cui, W., Zdravković, L., Haji Kasri, M.S. 2017. Numerical modelling of thermos-active piles in London Clay. *Proceedings of the Institution of Civil Engineers - Geotechnical Engineering* **170**(3): 201-219.

Potts, D.M., Addenbrooke, T.I. 1997. A structures influence on tunnelling induced ground movements. *Proceedings of the Institution of Civil Engineers-Geotechnical Engineering* **125**(2): 109-125.

Taborda, D.M.G., Kontoe, S., Tsiampousi, A. 2023a. IC MAGE Model 01—strain-hardening/softening Mohr-Coulomb failure criterion with isotropic small strain stiffness (Version 2.1). Zenodo.

Taborda, D. M. G., Kontoe, S., Tsiampousi, A. 2023b. IC MAGE UMIP – universal model interface for PLAXIS (Version 3.5). Zenodo.

Taborda, D.M.G., Kontoe, S., Tsiampousi, A. 2023c. IC MAGE Flow Model 01–Nonlinearly varying anisotropic permeability (Version 1.0). Zenodo.

Deep Basement Excavation - Park Street, Cambridge

I. Garmendia Odriozola[1*], J.M Slattery[1]

*Corresponding author: inigogodriozola@cgl-uk.com

[1]*Card Geotechnics Limited (CGL)*

Abstract

Card Geotechnics Limited (CGL) designed, in collaboration with Dawson Wam (DW) and Gilbert Ash (GA), the retaining walls, associated temporary works, as well as excavation/construction sequencing and Ground Movement Analysis (GMA), required to enable the construction of what is understood to be the deepest basement in Cambridge to date. The value engineered basement solution was informed through detailed 3D FEA modelling and resulted in an optimised construction sequence and reduced programme and costs.

Proposed Development

The proposed development comprised the demolition of an existing multi-storey car park and the construction of a new six-storey hotel building with a three-storey basement up to 13m deep. A number of sensitive assets/constraints are present around the proposed basement, including party walls, neighbouring listed buildings and roads.

Figure 1. Basement Excavation and Propping

Geological Context

Ground conditions on site comprise a variable thickness of predominantly granular Made Ground and River Terrace Deposits directly underlain by Gault Clay. Groundwater was approximately 2.5m below ground level. The underlying soils were characterised using laboratory and insitu testing, as well as relevant literature (British Geological Survey, 1995) to derive 'moderately conservative' design parameters, particularly for retaining wall analysis where the strain level of 0.01% and 0.1% is generally applicable.

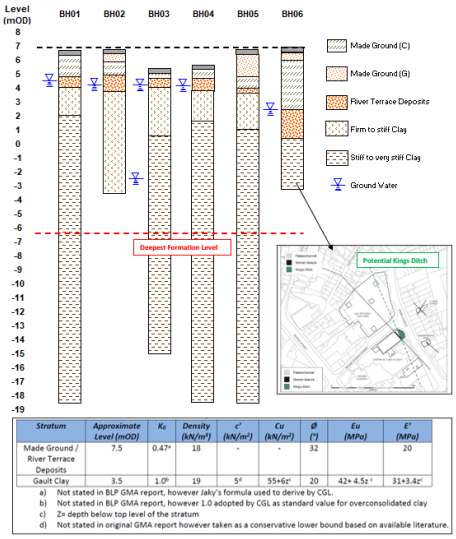

Stratum	Approximate Level (mOD)	K_0	Density (kN/m³)	c' (kN/m²)	Cu (kN/m²)	Ø (°)	Eu (MPa)	E' (MPa)
Made Ground / River Terrace Deposits	7.5	0.47[a]	18	-	-	32		20
Gault Clay	3.5	1.0[b]	19	5[c]	55+6z[c]	20	42+ 4.5z[c]	31+3.4z[c]

a) Not stated in BLP GMA report, however Jaky's formula used to derive by CGL.
b) Not stated in BLP GMA report, however 1.0 adopted by CGL as standard value for overconsolidated clay
c) z= depth below top level of the stratum
d) Not stated in original GMA report however taken as a conservative lower bound based on available literature.

Figure 2. Ground Model & Characteristic Parameters

Potential variation in ground conditions locally associated with the 'Kings Ditch' (Cessford D and Dickens A, 2019) was de-risked through sensitivity analysis on potential design implications of this feature on relevant sections.

Tender Stage Value Engineering (VE)

CGL in conjunction with DW value-engineered a 900mm diameter hard/firm secant piled wall with hard piles spaced at 1.35m c/c to a 750mm hard/hard secant pile wall, with male

piles spaced at 640mm c/c. The alternative optimised basement methodology also allowed for the removal of extensive enabling works, which was achieved by raising the capping beam levels around the perimeter and moving the secant pile wall line closer to the boundary. The latter was possible due to the use of vibration-free cased CFA system, which enables close proximity piling with improved installation verticality tolerances. During the tender stage the temporary propping requirements were optimised to two levels, including a new buttress pile wall, that enabled early quadrant excavation and erection of the tower crane, resulting in substantial programme benefits.

A preliminary ground movement analysis was undertaken and demonstrated that the alternative basement piled wall and construction methodology/sequencing provided consistent or improved results with regard to predicted ground movements and corresponding impact on the critical constraints/assets assessed for the existing party wall agreements and approvals to remain appropriate.

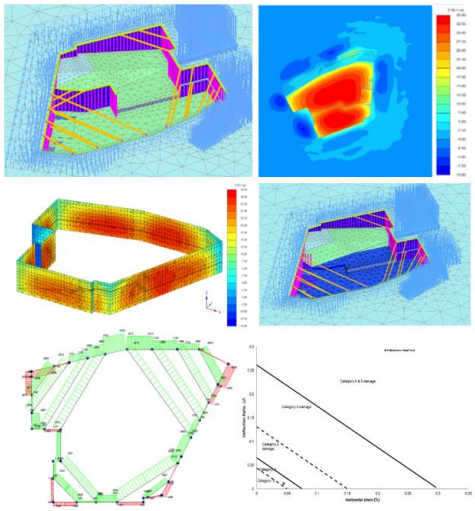

Figure 3. Detailed FE modelling & Impact Assessments

Detailed Design

CGL refined the PLAXIS 3D FEA modelling, undertook verification checks using non-FE 2D WALLAP and used the critical actions predicted to undertake a detailed geo-structural design of the secant wall, temporary buttress wall and temporary propping frames. The piled wall was designed to cantilever up to 3m initially to enable efficient and unrestricted archaeology investigation and clearance. The foundation system was also value engineered, adopting a raft with strategically placed tension piles. A detailed monitoring strategy was developed and refined to include in-place inclinometers in the secant pile wall and arrays of 3D EDM targets on the façades of all neighbouring buildings, and trigger limits and contingency measures set to control and manage risk during the works in line with the principles of the Observational Method (CIRIA 1999).

Live Construction Support

Reactive support and regular monitoring performance reviews were undertaken during the works, which enabled early prop removal locally through back analysis of wall performance from the monitoring to allow the main core walls to progress to ground level earlier than planned, which unlocked considerable programme advantages for the contractor. Also, reactive contingency prop design was undertaken in the localised area where the ‘Kings Ditch’ was encountered, and wall deflection exceeded the amber trigger limit locally in the corresponding inclinometer location.

The information, data and experience gathered from this scheme will be used to produce a case study paper in relation to the ground movements from underpinning, piling and retaining wall deflection, which will be used to inform future similar developments.

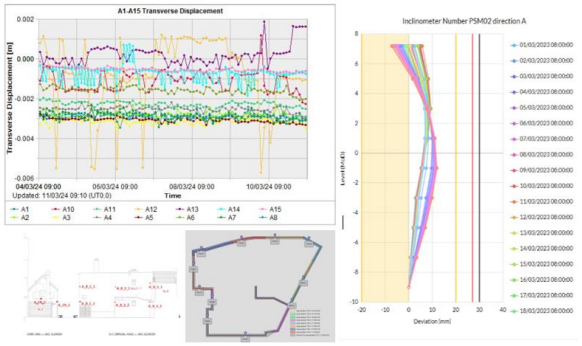

Figure 4. Real Time Monitoring Review

References

British Geological Survey. 1995. Engineering Geology of British rocks and soils: Gault Clay

Cessford C and Dickens A. 2019. Medieval to Modern Material Culture and Sequence at Grand Arcade, Cambridge: Archaeological Investigations of an Eleventh Century Suburb and Town Ditch.

CIRIA. 1999. The Observational Method in ground engineering: principles and applications (R185)

The Behaviour of Integral Abutment Bridges Under Earthquake Loading Using Centrifuge Modelling

Y. B. Asia*[1] and G. S. P. Madabhushi [2]

*Correspondence: *ybya2@cam.ac.uk*

[1] *Schofield Centre, Department of Engineering, University of Cambridge, Cambridge, UK. Email: ybya2@cam.ac.uk*
[2] *Schofield Centre, Department of Engineering, University of Cambridge, Cambridge, UK. Email: mspg1@cam.ac.uk*

Abstract

Integral abutment bridges (IABs) are gaining popularity globally over traditional bridges because they eliminate expansion joints and bearings. However, there is a lack of comprehensive unified codes or guidelines, and the dynamic interaction between these bridges and soil has not been thoroughly studied. To address these gaps, a series of centrifuge tests were carried out at the Schofield Centre, University of Cambridge. This paper discusses the benefits and drawbacks of IABs and offers a summary of the various testing setups used in the study.

Introduction

Integral abutment bridges (IABs) represent a significant evolution in bridge design and construction, offering numerous advantages over conventional bridges equipped with expansion joints and bearings; see Fig. 1. These bridges are distinguished by their seamless connection between the superstructure and abutments, where the abutments are engineered to accommodate thermal movements and other deformations without necessitating joints. This design effectively mitigates potential maintenance issues associated with joints, such as the accumulation of debris and degradation from exposure to weather (Burke, 2009).

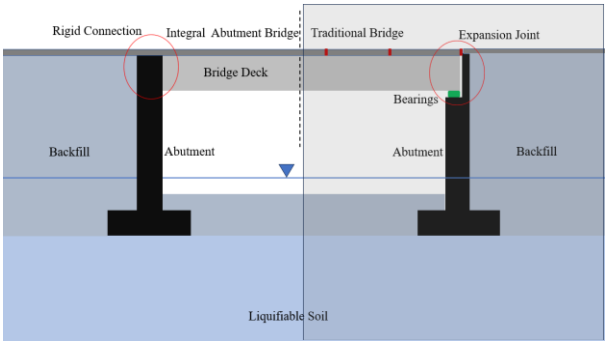

Figure 1. The salient differences between integral abutment bridges and conventional bridges.

Integral abutment bridges are typically constructed with a continuous deck supported by abutments that are integral to the bridge substructure. This integration enhances the structural resilience of the bridge by reducing vulnerability to seismic movements and improving overall durability (Haskell et al., 2013). By distributing forces more evenly and minimising stress concentrations, these bridges can offer enhanced performance and longevity.

Moreover, integral abutment bridges can be more cost-effective over their lifespan than bridges with expansion joints and bearings, as they require less maintenance and are less prone to structural wear. They also contribute to smoother driving experiences for motorists due to the absence of jolts and bumps typically associated with joints (White et al., 2010).

The design and construction of integral abutment bridges involve careful consideration of soil-structure interaction, as the behaviour of the backfill supporting the abutments plays a crucial role in maintaining stability and functionality.

The literature review shows the need for more research on the dynamic interaction of integral bridge-backfill soil under earthquakes (Mitoulis, 2020). Caltrans (1999) mainly focuses on the structural behaviour of integral abutment bridges (IABs) and neglects the soil-bridge interaction. However, this may alter the bridge

response under earthquakes due to the contribution of soil stiffness. Eurocode 8 (2005) limits the bridge displacement to 30 mm.

Centrifuge Modelling

A series of centrifuge experiments have been conducted at the Schofield Centre, University of Cambridge, to investigate the bridge-soil interaction during seismic events; Fig. 2 shows a typical testing setup for the conducted centrifuge tests. These tests are classified as:

- Two centrifuge experiments were conducted on a semi-integral bridge abutment. In the first experiment, the soil was completely dry, whereas in the second experiment, the foundation soil up to the bridge abutment footing was fully saturated. The purpose of these tests was to analyse the deformation mechanisms of a bridge abutment built on either dry soil or soil prone to liquefaction, and to highlight the importance of the rigid connection between the superstructure and bridge abutments in the overall stability of the bridge and its abutments.

- Four centrifuge experiments were conducted on a single-span integral abutment bridge constructed on a spread-wide footing. These tests included the following configurations: a benchmark test with completely dry soil, saturated soil up to the footing level to assess vulnerability to liquefaction damage, saturated soil up to the footing level with a geofoam layer behind abutments to investigate the impact of reducing interaction between bridge abutments and backfill soil on overall bridge stability and soil deformation mechanisms, and saturated soil up to the deck level to examine the effects of global warming and increased water table levels on serviceability and strength limit states.

- Three centrifuge tests were conducted on a single-span integral abutment bridge supported by piled footings. The testing included a benchmark test using dry soil, dry soil with a geofoam layer between the bridge abutments and backfill sandy soil to study the backfill deformation mechanisms of the backfill and the stresses induced on abutments and piles compared to the benchmark test. The configuration of the final test involved fully saturated soil up to the cap of the piles to examine the impact of liquefaction on the structural response of the bridge and soil movements.

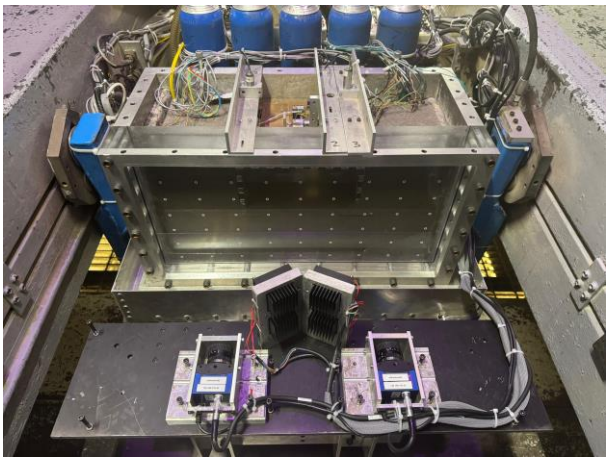

Figure 2. Typical centrifuge testing setup for a single-span integral abutment bridge.

References

Burke Jr, M. P. 2009. Integral and semi-integral bridges. John Wiley & Sons.

Caltrans 1999. Caltrans Seismic Design Criteria, Version 1.1. California Department of Transportation.

Eurocode 8, B. 2005. Eurocode 8: Design of structures for earthquake resistance. Part, 1,1998–1.

Haskell, J., Madabhushi, S., Cubrinovski, M., and Winkley, A. 2013. Lateral spreading-induced abutment rotation in the 2011 christchurch eartquake: Observations and analysis. Géotechnique, 63(15), 1310–1327.

Mitoulis, S. A. 2020. Challenges and opportunities for the application of integral abutment bridges in earthquake-prone areas: A review. Soil Dynamics and Earthquake Engineering, 135,106183.

White, H., Pétursson, H., and Collin, P. 2010. Integral abutment bridges: the european way. Practice periodical on structural design and construction, 15(3), 201–208.

Comparing the strain ratcheting of soil behind integral bridge abutments in field and physical modelling data

D.G. Morley *[1], G.S.P. Madabhushi [1]

*Correspondence: dm909@cam.ac.uk

[1] *Dept. of Engineering, University of Cambridge, Cambridge, UK*

Abstract

Integral bridge abutments are designed to withstand an increase in earth pressure caused by repeated thermal movements of the bridge deck. UK design is largely based on physical modelling due to challenges in recording long-term pressures in the field, however, there is a need for agreement between the two. This study compared the findings from field monitoring and physical modelling reported in the literature to explore the development of earth pressures in the backfill of integral bridges. The results show similarities between field and modelling data, with a limited pressure increase expected for many bridges due to the low strains experienced. However, the design temperature range used to estimate thermal movements may cause an overprediction of long-term pressures.

Introduction

Integral bridges do not have joints or bearings between the abutments and deck, therefore thermal movements are transferred to the backfill through the abutments. This causes an accumulation of strain over time, leading to an increase in earth pressures imposed on the abutments (strain ratcheting). Predicting this increase is important to prevent cumbersome abutment designs (Sandberg *et al.*, 2020).

Background

The development of earth pressure behind a retaining wall undergoing monotonic rotation (Δ/H), and strain ratcheting, is illustrated in Fig. 1 (Terzaghi, 1954). Springman et al. (1996) described how input shear strain can be taken as $\gamma_i = 2\Delta/H$, and for symmetrical rotation this can be simplified to $\gamma_i = d/H$. This term is the basis for calculating ratcheting earth pressures according to PD 6694-1 (BSI, 2020)

$$K^* = K_0 + [(Cd')/H]^{0.6}\, K_p \qquad (1)$$

where C is the foundation stiffness and d' is the thermal movement at H/2. Field data must be recorded over several years to observe strain ratcheting, and it is often concluded that further monitoring is required. Due to this, small-scale and centrifuge models are more reliable and generally show a logarithmic increase that is most dramatic in the early cycles (Fig. 1). The disparity between early pressure generation in modelling, and its absence in field monitoring, is explored in this work.

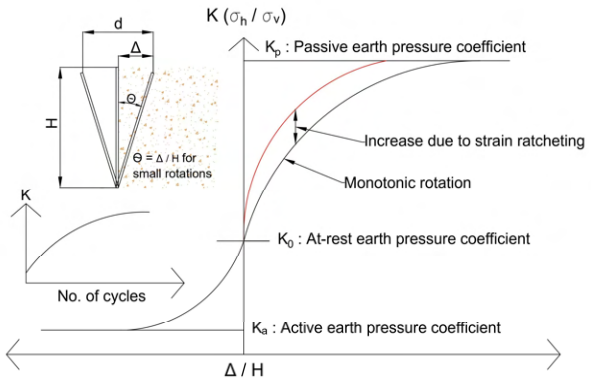

Figure 1. Earth pressure generation due to wall rotation.

Data Processing

With Eq. 1 based largely on the results of physical modelling (Denton *et al.*, 2010), field monitoring data in the literature was compared to these studies. The input shear strain, d/H, and annual cycle number were considered the main causes of pressure increase, and the extent of strain ratcheting was taken as the pressure generated following the first phase of bridge deck expansion, $K^* - K_{p,1}$. Alongside this, thermal movements recorded in the field were compared to design predictions to assess the accuracy of input shear strain estimations.

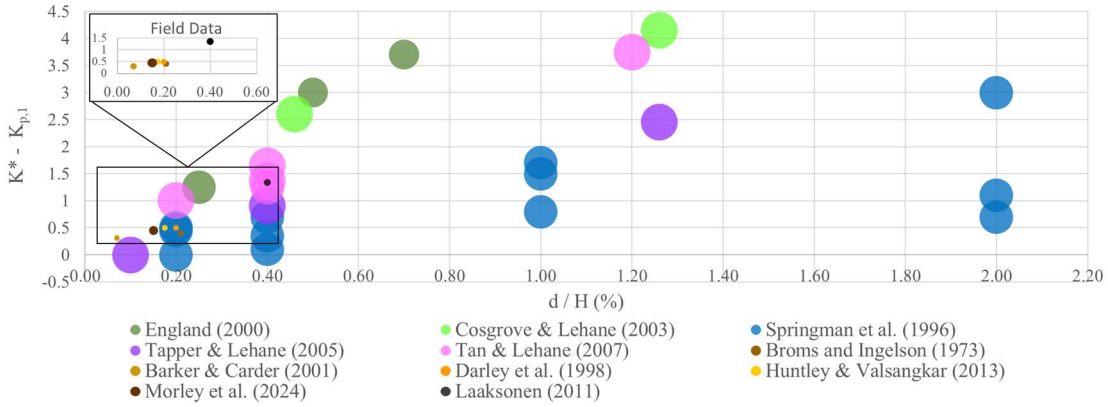

Figure 2. Earth pressure increase with abutment rotation, where marker size indicates the number of annual cycles.

Pressure Comparison

Fig. 2 shows a positive trend between the extent of strain ratcheting and input shear strain, where field data is distinguishable by the small marker sizes. All but one of the field studies fall around or below an input shear strain of 0.2% and experience limited ratcheting. The physical modelling data suggests that, at this magnitude of strain, pressures are unlikely to develop much further. Measuring K^* pressures against $K_{p,1}$, rather than K_0, is useful as field studies often record a high $K_{p,1}$ from initial rotation.

Thermal Movement Comparison

Tab. 1 compares thermal movements recorded in the field with predicted values. The bridges considered showed an overestimation of movement, and therefore ratcheting pressures, expected during design. A similar relationship was found for the temperature range, where UK design considers 1 in 50-year temperatures to occur every year (BSI, 2003). This appears to be overly conservative even when climate change is taken into account.

Table 1. Predicted and measured thermal movements.

Research	Design Movement, d_k[1] (mm)	Measured Movement (mm)	Movement Ratio
Morley (2024)	22	10	2.2
Barker and Carder (2001)	12	7	1.7
Darley et al. (1998)	14	6	2.3

[1] $d_k = \alpha^{(2)} L_x (T_{e;max} - T_{e;min})^{(3)}$ (BSI, 2020)
[2] α:coefficient of thermal expansion, 10E^{-6}/°C (BSI, 2023).
[3] $T_{e;max} - T_{e;min}$: deck temperature variation (BSI, 2003).

Conclusion

Integral bridge field data agrees with physical modelling, showing that strain ratcheting increases with abutment rotation. All except one of the bridges experienced a small input shear strain and hence limited long-term ratcheting could be expected. However, field measurements show that overprediction of the design temperature range may lead to the cumbersome design of some abutments.

References

Barker, K. J. and Carder, D. R. (2001) 'Performance of an integral bridge over the M1-A1 Link Road at Bramham Crossroads (TRL Report 521)', *Transport Research Laboratory*. Crowthorne.

Broms, B. B. and Ingelson, I. (1973) 'Lateral earth pressures on walls and measurements under different temperature conditions', *Swedish Geotech. Institute*.

BSI (2003) 'NA to BS EN 1991-1-5:2003 - UK National Annex to Eurocode 1: Actions on structures – Part 1-5: General actions – Thermal actions', *British Standards Institution*, London, UK.

BSI (2020) 'PD 6694-1:2011+A1:2020 - Recommendations for the design of structures subject to traffic loading to BS EN 1997-1:2011+A1:2020', *British Standards Institution*, London, UK.

BSI (2023) 'BS EN 1992-1-1:2023 - Eurocode 2 — Design of concrete structures: Part 1-1: General rules and rules for buildings, bridges and civil engineering structures', *British Standards Institution*, London, UK.

Cosgrove, E. F. and Lehane, B. M. (2003) 'Cyclic loading of loose backfill placed adjacent to integral bridge abutments', *International Journal of Physical Modelling in Geotechnics*, 3(3), pp. 9–16.

Darley, P., Carder, D. R. and Barker, K. J. (1998) 'Seasonal Thermal Effects over Three Years on the Shallow Abutment of an Integral Bridge in Glasgow (TRL Report 344)', *Transport Research Laboratory*. Crowthorne.

Denton, S. *et al.* (2010) 'Developments in integral bridge design', in Denton, S. (ed.) *Bridge Design to Eurocodes: UK Implementation*, pp. 463–480.

England, G. L., Tsang, N. C. M. and Bush, D. I. (2000) *Integral bridges - A fundamental approach to the time-temperature loading problem.* London: Crown Copyright and Thomas Telford Limited 2000.

Huntley, S. A. and Valsangkar, A. J. (2013) 'Field monitoring of earth pressures on integral bridge abutments', *Canadian Geotechnical Journal*, 50(8), pp. 841–857. .

Laaksonen, A. (2011) *Structural behaviour of long concrete integral bridges*, *Tampere University of Technology. Ph.D. thesis*. Tampere University of Technology.

Morley, D. . *et al.* (2024) 'Extended monitoring of earth pressures behind a 90 m integral bridge', *ASCE Journal of Bridge Engineering*, In review.

Sandberg, J. *et al.* (2020) 'The integral bridge design concept for the third runway at Heathrow, UK', *Proceedings of the Institution of Civil Engineers: Bridge Engineering*, 173(2), pp. 112–120. doi: 10.1680/jbren.19.00044.

Springman, S. M., Norrish, A. R. M. and Ng, C. W. W. (1996) 'Cyclic loading of sand behind integral bridge abutments (TRL Report 146)', *Transport Research Laboratory*. Crowthorne.

Tan, E. L. and Lehane, B. M. (2007) 'Lateral stress development on integral bridge abutments', *The University of Western Australia, Honours Dissertation*. Perth.

Tapper, L. and Lehane, B. (2005) 'Lateral stress development on integral bridge abutments', in Deeks, A. J. and Hao, H. (eds) *Developments in Mechanics of Structures and Materials*. 2nd edn. Perth, Australia: CRC Press, pp. 1069–1075.

Terzaghi, K. (1954) 'Anchored bulkheads', *Transactions of the American Society of Civil Engineers*, 119(1).

Centrifuge modelling of TBM tunnelling in soft clay

A.S.N. Alagha*[1], G.M.B. Viggiani[1], and S.K. Haigh[1]

*Correspondence: asna2@cam.ac.uk

[1] *Department of Engineering, University of Cambridge, UK*

Abstract

Understanding the effects of constructing a new tunnel on nearby structures and services relies on grasping the mechanisms caused by Tunnel Boring Machines (TBMs).The high cost and complexity of urban field monitoring, coupled with limited research on modelling the real-world tunnelling process, make simulating the advancement of a TBM in a geotechnical centrifuge an attractive alternative. A novel miniature TBM (mini-TBM) has been designed and developed for use in the Cambridge geotechnical centrifuge to model the major tunnelling processes in-flight as it excavates through soft clay. In this extended abstract, a brief description of the mini-TBM is presented and the results of a greenfield test are discussed. The mini-TBM has been shown as an effective model for the tunnelling process, providing a reliable approach for modelling tunnel-soil-structure interaction problems.

Introduction

The continuous growth of cities around the world has placed ever-increasing demands on their travel networks, resulting in a growing development of the underground landscape within urban areas. The construction of new underground lines will most probably take place nearby pre-existing structures, where limiting the tunnelling-induced ground deformations, that may adversely affect neighbouring structures, is the main design requirement. The control of these deformations has improved significantly in the last few decades due to the technological advancements of mechanised tunnelling technologies such as TBMs. Earth Pressure Balance (EPB) machines are the predominant type of TBMs used for tunnelling in urban areas, particularly in soft ground conditions. These machines cause stress changes in the soil mass around the tunnel which in turn result in ground movements that propagate to the ground surface and manifest as a three-dimensional settlement trough.

Different approaches have been proposed to simulate the mechanised tunnelling process. Field observations (*e.g.,* Selemetas, 2005) are considered one of the most reliable techniques due to the data being reported from real-life projects; however, the high cost and complexity associated with such approach make modelling the advancement of a TBM at high centrifugal gravity an appealing approach. That said, the demands for miniaturisation at increased gravity, coupled with the complex nature of centrifuge testing, have meant that the tunnelling process has been greatly simplified. In fact, in most geotechnical centrifuge studies of tunnelling, excavation has been simulated in a rather plane strain scenario using fluid filled flexible tubes in which the volume loss associated to tunnelling is simulated by extracting known volumes of fluid, either uniformly along the model tunnel length (*e.g.,* Marshall, 2009) or in stages (*e.g.,* Gue, 2017). Only one study so far (Nomoto et al., 1999) has sought to reproduce some of the main physical processes taking place during mechanised tunnelling in the centrifuge but, typically, at relatively low g-levels.

The development of a miniature TBM capable of excavating in flight at high gravity levels would therefore represent a significant technological breakthrough, allowing realistic simulation of tunnelling-induced soil-structure interaction.

Description of the New Model TBM

A miniature TBM, able to reproduce the mechanisms of shield tunnelling at high gravity and to account for most sources of volume loss, has recently been developed at the University of Cambridge, see Fig. 1.

The cutterhead, with a diameter of 78 mm, sits ahead of the shield, which has a diameter of 77.2 mm. This creates an overcut of approximately 1%, within the 0.2% to 1.6% range reported in the literature (*e.g.,* Bezuijen

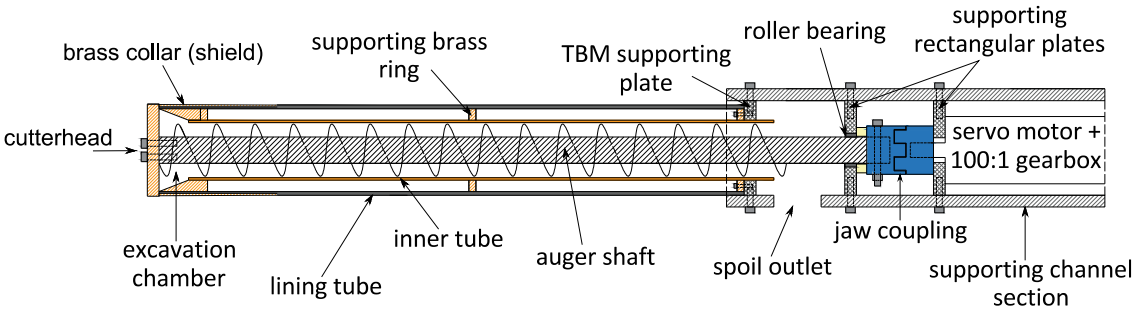

Figure 1. Components of Cambridge mini TBM.

and Talmon, 2008). This cutterhead was used without cutting tools and with a hatch ratio of around 45% as it was designed to mainly operate in soft clay. A conical brass collar was utilised to simulate a tapered shield, decreasing from 77.2 mm at the cutterhead junction to 76.2 mm at the tail. The 100 mm shield length, with a 1.3 length-to-diameter ratio, meets the 1.2 - 3 range recommended by ITA (2000). The taper gradient of 0.5% is consistent with the 0.1 – 1% values reported in the literature (Bezuijen and Talmon, 2008). The soil is removed from behind the cutterhead by a horizontal auger, housed by an inner tube, with a diameter of 40 mm. The auger is centred by a needle roller bearing at the rear and a bolted connection at the cutterhead front. The front 100 mm of the lining tube was reduced radially by 1.5 mm to accommodate the brass collar. The total length of the lining tube is 500 mm, allowing for at least 300 mm of TBM drive.

Finally, the auger is powered by a servo motor and a 100:1 reduction drive gearbox, providing a maximum torque of 27 Nm. The TBM is advanced into a soil-filled strongbox using a linear actuator capable of delivering up to 20 kN of thrust.

The following section shows selected results of centrifuge tests conducted at 50g, simulating a 4m diameter prototype tunnel in soft clay.

Sample Results

An initial greenfield test was conducted to calibrate the operating parameters of the mini-TBM that will produce a volume loss of 2 – 3%. The model TBM advance rate was found to be at 14 mm/min, while the auger speed was 1.35 rpm. Fig. 2 shows the development of the transverse settlement trough as the TBM advances. The overall settlement profile aligns well with the general pattern found in the literature (Peck, 1969). The settlement trough develops rapidly in the first 150 mm of tunnelling (x/D ~ 2), corresponding to the passage of the mini-TBM's tail under the monitoring section MS. This indicates that most of the displacements occur around the shield, as expected. Other results concerning longitudinal settlement profiles and excess pore pressures, and the limitations of the current mini-TBM can be found in Viggiani et al., 2022.

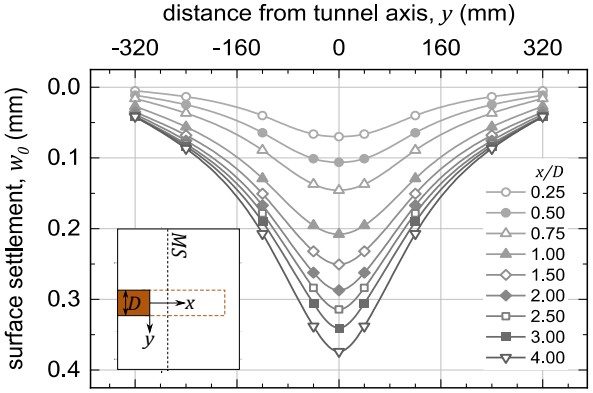

Figure 2. Development of transverse settlement trough.

References

Marshall, A. 2009. Tunnelling in sand and its effect on pipelines and piles. PhD thesis. *University of Cambridge.*

Gue, C.Y. 2017. Effects of Tunnelling under an Existing Tunnel in Clay. PhD thesis, *University of Cambridge.*

Nomoto, T., Imamura, S., Hagiwara, T., Kusakabe, O. and Fujii, N. 1999. Shield tunnel construction in centrifuge. *J. Geotech. Geoenvironmental Eng. - ASCE*, 125(4): 289-300.

Selemetas, D. 2005. The response of full-scale piles and piled structures to tunnelling. PhD thesis. *University of Cambridge, UK*.

Bezuijen, A. and Talmon, A. M. 2008. Processes around a TBM. *Proc. of the 6th Intr. Sy. on Geo. Aspects of Ungrnd. Construction, IS-Shanghi*, 1-11.

ITA, W. 2000. Mechanized Tunnelling: *Guidelines for Tunnel Boring Machines*. *International Tunnelling Association, Lausane, Switzerland*.

Peck, R.B. 1969. Deep excavations and tunneling in soft ground. *Proc. 7th ICSMFE*, 225-290.

Viggiani, G., Alagha, A.S.N. & Haigh, S.K. 2022. Reduced scale modelling of mechanised tunnelling -challenges and perspectives. *Proc. of the 10th International Conference on Physical Modellingin Geotechnics.*

Mechanical behaviour of earthquake-resistant jointed ductile iron pipeline under biaxial tension force

Qinglai Zhang[*1], Shih-Hung Chiu[2], Kenichi Soga[3] and Zili Li[4]*
*Correspondence: 120224300@umail.ucc.ie

[1,4]*Civil, Structural and Environmental Engineering, University College Cork, Ireland*
[1,2,3]*Civil and Environmental Engineering, University of California, Berkeley, USA*

Abstract

Bell-spigot jointed ductile iron (DI) pipelines, commonly used in seismic zones for water distribution, face significant risks from earthquake-induced tension and bending forces, leading to potential damage and leakage, particularly at the vulnerable joint sections. Previous research has largely focused on physical tests subject to separate loading condition, such as axial tension and four-point bending tests. However, pipelines often face a combination of axial and bending stresses, leading to an increased likelihood of leakage. Building on these prior studies, this study aims to investigate the response of an 8-inch diameter jointed DI pipeline to more realistic conditions through full-scale biaxial tension tests using distributed fiber optic sensor (DFOS) and 3D finite element (FE) methods.

Introduction

(O'Rourke and Liu., 2012) examined common failure mechanisms in jointed pipelines within seismic zones, highlighting axial pull-out combined with angular deflection at joints. Earlier studies (Christina Argyrou, 2018) focused on the behaviour of earthquake-resistant DI pipelines, mainly through axial tension and four-point bending tests, with limited exploration of biaxial tension tests. These studies heavily rely on traditional strain gauges and primarily employed 2D shell FE models to investigate the pipeline mechanical behaviour. This study extends previous research to conduct innovative full-scale biaxial tension tests, capturing hoop and axial strains with DFOS along with 3D continuum FE models.

Full-scale experimental test and FEM

The 8-inch TR-XTREME™ DI pipeline (US Pipe, 2020), previously separately tested for axial tension (Chiu et al.,2023a) and four-point bending (Chiu et al.,2023b), undergoes new biaxial tension tests at the Center for Smart Infrastructure, Berkeley (CSI). As depicted in Figure 1, the pipeline is vertically supported by two jackets with inner and outer spans of 35.5 in. (902 mm) and 65 in. (1651 mm), respectively, and features a midpoint bell-spigot joint. The pipeline is initially bent to 8 degrees before axial tension is applied until failure or leakage. Tests are performed on two specimens with different orientations of locking segments.

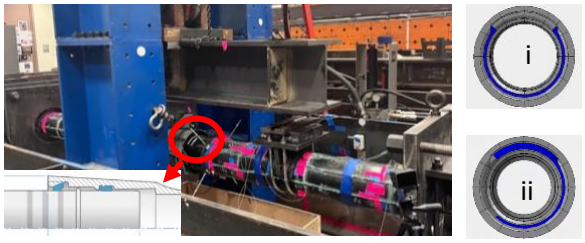

(a) (b)

Figure 1. Experimental setup:(a) Bell-spigot position (b) Orientations of locking segments: i-12 o'clock ii-9 o'clock

Fiber optic cables were attached along the pipeline to effectively monitoring continuous strain distribution in both axial and hoop directions, as depicted in Figure 2.

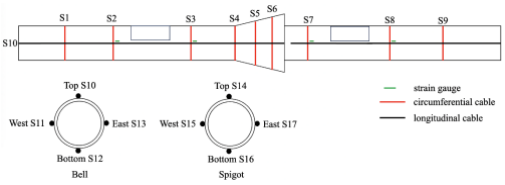

Figure 2. Locations of fiber cables and strain gauges

3D FE models, mirroring the specimen's geometry, materials and setup, were constructed with over 320,000 elements and 147,000 nodes using C3D8R elements, as

depicted in Figure 3. Key material properties for the simulation are listed in Table 1.

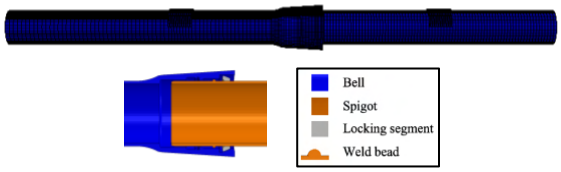

Figure 3. 3-D FE model setup

Table 1. Material properties (1 ksi = 6.89 MPa)

Young's modulus(ksi)	Poisson' ratio	Yield strength(ksi)	Ultimate strength(ksi)	Elongation
23,500.00	0.29	42.00	60.00	10%

Results & Discussions

Figure 4 shows the relationship between axial force and joint opening during the pull stage for both specimens, while Figure 5 illustrates the joint pull-out mechanism. The spigot's weld bead slides to contact the locking segments, primarily at the top and sides, leading to peak forces. Specimen 2, with locking segments at the 9 o'clock position, has a greater restraining area, providing higher axial pull capacity: reaching about 171 kips (761 kN) with a 2.3-inch (58.4-mm) opening. In contrast, Specimen 1 reached a peak force of 145 kips (645 kN) and a 2-inch (50.8-mm) opening.

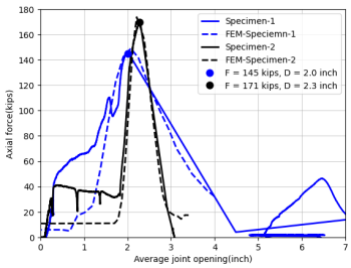

Figure 4. Axial force vs. average joint opening

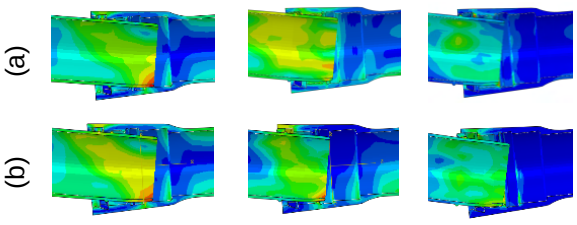

i:8-deg deflect ii:bell crack iii:leakage

Figure 5. Joint pull-out mechanism

Strain results from DFOS and simulation are presented in Figure 6, showing hoop strain S6 at the joint and axial strain S12 at the bottom bell section for both specimens. The orientation of locking segments has an influence on the distinct strain distribution of S6, captured by DFOS ranging from -1000 to 1500 με. S12 exhibited a similar axial strain trend, peaking at around 1500 με. Both specimens initially cracked at the same location due to similar stress concentrations (Figure 7). However, the locking segments orientation affected the failure progression, resulting in a more expansive and diagonally oriented crack in Specimen 2.

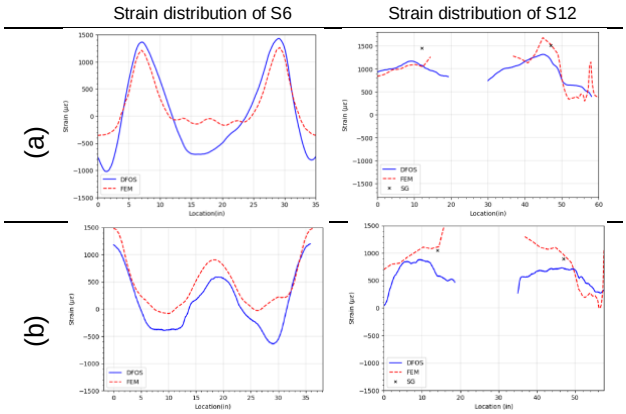

Figure 6. Strain distribution before failure: (a) Specimen 1 (b) Specimen 2

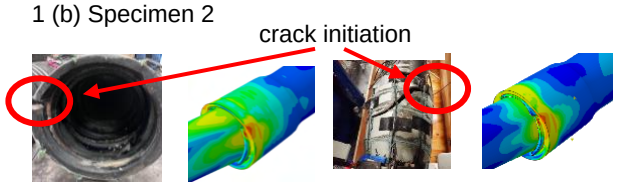

(a) (b)

Figure 7. Failure mode: (a) Specimen 1 (b) Specimen 2

Conclusions

This study highlights the critical impact of locking segment orientations on pipeline performance under biaxial tension forces. Full-scale testing using DFOS, and simulations comprehensively assessed the pipeline's capacity and failure mechanisms, providing valuable insights for future joint optimization.

References

Argyrou, C.2018. Pipeline response to earthquake-induced ground deformation.

Chiu, S.H., Zhang, Q., Takhirov, S., Soga, K., 2023. Direct Tension Testing of 8-in. (200-mm) Diameter TR- XTREME™ Ductile Iron Pipe.

Chiu, S.H., Zhang, Q., Takhirov, S., Soga, K., 2023. "Four-Point Bending Testing of 8-in. (200-Mm) Diameter TR- XTREME™ Ductile Iron Pipe."

O'Rourke, M.J., Liu, X. 2012. Seismic Design of Buried and Offshore Pipelines.

Suitability of excavation and mining clay wastes for geopolymer precursors in earthen construction.

P.I. Harding*, S. Rengaraju, and A. Al-Tabbaa

*Correspondence: pih24@cam.ac.uk

Department of Engineering, University of Cambridge, Cambridge, CB2 1PZ, UK

Abstract

Geotechnical engineering faces a critical challenge in addressing climate change, necessitating global efforts to minimize carbon emissions and enhance climate change adaptation. Targeting the production and utilisation of concrete offers a promising avenue, with calcined clay emerging as a viable supplementary cementitious material. However, research into applications beyond concrete remains scarce. This paper examines calcined clay reactivity and its potential as a pozzolanic material, focusing on utilisation as a geopolymer-based binder in earthen construction. Specifically, this study explores waste clay reactivity, focusing on 2:1 clay mineral content, an area that has received limited attention across literature. R3 tests confirmed that certain waste clays can exhibit similarities to pure 2:1 clays like bentonite. While kaolinite is preferred, moderate to high proportions of 2:1 clay minerals show promise as geopolymer precursors due to their aluminosilicate composition. The novelty of this research lies in the application in earthen construction, rather than conventional concrete. Future studies will explore the implications of this research on the strength and durability requirements of earthen construction materials. By evaluating the chemical performance of calcined clay in earthen applications, this study aims to highlight its value as an abundant, low-carbon material, facilitating the industry's transition towards net-zero emissions.

Introduction

Earth is a traditional building material with minimal associated emissions; however, its inherent weaknesses in terms of strength and durability often require stabilisation. Central to earthen stabilisation are pozzolanic reactions – a mechanism drawing upon the high reactivity of pozzolans i.e., aluminosilicates which react with portlandite and water to form cementitious characteristics. Conventional stabilisation uses cement; however, high associated emissions remain. Geopolymers offer an alternative approach. They function by harnessing the reactivity of alkali-activated aluminosilicates to yield significant mechanical improvements. Various methods exist to quantify a clay's pozzolanic reactivity, with the R3 test emerging as one of the most effective options. This procedure emulates the reaction environment observed during cement hydration. Pozzolanic materials like GGBS, PFA, and metakaolin are often considered as geopolymer precursors. Notably, excavation and mining clay waste can also exhibit significant pozzolanic tendencies. However, a major limitation is their diverse composition of 1:1 and 2:1 clay minerals, and inert materials such as quartz. A clay's reactivity is intrinsically linked to its mineralogy; kaolinite-rich samples have a greater reactivity, while those high in quartz exhibit low reactivity. The abundance of 2:1 clay minerals in common clays adds an additional complexity. Research into their moderate reactivity, and suitability as geopolymer precursors is sparse, therefore constituting a focal point of this study.

Methodology

The minerology and reactivity of four waste excavation clays and one mining waste clay (dried kaolinitic slurry) are studied, with the results compared against reagent kaolin and bentonite. All waste clays were air dried, manually ground, and calcined at 800 ˚C for a burning time of one hour, in line with the work carried out by Avet et al. (2016). Chemical compositions were determined using thermo-gravimetric analysis and x-ray diffraction (XRD). Pozzolanic reactivity was established through the R3 test, in accordance with ASTM C1897 (2020).

Results and Discussion

The XRD analysis in Figure 1 indicates the presence of the 1:1 clay mineral, kaolinite, and the lesser reactive 2:1 clay minerals, illite and montmorillonite. The influence of 2:1 clay mineral reactivity is more pronounced in clays with a low kaolinite content, such as the excavation clays examined. Additionally, Figure 1 reveals significant proportions of quartz in all waste clay, as indicated by significant peaks at 26.6°, with A30 and A391 exhibiting the highest quartz contents.

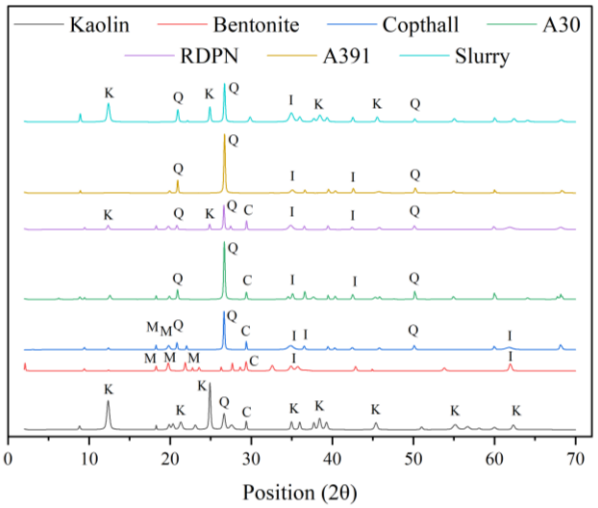

Figure 1. XRD patterns of raw clays. C: Calcite, I: Illite, K: Kaolinite, M: Montmorillonite, Q: Quartz.

Figure 2 depicts the cumulative heat released during the R[3] test, confirming kaolin's superiority. This value falls within the reported literature range, affirming the study's accuracy. Kaolinitic slurry, despite considered low-grade, outperforms the excavation waste due to a higher kaolinite content. Illite is predominant in excavation clays but has a lower reactivity than montmorillonite, underscoring the significance of clay composition (Overmann, 2024). Among the excavation waste, RDP North exhibited promising performance as a geopolymer precursor, aligning closely with the outcome observed with bentonite, with Copthall following suit. An intriguing observation emerges from the near-identical heat released from bentonite and Copthall within the first 24 hours. The identification of kaolinite and montmorillonite, coupled with similar dehydroxylation patterns at higher temperatures, indicates similar proportioning, and therefore, overall reactivity.

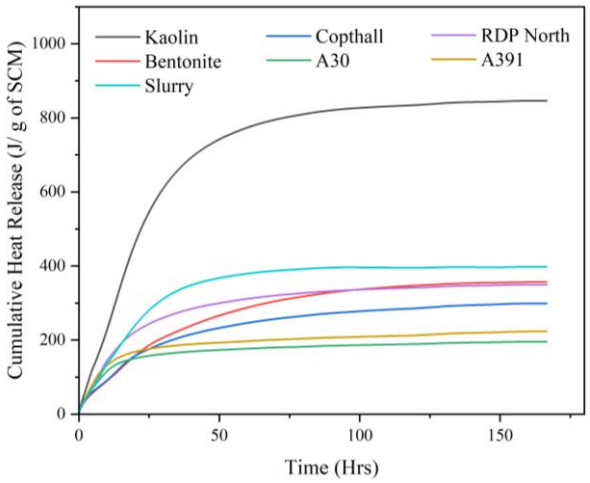

Figure 2. Reactivity assessment of waste clays against kaolin and bentonite using R3 method.

Conclusion and Future Work

This study indicates the potential of excavation and mining clay wastes, all low in quartz but with sufficiently high 1:1 and 2:1 minerals, as geopolymer precursors. While the presence of kaolinite significantly influences reactivity, reactivity comparable to typical geopolymer precursors like GGBS or PFA can be achieved using waste, illite- and montmorillonite-rich clays (Ramanathan, 2020, Vallina, 2023). Future studies will explore the implications of utilising waste clays on the mechanical and durability properties of earthen construction following geopolymer-based stabilisation.

References

ASTM. 2020. Standard Test Methods for Measuring the Reactivity of Supplementary Cementitious Materials by Isothermal Calorimetry and Bound Water Measurements. *ASTM C1897-20.*

Avet, F., et al., 2016. Development of a new rapid, relevant and reliable (R3) test method to evaluate the pozzolanic reactivity of calcined kaolinitic clays. *Cement and Concrete Research.* **85**: p. 1-11.

Overmann, s., et al. 2024. Reactivity of calcined clays as SCMs: A review. *Materials,* **17,** 312.

Ramanathan, S., et al., 2020. Linking reactivity test outputs to properties of cementitious pastes made with supplementary cementitious materials. *Cement and Concrete Composites*. **114**: p. 103742.

Vallina, D., et al., 2023. Supplementary Cementitious Material Based on Calcined Montmorillonite Standards. *Construction Building Materials*.

Effects of steam treatment on the microstructure of coal

Y.J. Li*[1,2] and C. Zhai[2]

*Correspondence: yujie.li@ucl.ac.uk

[1] *Department of Civil, Environmental and Geomatic Engineering, University College London, WC1E 6BT, United Kingdom*
[2] *School of Safety Engineering, China University of Mining and Technology, Xuzhou, Jiangsu 221116, China*

Abstract

Based on the advantages of steam in applications of coal gasification, drying of low-rank coals, and heavy oil recovery, steam is considered to have great potential in the recovery of coalbed methane (CBM). In this study, the effects of steam on the surface morphology and pore structure of coal were examined. The results indicated that new pores were generated after steam treatment, and the coal pore volume and pore diameter were increased, which could provide additional space for CBM flow. The decrease of the complexities of the mesopores and macropores of the coal could also facilitate gas flow and benefit CBM recovery.

Introduction

Coalbed methane (CBM) is an important clean energy source and a high-quality chemical material (Yang et al., 2019). However, the great burial depth, low permeability and strong gas adsorption capacity of the CBM reservoirs, particularly in China, have caused a low efficiency of CBM recovery (Zheng et al., 2021). Thermal stimulation can effectively reduce CBM adsorption capacity and improve coal seam permeability (Liu et al., 2021), thus promoting CBM recovery. Hot steam has been used as an excellent fluid medium to improve the recovery of heavy oil and bitumen resources for many years (Jamshid-nezhad, 2022). It has great potential in CBM recovery enhancement.

When steam is injected into the coal seam, complex interactions between coal and pore fluids occur, including steam condensation within the coal, the evaporation of water from coal, and changes in the physicochemical structure of coal, etc. These interactions have a great impact on the adsorption, desorption and migration of CBM.

Methods and experiments

To better understand the interactions between steam and coal, the surface morphology and pore structure of a Chinese lignite was characterized before and after treatment with steam for 3 h at different temperatures (200 °C, 300 °C, and 400 °C) using scanning electron microscopy (SEM) and low-temperature nitrogen adsorption (LTNA), respectively.

Results and discussion

As shown in Figure 1, after treatment with steam at 200 °C, there was no apparent change in the surface morphology of the coal. However, after steam treatments at 300 °C and 400 °C, the surface of the coal became rough and uneven, accompanied by the formation of small blowholes and microcracks. Generation of the blowholes was primarily attributed to evaporation of volatile substances (including water) from the coal surface. Additionally, pyrolysis of the coal matrix led to a roughened surface and the formation of pyrolytic pores. Volatilization of these substances and pyrolysis of the coal matrix could provide more space for gas flow and were conducive to CBM recovery.

To quantitatively analyze changes in the coal pore structure, the specific surface areas and pore size distributions of the coal were calculated with the BET and BJH models, respectively. The results are presented in Table 1 and Figure 2. With the rise of steam temperature, the proportion of the micropore and mesopore volumes as well as that of the mesopore surface area gradually decreased, while the proportion of the macropore volume and surface area increased. Some micropores and mesopores were transformed into macropores.

The increased total pore volume was mainly attributed to the expansion of the initial small pores, evaporation of volatile substances and moisture in the coal, and generation of new pores induced by pyrolysis of the coal matrix.

The fractal dimension D_1 was used to characterize the surface roughness of the coal micropores, while D_2 described the complexities of the coal mesopores and macropores. As presented in Figure 3, D_1 gradually increased while D_2 decreased with increasing steam temperatures, indicating that the micropores in the coal became rougher, while the complexities of coal mesopores and macropores decreased.

Conclusions

After steam treatment, the evaporation of the volatile substances (including water) from the coal surface facilitated the formation of small blowholes, and pyrolysis of the coal matrix led to the generation of pyrolytic pores. The generation of new pores and the increases in the pore volume and pore diameter could provide additional space for gas flow and were conducive to CBM recovery. The decrease of the complexities of the mesopores and macropores would also facilitate gas flow.

Tables

Table 1. Variations in coal pore structural parameters (SSA - specific surface area; CPV - cumulative pore volume; APD - average pore diameter)

Samples	SSA (m^2/g)	CPV (mL/g)	APD (nm)
Raw lignite	1.7001	0.0047	11.0562
200 °C	1.0743	0.0059	24.8998
300 °C	0.9840	0.0071	35.5133
400 °C	0.9295	0.0084	48.1100

Figures

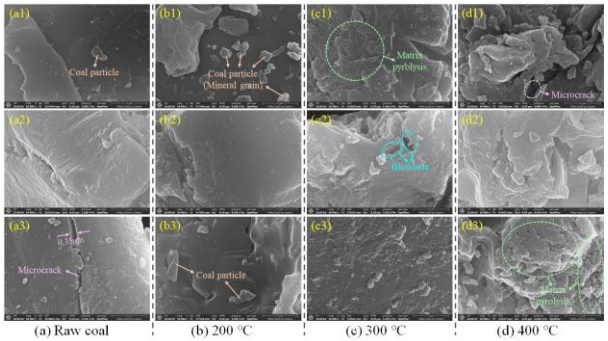

Figure 1. Changes in the coal surface micromorphology before and after steam treatment

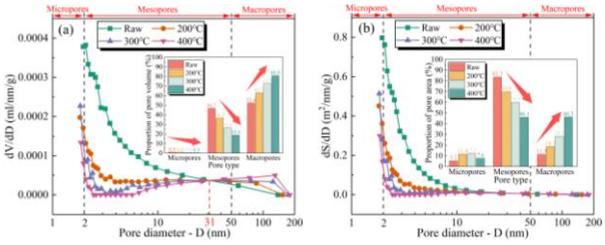

Figure 2. Variations in (a) pore volumes and (b) surface areas of the coal versus pore sizes

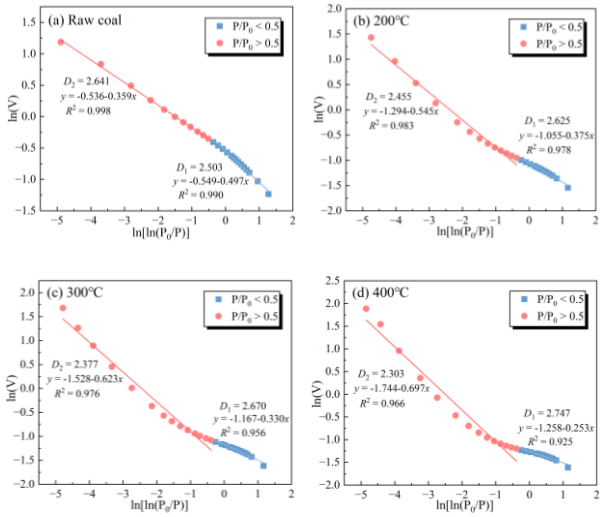

Figure 3. Pore fractal dimensions of the coal based on N_2 adsorption isotherms

References

Jamshid-nezhad, M. 2022. Steam alternating non-condensable gas injection for more heavy oil recovery. *Energy* **240**: 122476.

Liu, J., et al. 2021. Investigation of enhancing coal permeability with high-temperature treatment. *Fuel* **290**: 120082.

Yang, R.Y., et al. 2019. Coal breakage using abrasive liquid nitrogen jet and its implications for coalbed methane recovery. *Applied Energy* **253**: 113485.

Zheng, Y.F., et al. 2021. Experimental Study on the Effect of Coal Particle Size on the Mechanics, Pore Structure, and Permeability of Coal-like Materials for Low-Rank Coalbed Methane Reservoir Simulation. *Energy & Fuels* **35** (21): 17566–17579.

Feasibility study of modulating the microbially induced calcium carbonate precipitation (MICP) process through the application of electric fields

Chao Lv[1], and Chao-Sheng Tang*[1]

*Correspondence: tangchaosheng@nju.edu.cn.

[1] School of Earth Sciences and Engineering (Nanjing University, 163 Xianlin Avenue, Nanjing 210023, China)

Abstract

To investigate the influence of applied direct current electric fields on microbially induced calcium carbonate precipitation (MICP) process, we simulated sandy soil matrices to design and fabricate microfluidic chips. The microfluidic chip allowed exploration of bacterial behaviour and $CaCO_3$ precipitation patterns with and without an electric field. Experimental findings demonstrate that both bacteria and $CaCO_3$ precipitation distributed uniformly within the porous medium without an electric field. However, in the presence of an electric field, bacteria migrated towards the anode, while most $CaCO_3$ precipitated around the cathode.

Introduction

Microbially induced calcium carbonate precipitation (MICP) technology finds significant applications in geotechnical field (DeJong et al., 2010). However, challenges associated with non-uniform cementation may arise when employing MICP technology to treat problematic soils (Van Paassen et al., 2010). Given the charged nature of bacteria and chemical ions, electrokinetic methods hold potential for adjusting the distribution of bacteria and chemical ions during the MICP process (Terzis et al., 2020), thereby regulating the entire bio-mineralization process both temporally and spatially. This regulation can lead to a relatively homogeneous cementation effect.

Method

We designed and fabricated a microfluidic chip to simulate the pore structure of sandy soil based on the research conducted by Wang et al. (2019). To investigate the influence of a direct current (DC) electric field on the MICP reaction process, 1 mm diameter holes were punched at the top and bottom ends of the microfluidic chip to serve as electrode ports for accessing the DC power supply, as illustrated in Fig. 1. An activated bacterial solution (OD_{600} = 0.2) was injected into the prepared microfluidic chip at a flow rate of 1 μL/min through a syringe pump. Approximately 1.5 times the pore volume of the microfluidic chip was injected with bacterial solution during each round of MICP treatment. Subsequently, approximately 18 times the pore volume of the cementation solution, consisting of 0.1 M $Ca(CH_3COO)_2$ and 0.1 M urea, was injected into the chip at the same flow rate as the bacterial solution. A microscope with an integrated camera was employed to observe and record the MICP reaction process. Five rounds of MICP treatments were carried out with and without the application of a DC electric field of 3 V/cm, respectively. The chip was allowed to stand for 24 hours after each round of injection, during which bacterial behaviour and crystallisation process of $CaCO_3$ were observed. Note that, for the experimental group, the injection of the cementation solution and the application of the electric field were carried out simultaneously, with a duration of 1 hour per round.

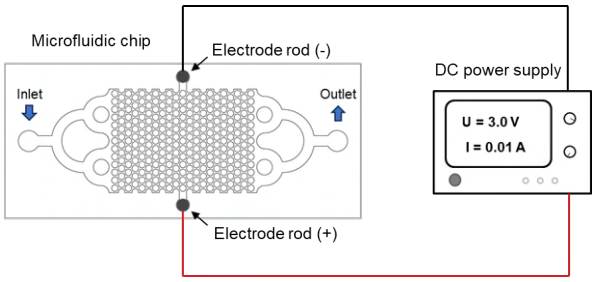

Figure 1. Schematic illustration of a microfluidic chip connected to a DC power supply via wires.

Results and Discussion

Continuous microscopic observation of the centre of the microfluidic chip (Fig. 2a) showed that, in the absence of an electric field, bacteria dispersed uniformly within the microfluidic chip throughout the MICP treatment period, and $CaCO_3$ crystals also precipitated evenly in the porous medium (Fig. 2b). Moreover, despite the drainage of some bacteria caused by the injection of cementation solution, the bacteria count within the porous medium increased with the number of MICP treatment rounds. As the MICP treatment rounds increase, the number of $CaCO_3$ crystals also rose, eventually reaching a plateau. Under the influence of a 3 V/cm DC electric field, experimental results demonstrated that most bacteria were driven by the electric field and aggregated around the anode duo to their negative charge. However, a portion of bacteria remained stationary in the electric field, which may be attributed to the interfacial cohesion with the inner pore surfaces. Regarding $CaCO_3$ precipitations, they initially occurred near the cathode during the MICP process, with the majority ultimately distributed in the region close to the cathode, with a small portion near the anode (Fig. 2c). Furthermore, the average size of $CaCO_3$ crystals precipitated near the cathode was larger than that near the anode. The preferential precipitation at the cathode primarily occurred because Ca^{2+} in the pore solution aggregated towards the cathode under the influence of the electric field, increasing the supersaturation in its vicinity. Compared to Ca^{2+}, CO_3^{2-} are less affected by electric field forces due to the time required for bacteria to hydrolyse urea to produce CO_3^{2-}. This dominance of Ca^{2+} in controlling the distribution of $CaCO_3$ precipitation suggests that the application of a DC electric field enables the preferential precipitation of $CaCO_3$ crystals at specific locations, providing new insights for optimising MICP treatment strategies.

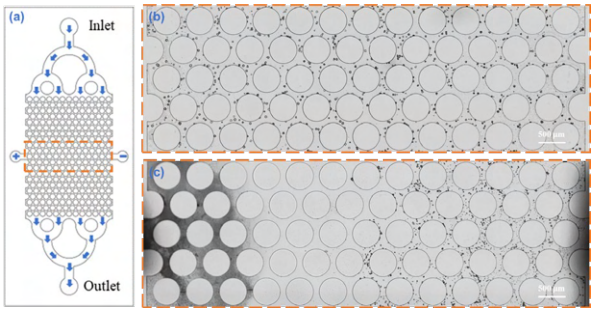

Figure 2. (a) Observation region within the microfluidic chip under the microscope; Microscope image depicting the centre of the microfluidic chip at the end of the fifth MICP treatment (b) without a DC electric field; (c) with a DC electric field.

Conclusions

This study investigated the influence of a DC electric field on MICP reaction process using a microfluidic system. The application of electric fields caused bacteria to migrate towards the anode and Ca^{2+} to accumulate towards the cathode, resulting in the preferential precipitation of $CaCO_3$ near the cathode. The experimental results confirm the feasibility of regulating the MICP process by applying a DC electric field.

References

DeJong, J.T., Mortensen, B.M., Martinez, B.C., Nelson, D.C. 2010. Bio-mediated soil improvement. *Ecological Engineering* **36** (2): 197-210.

Terzis, D., Hicher, P., Laloui, L. 2020. Direct currents stimulate carbonate mineralization for soil improvement under various chemical conditions. *Scientific Reports* **10** (1): 17014.

Van Paassen, L.A., Ghose, R., van der Linden, T.J., van der Star, W.R., van Loosdrecht, M.C. 2010. Quantifying biomediated ground improvement by ureolysis: large-scale biogrout experiment. *Journal of Geotechnical and Geoenvironmental Engineering* **136** (12): 1721-1728.

Wang, Y.Z., Soga, K., DeJong, J.T., Kabla, A.J. 2019. Microscale visualization of microbial-induced calcium carbonate precipitation processes. *Journal of Geotechnical and Geoenvironmental Engineering* **145** (9): 04019045.

Salinity constraints for bentonite barrier/backfill in GDF

Han Ming Lai*[1], Lidija Zdravkovic[1] and David M. Potts[1]

*Correspondence: h.lai23@imperial.ac.uk

[1] *Imperial College London, London, United Kingdom.*

Abstract

Compacted bentonite clay is the leading candidate for engineered barriers in the containment of radioactive waste in a geological disposal facility (GDF). Most of recent research on the behaviour of bentonite as a barrier material is limited to investigations under freshwater conditions. However, the chemical composition of groundwater can significantly inhibit bentonite's swelling behaviour, thus adversely affecting the functionality of the barrier. This is particularly of concern for geological environments containing soluble carbonates or evaporites, as groundwater salinity can significantly exceed seawater concentrations. This study evaluates the predictive capabilities of existing numerical modelling tools for simulating unsaturated, highly expansive compacted clays in varying pore fluid salinity. A fully coupled thermo-hydro-mechanical (THM) finite element (FE) model for unsaturated soils was employed, alongside an unsaturated dual-porosity mechanical model and appropriate soil water retention (SWR) and permeability models. Microstructural compressibility parameter, which decreases with increasing salinity, governs the ultimate bentonite swelling pressures. Increased permeability of bentonite due to salinity improved numerical prediction of swelling pressure evolution under saline conditions. The results identify further numerical developments, both in constitutive model formulation and in the extension of the governing FE equations from THM to THM-chemical coupling.

Introduction

While the UK government aims to expand nuclear power to achieve net zero objectives (UK GOV, 2022), managing legacy wasteforms remains a significant environmental challenge. High-Level Waste (HLW) and Spent Nuclear Fuel (SNF), with highest radioactivity, are currently stored above ground across multiple UK sites. This highlights the urgent need for more effective nuclear waste management. Geological disposal facility (GDF) offers a long-term solution for sustainable nuclear waste disposal, employing a multi-barrier approach to contain these wasteforms (NWS, 2022). Compacted bentonite is a promising barrier material due to its low permeability and self-sealing properties. Groundwater salinity is one major concern in a GDF as salinity can potentially inhibit its swelling behaviour. Experimental investigations involving the exposure of bentonite to saline solutions are currently limited. However, hypersaline groundwater is anticipated in potential UK GDF host rocks, such as evaporitic formations (Smedley et al., 2023). Further research is necessary to advance our understanding of bentonite behaviour under saline conditions.

Literature Review

Available literature indicates that salinity imposes significant effects on the swelling properties of bentonite clay. Studies (e.g. Dixon et al., 2018; Lloret et al., 2004) demonstrate that swelling of bentonite decreases with increasing salinity, but further increase to highly saline conditions does not affect swelling properties significantly. Samples subjected to saline solution attained final swelling pressure in shorter time periods, potentially attributable to the changes of hydraulic properties of bentonite. Studies revealed that permeability tends to increase with salinity when subjected to high saline conditions (e.g. Dixon et al., 2018).

Numerical Analyses and Discussion

The swelling pressure tests of FEBEX bentonite under different concentrations of NaCl solutions (Lloret et al., 2004) were simulated using the finite element (FE) software ICFEP, Potts and Zdravkovic (1999). ICFEP has a fully coupled THM FE formulation for saturated and unsaturated soils, (Potts et al., 2021), a dual-porosity mechanical model for compacted ben-

tonite, ICDSM (Ghiadistri, 2019), and a complement of SWR and permeability models.

As swelling of bentonite is believed to mainly occur at the microstructural level (Jiang et al., 2014), ICDSM microstructural parameters are subjected to investigation. The model results (Fig. 1) indicate that by varying the values of microstructural compressibility parameter, κ_m, the reduction of swelling pressure due to increasing salinity can be reasonably captured, but not so its temporal evolution. As the swelling of bentonite is closely linked to its response to wetting, it becomes essential to consider the hydraulic properties of the clay. By increasing the value of saturated permeability with increasing salinity in a variable permeability model, the prediction of swelling pressure evolution is much improved on average (Fig. 2).

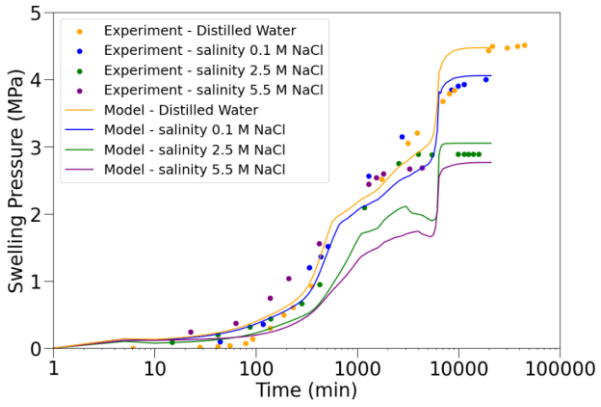

Figure 1. Model results for variation of κ_m

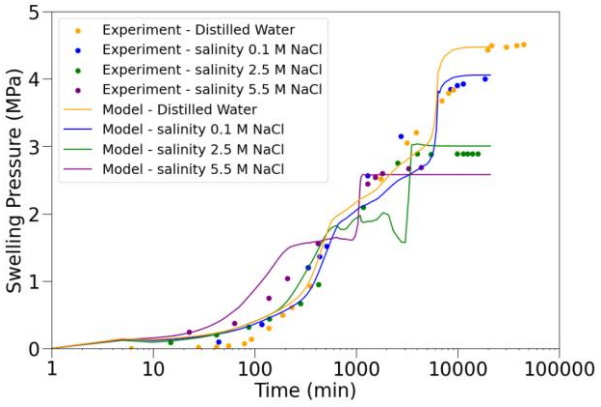

Figure 2. Model results for variation of permeability

Conclusion

This study highlights the importance of understanding bentonite behaviour under varying salinity conditions for effective GDF design. Future research would focus on incorporating salinity concentration as an input parameter and extending the existing THM formulation with chemical coupling (THM-C).

Acknowledgements

This research receives funding from the Nuclear Waste Services UK and the Imperial College Skempton Scholarship. The Imperial College Geotechnics Section supported the first author to attend the BGA YGES 2024.

References

Dixon, D.A., Man, A., Rimal, S., Stone, J., Siemens, G. 2018. Bentonite Seal Properties in Saline Water. Technical Report NWMO TR-2018-20, Nuclear Waste Management Organization.

Ghiadistri, G.M. 2019. Constitutive modelling of compacted clays for applications in nuclear waste disposal. PhD thesis, Imperial College London. Available: https://spiral.imperial.ac.uk/handle/10044/1/78499

Jiang, H., Xiang, G., Xu, Y., Chen, T. 2014. Study on the swelling mechanism and characteristics of bentonite. Soil behavior and geomechanics, 43-53.

Lloret, A., Romero, E., Villar, M.V. 2004. FEBEX II Project Final report on thermo-hydro-mechanical laboratory tests.

Potts, D.A., Zdravkovic, L. 1999. Finite element analysis in geotechnical engineering: theory. London: Thomas Telford Publishing.

Potts, D.M., Cui, W., Zdravkovic, L. 2021. A coupled THM finite element formulation for unsaturated soils and a strategy for its nonlinear solution. Computers and Geotechnics **136**: 104221.

Nuclear Waste Services (NWS), UK. 2022. NWS - GDF - Introduction to Geological Disposal. [Online]. Available: https://www.nws.uk/gdf/introduction-to-geological-disposal. (Accessed: Feb. 2024).

Smedley, P. L., Bearcock, J. M., Newell, A. J., Stewart, M. A., Metcalfe, R., Zagorscak, R., & Bailey, M. (2023). Guide to Reference Groundwater and Porewater Compositions. [Online]. Available: https://www.gov.uk/government/publications/guide-to-reference-groundwater-and-porewater-compositions. (Accessed: Apr. 2024).

UK, GOV., 2022. British energy security strategy. [Online]. Available: https://www.gov.uk/government/publica-tions/british-energy-security-strategy. (Accessed: Feb. 2024).

Comparative Study on the Small-Strain Stiffness of Recycled Concrete Aggregates Before and After Coating Removal with Acid Washing

Man LI[1,2], Huan HE[1,*], Guojun CAI[3]

*Correspondence: h_he@seu.edu.cn

[1] *School of Transportation, Southeast University (Nanjing, China)*
[2] *Department of Civil, Environmental and Geomatic Engineering, University College London (London, The United Kingdom)*
[3] *College of Civil Engineering, Anhui Jianzhu University (Hefei, China)*

Abstract

As urban infrastructure continues to age, the demand for the reuse of recycled concrete aggregates (RCA) increases, yet challenges arise due to cement mortar coatings on RCA surfaces. This study investigates an acid washing technique using dilute hydrochloric acid to remove these coatings. The focus is on the effects of the cement coating on the small-strain stiffness of RCA. The results indicate that stiffness decreases following acid washing, with significant impacts on the dynamic properties of treated versus untreated RCA.

Introduction

Recently, global construction activities and renovations generated a massive amount of waste. Rising construction waste and strict bans on extracting natural aggregates have heightened environmental concerns (Tam & Soomro, 2018). In geotechnical engineering, recycled concrete aggregates (RCA) have significant potential for use as fill material (Poon & Chan, 2006), thus rendering the investigation of its dynamic properties crucial. Small-strain stiffness (G_{max}) is a key parameter for assessing the dynamic properties of soils. It refers to a material's ability to resist deformation during the initial loading phase under small strain conditions. The stiffness of soils is often influenced by factors such as the coefficient of uniformity, particle shape, and inter-particle contact behaviour. However, due to the unique presence of cement mortar coatings, the stiffness properties of RCA often differ from those of natural sand. Consequently, this study will employ an acid washing technique to remove the cement mortar coatings from the surface of RCA. Combined with bender element tests, the study aims to evaluate the small-strain stiffness properties of RCA before and after acid washing.

Materials and Methods

Recycled concrete aggregate sourced from the demolition of ageing buildings and concrete pavements in China was employed. The RCA with the original gradation (coefficient of uniformity C_u=12.78) is investigated, as shown in Fig. 1.

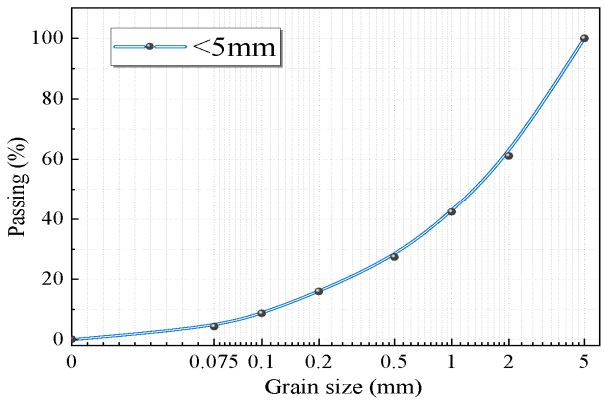

Figure 1. Particle size distribution curve

The acid wash procedure, using dilute hydrochloric acid, was implemented to remove the surface coating. Fig. 2 (a) and (b) display representative images of RCA grains before and after the acid-washing process, respectively. After acid washing, the core aggregate surfaces are cleaner and more distinct. Cylindrical samples with a diameter of 50 mm and a

height of 100 mm were prepared using a 3D-printed split mould for testing. The samples were prepared through air-pluviation and compaction methods, and the same density was maintained before and after acid washing. The small-strain shear stiffness of the RCA samples was assessed using bender element tests.

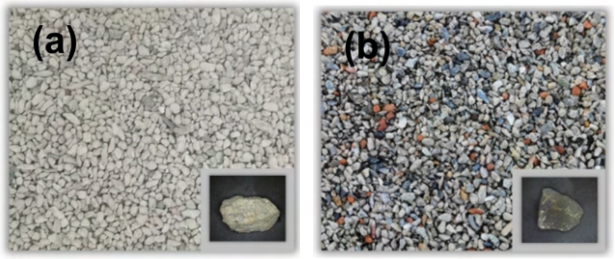

Figure 2. RCA particle before and after acid washing

A computer-controlled triaxial testing apparatus equipped with integrated piezo-element inserts was utilised for these tests. Bender element tests were conducted under isotropic confining stresses ranging from 25 kPa to 800 kPa, measuring wave velocities during loading and unloading at different pressures. By recording the propagation time of these waves and measuring the distance between the insert tips, the shear wave velocity (V_s) is determined. Subsequently, the G_{max} is computed using the equation (1), where ρ denotes the mass density of the RCA sample.

$$G_{max} = \rho V_s^2 \quad (1)$$

Results and Discussion

Fig. 4 reveals the trend of G_{max} variation with confining pressure in RCA samples before and after acid washing. Several observations can be made from Fig. 4: (1) The G_{max} of the acid-washed specimens is significantly lower than that of the original specimens at the same confining pressure. (2) The G_{max} of RCA demonstrated a significant increase during the unloading stage. (3) Although stiffness also increased in specimens following the acid-washing process, the magnitude of this increase was less pronounced compared to that observed in untreated specimens. To quantify the influence of various factors on small-strain stiffness, the general expression for G_{max} of granular materials is given in Equation (2).

$$G_{max} = A_G f(e) \left(\frac{p'}{p_n} \right)^{n_G} \quad (2)$$

Where G_{max} represents small-strain stiffness in MPa; e and p' (kPa) are void ratio and mean effective stress; p_n denotes standard atmospheric pressure (in this study 100kPa was adopted). A_G (MPa) and n_G are material constants.

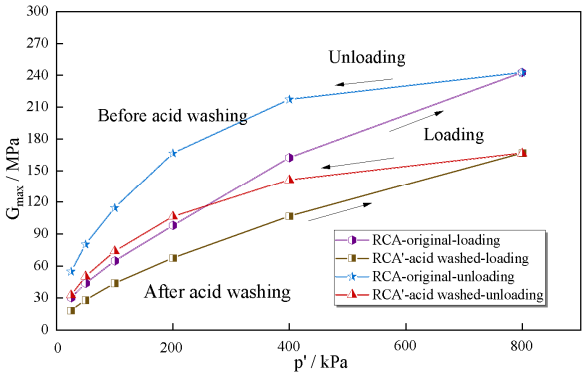

Figure 4. G_{max} of RCA particle before and after acid washing

By fitting the data points in Fig. 4 using Equation (2), it can be observed from Table 1 that compared to the G_{max} of acid-washed specimens, the original specimens exhibit a higher sensitivity to confining stress (i.e., higher n_G values). For RCA samples before and after acid washing, both of the sensitivity to confining pressure during the unloading stage is weaker compared to the loading stage (i.e. n_G> n_{uG}).

Table 1. The constants of specimens before and after acid washing: n_G, n_{uG}

	n_G	n_{uG}
Original RCA	0.60	0.37
Acid washed RCA	0.56	0.36

References

Tam V.W.Y., Soomro M., Evangelista A.C.J. 2018 A review of recycled aggregate in concrete applications, *Construction and Building Materials* **172**: 272–292.

Poon C.S., Chan D. 2006 Feasible use of recycled concrete aggregates and crushed clay brick as unbound road sub-base, *Construction and Building Materials* **20**: 578–585.

Numerical analysis of soil-plant-atmosphere interaction on a slope

M.S. Maddah Sadatieh*[1], A. Tsiampousi[1], and A. Paschalis[1]

*Correspondence: m.maddah-sadatieh22@imperial.ac.uk

[1] *Imperial College London, Exhibition Rd, South Kensington, London, UK (SW7 2AZ).*

Abstract

Surface geotechnical infrastructure is affected by the surrounding environment; therefore, it is important to comprehensively model soil-plant-atmosphere interaction (SPAI) and its effects on the infrastructure's safety and serviceability. Vegetation can have a positive effect on generating suctions and subsequently improving the factor of safety on infrastructure slopes. However, vegetation can also have negative effects, such as causing serviceability issues and larger displacements especially at the bottom of the excavation by contributing to cyclic volume change (swelling/shrinkage) of the soil. The balance between safety and serviceability should be investigated carefully and can be achieved through vegetation management. In this paper, the hydrological and mechanical properties of a column analysis modelled in an ecohydrological model (T&C) were compared with a numerical model in PLAXIS 2D, which accounts in a fully coupled flow-deformation analysis for the interaction between the soil and the atmosphere. It was shown that the results are in accordance, which indicated that the output results of T&C can be used to determine the boundary conditions for the geotechnical model.

Introduction

Climate change alters the environmental loads that are applied to geotechnical infrastructures, such as cuttings and embankments (Vardon, 2015). Thus, it is important to model the boundary conditions as accurately as possible (Dehn et al., 2000).

The safety of these infrastructures is highly connected to Pore Water Pressures (PWP) which in turn are related to the weather conditions, type of soil, and its vegetation cover. Rainfall induced slope failures are either due to the decrease of matric suction near the surface of the slope or because of the increase in the elevation of the water table and an increase in the PWP which result in the decrease of the effective stresses (Jamalinia et al., 2021).

Vegetation affects both the soil mechanical properties and its hydrological response to climate conditions. Vegetation management has the potential to enhance the stability of natural and man-made slopes in a sustainable manner, while having many positive environmental effects. Vegetation affects the pore water pressures and the soil strength via its roots. It decreases the infiltration rate and protects the soil against erosion. For heavier vegetation such as trees, the vegetation's weight will also play an important role (Greenwood et al. 2004). Changes in PWP will result in soil shrinkage/ swelling which may create serviceability issues. Drying of the soil may lead to cracking and increased permeability, which can result in a decreased soil strength and ultimately lead to slope failure (Elia et al., 2017). This shows the important of vegetation management.

In this paper, a column analysis modelled in T&C is compared against a numerical model of the hydrological and mechanical properties of the Newbury slope analysed as a column analysis in PLAXIS 2D (Sequent, 2023). Furthermore, it is shown that the output of T&C can be used to define the boundary conditions of the geotechnical model.

Numerical Modelling

An ecohydrological model (T&C) has been used to calculate the necessary parameters to capture the SPAI (Fatichi et al., 2012). The input for T&C is meteorological data such as precipitation, wind speed, radiation, humidity, temperature, and cloud cover. T&C uses these parameters and calculates the parameters shown in Fig. 1 for a column of soil. The net infiltration is applied as a surface infiltration boundary

condition in the hydro-mechanical model in PLAXIS as shown in Eq.(1):

$$I = P - E - T - E_{snow} - E_{int} - R \quad (1)$$

where I is infiltration. P, T and R are precipitation, transpiration, and run-off, respectively. E, E_{snow} and E_{int} are evaporation from bare ground, snow, and intercepted evaporation, respectively.

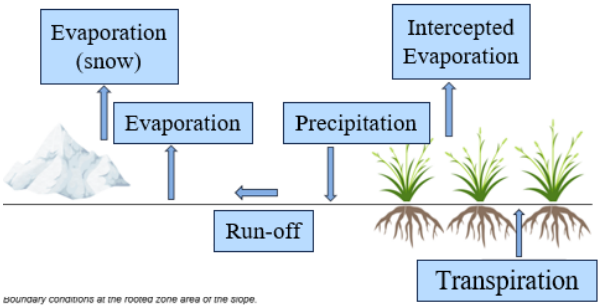

Figure 1. Boundary conditions at the rooted zone of the slope.

In order to see if the results from the ecohydrological model are in accordance with PLAXIS, a column analysis was also conducted in PLAXIS. The column of soil consists of 3 m of weathered London clay (including 0.8 m of rooted zone), 46 m of intact London Clay and 23.5 m of Lambeth Group Clay. After comparing these results, it was seen that the results from both models have the same order of magnitude and follow the same trends. The result for suction is shown in Fig. 2.

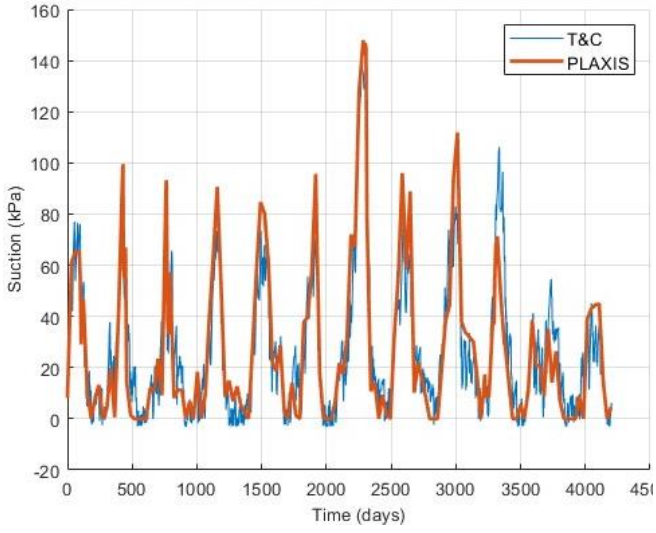

Figure 2. Suction values at 0.3 m in depth.

Conclusions

After comparing the results from the ecohydrological and geotechnical model and noting that the results are in accordance, it is showed that the output results from T&C can be used as input data for the geotechnical model.

For future study, the 2D model of the Newbury slope can be conducted and the results can be compared with field observations (Smethurst et al., 2012). Furthermore, a safety analysis can be performed to emphasize on the positive effects of vegetation on safety and the effect of future climate projections can be investigated.

References

Dehn, M. et al. (2000) Impact of climate change on slope stability using expanded downscaling, *Engineering Geology*. 55: 193-204.

Elia, G. et al. (2017) 'Numerical modelling of slope-vegetation-atmosphere interaction: An overview', *Quarterly Journal of Engineering Geology and Hydrogeology*, 50(3): 249–270.

Fatichi, S., Ivanov, V. Y., & Caporali, E. (2012). A mechanistic ecohydrological model to investigate complex interactions in cold and warm water-controlled environments: 1. Theoretical framework and plot-scale analysis. *Journal of Advances in Modeling Earth Systems*, 4(2).

Greenwood, J., Norris, J., and Wint, J. 2004. Assessing the contribution of vegetation to slope stability. *Proceedings of the Institution of Civil Engineers – Geotechnical Engineering*, 157(4): 199–207.

Jamalinia, E. et al. (2021) 'A data-driven surrogate approach for the temporal stability forecasting of vegetation covered dikes', *Water (Switzerland)*, 13(1): 1-25.

Sequent. 2023. PLAXIS 2D (2023.02).

Smethurst, J. A., Clarke, D., & Powrie, W. (2012). Factors controlling the seasonal variation in soil water content and pore water pressures within a lightly vegetated clay slope. *Geotechnique*, 62(5): 429–446.

Vardon, P.J. (2015) 'Climatic influence on geotechnical infrastructure: A review', *Environmental Geotechnics. ICE Publishing*, 5(1): 166–174.

Compilation and interpretation of historic inventory for landsliding between 1836 to 1919 in Wales, UK

D. Tudor*[1], and T. St John[2]

*dafydd.tudor@mottmac.com

[1,2] *Mott MacDonald, Cardiff, UK*

Abstract

Understanding historical landslide occurrence, distribution and impacts can help to inform modern risk mitigation strategies. By reviewing the National Library of Wales' recently digitised catalogue of over 15million historic newspaper articles, it was possible to compile a database of 529 unique landslide events for the years 1836 to 1919. The mass movements were catalogued and geolocated with extent and timing information as well as failure mode, impacts, antecedent weather and trigger mechanisms. A wide range of transport infrastructure, commercial activities and residential buildings were found to be impacted. 119 fatalities were identified. Landslide events were found to occur predominantly in winter and the dataset shows an apparent increase in landslide frequency from 1870 to 1909. The paper explores the links between landsliding and industrial development as well as weather events. Early approaches to landslide mitigation and remediation are considered.

Introduction

Wales has a generally moderate to high landslide susceptibility. There are some 2735 landslides recorded in Wales by the British Geological Survey (BGS) (pers. comm., 2021). Landslides include dormant sites reactivated by rainfall, erosion or human activities as well as first-time slides (e.g., within infrastructure earthworks). Landslides continue to cause adverse impacts and there is value in understanding historic landsliding to aid modern mitigation strategies.

Welsh Newspapers Online (WNO) launched in 2013. Over 1,100,000 pages from 120 publications are digitised for the period 1804 to 1919. Searches of WNO were undertaken using terms for mass movement, including 'landslide' and 'landslip' as well as Welsh equivalents. 529 mass movements were identified from >6400 articles (see Fig. 1). For each event, the description, location, timing, failure characteristics, possible triggers and impacts were populated.

Inventory Characteristics

526 events could be located to a county (Principal Area, PA). Events occurred in all 22 PAs, with the most (63 events, 12%) in Gwynedd, followed by Caerphilly and Rhondda Cynon Taf (each 61 events, 11.6%). There was no correlation between landslide quantity and county surface area. Confidence in positional accuracy was ranked, with the majority of events located with an accuracy of >100 m to <500 m.

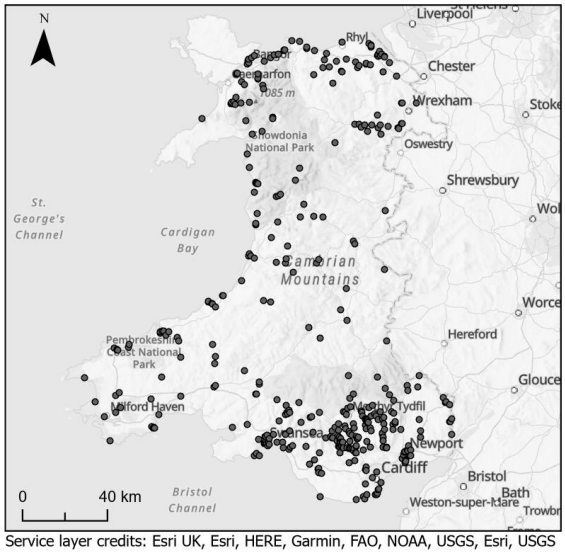

Figure 1 Landslides locations.

238 events (45%) were linked to a confirmed year, month and day. 97 landslides (35%) with month information were found to have occurred in winter months, with most in January followed by February. Equal proportions (18% each) occurred in spring and summer, whilst 30% occurred in autumn.

The timing was reported for 176 (33%) events. 49 events (28%) had timing reported to within the nearest hour. 119 fatalities were recorded across 54 events (10% of all events). Quarry rockfalls striking workers represent the most frequent cause of fatality. The average fatality rate for the study period was 1-2 persons/yr.

The incurred or estimated damage cost was described for 27 events. The November 2023 equivalent for the range of costs reported (considering the date of reporting) is £627 to £1.91M. Taking the lower bound, the average landslide economic impact reported (representing remedial works) is approximately £200,000 (2023 equivalent). This value is likely to be skewed by the tendency to report high-cost landslides. Adverse impacts on infrastructure were described for 339 events (64%) with roads and railways being the most affected, whilst the most affected industries were quarrying and coal mining. 53 events impacted buildings, including the flowslide of hundreds of thousands of tons of colliery spoil at Pentre, Rhondda Cynon Taf, in February 1909 which destroyed four houses and led to a fatality.

Remedial measures were basic, comprising debris clearance, void filling, wall and culvert construction. In some cases, new roads were proposed to avoid the hazard. Risk mitigation included watching briefs and road closures.

Inventory Interpretation

342 events were identified as new additions to the BGS landslide database. It was inconclusive whether a further 84 events may be additional inventory. The study findings represent a 13-16% increase in the number of Wales landsides in the BGS database. The dataset in this study indicates three to four events per year for the entire study period (1836-1919) but up to 22 events occurring in 1909. For modern context, BGS (2024) data indicates one to 10 landslides per year between 2013 to 2024, with exceptions (18-20 events) following extreme rainfall in 2013 and 2020.

Rainfall as a precursor for most events indicates a meteorological and seasonal control on landslide occurrence. Preliminary review of the 1km annual precipitation for Wales (Met Office, 2023) shows that annual rainfall peaks are not coincident with increased landsliding. It is likely that annual rainfall for the whole of Wales is too coarse a dataset for meaningful comparison, with regional variations in rainfall and short-term antecedent conditions likely important for landslide triggering.

The inventory shows an apparent increase in reported landslides (see Fig. 2). Census data shows that this period was a time of rapid population growth. In southeast Wales (the location of 47% of the landslides), rural areas became congested urban centres with new road and rail links excavated into valley sides. Extensive mining and lack of flat land led to tipping of spoil on slopes. Therefore, geohazards increased in number as did the potential receptors to landslide events. The apparent increase in landsliding likely reflects the increased reporting with more infrastructure and industry impacted. Media reporting is expected to have been biased towards events in populated areas which caused adverse impacts, with many landslide occurrences unreported.

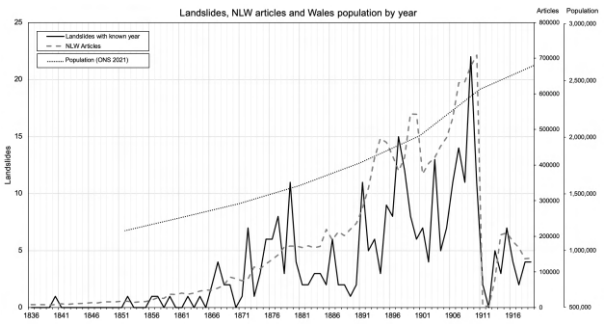

Figure 2 Landslides, WNO articles and population.

The inventory will prove useful for the identification of landslide potential as well as provide records of historic events at sites of existing instability, which may aid risk mitigation and remediation design. With the detail available in some articles, further work can be started to understand rainfall trigger conditions.

References

BGS. 2024. Rainfall and landslides. Available at: bgs.ac.uk/geology-projects/landslides.

Met Office. 2023. HadUK Wales precipitation.

National Library of Wales. 2022. Welsh Newspapers Online. Available at: library.wales.

Numerical Simulation of Landslides through a Stabilised Material Point Method with SANISAND Model

M. Xie *[1], P. Navas [2], and S. López-Querol [1]

*Correspondence: mian.xie.18@ucl.ac.uk

[1] *University College London, Gower Street, London, WC1E 6BT, UK*
[2] *Universidad Politécnica de Madrid, 28040 Madrid, Spain*

Abstract

This research presents a new semi-implicit two-phase double-point MPM formulation for modelling large-deformation geotechnical problems such as landslides. The proposed method addresses instabilities in traditional single-point MPM by using distinct sets of material points to model the soil and water phases separately (double-point approach). A modified F-bar technique is derived to stabilise advanced soil constitutive models such as SANISAND, allowing for a more realistic simulation of soil behaviour. The water phase is solved implicitly, enabling significantly longer time steps compared to fully explicit MPM approaches. Landslide examples using the SANISAND constitutive model are presented in this paper, demonstrating the performance of the modified F-bar method and highlighting the importance of the double-point approach.

Introduction

The Material Point Method (MPM) has a very similar formulation to the Finite Element Method (FEM), except that the iteration points (called material points in MPM) are allowed to move independently from mesh, providing the ability of this method to solve large deformation problem without mesh distortion. MPM has become a popular method to solve the geotechnical problem of large deformation. However, the current literature usually uses a basic constitutive model (e.g. Mohr-Coulomb) with a single-point MPM (i.e. use a single layer of material points to represent both soil and water) to model the soil-water coupled problems. Also, instabilities in MPM are usually overlooked. To address these issues, we proposed a new stabilised semi-implicit two-phase double-point MPM formulation. In this paper, we present some numerical examples of landslides using the proposed method with the SANISAND constitutive model to highlight the importance of stabilisation and the double-point method. The details of mathematical derivation, stabilisation method, and validations can be found in our extended paper (Xie et al., 2024).

Numerical Simulations

The SANISAND constitutive model (Taiebat & Dafalias, 2008) is implemented. Fig. 1 shows the validation of the numerical implementation against the original paper. Taiebat & Dafalias (2008) calibrated a set of SANISAND parameters for Toyoura sand with the drained and undrained triaxial tests. We adopt the same parameters for Toyoura sand to study landslides under dry and fully saturated conditions, except that a strength reduction factor 2 is applied (i.e. the parameter $\alpha_c^c = 0.6$) to generate catastrophic landslides. In this study, we also use the following parameters: soil particle density is 2650 kg/m^3, the water density is 1000 kg/m^3, the initial void ratio is 0.65, the initial porosity is 0.4, and initial permeability is 5e10^{-3} m/s.

The geometry and boundary conditions are illustrated in Fig. 2. A 0.05 m wide square mesh with 3^2 material points per cell is used. Rollers and fixed boundary conditions are applied on the side and bottom of the background mesh, respectively. The initial stress conditions are obtained through a gradually increasing gravity load in 1 s while keeping the model elastic. After initialisation, the plasticity suddenly is allowed to generate landslides. The final simulation times are set as 3 and 5 s excluding the initialisation for the dry and fully saturated landslides, respectively. In these times, the movement of landslides becomes negligible.

Discussion and Conclusion

In the case of dry conditions, the performance of the newly proposed modified F-bar stabilisation (Xie et al., 2023; Xie et al., 2024) is evaluated. As shown in Fig. 3, the original F-bar method fails to stabilise the volumetric locking for the dilative SANISAND soil, resulting in even more instability compared with the case without stabilisation. In contrast, the modified F-bar method has excellent performance with SANISAND, and the stress contour becomes smoother after increasing the mesh density. However, a 0.05 m mesh is sufficient for this type of problem. Further refining the mesh does not increase the accuracy significantly, as shown in Figs. 3 (c) and (d).

For the fully saturated landslides, we compared the performance of semi-implicit single- and double-point MPMs. Both methods are stabilised with a modified F-bar method. Fig. 4 shows the simulations of both methods at the final stage. The single- and double-point MPMs generate significantly different results, as shown in Fig. 4. The single-point approach has an unrealistic settlement in the water field. In contrast, the water field in the double-point method is realistic and stable. The soil field (grey material points on the background) between the single- and double-point methods are significantly different as well. The single-point method is stiffer, resulting in an underestimated run-out distance and an overestimated repose angle. These phenomena are consistent with previous findings in MPMs with the Nor-Sand constitutive model (Xie et al., 2024). In addition, the double-point method only increases about 15% of the increment in total computational time.

References

Taiebat, M., Dafalias, Y.F. 2008. SANISAND: Simple anisotropic sand plasticity model. *International Journal for Numerical and Analytical Methods in Geomechanics* **32**(8): 915–948.

Xie, M., Navas, P., López-Querol, S. 2023. An implicit locking-free B-spline Material Point Method for large strain geotechnical modelling. *International Journal for Numerical and Analytical Methods in Geomechanics* **47**(15): 2741–2761.

Xie, M., Navas, P., López-Querol, S. 2024. A stabilised semi-implicit double-point material point method for soil-water coupled problems. *arXiv*: 2401.11951

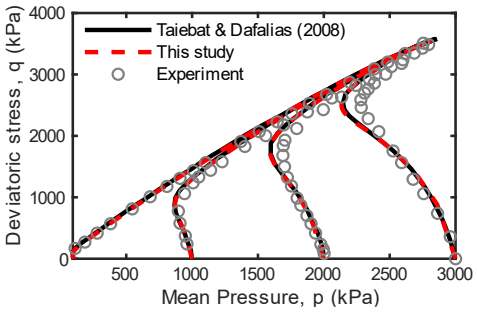

Figure 1. Validation of the SANISAND constitutive model: stress paths of the undrained triaxial test of Toyoura sand under different confining pressures

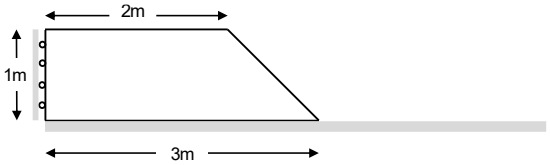

Figure 2. Graphical illustration of the numerical model

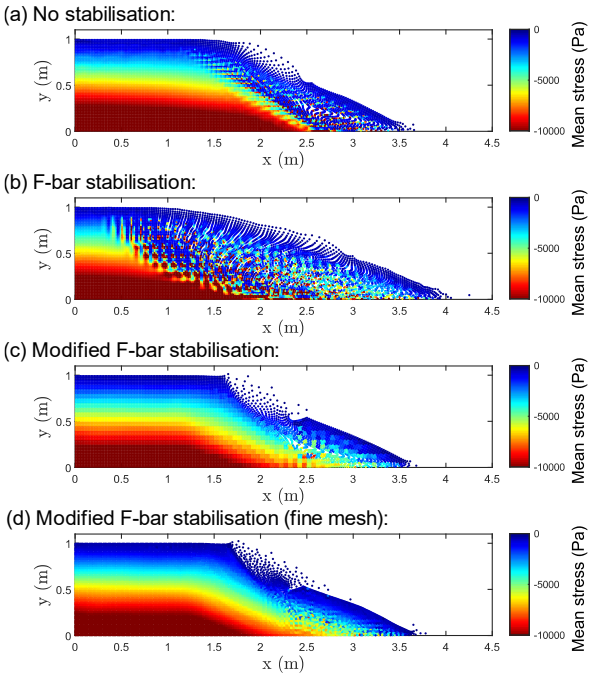

Figure 3. The stress contours of the landslides under dry conditions given by MPM with different stabilisations

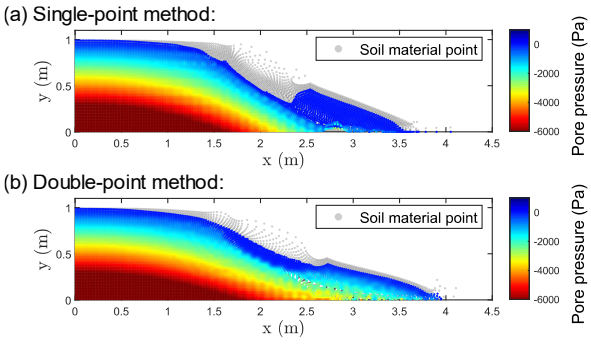

Figure 4. Pore pressure contours of the fully saturated landslides given by single- and double-point MPM

A sustainability analysis of major slope remediation techniques: A case study of failed slopes in England

C. Stafford and D. Akinniyi

Correspondence: chad.stafford2@gmail.com

Affiliation (Coventry University, Priory St, Coventry, CV1 5FB, United Kingdom)

Abstract

Achieving the UK's United Nations Sustainability Development Goals and 2050 net zero emissions target will require substantial research into high carbon production activities such as slope remediation. In this study, two failed UK slopes were remediated using sheet pile retaining wall, gabion basket wall and soil nail array design solutions. Thereafter, an embodied carbon assessment was conducted to provide insights to the most sustainable remediation method. Results show that the soil nail design proved significantly fewer tonnes of CO2e emissions could be achieved with the same factor of safety and 120-year design life. Reductions in the total values of tCO2e emissions ranged from 37%-83% when compared to the sheet pile wall designs, and 69%-86% to the gabion basket wall designs. Travel distance to locations for material supply and disposal are suggested as crucial factors towards achieving a safe and a sustainable slope remediation.

Key Words: Slope Remediation, Sustainability, Carbon Emission.

Introduction

The construction industry, through its activities and methods, contributes about 25% to global carbon emissions, hence, it is essential to give adequate attention to reduction of emission in construction activities. In the UK, ground engineering related construction is a major activity. According to network rail review report of earthworks management in 2021, there are over 190,000 earthwork assets in the UK, comprising of 70,000 soil cuttings and 100,000 embankments. Slopes continue to fail in UK for various reasons ranging from oversaturation, to changes in slope geometry (Mair, 2021). When slope failure occurs, a range of remediation methods are deployed, many of which rely on detrimental materials and construction processes for the environment. To align with the UK's efforts at combating climate change and conforming to the United Nations Sustainability Development Goals (UNSDG), the use of these remediation methods should be refined, to reduce values of GWP (Global Warming Potential). The high carbon emission results mainly from energy used in excavation, processing and transporting earth materials. It is therefore important to quantify the embodied energy different remediation techniques so as to understand the associated environmental impacts such as resource depletion and greenhouse gas emission.

The study aims to identify the most sustainable solution of three conventional geotechnical slope remediation method, namely, sheet pile retaining wall, gabion basket wall and soil nail array design solutions.

Methods

A preliminary assessment was conducted for two failed slope cases studies, based on buildability and geotechnical theory for stabilising the failure plane of the slope. The result of this assessment justified a cantilever sheet pile retaining, gabion basket gravitation wall and a soil nail array are viable solutions for each case study. Relevant Geotechnical parameters as required by Eurocode 7 – Geotechnical design – Part 2: Ground investigation and testing were obtained from existing ground investigation data for each case study. Analysis software RocScience Slide2 and Geosolve WALLAP was used to carry out global stability and FEM calculations. The National Highways Carbon Tool was used to conduct a sustainability embodied carbon analysis.

Results & Conclusion

Figure 1 shows the model for each remediation method for case study 1. It can be observed the minimum FOS was achieved in the soil nails design. The limited horizontal extents resulted in a steep pinned slope angle, causing difficulty in achieving a safe global stability.

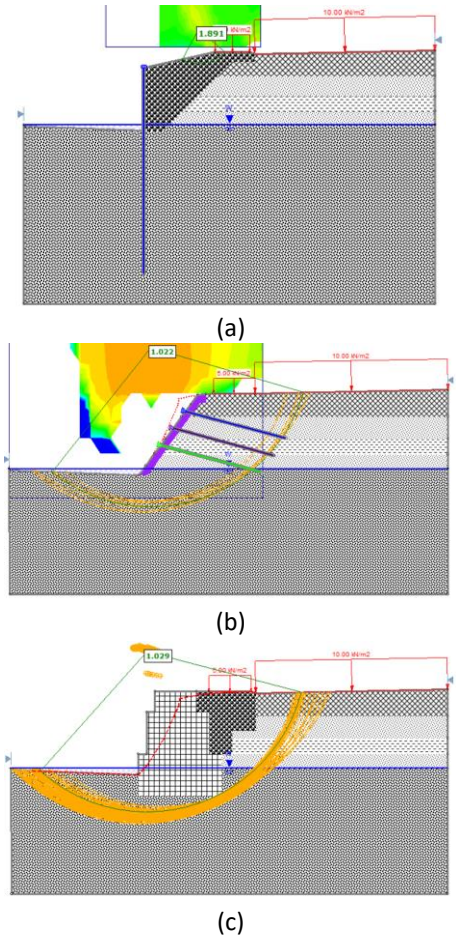

Figure 1. Case Study 1 Remediation Method Models: a) Sheet piles, b) soil nail, and c) Gabion basket

Figure 2 shows that the minimum FOS was obtained in the sheet pile wall design. Achieving a stable slope angle behind the wall provide difficult due the limited horizontal extents. The incorporation of 10% unplanned excavation in front of the wall further penalised the FOS when increasing the retained height to reduce the slope angle.

Figure 3 shows that the most sustainable slope remediation method, in tCO2e, is the use of soil nails, when compared to a sheet pile wall or gabion basket wall design for the same failed slope, 120-year design life and factor of safety (1).

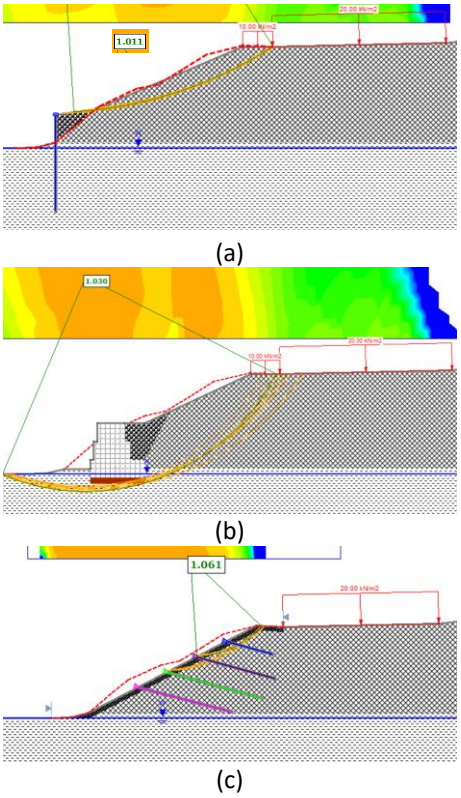

Figure 2. Case Study 2 Remediation Method Models a) Sheet piles, b) soil nail, and c) Gabion basket

The different colours display that by halving the transport distance, a maximum reduction of 43% in the total tCO2e was achieved.

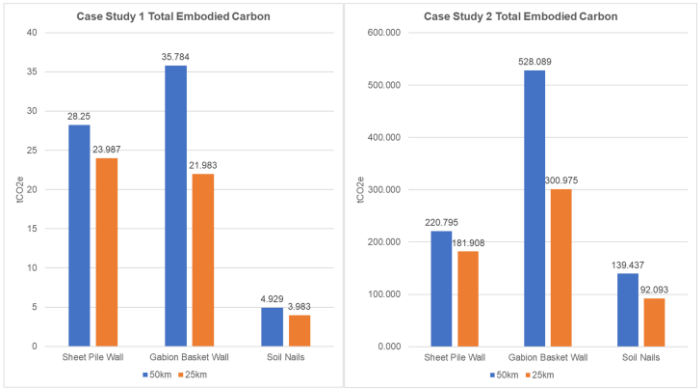

Figure 3. Total Embodied Carbon Graphs

In conclusion, soil nails rely on minimal materials due to the hollow small diameter bars and require little excavation of the failed slope for their installation. Hence, substantially less raw materials are required, and reduced material transport emissions.

References

R, Mair. 2021. A Review of Earthworks Management. London. Department for Transport.

Incorporation of Tyre Waste into Class 1 Embankment Materials in the UK

Judy Eid*[1]

*Correspondence: judy.eid@tonygee.com

[1] *Tony Gee and Partners LLP (Company, Hardy House, 140 High Street, Esher, Surrey, UK)*

Waste tyres present a significant global challenge. In the UK there has been an over reliance on exportation which has resulted in a significant quantity of waste tyres being sent to developing countries, where the lack of appropriate technology and environmental legislation has resulted in the tyres being treated in an unsustainable manner. Applications of waste tyre products in geotechnical engineering have been the subject of research for several years. The current research is co-funded by ICE, Imperial College, and Tony Gee, and will build on previous research produced by the author as part of an MSc. The research will focus on understanding strength, stiffness, mixture's packing state, and performance of soil skeleton. The aim will be to define the optimum rubber content for earthworks based on a pre-determined envelope of Class 1 material, so that it can be economically and sustainably used in earthwork projects.

Introduction

Studies estimated that approximately 1 to 1.8 billion waste tyres are discarded yearly all around the world (Pilkington, 2021). Figure. 1a shows the UK tyre waste generation per annum. In 2019, European Tyre and Rubber Manufacturers Association, provided a statistical estimate of the fate of waste tyres in Europe, as shown in Figure. 1b.

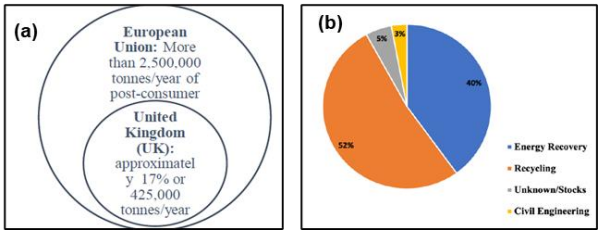

Figure 1. (a) UK Tyre Waste Generation (ETRMA, 2015) and (b) Fate of Waste Tyres in the EU (ETRMA, 2015)

In the UK there has been an over reliance on exportation which has resulted in a significant quantity of waste tyres being sent to developing countries, where the lack of appropriate technology and environmental legislation has resulted in the tyres being treated in an unsustainable manner. The UK government's Environment Bill promises "powers which will allow government to stop the export of waste…to developing countries." It is considered likely that this will restrict the export quantity of tyres.

Applications of waste tyre products in geotechnical engineering have been the subject of research for several years.

Background

In 2021 Tony Gee (TG) proposed and supported an MSc research project at Imperial College London (ICL) to carry out a literature review of the recent research. The review found that there was conflicting published data on the mechanical behaviour of soil/rubber admixtures, some indicating an enhancement or a degradation in behaviour, depending on the percentage of rubber used. The published research however focussed on the addition of rubber granules (<30mm) to sand and so did not replicate the size scale of typical earthworks materials, see Figure 2. The MSc thesis concluded that there was some evidence that coarser size-reduced rubber products, such as rubber chips or shreds exhibited higher strength in rubber-soil mixtures and therefore recommended further literature research and investigation be conducted in this area.

In early 2022 Tony Gee (TG) in collaboration with ICL instigated two further MSc research projects to extend the 2021 study by completing addition literature research and undertaking controlled laboratory testing to investigate

the mechanical behaviour of the addition of increasing percentages of tyre chips to Class 1 and Class 2 earthworks materials.

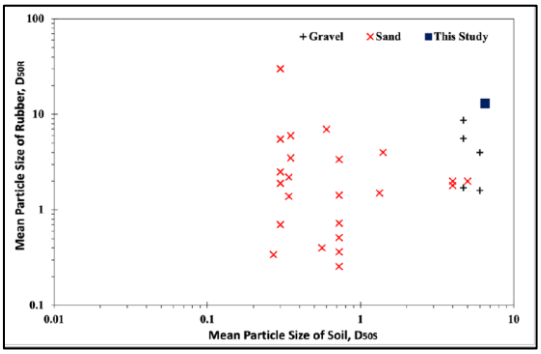

Fig 2. Previous investigations of granular soil and rubber

The current research project builds on previous research produced as part by the author's 2022 MSc. It is co-funded by the ICE, ICL and TG and aims to demonstrate that the inclusion of processed tyre chips does not adversely impact the overall performance of Class 1 fill and define the optimum rubber content for earthworks.

Research Programme

Preliminary laboratory assessments have found that the increase in the rubber content mainly affects the coarser materials in the mixture influencing compaction and so the unit weight. The author will characterise the geotechnical properties of rubber chips, Class 1 fills, and soil and rubber mixtures through further laboratory testing to evaluate compaction behaviour, strength, and stiffness of the mixtures.

A large triaxial cell developed at Imperial college, London Geotechnical laboratory will be employed to investigate the behaviour of the mixture, Figure 3. The research will focus on understanding the mixture's packing state and performance of soil skeleton as shown in Figure 4 and 5.

Finally, this project will enable site compaction trials and the construction of a full-scale embankment trial as a part of an operational highway scheme.

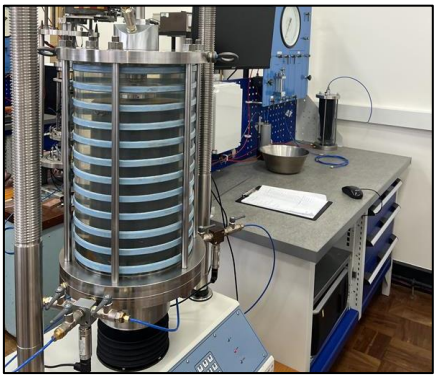

Figure 3. 150 mm Triaxial Cell developed at the Imperial College, London Geotechnics Laboratory

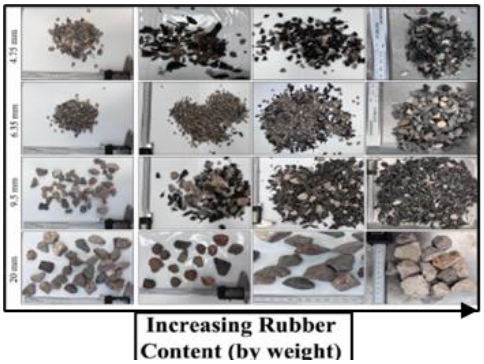

Figure 4. Soil Skeleton vs size fraction

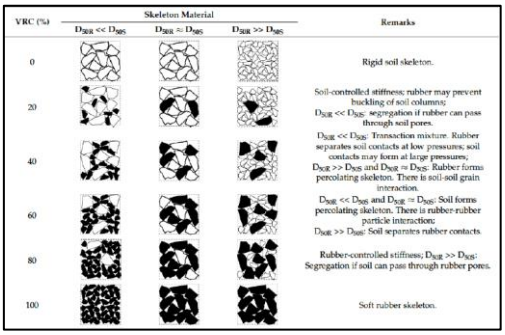

Figure 5. Distinct Skeleton Materials (Tasalloti, et al., 2021)

References

Specification for Highway Works, 2016, Manual Of Contract Documents For Highway Works Volume 1 Specification For Highway Works, Series 600.

ETRMA, 2015. End-of-life Tyre Report, s.l.: European Tyre and Rubber Manufacturers Association.

Kim, H. & Santamarina, J., 2008. Sand–rubber mixtures (large rubber chips). Can. Geotech. J, Volume 45, p. 1457–1466.

Tasalloti, A., Chiaro, G. & Murali, A., 2021. Physical and Mechanical Properties of Granulated Rubber Mixed with Granular Soils—A Literature Review. Sustainability, 13(4309).

Engineering Soil Barriers for the Prevention and Mitigation of Gully Erosion Menace in Nigeria

E.O. Mezie*[1], K. Tsiampousi[1], and K. Vinck[1]

*Correspondence: e.mezie23@imperial.ac.uk

Department of Civil and Environmental Engineering, Skempton Building, Imperial College London, United Kingdom

Abstract

In this study, the principles of unsaturated soil mechanics are intended to be applied to investigate landslide menace ravaging the state of Anambra in Nigeria. Reviews of literature have shown that the geology of the region, soil characteristics, topography and climatic factors favours rainfall-induced landslides. It is anticipated that the research outcome will enable the development of sustainable engineered barriers as solution.

1.0 Introduction

The state of Anambra in southeastern Nigeria has witnessed severe land degradation in the form of large-scale landslides leading to loss of lives and properties; a situation that is exacerbated by climate change. According to recent research, recommendations in previous studies and strategies employed to remedy the situation have not been effective due to gaps in understanding and in design strategies (Amangabara, 2023).

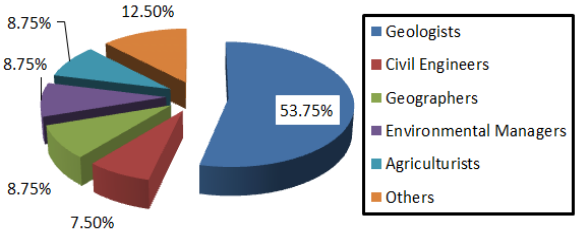

Fig. 1: Statistics of researchers on the menace (Authors)

Leroueil (2001) highlighted that good understanding of slope movement requires the joint efforts of geologists, hydrologists, hydrogeologists, geomorphologists and geotechnical engineers but statistics from the region proved otherwise – see Fig. 1 based on 80 research articles on the menace reviewed from the region. The failure of previous strategies points to the fact that the root cause of the problem is yet to be unravelled.

Large, well-developed gullies are found in the region (Fig. 2) numbering as much as 700 active ones and covering more than 40% of the state (Fig. 3a & b).

Fig. 2: Typical features of gullies in Anambra state

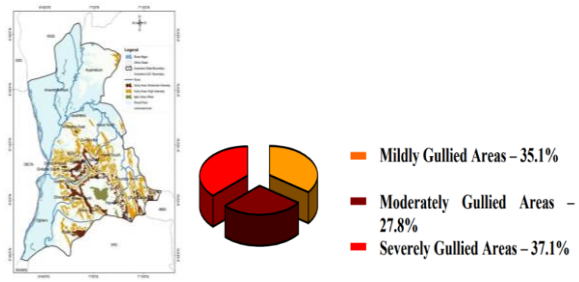

Fig. 3: (a) Map of Anambra state showing areas of gully concentration (Amangabara, 2023); (b) Statistics showing the extent of gullying (Igbokwe et al., 2008)

2.0 Key Contributory Factors of Gully Erosion

Nigeria witnesses two seasons in a year: a rainy season that runs from April to October

(associated with a Southwest trade wind blowing from across the Atlantic Ocean) and a dry season that runs from November to March (associated with a Northeast trade wind blowing from across the Sahara Desert). Anambra state located close to the southern border of Nigeria with the Atlantic Ocean witnesses high annual average rainfall of 1800 – 2050 mm (Onafeso, 2023) with intensities up to 100 – 125 mm/hr occurring up to 5 times in a year during the rainy season (Egboka et al., 2019). Although not having the highest annual average rainfall in the country which is as much as 3000 mm (Onafeso, 2023), it bears the largest menace of landslides which points to the contribution of soil characteristics and topography.

Nigeria possesses large depths of unsaturated soils while the state of Anambra has been shown to possess geological formations and soil characteristics that favours landslides. Table 1 shows the characteristics of some soil samples collected from Nanka, the most affected town in Anambra state.

Table 1: Soil characteristics of Nanka

Gravel (%)	-	16.97	17.70
Sand (%)	96	68.06	69.20
Fines (%)	4	14.97	13.1
MDD (g/cm^3)	1.6	1.88	1.98
OMC (%)	11.5	17.10	13.65
K (cm/s)	2.4×10^{-3}	8.52×10^{-5}	6.36×10^{-5}
Porosity, n (%)	-	45	51
C	23 kPa	7 kPa	2 kPa
ϕ^o	24	33	33

The state also contains high topography (see Fig. 4) that enhances the speed of runoff water which aids the instability of slopes.

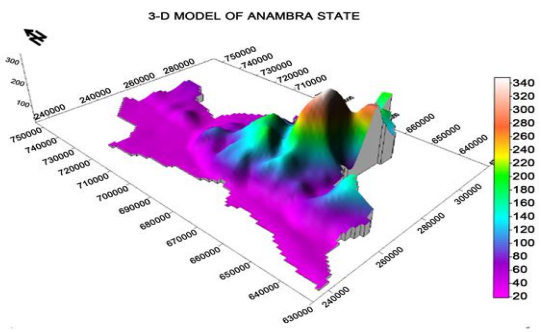

Figure 4: Topography of Anambra state (Udo et al., 2021)

3.0 Conclusion

This study postulates that the cause of large-scale landslides may be the loss of soil suction associated with high rainfall infiltration into the porous unsaturated soils, causing loss of shear strength and instability. Thus, it intends to investigate this presumption in-depth using the principles of unsaturated soil mechanics, an approach that is novel for the region, and to also develop sustainable engineered barriers based on research findings as solution.

References

Amangabara, G.T. 2023. Gully Erosion Sites in Southeast Nigeria: Prospects for Geotourism. In: Faniran, A., Jeje, L.K., Fashae, O.A., & Olusola, A.O. (eds.) *Landscapes and landforms of Nigeria*. Springer, Cham, Switzerland, World geomorphological landscapes, 225 – 242.

Egboka, B.C.E., Orji, A.E. & Nwankwoala, H.O. 2019. Gully Erosion and Landslides in Southeastern Nigeria: Causes, Consequences and Control Measures. *Global Journal of Engineering Sciences*, **2** (4).

Igbokwe, J.I., Akinyedebe, J.O., Dangc, B., Alaga, T., Onoa, M.N., Nnodu, V.C., and Anike, L.O. 2008. Mapping and Monitoring of the impact of Gully Erosion in Southeastern Nigeria with Satellite Remote Sensing and Geographic Information System. *The International Archives of the Photogrammetry, Remote Sensing and Spatial Information Sciences*. Vol. XXXVII. Part B8. Beijing, China.

Leroueil, S. 2001. Natural slopes and cuts: movement and failure mechanisms. *Geotechnique* **51** (3): 197 – 243.

Onafeso, O.D. 2023. The climate of Nigeria and its role in landscape formation. In: Faniran, A., Jeje, L.K., Fashae, O.A., & Olusola, A.O. (eds.) *Landscapes and landforms of Nigeria*. Springer, Cham, Switzerland, World geomorphological landscapes, 33 – 38.

Udo, E.A., Ojinnaka, O.C., Chukwuocha, A.C. and Uchenna, U.D. 2021. Terrain Modeling and Analysis Using Earth Observation System Based Data: A Case Study of Anambra State, Nigeria. *Open Access Library Journal* **8**: 1-18.

Reliability-Based Serviceability Limit State Design of Spread Foundations Under Uplift Loading

J.M. Han*[1]

*Correspondence: jayne.han@eng.ox.ac.uk

[1] *University of Oxford, Department of Engineering Science, Parks Road, Oxford, OX1 3PJ, United Kingdom*

Abstract

This research aims to develop a reliability-based serviceability limit state (SLS) design method for spread foundations under uplift loading in cohesionless soils. A probabilistic framework was adopted for the empirical characterisation of the compiled load-displacement curves and the quantification of the associated uncertainties. By using the obtained statistics of the curves, reliability analysis was carried out with Monte-Carlo simulations to calibrate the resistance factors within the load and resistance factor design (LRFD) framework. In addition, the relationship of the SLS with the ultimate limit state (ULS) was assessed, including the governing limit state at each allowable displacement level, and the probability of ultimate failure of the foundation at the SLS condition.

Introduction

The design of foundations involves uncertainties that arise from various sources (e.g. natural variability of the soil properties, and model uncertainties). To address these uncertainties and the associated risks, reliability-based design (RBD) methods have been developed and implemented in several design codes. In the RBD of foundations, the probability of the foundation reaching the limit state is assessed.

Specifically in the context of spread foundations for four-legged transmission towers, the limit states are governed by the uplift behaviour of the foundation. The applied uplift forces are induced by the overturning effects that are caused by the horizontal loads acting on the tower structure (e.g. wind loads, and differential wire tension). The resulting displacements and differential settlements of the foundation can lead to buckling failure in the tower structure, which may be a more crucial consideration than foundation failure (Farkas & Marczal 1995). Particularly for large spread foundations, the design is often governed by the serviceability requirements of the supported structure, due to their high susceptibility to significant displacements before failure (Orr & Farrell 2001). However, to date, there has been limited development of the reliability-based serviceability limit state (RBSLS) design methods for this specific design condition.

Thus, this paper aims to develop the RBSLS design method for spread foundations under uplift loading in cohesionless soils by adopting the probabilistic framework of using an empirical bi-variate model.

Statistical Characterisation of the Load-Displacement Curves

A database of 61 load test data from spread foundations under uplift loading in cohesionless soils was compiled to quantify the uncertainties in the uplift load-displacement behaviour. The database consists of the load-displacement curves and the associated properties of the soil and foundation, obtained from various field tests and centrifuge model tests. When compiling the database, the following criteria were considered: (1) cohesionless soils above the foundation base that is relatively dry and uniform; (2) uniaxial, monotonic uplift loading conditions; (3) foundation widths $B \geq 0.30$m to ensure that the data is representative of full-scale foundations; (4) shallow foundations with the embedment depth D of less than $6B$.

As shown in Figure 1, the compiled load-displacement curves were normalised by dividing the load by the slope tangent capacity

with the offset of 0.01B ($Q/Q_{0.01B}$), and the displacement by the equivalent circular foundation width ($\eta = \delta/B'$). Then, a hyperbolic function (Eq. (1)) was fitted to the normalised curves to obtain the fitting coefficients (θ_1, θ_2). The statistics of the fitting coefficients represent the statistical characteristics of the load-displacement curves, and hence are used as inputs for the reliability analysis and LRFD calibration.

$$\frac{Q}{Q_{0.01B}} = \frac{\eta}{\theta_1 + \theta_2 \eta} \quad (1)$$

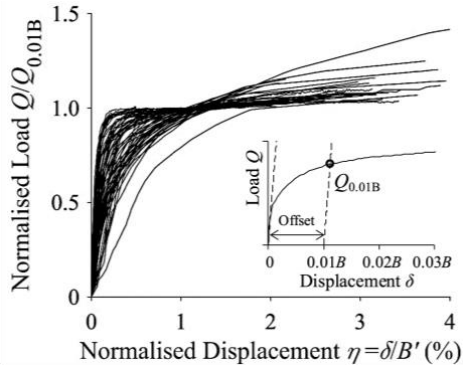

Figure 1. Normalised load-displacement curves

Reliability Analysis & LRFD Calibration

The LRFD calibration was carried out for both the serviceability and ultimate limit states by considering the context of transmission tower foundations subjected to uplift loads. In the LRFD framework, the following inequality is considered, where the nominal resistance (R_n) factored by the resistance factor (ψ) should be greater than or equal to the sum of the nominal loads (Q_n) factored by the load factors (γ).

$$\psi R_n \geq \sum \gamma_i Q_{i,n} \quad (2)$$

Based on this framework, the performance function was formulated to calibrate the resistance factors for both SLS and ULS designs. The target reliability index, or targeted probability of failure, was selected as β_{SLS} = 2.33 ($p_f = P(\delta > \delta_{all})$ = 1%) and β_{ULS} = 3.2 (p_f = 0.07%).

Figure 2 shows the calibrated resistance factors. It is demonstrated that the ULS becomes the governing condition, when the allowable displacement (i.e. SLS displacement) exceeds a relatively small value of 0.002B'; this highlights the importance of considering both limit states for design, particularly in the context of reliability-based design where the targeted probability of failure is significantly lower for the ULS condition.

Additional analysis was carried out to assess the probability of the ULS being reached, when the foundation reaches the SLS condition, or the allowable displacement level (δ_{all} or η_{all}) (Figure 3). The estimated probability can be used to evaluate the relative reliability of the foundation in the overall foundation-structure system; this would allow for the coordination of the failure sequences in the system, as referred to by several transmission tower design standards including the ASCE-74 guidelines and the international standard IEC 60826.

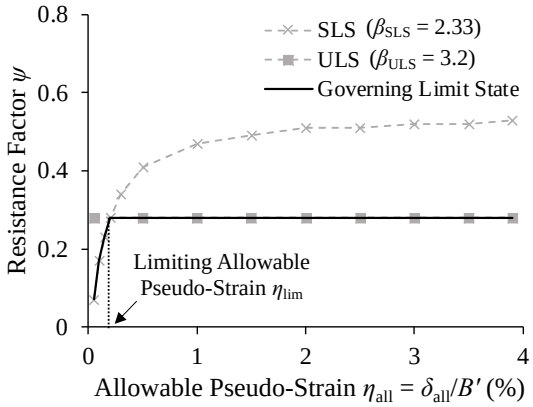

Figure 2. Calibrated resistance factors and the determination of the governing limit state

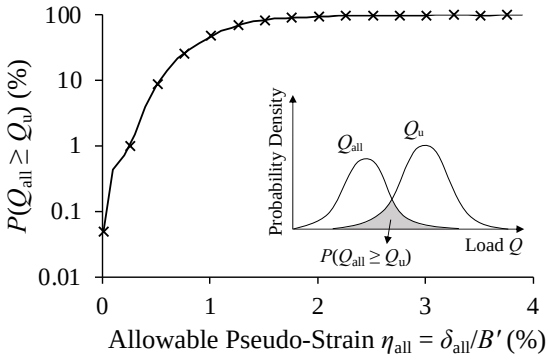

Figure 3. Probability of ultimate failure of the foundation occurring at the allowable displacement level

Based on the outcomes of this study, it is seen that the identified relationships between the foundation reliability against SLS and ULS failures could be incorporated into the foundation design procedures to allow for more a holistic design, compared to the conventional design approach.

References

Farkas, J., Marczal, L. 1995. Foundation of a 157 m High Transmission Tower. *Int. J. Rock Mech. Min. Sci. & Geomech. Abstr.* **32** (6): A282.

Orr, T.L.L., Farrell E.R. 2001. Use of Serviceability Limit State Calculations in Geotechnical Design. *15th Int. Conf. Soil Mech. Found. Eng.* Istanbul, 27-31 August 2001. Lisse: A. A. Balkema.

Image-based Constitutive Model Parameter Calibration

J.D.K. Smith [*1] and S.A.Stanier[1]

*Correspondence: jdks2@cam.ac.uk

[1] *Cambridge University Engineering Department, Trumpington Street, Cambridge CB2 1PZ, UK*

Abstract

Since geotechnical design requires carefully calibrated constitutive models, experimental techniques to define the parameters is of the upmost importance. Conventional element testing (e.g. triaxial tests) are the most commonly used means to calibrate constitutive models, however, they fail to quantitatively capture the effects of the natural state of soils, including heterogeneity (Wood, 2012) and uncertainty. Given developments in imaging and data processing, can material characterisation be improved? In this project, a work-based framework was trialled to calibrate strain-softening parameters in Structured Modified Cam Clay (SMCC) (Masin, 2006) using cyclic T-bar penetration and Particle Image Velocimetry (PIV) post-processing. Ultimately, it was found that element issues remained but could potentially be addressed in the future.

Introduction

Constitutive models are simplifying mathematical idealisations, founded on pedagogical understandings of complex material behaviour, for the purposes of engineering design. To ascribe physical meaning and verify suitability, it is imperative to calibrate constitutive models experimentally.

However, several issues have been identified with conventional calibration tests, namely: (i) implicitly assumed deformation homogeneity, (ii) lacking account for inherent uncertainty in results and (iii) subjectivity in evaluation by direct comparison. Thus, conventional calibration is rendered problematic, particularly for behaviours exhibited beyond heterogeneous shear band formation.

In response, an alternative framework, applied to strain-softening parameter calibration, is trialled in this extended abstract, providing an overview of the author's PhD thesis.

Work-based Calibration Methodology

The proposed framework, based on the Virtual Fields Method (VFM) (Grédiac, 1989), performs calibration by minimising a work-based objective function Eq.(1):

$$\Delta W_I(\sigma, \epsilon) - \Delta W_E = 0 \qquad (1)$$

where ΔW_I and ΔW_E are internal and external work increments respectively. As a function of stress, σ, and strain, ϵ, the former is constitutively dependent, thereby relating parameter values with an error quantity. Furthermore, full-field heterogeneous deformation data, obtainable through photogrammetric techniques e.g. Particle Image Velocimetry (PIV), is inherently incorporated into calibration.

Following on from Singh (2022) and Charles (2020), this project develops the framework for large deformations and realistically complex constitutive models.

Cyclic T-bar Penetration Testing

Figure 1. The cyclic T-bar penetration test configuration.

Cyclic T-bar penetration (as displayed in Figure 1) was conducted to provide full-field deformation data since the full-flow mechanism induced observes strain-softening and the geometry enforces plane-strain

conditions (i.e. the surface was assumed representative). The test was performed upon a sandy-clay composite (Kaolin clay and Hostun sand) normally-consolidated to 80kPa. The T-bar, consolidated in situ, completed 20 oscillations (10mm amplitude) at 1mm/s (undrained).

For calibration, the external work was directly calculated from the force-displacement response of the T-bar (Figure 2(a)). Furthermore, the degradation curve (Figure 2(b)) indicates the initial nominal sensitivity, $s_i \approx 4.45$.

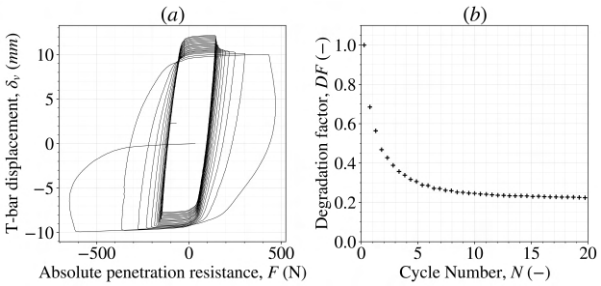

Figure 2. The cyclic T-bar (a) force-displacement response and (b) strength degradation curve.

Quantitative Image Post-Processing

Pre-existing PIV packages lacked the features necessary for temporal data storage, motivating the development of "geopyv". Pivotally, by using Material Point Method (MPM) and Strain Path Method (SPM) techniques, "particles" (material volume discretisation) interpolated incremental strain paths from optimised analysis meshes. Subsequently, corresponding stress paths were computed by assuming a constitutive model. Other developments included higher order structures, automated wild vector correction and adaptivity.

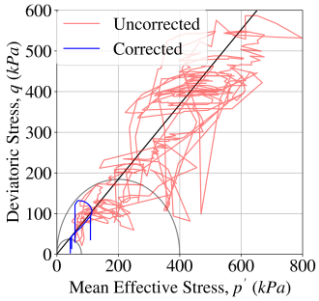

Figure 3. A particle stress path (within the mechanism) with and without volumetric error correction for Structured Modified Cam Clay (SMCC).

Geometrically-induced volumetric strain error, associated with mechanism discontinuities, proved problematic, as demonstrated in Figure 3. However, if volumetric strain correction can be justified given drainage conditions, model-dependent internal work can be evaluated.

Calibration and Model Comparison

Evaluation by Bayesian inference, rather than direct comparison, inherently incorporates and quantifies model and experimental uncertainty into the calibrated parameters. In Figure 4, parameter sets are compared for fit accordingly. By extension, uncertainty comparison can inform model suitability.

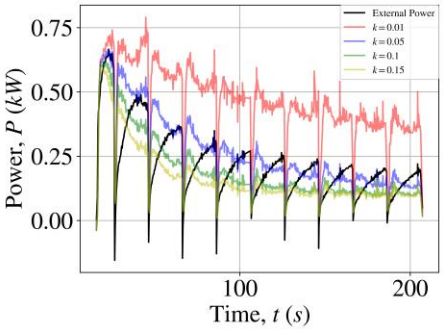

Figure 4. Comparison of internal (SMCC model) and external power curves about the peak likelihood with sensitivity, $s_i = 8.0$, and various degradation rates, k.

Conclusions

While advancing calibration, without the caveat of volumetric strain correction, the technique remains limited by element assumptions. Further improvement requires splining element shape functions or work-coupling strain measurements. Trialling the technique on triaxial compression with stereo-photogrammetry would improve applicability.

References

Grédiac, M. 1989. Principle of Virtual Work and Identification. Comptes Rendus de l'Académie des Sciences **309** (1): 1-5.

Singh, V. 2022. Unlocking the changing strength of fine-grained soils in numerical analyses. PhD Thesis. UWA.

Charles, J.A. 2020. Reconstuction of Soil Stress-Strain Response Using Optimisation. PhD Thesis. University of Sheffield.

On Applications of Geometric Singular Perturbation Theory within Hyperplasticity Accelerated Ratcheting Models

M.E. Rasmussen*[1]

*Correspondence: magne.rasmussen@eng.ox.ac.uk

[1]University of Oxford, Department of Engineering Science, Parks Road, Oxford OX1 3PJ, UK

Introduction

A robust design practice for foundations of offshore wind turbines includes consecutive and interconnected steps: material selection, defining pile dimensions, load calculations, fatigue analysis, and an understanding of the lateral & rotational responses at an ultimate limit state (Abadie, 2015). This study focuses on fatigue analysis, more specifically modelling monopile responses to cyclic lateral loading from wind and waves causing non-linear hysteretic and potentially ratcheting behaviour if loads are biased due to predominant wind/wave directions.

To theoretically model the soil response of a larger number to natural loading cycles varying in both frequency and amplitude, a thermodynamical theoretic macro scale incremental framework denoted by the 'Hyperplasticity Accelerated Ratcheting Model' (HARM) is in use (Houlsby, 2017). As a complement to the incremental framework, an alternative analytical approach is presented attempting to avoid stiff ordinary differential equations solvers. It entails establishing an equivalent set of algebraic-differential equations and the proof of a slow-fast dynamical system within the continuous HARM version. The work represents the first-ever exploration, motivation, and analysis of slow-fast dynamics for the HARM mass-spring system.

HARM - a Kinematic Hardening Model

HARM models are a subgroup of the wider field of kinematic hardening models. At its core is a macro-model consisting of a series of spring, dashpot, slider components selected to be able to accurately model:

- Kinematic hardening
- Rate effects
- Ratcheting
- Softening

(Houlsby, 2017). The model is formulated using a hyperplasticity approach, adhering to the first two laws of thermodynamics. The system incorporates multiple plasticity surfaces, see Fig. 1, allowing plasticity to be evaluated based on recent historical strain-stress behaviour.

HARM is built from 2 potentials: A potential for Helmholtz free energy (f) and one for dissipation (d). For the series multi surface model without ratcheting the equations are

$$f = \frac{H_0}{2}\left(\varepsilon - \sum_{i=1}^{N_s}\alpha_i\right)^2 + \sum_{i=1}^{N_s}\frac{H_i}{2}\alpha_i^2 \qquad (1)$$

$$d = \sum_{i=1}^{N_s} K_i|\dot{\alpha}_\iota| + \frac{\mu_i}{t_{\mathrm{ref}}}\dot{\alpha}_\iota \sinh^{-1}\left(|\dot{\alpha}_\iota|\, t_{\mathrm{ref}}\right) \qquad (2)$$

where H_{i}, $\mathrm{K_i}$, μ_i are spring, slider and dashpot coefficients for the i'th surface. t_{ref} decides the non-linearity of the elastic-viscoplastic part of the model. Letting $t_{\mathrm{ref}} \to 0$ implies a Bingham elastic-viscoplastic model. Lastly, (1, 2) also introduce internal strains α_i and global strain ε.

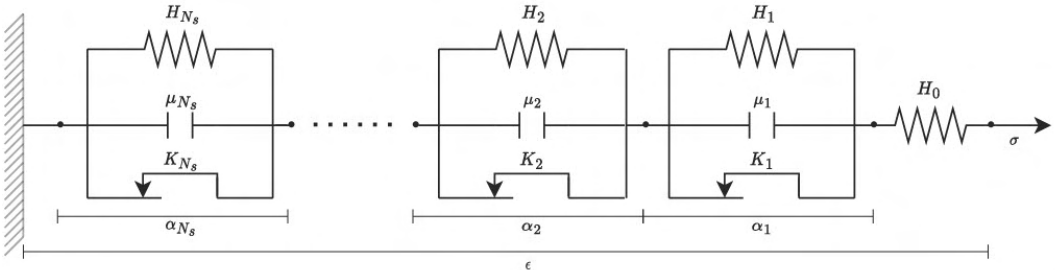

Figure 1 Physical representation of a rate-dependent, series, kinematic hardening model aligning with equations (1, 2).

For $i = 1, \ldots, N_s$:

$$\sigma = H_0 \left(\epsilon - \sum_{i=1}^{N_s} \frac{\left(\prod_{\substack{j=0 \\ j \neq i}}^{N_s} H_j \right) \epsilon - \left(\sum_{\substack{j=0 \\ j \neq i}}^{N_s} \prod_{\substack{w=0 \\ w \neq \{i,j\}}}^{N_s} H_w \right) \chi_i + \sum_{\substack{j=1 \\ j \neq i}}^{N_s} \left(\prod_{\substack{w=0 \\ w \neq \{i,j\}}}^{N_s} H_w \right) \chi_j}{\sum_{j=0}^{N_s} \prod_{\substack{w=0 \\ w \neq j}}^{N_s} H_w} \right)$$

$$\dot{\chi}_i = H_0 \dot{\epsilon} - (H_0 + H_i) \frac{S(\chi_i)}{t_{\text{ref}}} \sinh\left(\frac{t_{\text{ref}} \langle |\chi_i| - K_i \rangle}{\mu_i} \right) - H_0 \sum_{j \neq i} \frac{S(\chi_j)}{t_{\text{ref}}} \sinh\left(\frac{t_{\text{ref}} \langle |\chi_j| - K_j \rangle}{\mu_j} \right)$$

Figure 2 System of algebraic-differential equations for a rate-dependent, series, kinematic hardening model. The system is set up with respect to strain control. S(·) is the modified signum function (Rasmussen, 2023).

With strain control (ε known) and utilizing Maxwell relations for stress and internal stresses

$$\sigma = \frac{\partial f}{\partial \epsilon}, \chi_i = -\frac{\partial f}{\partial \alpha_i}, \ i = 1, \ldots, N_S \tag{3}$$

we can via first integration with initial conditions set to zero and by solving a full rank linear system of equations find a novel continuous equivalent kinematic hardening model. The complete system is included in Fig. 2.

The Applications of Geometric Singular Perturbation Theory within HARM

Geometric singular perturbation theory (GSPT) is built around a specific approach within the realm of singular perturbation theory. In a nutshell, the theory aims to systematically construct an approximation of solutions to problems that are otherwise intractable. GSPT makes use of multiple timescales relying on the existence of a small parameter in the differential system. (4) and (5) combine for a normal form of the GSPT differential equations:

$$x' = \frac{dx}{dt} = \delta f(x, y, \delta) \tag{4}$$

$$y' = \frac{dy}{dt} = g(x, y, \delta) \tag{5}$$

where $x \in \mathbb{R}^n$, $y \in \mathbb{R}^m$, $0 < \delta \ll 1$ and with the conditioning that f and g are at least piecewise smooth (Jones, 1995).

The algebraic-differential equivalent system in Fig. 2 is constructed such that the algebraic equation with respect to stress, σ, is solely a response equation and does not interact with the differential equations. Let now K_i be partially ordered such that $K_1 \leq K_2 \leq K_3$ without loss of generality, then for the system of differential equations (Fig. 2) we can utilize the limit of the empirically shown small parameter K_1/H_0 to create a fast and a slow system for the differential equations concerning χ_i leading to the knowledge of sudden jumps in χ_i values and thereby also jumps in the response variable, σ. In other words, the hyperbolicity of the critical manifold from the GSPT analysis align with unloading / reloading parts of each cycle.

(Rasmussen, 2023) rigorously covers the steps elucidated in this abstract to show the existence of a slow-fast system for the 0-D macro model with arbitrarily many plasticity surfaces. Two main research directions are heavily motivated by the found slow-fast system:

• First, a study in the performance of GSPT as a standalone tool to obtain integrable and non-conservative upper bounds for experienced ratcheting along pile depth. If the results are in alignment with experiments/simulations, they can be used as immediate design parameters.

• Second, a study on the new knowledge of where HARM becomes stiff for current numerical solvers. An idea is to model the fast and slow parts separately. By avoiding issues with machine number precision, it might lead to not only faster results but also better accuracy.

References

Abadie, C., 2015, “Cyclic lateral loading of monopile foundations in cohesionless soils,” Ph.D. dissertation, Oxford University

Houlsby, G., Abadie, C., Beuckelaers, W., and Byrne, B., 2017, A model for nonlinear hysteretic and ratcheting behaviour, International Journal of Solids and Structures, vol. 120, pp. 67–80

Jones, C. K. R. T., 1995, Geometric singular perturbation theory. Berlin, Heidelberg: Springer Berlin Heidelberg, pp. 44–118.

Rasmussen, M. E., 2023, On applications of geometric singular perturbation theory to mass-spring systems close to the continuum limit, Master Thesis, DTU Denmark.

Behaviour of small-scale piles jacked in soft rock

T. Riccio*[1], M. Ciantia[1,2], M. Previtali[1], M.J Brown

*Correspondence: 140007677@dundee.ac.uk
[1] University of Dundee, Nethergate DD1 4HN, United Kingdom
[2] University of Milano Bicocca, Piazza della Scienza, 4, 20126 Milano MI, Italy

Abstract

Open-ended (OE) pile field tests in low to medium density chalk have demonstrated a unique post installation response which impacts their axial short and long-term performance. Field-scale pile tests, although crucial for the development of new empirical based design approaches, are costly and time-consuming. Alternatively, characteristics observed at the field-scale can be broadly replicated at a small-scale for a lower cost and with more flexibility. In this scope the ICE-PICK testing campaign, a numerical and experimental study on installation effects and their long-term impact pile performance, will be discussed. Focus is drawn to the small-scale experimental pile tests conducted and the advanced techniques (namely a new versatile loading frame apparatus and X-ray CT) used to study the risks associated with pile installation in soft rocks.

Introduction

Soft rock is a unique geomaterial characterised by its structured, highly porous nature. The mechanical behaviour of soft rock makes pile installation a challenging task and gives rise to risks such as pile refusal and conversely pile free-fall. Field-scale test observations show that as piles are driven in to soft rock, they generate damage zone around the pile annulus which corresponds to low driving resistance, and short-term axial capacity. Whilst field-scale tests are crucial in developing new design approaches (such as the ICP-18 (Jardine et al., 2023)), they can be expensive and time consuming to conduct. Therefore, to aid a better understanding of the complex phenomena observed in the field, small-scale 1*g* tests combined with advanced numerical simulations may be used to conduct systematic parametric studies. These can carefully investigate the mechanisms which contribute to the unique installation behaviour observed in the field which varies in different rocks.

As part of the ICE-PICK project, a large campaign of small-scale physical modelling using novel X-ray CT, after Alvarez-Borges et al. (2021), was performed. This study, facilitated by a new multi-axis loading frame (Riccio et al., 2024) is actively contributing to the numerical package of the ICE-PICK project which aims to grow the understanding of pile installation behaviour in soft rock (Previtali et al., 2023). This paper highlights the development of the multi-axis frame as well as some brief insights into the extensive experimental test campaign.

The ICE-PICK multi-axis frame

The multi-axis frame (Fig. 1) was designed to fulfil criteria for pile installation and loading in soft rock ($UCS \approx 1-3$ MPa). It was also developed to be compact enough to fit within the University of Dundee SMART Lab CT scanner.

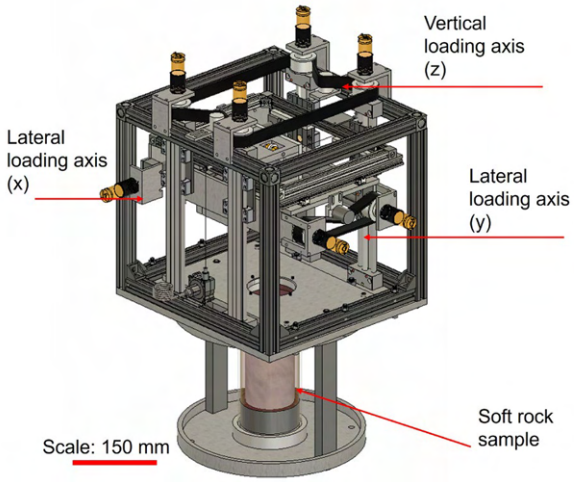

Figure 1. Multi-axis loading frame in small-chamber arrangement prepared with a soft rock sample for testing

Despite its size (see Fig. 1), it was able to actuate vertical and horizontal loads up to 5kN and 500 N, respectively. Details associated with the development may be found in (Riccio et al., 2024). Tests performed in different soft

rock samples using the frame consisted of installation, lateral monotonic and cyclic, and long-term axial tests to study pile set up. Continuous testing (i.e., install and then subsequent test stages) meant that the impact of installation could be evaluated. Whilst wished-in-place conditions adopted in experimental and numerical simulations may be appropriate for granular materials, neglecting the installation process in soft rock overlooks a significant precursor to pile performance.

Examples tests and discussion

Examples here consist of 15.4 mm piles axial tested after slow jacking into 100 mm diameter samples of calcarenite from Gravina Di Puglia, Italy ($UCS \approx 2$ MPa, $e_0 \approx 1$) after Ciantia and Hueckel (2013) and a white chalk from the St. Nicholas at Wade site (SNW), UK ($UCS \approx 3$ MPa, $e_0 = 0.85$). Jacking forces for both are shown in Fig 2a.

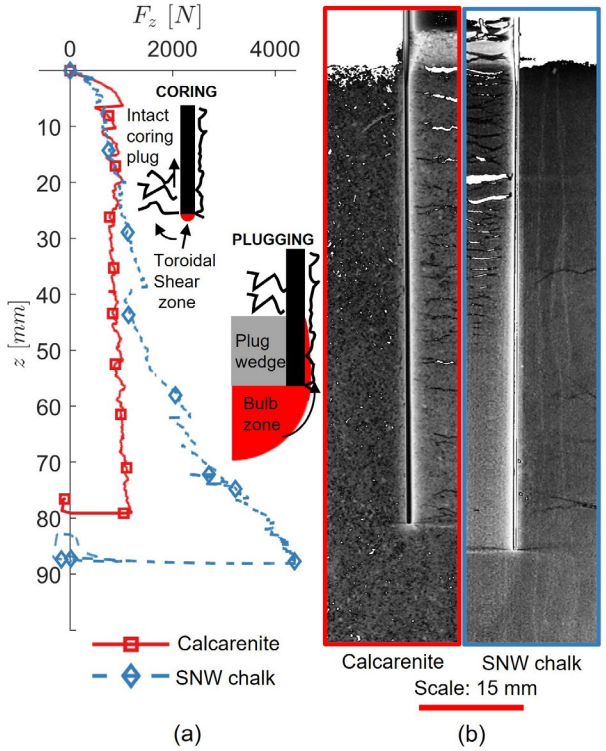

Figure 2. (a) Pile installation response of 15.4 mm piles installed in a highly porous calcarenite and white chalk (b) X-ray CT observations for both tests

Both cases exhibited a similar force-displacement response at shallow 'unconfined' penetration (<20-30 mm). In the chalk however, a marked increase in load at ~50 mm was observed, which grew until the end of insertion, contrasting the calcarenite case. Post-test X-ray CT (Fig 2b) showed that changes in jacking resistance for the chalk was associated with the formation of a plug. Both tests showed that a damage zone formed around the annulus of the pile, which was approximately the thickness of the pile wall, consistent with field observations reported by Jardine et al. (2023). In the chalk case, at deeper penetration depths, the plug led to a punching mechanism, contributing to a higher damage extent. Differences in installation stem from variability in the constituent materials (e.g., $d_{50,\text{calcarenite}} = 86\,\mu m$ vs $d_{50,\text{chalk}} = 5\,\mu m$), porosity and strength. In both cases, the installation process, paired to the bonded state of the far field material and marked destructurisation of near-pile material contributed to a low uplift capacity.

Conclusion

In summary, a new multi-axis loading frame was developed offering insight into the installation characteristics of piles installed in different soft rocks. X-ray CT revealed insights into pile insertion in soft rock not seen previously whilst also providing valuable data for validating numerical models.

References

Alvarez-Borges, F., Ahmed, S., Madhusudhan, B. N., & Richards, D. (2021). Investigation of pile penetration in calcareous soft rock using X-ray computed tomography. International Journal of Physical Modelling in Geotechnics.

Ciantia, M.O. and Hueckel, T., (2013). Weathering of submerged stressed calcarenites: chemo-mechanical coupling mechanisms. *Géotechnique*, *63*(9), pp.768-785.

Jardine, R. J., Buckley, R. M., Liu, T., Andolfsson, T., Byrne, B. W., Kontoe, S., McAdam, R. A., Schranz, F., & Vinck, K. (2023). The axial behaviour of piles driven in chalk. Géotechnique, 19(6), 1–45.

Previtali, M., Ciantia, M. O., & Riccio, T. (2023). Numerical installation of OE piles in soft rocks within the G-PFEM framework. Proceedings of the 10th European Conference on Numerical Methods in Geotechnical Engineering, 322–328.

Riccio, T., Romero, T., Mánica, M., Previtali, M., & Ciantia, M. (2024). A 4D soil-structure interaction model testing apparatus. Submitted to Geotechnical Testing Journal, 1(1), 1–12.